

THE UNIVERSITY
of EDINBURGH

This thesis has been submitted in fulfilment of the requirements for a postgraduate degree (e.g. PhD, MPhil, DClinPsychol) at the University of Edinburgh. Please note the following terms and conditions of use:

This work is protected by copyright and other intellectual property rights, which are retained by the thesis author, unless otherwise stated.
A copy can be downloaded for personal non-commercial research or study, without prior permission or charge.
This thesis cannot be reproduced or quoted extensively from without first obtaining permission in writing from the author.
The content must not be changed in any way or sold commercially in any format or medium without the formal permission of the author.
When referring to this work, full bibliographic details including the author, title, awarding institution and date of the thesis must be given.

Is Small Vessel Disease a Disease of the Blood Brain Barrier?

Rikesh M. Rajani



Doctor of Philosophy

The University of Edinburgh

2015

Declaration

I declare that this thesis was composed by myself and that all of the research described within it, except where specifically acknowledged in the text, is my own. This thesis has not been submitted for any other degree or professional qualification.

Rikesh M. Rajani, December 2015

Acknowledgements

Firstly, I would like to thank my supervisor Anna Williams, as well as my co-supervisors Joanna Wardlaw and Colin Smith, for providing guidance throughout the project and always being available for support. I would also like to thank the Medical Research Council for funding both myself and the project.

Secondly, I would like to thank those who have helped contribute to the work in this thesis. Anna Dominiczak for giving permission to use the stroke prone spontaneously hypertensive rats (SHRSP), Delyth Graham and Elisabeth Beattie for maintaining the colony, providing me with animals and helping with perfusions, and everyone at the Glasgow BHF animal unit who has helped, especially Charlie and David. I would like to thank my Master's student, Silvie Ruigrok, who helped validate gene lists and carried out some of the conditioned media experiments. I would also like to thank the MRC Sudden Death Brain Bank for providing me with human tissue, Santosh Atanur for providing me with a list of coding SNVs in SHRSPs, Bryan Serrels for use of his microarray scanner for the antibody array, the SuRF facility for help with paraffin embedding, the imaging and tissue culture staff at the Centre for Regenerative Medicine, and everyone in the Williams and ffrench-Constant labs who has shown me various techniques and guided me.

Completing a PhD relies as much on moral support as academic support, and for this I would like to thank my family, all the other students at SCRM, all the flatmates I have had in Edinburgh, RS, the Bathers, and all of my friends, both close by and further away, who have always been available for a chat and a pint.

Finally I would like to thank Laura – my best friend, my partner, my constant support. I could not have done it without you.

Abstract

Cerebral small vessel disease (SVD) is a vascular neurodegenerative disease which is the leading cause of vascular dementia and causes 20% of strokes. 20-30% of those over 80 show signs of the disease as white matter hyperintensities on MRI scans, doubling their risk of stroke and trebling their risk of dementia. Sporadic SVD is thought to be caused by hypertension but 30% of sufferers are normotensive and an alternative hypothesis implicates loss of integrity of the blood brain barrier (BBB).

To investigate this, I studied brains from normotensive people with early stage SVD and found reduced capillary endothelial claudin-5 (a BBB tight junction protein), more oligodendrocyte precursor cells (OPCs; the precursors to myelinating oligodendrocytes), and more microglia/macrophages compared to controls. Furthermore, in a relevant rat model of spontaneous SVD, the Stroke Prone Spontaneously Hypertensive Rat (SHRSP; disease model; DM) I found that reduced endothelial claudin-5 was the earliest change, appearing at 3 weeks of age, followed by OPC proliferation, appearing at 4 weeks, and then increased number of microglia/macrophages, appearing at 5 weeks. Importantly, all these changes occurred at a young age (< 5 weeks), before any measurable hypertension. These changes were confirmed in an *ex vivo* slice culture model (i.e. removing blood flow), ruling out direct damage by leakage of blood components through an impaired BBB and suggesting an inherent endothelial cell dysfunction as the primary cause, with secondary BBB defects.

This hypothesis of endothelial dysfunction is supported by increased endothelial cell proliferation in both human SVD tissue and the DM rats, and lower levels of endothelial nitric oxide synthase (eNOS) in brains of DM rats. To study this further I isolated primary brain microvascular endothelial cells (BMECs) from DM and control rats and found that those from DM rats formed less mature tight junctions (less membranous claudin-5) than control BMECs. I also found that conditioned media (CM) from DM BMECs causes OPCs in culture to proliferate more and mature less. This indicates that the endothelial dysfunction is inherent to the endothelial cells, rather than induced by other cell types, and through secreted factors causes OPC changes mirroring what is seen *in vivo*. Using an antibody array, I identified HSP90α

as a candidate secreted factor and showed that it is necessary (by blocking the protein in CM) and sufficient (by adding recombinant HSP90α) to induce the maturation phenotype in OPCs, but not the proliferation phenotype.

The idea that endothelial dysfunction causes SVD begs the question of what causes endothelial dysfunction, especially in our inbred DM rat strain. To establish this, I reanalysed sequencing data of the DM and control rats from a previously published study, searching for mutations which lead to truncated proteins in genes expressed in brain endothelial cells. We confirmed the candidate gene *Atp11b*, a phospholipid flippase, was mutated as predicted. I found that knocking down *Atp11b* using siRNA in a control endothelial cell line caused endothelial dysfunction and a loss of tight junction maturity, and that CM from these cells causes OPCs to proliferate more and mature less, mirroring what we see in primary DM BMECs and suggesting that *Atp11b* has a key function in promoting normal endothelial function. Furthermore, I showed that knocking down *Atp11b* causes cells to secrete increased levels of HSP90α. I propose a mechanism whereby ATP11B regulates the retention of HSP90α within endothelial cells, which in turns regulates eNOS levels and activity, as has been shown previously.

In summary, this work shows that there are many pre-symptomatic changes which occur in the brain in the development of SVD in DM rats, and that these are ultimately caused by endothelial dysfunction. As these changes are similar to those found in spontaneous human SVD, I propose that endothelial dysfunction is a key mechanism of human SVD, which may in the future lead to new therapies.

Lay summary

Cerebral small vessel disease (SVD) affects the small blood vessels in the brain, and causes cognitive and motor problems. Sufferers of SVD are also twice as likely to have a stroke and three times as likely to develop vascular dementia. SVD is a very common disease, with almost a third of people over eighty showing some signs of the disease. Despite this, there are currently no known treatment options and the disease is poorly understood.

One part of the brain which is damaged in SVD is the blood brain barrier (BBB). This structure prevents harmful substances in the blood from entering the brain. Using an animal model of SVD, I showed that a breakdown of the BBB is one of the first changes that happens in the brain during the development of the disease. Using a model where brain slices are grown in culture, I demonstrated that despite this early BBB breakdown, later disease changes are not caused by harmful blood products leaking into the brain. I then went on to show that another early change in SVD is a dysfunction of the endothelial cells (ECs), the cells which form the blood vessels. I demonstrated that this explains the BBB breakdown, and that these dysfunctional ECs release factors which cause other changes in the brain that we observe in SVD. I also demonstrated that a single gene mutation in the animal model of SVD that we use is responsible for a large part of this.

This thesis provides evidence that endothelial dysfunction is the cause of SVD. This knowledge can help us to develop better treatment options for this common, potentially debilitating disease.

Contents

Declaration 2

Acknowledgements 3

Abstract 4

Lay Summary 6

Contents 7

Chapter 1: Introduction 13

1.1 – Importance of SVD *13*

1.1.1 – Symptoms of SVD 13

1.1.2 – Consequences of SVD 14

1.1.3 – Prevalence of SVD 14

1.2 – Pathology of SVD 16

1.2.1 – Lacunar lesions 16

1.2.2 – Vascular pathology 17

1.2.3 – Other pathology 18

1.2.4 – Diseases with similar pathology to SVD 18

1.3 – SVD on neuroimaging 20

1.3.1 – Recent small subcortical infarct 20

1.3.2 – Lacune of presumed vascular origin 21

1.3.3 – WMH of presumed vascular origin 21

1.3.4 – Perivascular space 21

1.3.5 – Cerebral microbleed 22

1.3.6 – Brain atrophy 22

1.3.7 – Breakdown of the blood brain barrier 23

1.4 – The blood brain barrier 25

1.4.1 – Function of the BBB 25

1.4.2 – Composition of the BBB 26

1.4.3 – The BBB in SVD *30*
1.4.4 – The BBB in other diseases *30*
1.5 – Myelin 30
1.5.1 – Function of myelin *31*
1.5.2 – Oligodendrocytes *33*
1.5.3 – Myelin in SVD *35*
1.5.4 – Extrapolation from other diseases of the white matter – multiple sclerosis *35*
1.6 – Mendelian forms of SVD 36
1.6.1 – CADASIL *37*
1.6.2 – CARASIL *38*
1.6.3 – COL4-related angiopathies *38*
1.7 – Causes of sporadic SVD 38
1.7.1 – Hypertension *39*
1.7.2 – Diabetes *39*
1.7.3 – Smoking *40*
1.7.4 – Other risk factors *40*
1.8 – Animal models of SVD 41
1.8.1 – Animal models of Mendelian SVD *41*
1.8.2 – Inducible models of SVD *42*
1.8.3 – The stroke prone spontaneously hypertensive rat *43*
1.9 – Hypothesis 46
1.10 – Aims 46

Chapter 2: Materials and Methods **47**

2.1 – *In vivo* methods 47
2.1.1 – Animal housing and husbandry *47*
2.1.2 – Termination *47*
2.1.3 – Tracer experiments *48*
2.1.4 – Preparation of tissue *48*
2.2 – *In vitro* methods 49
2.2.1 – Preparation of brain slices *49*

2.2.2 – Preparation of BMECs 49
2.2.3 – Preparation of OPCs 50
2.2.4 – Preparation of microglia 51
2.2.5 – Maintenance of bEND.3 cell line 51
2.2.6 – Collection of conditioned media 52
2.2.7 – Experiments using conditioned media 52
2.2.8 – Treatment of bEND.3 cells with siRNA 52
2.3 – Immunostaining 53
2.3.1 – Fluorescent IHC on paraffin embedded rat tissue 53
2.3.2 – Fluorescent IHC on fixed frozen rat tissue 53
2.3.3 – Fluorescent IHC on paraffin embedded human tissue 53
2.3.4 – Colorimetric IHC on paraffin embedded human tissue 54
2.3.5 – Fluorescent IHC on ex vivo brain slices 54
2.3.6 – Immunocytochemistry 55
2.4 – Analysis of protein levels 55
2.4.1 – Extraction of protein from tissue 55
2.4.2 – Extraction of protein from cells 56
2.4.3 – Quantification of total protein 56
2.4.4 – Western blotting 56
2.4.5 – Antibody array 57
2.5 – Molecular biology 58
2.5.1 – Extraction of DNA 58
2.5.2 – Extraction of RNA 58
2.5.3 – Synthesis of cDNA 58
2.5.4 – Polymerase chain reaction (PCR) 59
2.5.5 – Sequencing of DNA and cDNA 59
2.6 – Other methods 59
2.6.1 – Assay of nitric oxide synthase activity 59
2.7 – Imaging, analysis and statistics 60
2.7.1 – Imaging 60
2.7.2 – Imaging analysis 60
2.7.3 – Quantification of western blots 61

2.7.4 – Statistics *61*
2.8 – Materials: human tissue blocks 61
2.9 – Materials: *in vitro* reagents and plastics 63
2.9.1 – List of all cell culture plastics *63*
2.9.2 – List of all cell culture solutions *63*
2.9.3 – List of siRNAs *64*
2.10 – Materials: list of antibodies 64
2.10.1 – Primary antibodies used for IHC and ICC *64*
2.10.2 – Primary antibodies used for western blots *65*
2.10.3 – Secondary antibodies used *66*
2.11 – Materials: list of primers 66
2.12 – Materials: list of kits and other chemicals 67

Chapter 3: What are the Early Pathological Changes in Small Vessel Disease: Descriptive Results 69

3.1 – Introduction 69
3.2 – Results of tissue staining 71
3.2.1 – BBB tight junctions *71*
3.2.2 – OPCs *76*
3.2.3 – Macrophages/microglia *81*
3.2.4 – Other components of the BBB *83*
3.3 – Discussion I 85
3.3.1 – BBB changes *85*
3.3.2 – OPC changes *86*
3.3.3 – Macrophage/microglia changes *87*
3.3.4 – Mechanisms *88*
3.4 – The slice culture model 89
3.5 – Results from slice cultures 90
3.6 – Discussion II 94

Chapter 4: What are the Effects of Endothelial Dysfunction in Small Vessel Disease: *In Vitro* Results **96**

4.1 – Introduction 96

4.1.1 – Role of nitric oxide *96*

4.1.2 – Endothelial nitric oxide synthase *97*

4.1.3 – Endothelial dysfunction vs. endothelial activation *97*

4.1.4 – Causes of endothelial dysfunction *98*

4.1.5 – Effects of endothelial dysfunction *99*

4.1.6 – Endothelial dysfunction in SVD *100*

4.2 – Results: evidence for endothelial dysfunction in SVD and DM rats 100

4.3 – Results: effects of endothelial dysfunction in DM rats 104

4.4 – Results: What mediates the effects of endothelial dysfunction in the DM rat 118

4.5 – Discussion 127

4.5.1 – The effects of endothelial dysfunction on microglia *127*

4.5.2 – Recombinant protein and blocking antibody experiments *128*

4.5.3 – Heat shock protein 90 alpha (HSP90α) *129*

4.5.4 – HSP90 and OPCs *131*

4.5.5 – Other secreted factors *132*

Chapter 5: What Are the Causes of Endothelial Dysfunction in the Disease Model Rat: Genetics Results **134**

5.1 – Introduction 134

5.2 – Reanalysis of genetic data 136

5.3 – Results: validation of genetic mutations 139

5.4 – Results: effects of knocking down *Atp11b* in ECs 143

5.4.1 – Knocking down Atp11b *143*

5.4.2 – Effects of knocking down Atp11b on ECs *146*

5.4.3 – Effects on OPCs *149*

5.5 – Discussion 154

5.5.1 – Analysis of genome sequence of DM rat *154*

5.5.2 – Knockdown of Atp11b *155*
5.5.3 – Function of ATP11B *157*
5.5.4 – Atp11b and endothelial dysfunction *159*

Chapter 6: General Discussion **162**

6.1 – Mechanism of development of SVD 162
6.1.1 – Summary of results *162*
6.1.2 – Possible mechanisms of action *164*
6.2 – Relevance of rat model findings to human disease 166
6.2.1 – SVD risk factors associated with endothelial dysfunction *167*
6.2.2 – Markers of endothelial dysfunction in humans with SVD *168*
6.2.3 – Endothelial dysfunction in Mendelian forms of SVD *170*
6.2.4 – Genetic polymorphisms linked to SVD and endothelial dysfunction *171*
6.2.5 – GWAS and endothelial dysfunction *172*
6.3 – Clinical relevance of findings 174
6.3.1 – Treatments tested to help SVD *175*
6.3.2 – Clinical trials involving antihypertensive therapy *176*
6.3.3 – Other therapies to improve endothelial function *177*
6.4 – Future directions 178
6.4.1 – Effects of secreted factors downstream of endothelial dysfunction *178*
6.4.2 – Upstream causes of endothelial dysfunction *179*
6.4.3 – In vivo experiments *183*
6.5 – Concluding remarks 185

List of abbreviations 186

References 193

Chapter 1: Introduction

Cerebral small vessel disease (SVD) is a disease of the small perforating arterioles in the central nervous system (CNS), which has an important impact on society as it is common, under-recognised, causes cognitive impairment, dementia and motor problems, increases the risk of large vessel stroke and worsens the symptoms of Alzheimer's disease (AD) (section 1.1). There are currently no known treatment options for this disease (Bath and Wardlaw, 2015). Single gene genetic forms of SVD occur, at early ages, and this supports SVD as a disease rather than being pathology associated with normal ageing (section 1.6). Its diagnosis relies in life on clinical presentation of lacunar stroke and/or magnetic resonance imaging (MRI), and post-mortem on characteristic pathological changes (sections 1.2 and 1.3). The risk of having sporadic SVD is increased by the usual vascular risk factors such as hypertension, diabetes and smoking, but a causal association has never been proven (section 1.7). Some evidence points to disruption of the blood brain barrier (BBB) as the cause of SVD, but the mechanism of this has not been shown. In this thesis, I will provide evidence that the endothelial cells (ECs) of the BBB are critical in the pathology of this disease. First, I will describe the clinical syndrome, imaging diagnostic changes and pathological changes associated with SVD. I will then describe the BBB and the current evidence that BBB disruption leads to SVD.

1.1 – Importance of SVD

1.1.1 - Symptoms of SVD

In the early stages, SVD is characterised by mild cognitive impairment, abnormal gait and balance, and depression (Baezner et al., 2008; Herrmann et al., 2007; de Laat et al., 2011; Prins et al., 2005; Smallwood et al., 2012). Affected functions can vary depending on where in the brain lesions occur, meaning that the severity of symptoms can vary. As well as symptomatic SVD, there are many people who have asymptomatic SVD, where they have imaging correlates and underlying pathology without showing any obvious symptoms (Vermeer et al., 2007). However, SVD still poses a huge burden to these people due to the other consequences of the disease.

1.1.2 - Consequences of SVD

As well as symptomatic changes, SVD significantly increases an individual's risk of suffering a stroke or dementia. SVD accounts for 25% of all ischemic strokes (Bamford et al., 1991), and people with SVD have double the risk of suffering a stroke (Debette and Markus, 2010). SVD is the leading cause of vascular dementia (Esiri et al., 1997; Smallwood et al., 2012; Verdelho et al., 2010), and individuals with SVD are three times as likely to develop vascular dementia (Debette and Markus, 2010). Thus, even in asymptomatic cases, SVD poses a huge risk for future neurological damage.

1.1.3 - Prevalence of SVD

SVD is a more prevalent disease than many people realise. As it primarily affects older people, looking at the overall prevalence of the disease can be uninformative. This is further compounded by the fact that many people with SVD are asymptomatic, so are not diagnosed with the disease (Vermeer et al., 2007). While this may not seem like a problem, these people still have the underlying pathology contributing to cognitive impairments which are frequently undiagnosed, and an increased risk of suffering a stroke or developing dementia. The extent of these cases of silent SVD can be seen by studies which have undertaken MRI of the general population and looked for radiological signs of SVD (detailed in section 1.3). Taken together, these studies show that approximately thirty percent of people over the age of eighty in the general population have some signs of SVD, even though they may be undiagnosed and asymptomatic (**Figure 1.1**) (Morris et al., 2009; Vermeer et al., 2007). Given that the leading cause of dementia, Alzheimer's disease (AD), only has a prevalence of sixteen percent in a similar age group (Alzheimer's Society, 2012), the potential burden of SVD for society is huge. Studies have shown that many AD patients also show signs of vascular dementia, suggesting an underlying SVD (Gorelick et al., 2011; Smallwood et al., 2012), and the outlook for these patients with dual pathology is worse (Smallwood et al., 2012). All this evidence demonstrates that the prevalence of

SVD is much higher than most people realise, and the potential problem which it poses to society is huge.

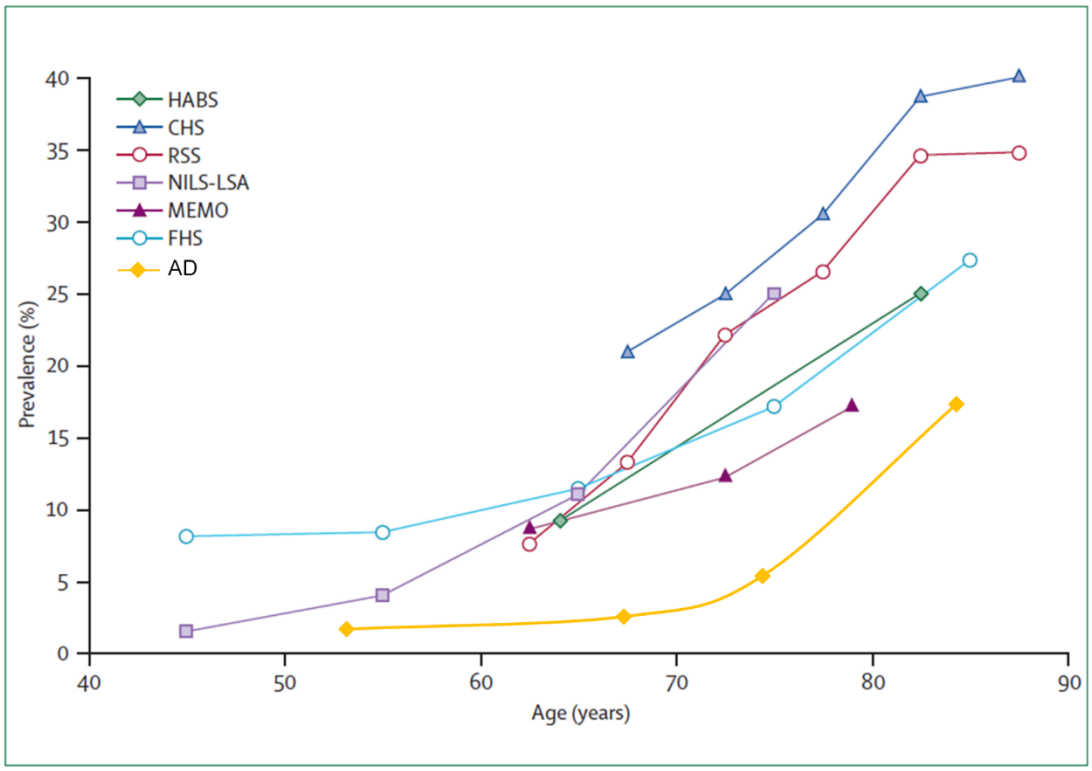


Figure 1.1: Graph showing increasing prevalence with age of silent small vessel disease (SVD) in the general population (adapted from Vermeer et al., 2007). The top six lines on this graph show the percentage of people in six population-based imaging studies who had silent brain infarcts on magnetic resonance imaging (MRI). This not only shows that SVD is highly prevalent in the general population amongst people without symptoms, but also that this prevalence increases with age to the point where between 25% and 40% of people over the age of 80 have silent brain infarcts. As a comparison, the bottom, yellow line shows the prevalence of Alzheimer's disease across similar age groups (data from Alzheimer's Society, 2012). This shows that silent SVD is far more prevalent than Alzheimer's disease, which reaches a maximum prevalence of 16% in those over 80. HABS: Helsinki Aging Brain Study, CHS: Cardiovascular Health Study, RSS: Rotterdam Scan Study, NILS-LSA: National Institute for Longevity Sciences-Longitudinal Study of Aging, MEMO: Memory and Morbidity in Augsburg Elderly study, FHS: Framingham Heart Study, AD: Alzheimer's Disease.

1.2 – Pathology of SVD

SVD has a range of pathological hallmarks in the brain, and to date many of these are poorly defined, with a lack of consensus as to what should actually be classed as SVD (Bailey et al., 2012). There are, however, a number of features which are universally considered as signs of SVD, which I will describe here. The term SVD originally derives from its implication as the cause of lacunes and lacunar stroke, and to begin describing the pathology of SVD we must first address the concept of a lacunar stroke.

1.2.1 - Lacunar lesions

A lacunar stroke is a clinical syndrome associated with a small subcortical infarct or haemorrhage. When this is due to a subcortical infarct, it is referred to as a lacunar ischemic stroke and is usually due to damage to small, deep penetrating arteries/arterioles (Bamford et al., 1991). It predominantly affects subcortical white matter and deep grey matter in the frontal lobe, basal ganglia, thalamus and brainstem (Kalaria and Erkinjuntti, 2006). Lacunar ischemic strokes account for 25% of all ischemic strokes (Bamford et al., 1991), however while most ischemic strokes affect the large arteries in the brain, causing potentially widespread damage to the areas to which these arteries provide a blood supply, lacunar strokes affect the deep penetrating arterioles causing a more localised, smaller area of damage (Fisher, 1969). The small size of lacunar infarcts (<2cm) (Lammie, 2000) means that the symptoms are often less severe, to the point where it is fairly common for someone to suffer a lacunar infarct without showing any symptoms at all (Vermeer et al., 2007). However, when a lacunar infarct occurs in a region of dense connectivity, the effects can be severe (Bailey et al., 2012; Valdés Hernández et al., 2015).

Separate from lacunar infarcts are lacunes. While these two terms are often used interchangeably in the literature, they in fact refer to different things (Potter et al., 2011). While a lacunar infarct is the original area of damage which may cause the clinical signs of lacunar stroke, a lacune is a fluid filled cavity which can be formed as a lacunar infarct cavitates (Wardlaw, 2008). The fact that lacunar infarcts tend not to be immediately fatal (Bamford et al., 1987) means that recent lacunar infarcts are

rarely found on histopathological sections from post-mortem tissue, as they have usually formed lacunes by that point. Thus, when describing the pathology of SVD based on studies of post-mortem tissue the bulk of the literature refers to lacunes. Despite their small size, the severity of lacunes, with a total loss of tissue, means that they can easily be seen on histopathological sections of brain tissue (**Figure 1.2 A**).

Another pathological feature of SVD is white matter lesions (WMLs), which are areas where there is a partial loss of myelin and neurons, but which have not fully cavitated (**Figure 1.2 B**) (Gouw et al., 2011; Schmidt et al., 2011). These are believed to be the alternative fate of lacunar infarcts – those that do not cavitate to form lacunes remain as WMLs (Moreau et al., 2012; Potter et al., 2010). Collectively, lacunar infarcts (where visible), lacunes and WMLs are often referred to as lacunar lesions on histopathology, though there is still no consensus on terminology in the literature.

1.2.2 - Vascular pathology

Studies to determine the cause of lacunes underpin the definition of SVD, and the vascular changes associated with lacunes were first described by C Miller Fisher (Fisher, 1969). These vascular changes are arteriosclerosis, in vessels between 200μm and 800μm in diameter, and, more commonly, lipohyalinosis, in vessels smaller than 200μm in diameter (Fisher, 1969). These vascular changes were originally thought to cause either occlusion, a complete loss of blood flow to an area, or hypoperfusion, a reduction of blood flow to a brain region. However, more recently it has been shown that the majority of lacunar lesions do not actually show any sign of vascular occlusion (Bailey et al., 2012).

Arteriosclerosis is a thickening and stiffening of the blood vessel walls, most commonly caused by atherosclerosis. Atherosclerosis is where plaques, formed of cholesterol, fats, cells and cellular waste products, build up on and within the luminal walls of arteries, narrowing the lumen (**Figure 1.2 C**). While the severity of arteriosclerosis is associated with the number of lacunar lesions (Dozono et al., 1991), it is also a common feature in, and is a leading cause of, large vessel stroke, and so is not unique to SVD.

Lipohyalinosis is the asymmetric thickening of the blood vessel wall with deposits of hyaline material (**Figure 1.2 D**). In its early stages, lipohyalinosis can also include fibrinoid necrosis, so-called due to the deposition of fibrin in the vessel walls and necrosis of vascular tissue (Lammie, 2002). Lipohyalinosis can cause vascular occlusion and also lead to leakage of the blood vessels (Lammie, 2002). This is thought to explain another of the histopathological features observed in SVD, cerebral microbleeds, where small amounts of blood leak out of a damaged blood vessel (Lammie, 2002).

1.2.3 - Other pathology

As well as changes to the vessels themselves, another vascular feature associated with SVD is the build-up of foamy macrophages, indicative of macrophages which have phagocytosed fatty material, both surrounding the vessels and in the walls of the vasculature. Hemosiderin-laden macrophages are also found in some lacunar lesions (Lammie, 2002). Macrophages are cells of the innate immune system which respond to both pathogenic invasion and tissue damage. They are able to phagocytose pathogens and tissue debris, as well as secrete factors thought to enhance tissue repair (Kotter et al., 2005). The fact that the macrophages are enlarged and filled with hemosiderin is thought to be a sign that they are actively phagocytosing (Batchelor et al., 1999).

1.2.4 - Diseases with similar pathology to SVD

The pathological definitions of SVD are sometimes confused with other neurovascular diseases, such as large vessel stroke and cerebral vasculitis. It is important to clarify these distinctions, as the aetiology of these diseases is likely to be very different. As detailed above (section 1.2.1), large vessel stroke differs from SVD in the size of the vessels involved, how far up the vascular tree these vessels are, and the size of the parenchymal lesion. It also differs in its vascular pathology – while arterial occlusion in the form of atherosclerosis or embolism is a common feature of large vessel stroke, there is no vascular remodelling in the form of lipohyalinosis. Vasculitis (also known

as angiitis) involves an infiltration of immune cells into the walls of small vessels, causing necrosis of the vessels (reviewed in Rehman, 2000). This immune cell build-up can occlude the blood vessel and cause stroke-like symptoms. While this may appear similar to SVD clinically, the pathology is in fact very different. The immune infiltrate in vasculitis is composed of macrophages, lymphocytes and leukocytes, and it is believed that overactivity of the immune system drives the disease. In SVD, the immune infiltrate, where present, consists exclusively of macrophages. Similarly, while fibrinoid necrosis is sometimes seen in the brains of vasculitis patients, lipohyalinosis is not.

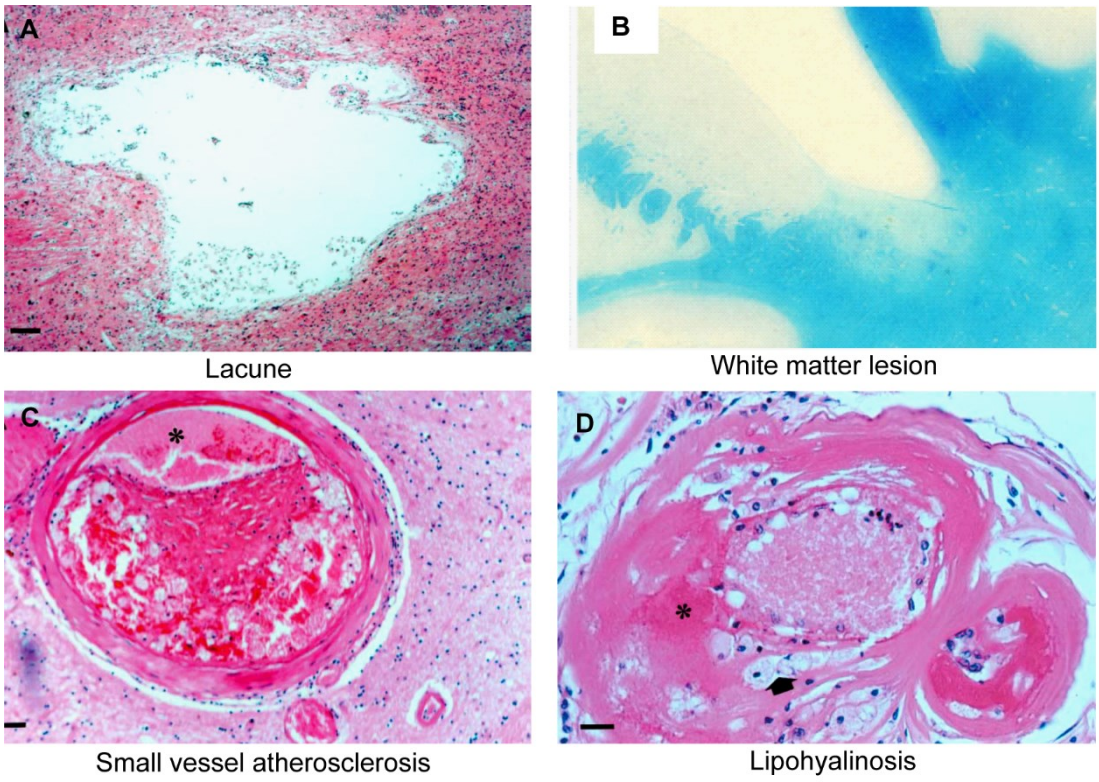


Figure 1.2: Histopathological hallmarks of small vessel disease (SVD) (adapted from Lammie, 2002; Schmidt et al., 2011). A, C, D: Images of sections of human brain tissue from people with SVD, stained with haematoxylin and eosin (H&E) (adapted from Lammie, 2002). The blue haemotoxylin stains nuclei, while the pink eosin stains other parts of the tissue with a different appearance depending on the tissue structure. B: Luxol fast blue stain around the ventricles of an individual with SVD (adapted from Schmidt et al., 2011). Darker blue areas are regions with more myelin. A: A lacune - the complete lack of any tissue in this lesion indicates a fully cavitated lacune. B: A white matter lesion - the pale blue area at the centre of this image indicates a loss of white matter, however there are still cells and tissue present, likely neurons and astrocytes, unlike in the fully cavitated lacune (A). C: An example of a small blood vessel with atherosclerosis. The atherosclerotic plaque is indicated by a star, and narrows the blood vessel. D: An example of a blood vessel with lipohyalinosis. This is seen by the glassy appearance of the thickened blood vessel wall, indicated by the star, and the fibrous, disorganised appearance of the other parts of the vessel wall.

1.3 – SVD on neuroimaging

The fact that lacunar infarcts are not usually immediately fatal (Bamford et al., 1987) means that studies of post-mortem tissue can only tell us so much about what is happening in SVD. To understand what is happening during the course of the disease, and to diagnose the disease, we must turn to imaging studies, which have been the major source of advances in understanding of epidemiology, risk factors, clinical feature associations and prognosis of SVD in the last twenty-five years. Using magnetic resonance imaging (MRI), we can achieve a clearer idea of what is happening in SVD, across a wider number of cases. Though many of the diseased vessels involved in SVD are too small to be directly observed on MRI, imaging studies can still tell us a lot about the parenchymal changes in SVD. Previously, radiological studies of SVD have suffered from many of the same problems as histopathological studies of SVD, namely a lack of consensus on definitions of certain features. Recently, however, standards for terminology and definitions of radiological features have been published, which should lead to a greater similarity between different researchers' definitions (Wardlaw et al., 2013a). This paper classes the many different terms used to describe radiological features of SVD into six types: recent small subcortical infarct, lacune of presumed vascular origin, white matter hyperintensity (WMH) of presumed vascular origin, perivascular space, cerebral microbleed and brain atrophy.

1.3.1 - Recent small subcortical infarct

Small subcortical infarcts are what are referred to as lacunar infarcts in histopathological sections. As described in section 1.2.1, they are small areas of tissue damage in subcortical white matter, in the territory of small, perforating arteries. The term lacunar infarct is discouraged in imaging studies as it is unclear what percentage of subcortical infarcts actually cavitate to form lacunes (Moreau et al., 2012; Potter et al., 2010). These infarcts are thought to be the immediate effect of vascular damage in SVD, as opposed to the longer term changes which cause lacunes and WMLs. On imaging they are identified as hyperintense areas on diffusion weighted imaging (DWI), which measures the movement of water molecules, smaller than 20mm in diameter (**Figure 1.3 A**) (Wardlaw et al., 2013a).

1.3.2 - Lacune of presumed vascular origin

As described in section 1.2.1, lacunes are fluid filled cavities, thought to derive from the cavitation of small subcortical infarcts. While in histopathological sections the distinction between the lacunes and recent small subcortical infarcts is unclear, as histopathological studies look at late stage pathology, on imaging the two can be clearly distinguished. Lacunes are seen as hypointense regions on fluid-attenuated inversion recovery (FLAIR), which removes the signal from fluids, between 3mm and 15mm (**Figure 1.3 B**) (Wardlaw et al., 2013a).

1.3.3 - White matter hyperintensity of presumed vascular origin

WMH are imaging correlates of WMLs seen on histopathological sections, which are strongly associated with SVD (Swieten et al., 1991). As described in section 1.2.1, these are areas of white matter loss and myelin damage believed to be the alternative outcome of small subcortical infarcts (Moreau et al., 2012; Potter et al., 2010). Though WMH are also associated with ageing, they have been shown to correlate strongly with many of the clinical symptoms of SVD, including disrupted gait and cognitive impairment (Baezner et al., 2008; Debette and Markus, 2010). They provide an interesting marker of SVD, as while many signs of the disease worsen over time, WMH can occasionally get smaller (Wardlaw et al., 2015). This suggests that one of the aspects of SVD which is correlated with symptoms is potentially reversible, which is promising when considering therapeutic options. WMH are visible as hyperintense regions on FLAIR and T2-weighted MRI (**Figure 1.3 C**) (Wardlaw et al., 2013a).

1.3.4 - Perivascular space

The perivascular space (PVS), also known as Virchow-Robin space, is the region around a blood vessel, between the vessel wall and astrocyte endfeet (see section 1.4.2). These spaces are normally invisible on MRI due to their small size, but can be visualised when they become enlarged, a feature seen with normal ageing (Groeschel

et al., 2006) and also associated with inflammation. Recent studies have shown that enlarged PVS on MRI are correlated with lacunar stroke, WMH and reduced cognition (Doubal et al., 2010; MacLullich, 2004). Histopathological correlation of these changes has been difficult, as the dehydration of tissue samples necessary to fix them can cause tissue shrinkage, especially around the blood vessels, leading to them being dismissed as artefacts for many years. This means that though enlarged PVS are histopathologically observed close to lacunar lesions, these have not yet been studied sufficiently to show an association greater than that seen with normal ageing (Bailey et al., 2012). PVS are observed on T2-weighted MRI as hyperintense regions which are linear (when imaged parallel to the course of the vessel) or ovoid of a diameter less than 3mm (**Figure 1.3 D**) (Wardlaw et al., 2013a).

1.3.5 - Cerebral microbleed

As the name suggests, cerebral microbleeds are small areas of blood leakage from the vasculature into the parenchyma. Though their cause is poorly understood, they are a common feature of SVD and there is some evidence to suggest that they are associated with cognitive impairment (Cordonnier et al., 2007; Patel et al., 2013; Vernooij et al., 2008). They are seen as signal voids on T2*-weighted MRI, less than 10mm in diameter (Wardlaw et al., 2013a).

1.3.6 - Brain atrophy

Brain atrophy is not a feature unique to SVD, and can be seen in many other neurological diseases. Though this means that it is not part of a diagnosis of SVD, descriptions of brain atrophy are important to understand the pathophysiology of SVD. Brain atrophy has been shown to be a sign of neuronal loss in the brain, and is thought to be one of the key correlates to cognitive decline with SVD (Carmichael, 2010; Mungas et al., 2001). It is seen as a shrinkage of the brain, which can be general or localised to a specific region (Wardlaw et al., 2013a).

1.3.7 - Breakdown of the blood brain barrier (BBB)

The BBB is the structure which limits the entry of cells and solutes into the brain (see section 1.4). Though it is not classed as a defining feature of SVD, a loss of BBB integrity, as measured by the leakage of intravenously administered gadolinium tracer (**Figure 1.3 E**), has recently been shown in several studies to be associated with SVD (Wardlaw et al., 2013b). While some histopathological studies investigating leakage of fibrinogen from blood vessels have not shown a strong association with SVD (Bridges et al., 2014), evidence from relevant experimental models, other histopathological studies and imaging studies (Farrall and Wardlaw, 2009) led to the suggestion over ten years ago that BBB impairment may have a major precipitating role in the pathogenesis of SVD (Wardlaw et al., 2003).

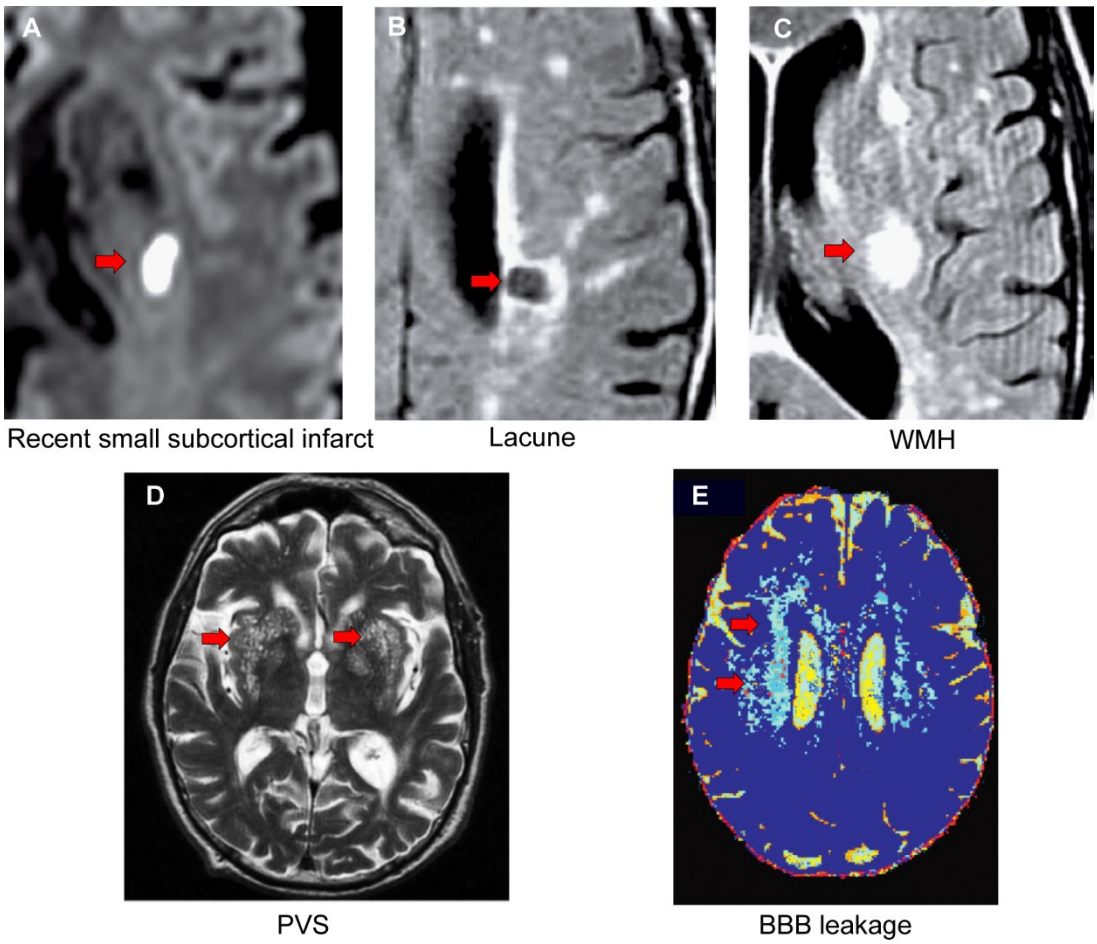


Figure 1.3: Radiological features of small vessel disease (SVD) on magnetic resonance imaging (MRI). A: Diffusion weighted imaging (DWI) scan showing a recent small subcortical infarct (bright white (hyperintense) region indicated by arrow) (adapted from Wardlaw et al., 2013a). B: Fluid-attenuated inversion recovery (FLAIR) scan showing a lacune (dark (hypointense) region surrounded by a hyperintense halo, indicated by arrow) (adapted from Wardlaw et al., 2013a). C: FLAIR scan showing a white matter hyperintensity (WMH; indicated by arrow) (adapted from Wardlaw et al., 2013a). D: T2-weighted MRI showing enlarged perivascular spaces (PVS; punctate hyperintensities indicated by arrows) (adapted from Doubal et al., 2010). E: Colour mapping of cerebrovascular permeability after intravenous administration of a gadolinium tracer. Dark blue indicates areas of low vascular permeability, while light blue, yellow and red indicate increasing permeability. The light blue regions indicated by arrows show areas where the gadolinium tracer is leaking out of the blood vessels due to an impaired blood brain barrier (BBB) (adapted from Wardlaw et al., 2013b).

1.4 – The blood brain barrier

As described in section 1.3.7 above, one of the key recent findings in the pathophysiology of SVD is the presence of BBB leakage. My thesis will develop this idea further. To understand how BBB disturbance may contribute to other aspects of the disease, we must first understand exactly what the BBB is.

1.4.1 - Function of the BBB

The BBB was first described by Ehrlich (Ehrlich, 1885), and the term is attributed to Lewandowski (Lewandowski, 1900), as a structure which stops coloured dyes injected into the blood from entering the brain, even though these same dyes were able to enter other organs. These experiments neatly demonstrate the primary function of the BBB – to control the entrance of cells and blood products into the brain.

Throughout most of the body, blood vessels are very permeable. This allows easy perfusion of tissues with required nutrients and solutes, and access for the various cells of the immune system (Hawkins and Davis, 2005; Wolburg and Lippoldt, 2002). This permeability, however, also allows for the easy entrance of pathogens into the organs. While in most tissues any cellular damage can be quickly repaired after a pathogen is subdued by the immune system, this process is limited in the central nervous system (CNS). The CNS has a very limited capacity to repair – neurons are not capable of dividing and the pool of adult neural stem cells is limited (Hallbergson et al., 2003; y Cajal, 1928). It is thought that this provides an evolutionary advantage by ensuring the stability of key neural networks. However, it also limits the brain's ability to repair after damage. Thus, structures are required to limit that damage, and the BBB exists to control the interstitial milieu within tight limits to allow electrically active cells like neurons to function, and to limit the damage from pathogens and toxins. The BBB also prevents fluctuations in ionic concentrations after meals from affecting the brain, and allows similar signalling molecules to be used in the brain and blood without interference (Abbott et al., 2006; Cserr and Bundgaard, 1984).

While the BBB plays a passive role in keeping these harmful substances out of the brain, it also plays an active role in allowing nutrients or cells which are needed into

the brain (reviewed in Abbott et al., 2006). The flow of nutrients is mediated by transport proteins on the luminal surface of endothelial cells (ECs) which can actively transport solutes across the barrier, such as the GLUT-1 transporter for glucose (Simpson, 2001). The movement of leukocytes across the barrier, when required, is mediated by the upregulation of receptors to which they can bind, such as intercellular adhesion molecule 1 (ICAM-1) (reviewed in Muller, 2011). Upon binding, leukocytes are then transported across the BBB either between endothelial cells (paracytosis) or through them (transcytosis) (Feng et al., 1998).

1.4.2 - Composition of the BBB

The cerebral blood vessels and surrounding cells are collectively known as the neurovascular unit (**Figure 1.4**). This is comprised of the ECs which form the blood vessel walls, pericytes directly apposing them, astrocytes, whose endfeet form the glia limitans, the outer barrier of the perivascular space, and macrophages in the perivascular space. Larger vessels in the brain also contain smooth muscle cells, however the focus of this project is the small vessels. Each of these cells has a structural and functional role to play, contributing to the barrier function of the BBB.

ECs are the cells which form all blood vessels in the body. They have an elongated shape, and curve to form the vessel wall, with the number of ECs in a vascular cross section determining the diameter of the vessel. The cells are highly polarised, expressing a different protein composition on their luminal and parenchymal surfaces (Dermietzel et al., 2006; McAllister et al., 2001). Throughout the body, ECs are joined to each other by adherens junctions. These loosely join the ECs together, with pores to allow nutrients and cells in the blood to pass between ECs. The spacing of these junctional proteins determines the permeability of the vessel – a vessel with more adherens junction proteins between its ECs will be less permeable. There is a limit to how impermeable these junctions can make ECs, and so in tissues where greater stability is needed another form of cell-cell junction exists – the tight junction (TJ).

TJs are so called due to their ability to hold cells together very tightly. They are found between ECs in the brain, lungs and kidneys, and also between epithelial cells in

various tissues of the digestive system (Wolburg and Lippoldt, 2002). TJs are formed by homodimers of tight junction proteins (TJPs) on two adjacent EC membranes. In the brain there are three main families of TJPs: occludins, claudins and junctional adhesion molecules (JAMs) (Furuse et al., 1993, 1998; Martìn-Padura et al., 1998). Recently, lipolysis-stimulated lipoprotein receptor (LSR; also known as angulin-1) has also been added to this list as a TJP which forms a homotrimer at the point where three ECs make contact, and is enriched in brain ECs compared to other ECs in the body, but little else is currently known about this protein (Sohet et al., 2015). These are all transmembrane proteins, with a strong affinity for themselves. The different TJPs bond with different strengths, and so tighten the vasculature to different degrees. Thus, a change in the composition and density of the TJs can greatly affect the permeability of a blood vessel, and this composition varies greatly between different organs.

When considering TJs in the BBB, the least permeable vasculature in the body, we expect to see the strongest TJPs. One TJP in particular, claudin-5, is much more highly expressed in brain ECs than in other ECs in the body, though it is also found in the lungs and kidneys (Morita et al., 1999). Claudin-5 is thought to be the tightest of the TJPs, responsible for limiting the pore size of the BBB to <800 Daltons (Nitta et al., 2003). It has been shown that a loss of claudin-5 alone in transgenic mice null for claudin-5, with normal expression of other TJPs, leads to severe leakage of small molecules through the BBB (Nitta et al., 2003). Thus, when investigating changes to the BBB, a loss of claudin-5 alone is taken as indicative of damage.

As well as the TJPs described above, there are also the intracellular proteins involved in TJ complexes. These are the zonula occludens proteins: ZO-1, ZO-2, and ZO-3. ZO-1, forming a dimer with either ZO-2 or ZO-3, binds to both the TJPs and the actin cytoskeleton, anchoring the TJP to the cytoskeleton, and the formation of this ZO complex is thought to be a crucial step in the development of TJs (Tsukita et al., 2009). As a consequence, ZO-1 expression at the cell membrane is a sign that there is at least some normal TJP expression.

While TJs form the tightest part of the BBB and prevent the entrance of solutes into the brain parenchyma, cells can cross the EC barrier by active processes, described in 1.4.1. While these processes are designed to allow benign cells into the brain, they can

also be exploited by pathogens. There is therefore a second line of defence – the glia limitans, formed by the astrocyte endfeet. These astrocyte endfeet are bound by gap junctions (Nedergaard et al., 2003). While these do not hold cells as tightly together as TJs, they nevertheless create a barrier too small for a cell to passively cross. In times of acute need, or in pathological situations, there are methods by which this barrier can be broken, including a destruction of the glia limitans by macrophages (Bechmann et al., 2007).

The proximity of the astrocyte endfeet to the blood vessels does not just play a barrier function. It also allows astrocytes to play a metabolic role. Astrocytes both metabolically support neurons, and use a lot of energy themselves when clearing up neurotransmitters (reviewed in Nedergaard et al., 2003). It is therefore advantageous for them to have a process close to blood vessels, the source of nutrients.

In between the glia limitans and the ECs is the perivascular space, containing two cell types which are also important for the function of the BBB. The first of these are macrophages, phagocytic cells which respond to injury or damage by consuming pathogens and debris. From their location in the PVS they can both defend against any pathogens which manage to cross the EC barrier, and easily access the brain parenchyma, by secreting matrix metalloproteases (MMPs) to break down the glia limitans (Bechmann et al., 2007).

The other cell type in the PVS is the pericyte. This directly apposes the ECs and is a contractile cell, from the same lineage as smooth muscle cells present around larger vessels (Korn et al., 2002). It provides support to the ECs and is vital for the formation and maintenance of the BBB, as mice without pericytes are unable to form a BBB, though the mechanism for this is unclear (Daneman et al., 2010; Ramsauer et al., 2002).

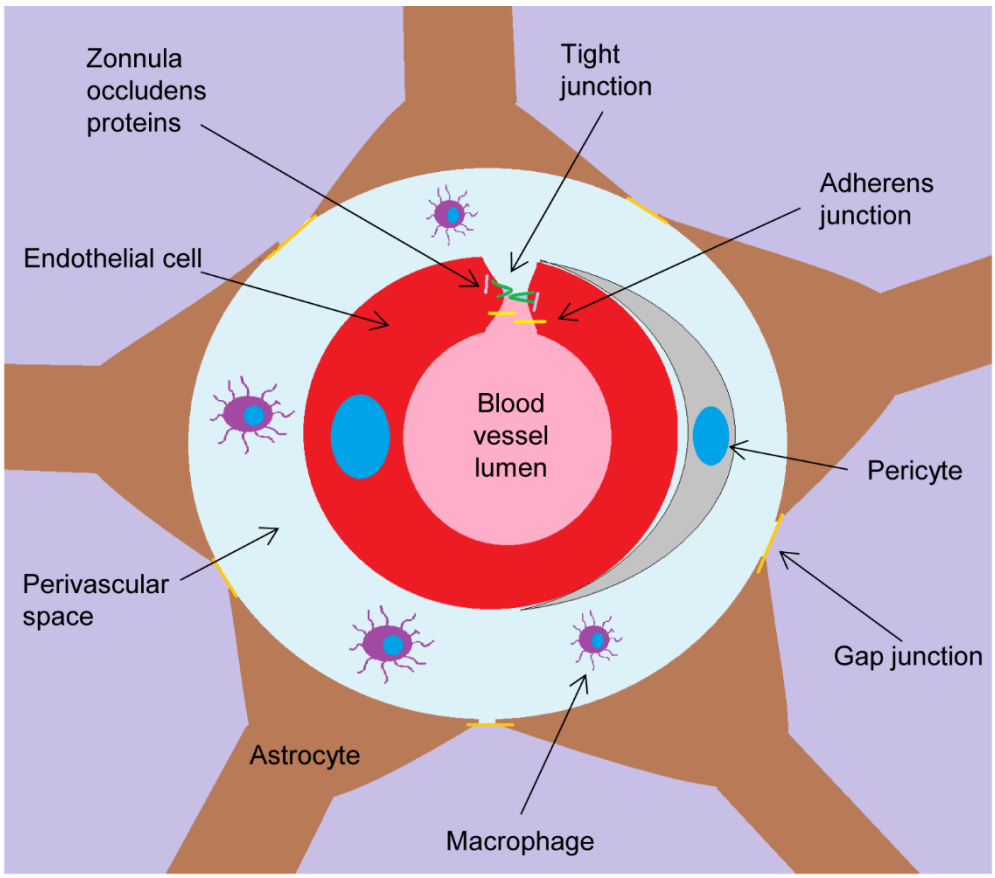


Figure 1.4: Diagram showing the components of the blood brain barrier (BBB). The BBB has many component cell types, together forming the neurovascular unit. This diagram represents a cross section through a cerebral blood vessel, showing these cells. The blood vessel is formed from endothelial cells (red), joined to each other by adherens junctions (yellow), which hold the cells loosely together, and tight junctions (green), which hold the cells together tightly and prevent molecules larger than 800 Daltons passing out of the blood vessel. The tight junction proteins are anchored to the cytoskeleton by zonnula occludens proteins (lilac). Immediately apposing the endothelial cells are pericytes (grey), contractile cells which support the endothelial cell and are neccesary for the maintenance of the BBB. At the edge of the neurovascular unit are astrocyte endfeet (brown), joined to each other by gap junctions (orange), forming the glia limitans. These provide a more porous barrier against any invading cells which get past the endothelial cells into the perivascular space. The perivascular space (light blue) is the fluid filled space between the glia limitans and the endothelial cells. It contains macrophages (purple) which consume any pathogenic cells which get past the endothelial cells into the perivascular space.

1.4.3 - The BBB in SVD

As described in section 1.3.7, BBB leakage appears to be associated with SVD, and has even been implicated as having a causative role. There are many ways by which this could happen. As detailed in section 1.4.1, the primary function of the BBB is to keep toxins and pathogens out of the brain. If these get into the brain through a damaged BBB, it is clear that this is likely to cause damage to cells inside the parenchyma. However, even without the invasion of pathogens or toxins into the brain, a leaky BBB could cause damage. Were a damaged BBB to allow more leukocytes through, this could be equally disastrous. Due to the low exposure of leukocytes to cells in the brain (Muldoon et al., 2013), there is an increased risk that the immune system may aberrantly class these cells as foreign bodies. Some neurological diseases, such as multiple sclerosis, are characterised by autoimmune damage of glia (Chastain and Miller, 2012). Damage to cells in the brain could also be caused simply by a change in the ionic composition of the cerebrospinal fluid (CSF), as this is very different to that of the blood (Abbott et al., 2006; Cserr and Bundgaard, 1984).

1.4.4 - The BBB in other diseases

Though leakage of cells and solutes through a damaged BBB is likely to cause damage, this does not necessarily mean that this is what is driving the damage in SVD. A number of other neurological diseases, such as epilepsy, brain tumours and head trauma, have been shown to also include a leakage of the BBB (reviewed in Abbott et al., 2006). However, in many of these cases the timing of the leakage suggests that it occurs after the onset of disease pathology, not as a precursor. It is believed that this may be part of an attempted inflammatory response to limit damage by the body. Thus, BBB leakage in SVD could be happening as a downstream effect of an upstream pathology, not acting as the root cause.

1.5 – Myelin

As detailed in sections 1.2.1 and 1.3.3, one of the key changes which occur in SVD, visible in both histopathological sections of brains and on MRI, is the occurrence of

WMLs. These are believed to be responsible for many of the symptomatic changes, and may even lead to the brain atrophy which contributes to dementia (Kloppenborg et al., 2012). To study these WMLs effectively, we must first develop a clearer understanding of the composition and function of white matter.

1.5.1 - Function of myelin

White matter, so called because it appears white due to its high fat content on unlabelled histopathological sections of brain, describes areas of nerves which are myelinated. The primary purpose of myelin sheaths is thought to be to allow faster transmission of electrical signals. Signals are transmitted along axons by the propagation of an electrical signal along their length. This is mediated by the opening of voltage gated sodium channels – as the electrical signal reaches a point in the axon, the voltage change triggers the opening of these channels allowing sodium to flood into the axon, further depolarising it and allowing the signal to travel further. In an unmyelinated axon these voltage gated sodium channels are distributed evenly along the length of an axon (Catterall, 2012; Vandenberg and Waxman, 2012). In myelinated axons, however, these sodium channels are clustered at Nodes of Ranvier, with the myelin sheaths, also known as internodes, covering the length of the axon in-between (Ritchie and Rogart, 1977; Waxman and Ritchie, 1985). This allows for a process known as saltatory conduction, whereby the electrical signal can jump between nodes (Huxley and Stampfli, 1949; Tasaki, 1939). As these signals propagate with the influx of sodium ions at fewer points, this allows for faster conduction of the signal.

The composition of myelin sheaths allows for this function of increasing the conduction velocity of axons. They are formed of multiple layers of compacted cell membrane wrapped around the axon (Geren and Schmitt, 1954). These layers increase the effective resistance of the axon membrane, preventing the leakage of current and so allowing the signal to travel further along the axon without becoming too weak to trigger the opening of the voltage gated sodium channels at the next node of Ranvier. Myelin sheaths are largely composed of a number of different lipid molecules, most notably cholesterol, which give myelin its white appearance in histopathological sections (Saher et al., 2005). As well as these lipids, there are a number of different

membrane associated proteins which contribute to the formation of myelin sheaths. The two most abundant proteins are proteolipid protein (PLP) and myelin basic protein (MBP), together making up 60-80% of the protein composition of myelin. PLP, a structural myelin protein with four transmembrane domains, is the major constituent of myelin in the CNS. While mice which have a deletion in the *Plp* gene appear to have normal myelin, they exhibit late stage axonal death, suggesting that PLP may be important for myelin interaction with axons (Griffiths, 1998). MBP is the second most abundant protein component of myelin, composing approximately thirty percent of total myelin proteins (Boggs, 2006). It binds to negatively charged phospholipids on the inner leaflet of the plasma membrane, allowing two adjacent lipid bilayers in compacted myelin to stably interact. Rodents with a mutated or deleted *Mbp* gene have major problems in forming compact myelin (Carré et al., 2002; Readhead et al., 1990). The other major protein components of myelin sheaths are myelin associated glycoprotein (MAG), thought to play a role in axon-glial interaction, and myelin/oligodendrocyte glycoprotein (MOG), thought to stabilise compact myelin (Johns and Bernard, 1999; Li et al., 1998).

As well as allowing for faster conduction velocities, myelin also plays a role in neuronal survival by providing both trophic and metabolic support to the axon. Numerous trophic factors secreted by oligodendrocytes have been shown to increase neuronal survival *in vitro* and *in vivo*, including insulin-like growth factor 1 (IGF-1) and brain derived neurotrophic factor (BDNF) (Linker et al., 2010; Wilkins et al., 2001). In addition to secreting trophic factors which promote axonal survival, oligodendrocytes also provide metabolic support to the axons. As well as compacted membranes, myelin sheaths have a cytoplasmic channel running through all the layers which comes to rest close to the axonal surface. Through these channels and lactate transporters, oligodendrocytes provide the axons with lactate, a precursor to pyruvate from which energy can be derived (Lee et al., 2012). It has been shown that knocking out monocarboxylate transporter 1 (MCT1), a lactate transporter highly expressed in oligodendrocytes, in mouse oligodendrocytes, leads to an axonopathy without any change in myelination (Lee et al., 2012). This demonstrates the key role myelin has to play in axonal survival.

1.5.2 - Oligodendrocytes

The cells which form the myelin sheath in the CNS are oligodendrocytes. Unlike myelination by Schwann cells in the peripheral nervous system (PNS), where one cell forms one internode, oligodendrocytes can form multiple internodes on multiple axons (Baumann and Pham-Dinh, 2001). Oligodendrocytes derive from oligodendrocyte precursor cells (OPCs; also known as oligodendrocyte progenitor cells), which arise from many different regions of the brain during development and are also present throughout the adult brain (Dawson et al., 2003; Richardson et al., 2011). As OPCs differentiate into immature, pre-myelinating oligodendrocytes and then into mature, myelinating oligodendrocytes they express different markers, which allow us to study them in more detail (**Figure 1.5**). Throughout this differentiation process, cells constitutively express the transcription factor Olig2, which allows us to use this as a marker for all cells of the oligodendroglial lineage. OPCs express the proteins platelet derived growth factor receptor alpha (PDGFRα) and the proteoglycan neural/glial antigen 2 (NG2) (Baumann and Pham-Dinh, 2001). Immature oligodendrocytes, which have started branching but are not yet myelinating, express the surface protein O4, and begin to express Nogo-A (Kuhlmann et al., 2007; Sommer and Schachner, 1981). Mature oligodendrocytes can be labelled with antibodies against myelin proteins, such as MBP or PLP.

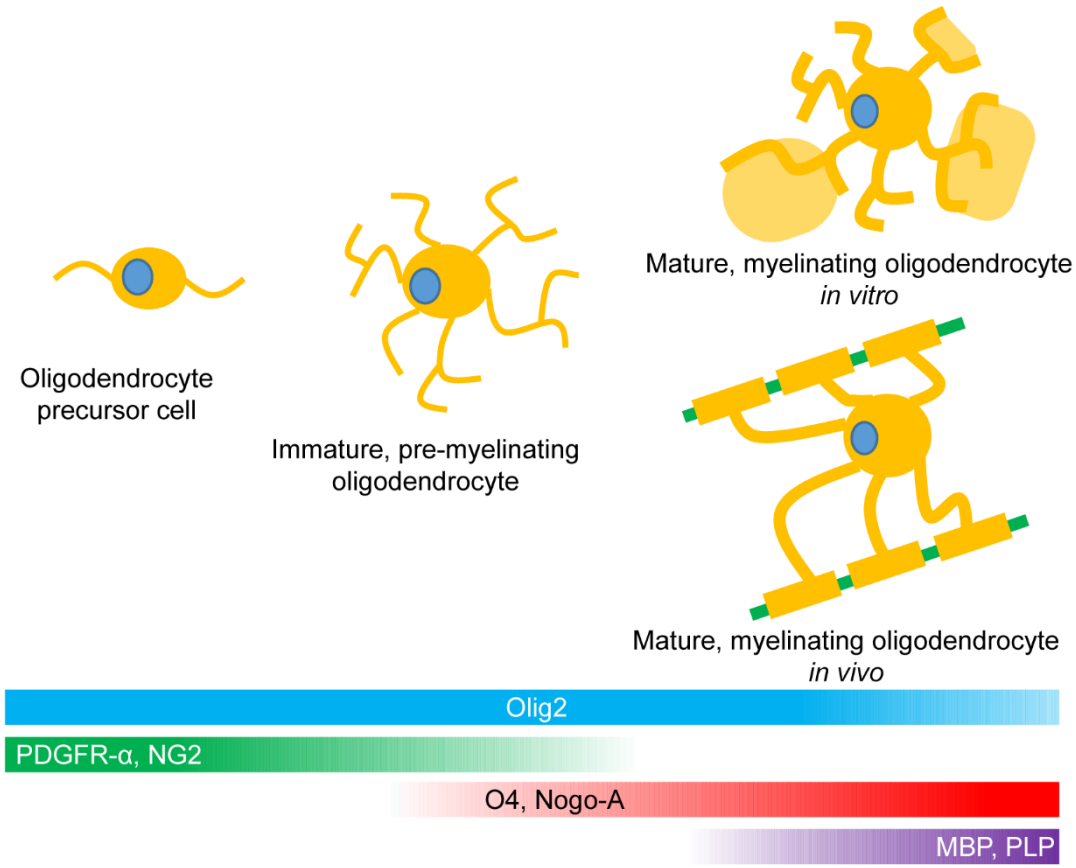


Figure 1.5: Diagram showing the changing morphology and marker expression of oligodendrocytes as they mature. The diagrams in the top part of the image depict oligodendroglia at different stages of maturation. The coloured bars along the bottom indicate the expression levels of different markers - a darker colour indicates a higher level of marker expression at that stage of maturation. As an oligodendrocyte matures from an oligodendrocyte precursor cell (OPC), it starts to form more processes. It downregulates the expression of the markers platelet derived growth factor receptor alpha (PDGFR-α) and neural/glial antigen 2 (NG2) which are at high levels in OPCs, and begins to express O4 and Nogo-A. As the oligodendrocyte matures further, it begins to myelinate. *In vitro*, in an isolated culture of oligodendrocytes without neurons, this begins with the expression of myelin basic protein (MBP), followed by more complex processes and the formation of membrane sheets. *In vivo*, this involves the formation of MBP and proteolipid protein (PLP) containing myelin sheaths, wrapped around axons. Throughout this entire oligodendroglia lineage, Olig2 is expressed.

1.5.3 - Myelin in SVD

As described in sections 1.2.1 and 1.3.3, white matter changes make up a large part of the pathologies associated with SVD. Not only are they associated with SVD, but they are also associated with cognitive decline, with a number of studies showing that increased number or severity of WMH is associated with increased cognitive decline (Debette and Markus, 2010). These data suggest that an understanding of the changes in the white matter is essential to understanding the progress of SVD and its contribution to vascular dementia.

1.5.4 - Extrapolation from other diseases of the white matter – multiple sclerosis

We may learn more about the structure and function of myelin by studying other demyelinating diseases. One of the best studied diseases of CNS myelin is multiple sclerosis (MS), which illustrates a number of the functions of myelin described above. MS is caused by an immune system mediated destruction of myelin in small localised areas centred on blood vessels (reviewed in Sriram, 2011; Wu and Alvarez, 2011), causing lesions which on MRI appear similar in some ways to WMH in SVD. In the early stages of MS (relapsing-remitting phase), the myelin debris is cleared by macrophages/microglia, OPCs proliferate and migrate into the lesion, and the axons are remyelinated as OPCs differentiate into mature myelinating oligodendrocytes. However, in later stages of the disease (secondary progressive phase) this remyelination process fails, leading to progressive loss of axons due to a lack of metabolic support from oligodendrocytes to axons. Initially myelin is lost (demyelination) but axons are intact, and patients can suffer disabilities and weaknesses of a range of severities, depending on where the lesion occurs (Noseworthy et al., 2000). This demonstrates the key role that myelin plays in increasing axonal conduction velocities – though axons remain intact, a decrease in conduction velocities can still lead to severe disability. These symptoms improve once the inflammation that causes the demyelination settles and the lesion has remyelinated. In later stages of MS, disabilities progressively become more severe and are permanent. This reflects the role of myelin in metabolically and trophically supporting axons – when myelin is lost and not regenerated, the axons progressively die.

This knowledge of the pathophysiology of MS may help to explain what is happening in SVD. Demyelination is seen in WMLs in SVD, which may lead to the death of axons in these regions and could explain why WMLs often cavitate to form lacunes, and could even explain some of the progressive brain atrophy in SVD which leads to dementia.

The work done on models of MS can also give us clues as to what other changes to look for in SVD. To repair (remyelinate) demyelinating lesions in animal models, there is first an increase in OPC number, due to both migration and proliferation, followed by OPC differentiation into mature myelinating oligodendrocytes (reviewed in Franklin and ffrench-Constant, 2008). This is relevant to determine whether there is a regenerative response in SVD, and whether some of the pathological changes are reversible.

The pathology of MS may also provide some insight into the changes in macrophages/microglia seen in SVD. In MS and its animal models increased numbers of activated macrophages/microglia are seen in demyelinated lesions, and are thought to be both clearing myelin debris and producing pro-regenerative factors to allow for effective remyelination of axons (Kotter et al., 2006; Ruckh et al., 2012). There is evidence that these macrophages/microglia migrate to the lesion site in response to a signal from damaged oligodendrocytes. In SVD, an increased number of phagocytic macrophages has been observed, both around diseased vasculature and areas of lesioned tissue (section 1.2.3) but it is not yet known whether these macrophages are carrying out similar functions.

1.6 – Mendelian forms of SVD

In the preceding parts of this chapter I have described the changes associated with sporadic SVD, however these provide little clue as to what causes the disease, though this thesis will develop the theme of BBB disruption in SVD further. It is thought that there is a significant genetic component to the sporadic disease, and estimates for the heritability of SVD range from 55% to 75% (reviewed in Haffner et al., 2015). In the vast majority of cases, the genetic component is unknown. However, for a small

proportion of people with SVD, the disease is caused by a known, inheritable genetic mutation. Studying these forms of the disease can give us an idea as to the mechanisms which might underlie sporadic SVD. The existence of these Mendelian forms of SVD also support the idea that SVD, whose pathologies and symptoms greatly overlap with those seen in normal ageing, is in fact a disease, as many of these patients develop pathology at a relatively young age. The best studied forms of Mendelian SVD are cerebral autosomal dominant arteriopathy with subcortical infarcts and leukoencephalopathy (CADASIL), cerebral autosomal recessive arteriopathy with subcortical infarcts and leukoencephalopathy (CARASIL), and COL4-related angiopathies, and I will describe these diseases in more detail here. While sufferers of other diseases, including retinal vasculopathy with cerebral leukodystrophy (RVCL), Fabry's disease and homocystinuria, also show signs of SVD (Haffner et al., 2015), these have not been as well studied, and I will not include details of these here.

1.6.1 - CADASIL

CADASIL has been described in various clinical studies since 1977 (Chabriat et al., 1995; Sourander and Walinder, 1977; Tournier-Lasserve et al., 1991), and in 1996 was shown to be caused by dominant mutations in the *NOTCH3* gene (Joutel et al., 1996). It is the most common form of Mendelian SVD, affecting as many as 5 in 100,000 people (Bianchi et al., 2014; Narayan et al., 2012). Individuals with CADASIL show many similar pathological features and symptoms to sporadic SVD, including subcortical infarcts, lacunes, white matter changes and dementia, with the key difference being a younger age of onset (Chabriat et al., 1995, 2009; Tournier-Lasserve et al., 1991). Studies in the mouse model of the disease suggest that CADASIL is caused by an accumulation of the NOTCH3 extracellular domain ($NOTCH3^{ECD}$) around blood vessels (Joutel et al., 2010). This suggests that there may be some disruption of the BBB involved, consistent with the theme of this thesis, though this has not yet been shown in the mouse model or in patients.

1.6.2 - CARASIL

CARASIL is a much rarer form of SVD, with only 50-100 cases having been reported (Fukutake, 2011). It was first described in 1976 as showing similar vascular pathology to SVD (Maeda et al., 1976). It has more recently been shown to present with other features common to SVD, including subcortical infarcts, white matter changes and cognitive defects (Fukutake, 2011; Nozaki et al., 2014; Oide et al., 2008). It has a much younger age of onset, with symptoms starting as young as 20 years of age, and most patients having dementia by the age of 50 (Fukutake, 2011). It is caused by recessive mutations in the *HTRA1* gene leading to a misregulation of transforming growth factor beta (TGF-β) signalling. Though it has not yet been shown how this may lead to the pathological changes, increased TGF-β signalling has been shown to disrupt the BBB (Shimizu et al., 2013), again consistent with the theme of this thesis, and this may yet explain the disease process.

1.6.3 - COL4-related angiopathies

Mutations in the *COL4A1* and *COL4A2* genes cause defects in the alpha 1 and alpha 2 chains of collagen IV respectively. Collagen IV is a key component of the basement membrane which supports blood vessels (Pöschl et al., 2004). *COL4A1* and *COL4A2* mutations can affect a range of organs, including the brain, retina and kidneys (Kuo et al., 2012). It has been shown relatively recently that mutations in these genes can lead to pathology similar to SVD, including vascular and white matter changes, in both humans and mice with the mutations (Gould et al., 2006; Verbeek et al., 2012). The fact that all of the organs affected by these mutations are areas which normally have TJs, suggests that a loss of BBB integrity, induced by the disruption to the basement membrane, may cause the pathology.

1.7 – Causes of sporadic SVD

Aside from the Mendelian forms of the disease described in section 1.6, the cause of SVD is not well defined, beyond the fact that incidence increases with age (Vermeer et al., 2007). While the root pathophysiology has been described to be narrowing and

stiffening of the blood vessel walls (section 1.2.2), this ignores that fact that in many lacunes the vasculature does not appear occluded (Bailey et al., 2012), and does not give any clue as to what causes this vascular pathology. There are many risk factors which have been associated with SVD, but there have not been any coherent attempts to describe how these may contribute to disease development and whether they are causal or exacerbating factors. Despite this, there are some risk factors which are widely described as causing SVD, and I will discuss some of these here. Those most often quoted are hypertension, diabetes and smoking.

1.7.1 - Hypertension

Hypertension is widely cited as the cause of SVD, largely due to its strong association with SVD (Thrift et al., 1998). Some studies have even shown that individuals with SVD who have a higher blood pressure also show more severe pathology on imaging (van Dijk et al., 2004). However, 30% of people diagnosed with SVD have completely normal blood pressure (Lammie et al., 1997), and this rate of hypertension is similar to that of the general population in age matched controls (Go et al., 2013; Yoon et al., 2010). This suggests that hypertension alone is not the cause of SVD, though it may well exacerbate it. Further to this, trials to treat SVD patients with antihypertensives have shown mixed results with some showing moderate success, while others show no effect at all (Bath and Wardlaw, 2015; SPS3 Group, 2013).

1.7.2 - Diabetes

Diabetes has a strong association with SVD and has been implicated as a cause, especially in younger, non-hypertensive cases (Ryu et al., 2014). Diabetic patients also suffer damage to a number of different parts of the body, including the retina, kidneys and peripheral nerves. It is believed that all of these changes are caused by a generalised vasculopathy (Cooper et al., 2001). The fact that patients with diabetes also suffer from accelerated large vessel atherosclerosis suggests that arteriolar occlusion could be the cause of many of these changes, including SVD. However, arteriolar occlusion has not been shown in the smaller vessels in organs damaged by

diabetes, and other vascular factors, such as angiogenesis in diabetic retinopathy, have also been implicated as a cause of pathology (reviewed in Cooper et al., 2001). Though diabetic vasculopathy may provide us with some clues as to the origins of vascular pathology in SVD, the fact that this affects multiple parts of the vasculature, rather than just the small vessels in the brain, and the fact that not all SVD patients are diabetic means that diabetes alone cannot tell the whole story.

1.7.3 - Smoking

Smoking has been implicated in SVD in many studies, showing an association with WMH and cognitive decline (Van Dijk et al., 2008). Smoking has long been associated with atherosclerosis, and this could provide a mechanism by which smoking can lead to arteriolar occlusion (Klein, 1984). However, as not all people with SVD are smokers, this is unlikely to be the sole mechanism by which SVD develops.

1.7.4 - Other risk factors

Other cardiovascular risk factors, such as high cholesterol, have also been associated with SVD (Khan et al., 2006). However, one of the issues with these and the other risk factors described above is that their association with lacunar infarcts is no different from that of large vessel stroke. Thus, while they may contribute to the development or worsening of SVD, they cannot be pointed to as the cause which sets SVD apart from other forms of ischemic stroke.

I described in section 1.3.7 how a loss of integrity of the BBB is also associated with SVD. While this is also seen in large vessel strokes, it is observed after an infarct, rather than in the build up to an infarct (Sandoval and Witt, 2008). Thus, a loss of BBB integrity is a feature associated with the development of SVD which is not seen in the development of large vessel stroke, suggesting that it may play a causal role in SVD.

1.8 – Animal models of SVD

The nature of sporadic SVD as a disease which has a late onset in life, and with few ways to predict who will get it, makes the study of disease development difficult. While genetic forms of SVD present us with an opportunity to study people who we know will go on to develop the disease, and so search for early disease related changes, this approach is limited by the nature of studying humans – we are limited to investigating disease progression by methods such as MRI, and to study aspects of pathology involves waiting for post-mortem tissue to become available. Therefore, an animal model is needed to study disease development effectively. This allows us to study the development of the disease from a young age. A number of different animal models exist which are currently used to model SVD, including genetic and inducible models. In this section I will describe the most common models used, and weigh the merits of each one.

1.8.1 - Animal models of Mendelian SVD

As described in section 1.6, there are a number of Mendelian forms of SVD, where mutations in a specific gene are known to cause the onset of disease. This means that mouse lines can be generated with those specific mutations, allowing us to model the disease and better understand the mechanisms involved in disease development. Models have successfully been developed of CADASIL and *COL4A1* mutations, and these have contributed to the understanding of the pathophysiology of these forms of SVD (Gould et al., 2006; Monet-Leprêtre et al., 2013). The extent to which these animal models mimic their respective human diseases varies. While *Col4a1* mutant mice show many late stage pathologies associated with the human disease, including subcortical microbleeds, CADASIL mice show some white matter and vascular pathology, but no lacunar infarcts (reviewed in Joutel and Faraci, 2014). However, studying the disease mechanism in genetic forms of SVD can only take us so far in understanding the causes of sporadic SVD. While these diseases have significant overlapping pathology with sporadic SVD, and are likely to have some similarities in underlying mechanisms, they only model a very specific cause of SVD caused by a single gene mutation, rather than allowing us to understand all the possible causes of

SVD. These models also suffer from the drawback that they are all mouse models. Mice have a much lower white matter to grey matter ratio (10:90) than rats (14:86) or primates (39:61), making them less effective at modelling SVD pathology and symptoms in humans who have a very high white matter to grey matter ratio (60:40) (Bailey et al., 2009). Therefore other models of sporadic SVD, which are not caused by a single gene mutation and which are in an animal with a greater proportion of white matter, are needed.

1.8.2 - Inducible models of SVD

As described in section 1.2.2, SVD is believed to stem from changes to the perforating arterioles in the brain, causing vascular occlusion and hypoperfusion. From this assumption, a number of animal models of SVD are based on inducing some form of occlusion or hypoperfusion in the vasculature. These fall broadly into four categories: embolism, middle cerebral artery occlusion (MCAO), perforating artery occlusion, and administration of a vasoconstrictive agent.

Models of embolism are thought to more closely mimic some forms of vascular occlusion in humans, such as clots formed from atherosclerotic plaques. In animal models, embolism has been induced by injection of artificial objects (microspheres, beads, rubber cylinders) or more natural components (preformed clots) into the internal carotid artery (reviewed in Bailey et al., 2009). The injection site of these artificial emboli means that the effects are unpredictable, and while smaller emboli in small numbers produce subcortical infarcts, most emboli produce cortical infarcts (i.e. large vessel stroke) (Macdonald et al., 1995). The unpredictable nature of these methods makes them poor models for SVD.

MCAO using an intraluminal thread is a common model for large vessel ischemic stroke (Engel et al., 2011). However, this method also causes subcortical infarcts, and can be adapted to cause almost exclusively subcortical infarcts. When MCAO is done for a shorter amount of time (less than 4 hours), large subcortical infarcts are produced which closely resemble striatocapsular lesions seen in human pathology (Bailey et al., 2009). Though this would therefore appear to be a good model of subcortical infarcts

in human disease, the vascular pathology has not been described, and the model involves inducing infarcts in a way known to be different to the development of infarcts in SVD (occlusion of large artery rather than small, perforating arteries).

Models of perforating artery occlusion involve either occluding a perforating artery on the cortical surface with forceps, or using photochemical irradiation to induce an occlusion (Pevsner et al., 2001; Wang and Walz, 2003). While these techniques would be predicted to lead to a good model of SVD, as they mimic the occlusion of perforating arterioles thought to cause SVD, they often lead to cortical as well as subcortical strokes, and have generally been poorly described (Bailey et al., 2009).

Rather than completely occluding a blood vessel, hypoperfusion of brain tissue can be induced by administration of a vasoconstrictive agent. The most common molecule used for this purpose is endothelin 1 (ET-1), injected directly into the brain parenchyma. While studies using this technique have shown myelin and neuronal damage, the description of vascular pathology and comparison of these changes to lacunar infarcts has been poor (Bailey et al., 2009).

Despite the lack of success of these common models to mimic SVD, there are inducible models which do closely resemble SVD. A mouse model of chronic cerebral hypoperfusion, induced by microcoils in the common carotid artery causing chronic constriction of the blood vessels, has shown many features of SVD, including lacunar infarcts and WMH on MRI, myelin damage and even vascular pathology in the form of lipohyalinosis and BBB damage (Holland et al., 2015; Reimer et al., 2011). However, this model, like all the models described in this section, suffers from the flaw of presuming an occlusive or hypoperfusive origin for SVD, which, as I described in section 1.2.2, is not necessarily the case.

1.8.3 - The stroke prone spontaneously hypertensive rat (SHRSP)

Rather than presuming a hypoperfusive origin of SVD, many studies have looked to existing rodent strains to see if they spontaneously develop SVD-like infarcts, so more closely mimicking sporadic SVD in humans where lesions spontaneously arise. One strain in particular, the stroke prone spontaneously hypertensive rat (SHRSP), appears

to model SVD very closely. The SHRSP was first established in 1974 as an inbred strain derived from the spontaneously hypertensive rat (SHR), originally derived from the Wistar Kyoto rat (WKY) (Okamoto, 1974). Numerous studies have described SVD-like features in this rat, and a number of systematic reviews have shown it to be the best animal model of SVD (Bailey et al., 2009, 2011a; Hainsworth and Markus, 2008). The SHRSP develops malignant hypertension (>200 mmHg) between the ages of six and twelve weeks of age (**Figure 1.6**) (Yamori and Horie, 1977). It first starts showing signs of SVD-like features, including WML, lipohyalinosis, microinfarcts and haemorrhage between the ages of eight and twelve weeks, and the animals start to suffer strokes after twenty weeks of age (**Figure 1.6**) (Bailey et al., 2011a; Lin et al., 2001; Yamori et al., 1976). The progressive, spontaneous nature of these changes makes the SHRSP a good model for SVD.

The fact that the SHRSP develops hypertension prior to the onset of SVD-like features can lead to the suggestion that this model presumes a hypertensive origin of SVD, in the same way that the inducible models of SVD described above presume an occlusive origin of SVD. However, by comparing the SHRSP to other rodent models of hypertension we can see that there is clearly more to this model than hypertension. Few hypertensive mouse models have been studied in relation to SVD, however one model, which overexpresses human renin and angiotensin (R^+/A^+), shows many features of SVD in certain conditions. When treated with a high salt diet and Nitro-L-arginine methyl ester hydrochloride (L-NAME), a nitric oxide synthase inhibitor, these mice develop haemorrhages in the basal ganglia, cerebellum and brainstem, similar to what is seen in patients with SVD (Iida et al., 2005). However, other types of lesions, including WMLs, have not been reported in this model. Rat genetic models of hypertension, such as the inducible hypertensive rat (IHR), similarly show little brain pathology under normal conditions, but multiple small haemorrhagic lesions when subjected to a high salt diet (Hainsworth and Markus, 2008). However, the best model for comparison to SHRSP is the SHR. The SHR is the closest related strain to the SHRSP, from which the SHRSP was initially derived, and develops similar levels of hypertension (>200 mmHg) (Lin et al., 2001). A study directly comparing the two strains showed that despite this similar genetic background and level of hypertension, the SHRSP develops WMLs, increased microglial activation and lipohyalinosis,

whereas the SHR does not (Lin et al., 2001). This suggests that the SVD-like phenotype of SHRSP is not solely due to its high blood pressure. Though the level of hypertension in SHRSP is far greater than that seen in hypertensive patients, I believe that the SHRSP is still the best animal model of SVD available, as it displays more SVD-like features than other models, and does not rely on any *a priori* assumptions as to the cause of the disease.

The majority of studies using SHRSPs have looked at their pathology after the onset of hypertension, with many looking even after the onset of strokes (Bailey et al., 2009, 2011a). This is likely because SVD is a disease of ageing, with hypertension believed to be a contributory factor. While earlier studies showed no apparent histopathological changes in SHRSPs prior to the onset of hypertension (Tagami et al., 1987), more recent studies have shown that at ages as young as five weeks there is reduced immunoreactivity of claudin-5, a key TJP of the BBB (Bailey et al., 2011b). This increased BBB permeability is present throughout adulthood in the SHRSP (Fredriksson et al., 1988; Schreiber et al., 2012), and increased BBB permeability has been found in humans with SVD by imaging (1.3.7). This suggests that BBB breakdown predates hypertension in SVD, and may even be responsible for many of the downstream tissue changes.

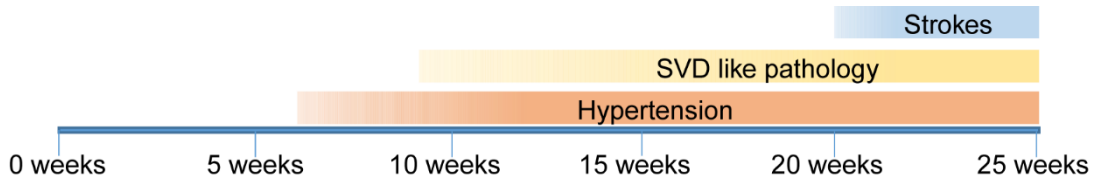


Figure 1.6: Schematic showing the timing of pathological changes in the stroke prone spontaneously hypertensive rat (SHRSP). The orange bar depicts the development of hypertension between six and twelve weeks of age. The yellow bar shows the first onset of small vessel disease (SVD) like pathology, between eight and twelve weeks of age. The blue bar shows the incidence of stroke symptoms, from twenty weeks of age.

1.9 – Hypothesis

Based on the evidence described here, showing that a loss of BBB integrity may predate hypertension in SVD, my initial hypothesis is that the primary cause of SVD is a breakdown of the BBB.

1.10 – Aims

- Describe the early pathological changes in SVD which predate hypertension and the onset of symptoms, both in human post-mortem tissue with early stage SVD and in the SHRSP model of the disease;
- Elucidate the mechanisms linking these early changes, to determine the role that the BBB plays in SVD.

Chapter 2: Materials and Methods

Details of all reagents, kits and antibodies used in the methods below are given in sections 2.9-2.12 at the end of this chapter.

2.1 – *In vivo* methods

All experiments were carried out in line with Home Office guidelines, under personal licence IF8E4EADA (Rikesh Rajani) and project licences 60/4268 (Delyth Graham) and 60/4524 (Anna Williams).

2.1.1 - Animal housing and husbandry

The stroke prone spontaneously hypertensive rats (SHRSP) and matched control strain, Wistar Kyoto rats (WKY), were kindly provided and housed by Delyth Graham and Anna Dominiczak at the University of Glasgow. Animals were fed standard chow and housed in line with Home Office guidelines. Breeding SHRSP pairs regularly had their blood pressure tested to ensure maintenance of the colony's phenotype. Male animals were exclusively used for both WKY controls and SHRSPs as these SHRSP animals display a more severe and consistent phenotype. For extraction of wild type oligodendrocyte precursor cells (OPCs), microglia and slice cultures Sprague Dawley rats housed at the University of Edinburgh were used.

2.1.2 - Termination

For extraction of OPCs, microglia and slices animals were terminated at postnatal day 0-2 by an overdose of Euthatal (150mg/kg) administered intraperitoneally. For extraction of brain microvascular endothelial cells (BMECs) animals were terminated at postnatal day 5-10 by a rising concentration of carbon dioxide (CO_2), as anaesthetics can affect endothelial cell function (Acharya et al., 2015). For extraction of protein lysates where fresh, frozen tissue was required, animals were terminated at the age of 5 weeks by an overdose of Euthatal (150mg/kg) and their brains extracted and flash

frozen in liquid nitrogen. For immunohistochemistry (IHC) animals were terminated at 3, 4 and 5 weeks of age by overdose of Euthatal (150mg/kg) and intracardiac perfusion fixation with 4% paraformaldehyde (PFA; diluted in phosphate buffered saline (PBS)).

2.1.3 - Tracer experiments

The tracer experiments were carried out on 5 week old animals by administering an overdose of Euthatal, intracardiac perfusion of the tracer mix (80µg/ml sodium fluorescein, 1.5mg/ml tetramethylrhodamine-isothiocyanate-dextran, 1mM calcium chloride in PBS) through the animal, followed by intracardiac perfusion fixation with 4% PFA.

2.1.4 - Preparation of tissue

For IHC, brains were extracted from animals after perfusion fixation and incubated overnight in 4% PFA at 4ºC, followed by an overnight incubation in 50% ethanol. Brains were then processed for paraffin embedding by immersion in increasing concentrations of ethanol before being embedded in paraffin wax (with the assistance of the SURF facility at the University of Edinburgh). 4µm thick sections were then cut on a microtome, and incubated overnight at 46ºC to stick to the slides. For tracer experiments the brains were extracted from animals after perfusion fixation and incubated overnight in 4% PFA at 4ºC, followed by incubations in 30% sucrose (overnight at 4ºC) and 50% sucrose (overnight at 4ºC). The brains were then embedded in optimal cutting temperature compound (OCT) and frozen on dry ice. Sections were cut at 8µm thickness using a cryostat.

2.2 – *In vitro* methods

Details of all solutions and plastics used can be found in section 2.9 at the end of this chapter.

2.2.1 - Preparation of brain slices

The following protocol was adapted from a previously published method (Levi and Meyer, 1941; Zhang et al., 2011). Brains were extracted from rats aged postnatal day 0-2, divided into hemispheres and trimmed to leave only mid-coronal regions (approximately Bregma +1 to Bregma -4) in L-15 medium. This was placed onto a McIlwan Tissue Chopper to cut 300μm thick coronal sections. These were teased apart with flat edge scalpels in slice culture medium and plated on Millipore cell culture inserts (2-4 slices per insert) in 6-well plates with 1ml slice culture medium (minimum essential medium (MEM) with 25% Earle's balanced salt solution (EBSS), 25% heat inactivated horse serum (HIHS), 1.5% glucose (45%), 1% glutamax, 1% penicillin/streptomycin (pen/strep), 0.5% Fungizone) underneath the insert. Medium was changed every 2-3 days, and slices were kept in culture for up to 5 weeks.

2.2.2 - Preparation of primary brain microvascular endothelial cells (BMECs)

The following protocol is based on a previously published method (Abbott et al., 1992). Brains were extracted from rats aged postnatal day 5-10 and divided into hemispheres with cerebellum removed in working buffer (Hank's balanced salt solution (HBSS) with 0.5% bovine serum albumin (chromatographically purified; BSA (cp)), 0.5% HEPES, 0.5% pen/strep). Meninges were removed before the brains were homogenised in 5ml working buffer with a Dounce tissue grinder. The homogenate was isolated from the buffer by centrifugation for 5 minutes at 1800 revolutions per minute (RPM) at 4ºC. Blood vessel fragments were pelleted from this homogenate by centrifugation in 22% BSA (cp) for 15 minutes at 3000 RPM at 4ºC. The pellet of blood vessel fragments was kept on ice in 1ml working buffer while the remainder was centrifuged again. This was repeated for a total of 5 spins. The blood vessel fragments were pipetted onto an upside down 70μm cell strainer to remove

single cells then washed into a pooled mixture with working buffer. This was spun down (5 minutes at 1800 RMP at 4ºC) and the pellet then digested in 10ml collagenase/dispase (1mg/ml) and DNase I type IV (40µg/ml) for 45 minutes at 37ºC. The resultant dissociated endothelial cells were washed in working buffer and plated at 500,000 cells/well on collagen IV and fibronectin (100µg/ml and 50µg/ml respectively; overnight at 4ºC) coated coverslips in a 24-well plate in 1ml Endothelial Growth Media-2 Bullet Kit (EGM-2; Lonza; Endothelial basal media-2 with 2% Fetal Bovine Serum (FBS), 0.4% hFGF-beta, 0.1% hEGF, 0.1% VEGF, 0.1% R3-IGF-1, 0.1% Ascorbic acid, 0.1% Gentamicin/Amphotericin-B, 0.1% puromycin (5mg/ml in Dulbecco's phosphate buffered saline (DPBS)) and 0.04% hydrocortisone). Cells were grown in 5% carbon dioxide (CO_2) and medium was changed every 2-3 days. Cultures were used in experiments once they had regions of confluence (10-14 days) and were kept for up to 4 weeks. For conditioned media (CM) experiments, BMECs were kept in EGM-2 until they had regions of confluence before being grown in medium of the target cell type (details in section 2.2.6).

2.2.3 - Preparation of oligodendrocyte precursor cells (OPCs)

The following protocol is based on a previously published method (McCarthy and de Vellis, 1980). Brains were extracted from rats aged postnatal day 0-2 and cortices isolated in MEM. Meninges were removed then cortices were minced with fine scissors and digested in 1ml MEM with papain (1.2U/ml), L-cysteine (0.24mg/ml) and DNase I type IV (40µg/ml) for 1 hour at 37ºC. Cells were diluted in 10ml culture medium (Dulbecco's modified Eagle medium (DMEM) with 10% FBS, 1% pen/strep), spun down (5 minutes at 1000 RPM), 5ml medium removed then triturated gently 3-4 times with a 19 gauge needle followed by 3-4 times with a 23-gauge needle. Cells were resuspended in culture medium (1.5 brains in 10ml per flask) and grown in vented T75 flasks coated with poly-D-lysine (PDL; 5µg/ml in water; minimum 1 hour coating at 37ºC) in 7.5% CO_2. Medium was first changed after 3-5 days, then every 2-3 days. 10-14 days after dissection, the vented cap of the flasks was sealed with parafilm and the flasks were placed on an orbital shaker at 240 RPM at 37ºC. After 1 hour the medium was removed (containing loosely attached microglia), fresh medium added, and the

flask returned to the shaker for 16-18 hours. This medium was removed and plated on 10cm plastic petri dishes for 20-25 minutes (to remove any remaining microglia) after which the cells were spun down (5 minutes at 1000 RPM). The cells were resuspended in 5ml culture medium, gently triturated 6-10 times through a 21 gauge needle, counted, and plated at a density of 50,000 cells in a 20µl droplet of SATO medium (DMEM with 1% pen/strep. 1% ITS supplement, 0.5% FBS, 16µg/ml putrescine, 400ng/ml L-thyroxine, 400ng/ml Tri-iodothyroxine, 60ng/ml progesterone, 100µg/ml BSA (fraction V)) per PDL coated coverslip in a 24 well plate, topped up to 0.5ml SATO medium per well after 20 minutes at 37ºC for cells to stick down. OPCs were grown for 2 days and the medium was not changed during this time.

2.2.4 - Preparation of microglia

Microglia were taken from the same preparations as OPCs, from the medium removed after the first hour on the orbital shaker. Microglia were plated at a density of 50,000 cells per well in culture medium (DMEM, 10% FBS, 1% pen/strep) and were grown for 24 hours on PDL (5µg/ml; 1 hour at 37ºC) coated coverslips in 24 well plates.

2.2.5 - Maintenance of mouse brain endothelial cell line, bEND.3

Cells were initially obtained from ATCC (catalogue number: CRL-2299) and donated to us by the ffrench-Constant group. Cells were grown in PDL (5µg/ml; 1 hour at 37ºC) and matrigel (1:40 in water; 1 hour at 37ºC) coated vented T75 flasks in culture medium (DMEM, 10% FBS, 1% pen/strep). The cells were plated at 1:10 of confluent density and split every week. To split the cells, they were first washed with DPBS and then incubated for 10 minutes at 37ºC in TVP (1.3mM ethylenediaminetetraacetic acid (EDTA; from BDH), 0.025% trypsin, 1% chicken serum in DPBS). The cells were then agitated and diluted in culture medium to stop the digestion, before being further diluted for splitting or plating. For experiments, cells were plated at 1:2 of confluent density on PDL and matrigel coated coverslips in 24-well plates as above.

2.2.6 - Collection of conditioned media

Endothelial cells (BMECs and bEND.3 cells) were grown in normal culture medium until reaching confluence and forming tight junctions (~ 10 days in vitro (DIV) for BMECs, 5 DIV for bEND.3 cells). At this point the media was changed for media of the target culture (SATO medium (2.2.3), microglia medium (2.2.4), or slice medium (2.2.1)), and the media was conditioned for 2-3 days. Media was then removed and stored at -20^{o}C until required. Media was filtered with a Millex 0.22μm syringe filter prior to use.

2.2.7 - Experiments using conditioned media

Cells grown in conditioned media were prepared as normal. Conditioned media was added to OPCs after the step at which they were left for 20 minutes to stick down. Microglia were resuspended in conditioned media before plating. Cells were left for 2 days in conditioned media before being fixed and analysed.

Slices grown in conditioned media were prepared as normal. After preparation, slices were grown in normal media for 1 day to settle into culture, before the media was changed for 0.8ml of conditioned media. Media was changed for fresh conditioned media every 2-3 days, and slices were grown for 5 weeks before being fixed and analysed.

2.2.8 - Treatment of bEND.3 cells with siRNA

After splitting, bEND.3 cells were plated at half confluent density in a 24-well plate (day 0). After 1 DIV, media was changed and cells were transfected with pre mixed siRNA (5pmol per well) and lipofectamine RNAiMAX (3μl per well) diluted in Opti-MEM. At 4 DIV, media was changed and cells were again transfected with pre-mixed siRNA and lipofectamine RNAiMAX. Cells were fixed and analysed at 7 DIV. To determine the efficiency of the knockdown, protein was extracted from unfixed cells at 7 DIV, as detailed in section 2.4.2.

2.3 – Immunostaining

Details of all antibodies used can be found in section 2.10 at the end of this chapter.

2.3.1 - Fluorescent immunohistochemistry (IHC) on paraffin embedded rat tissue

Sections were deparaffinised by immersion in Xylene (2x 5 minutes) and rehydrated by immersion in descending concentrations of ethanol (100%, 90%, 80%, 70%, 50%, 30%; 1 minute each) before being immersed in phosphate buffered saline (PBS). Antigen retrieval was carried out by boiling sections for 15 minutes in a microwave in citrate buffer. Sections were then cooled for 20 minutes in running tap water. Sections were blocked for at least 1.5 hours at room temperature in blocking solution (10% heat inactivated horse serum (HIHS), 0.3% triton in PBS). Primary antibodies, diluted in blocking solution, were added and the sections were incubated at 4^{o}C overnight in a humid chamber. The sections were washed in PBS (3x 5 minutes), then secondary antibodies, diluted in blocking solution, were added for 1.5 hours at room temperature (RT). Sections were washed in PBS (3x 5 minutes), Hoechst was then added (1 minute), then sections were washed again in PBS (5 minutes). Sections were mounted with Fluoromount.

2.3.2 - Fluorescent IHC on fixed, frozen rat tissue

IHC was carried out as above for paraffin fixed rat tissue (2.3.1), but without deparaffinisation or antigen retrieval steps.

2.3.3 - Fluorescent IHC on paraffin embedded human tissue

Sections were deparaffinised and antigen retrieval carried out as described above for paraffin embedded rat tissue (2.3.1). Sections were then washed with 0.3% triton in PBS before iFX signal enhancer was added (30 minutes). Sections were then washed with PBS (5 minutes) and blocking solution (10% HIHS, 0.3% triton in PBS) was added (2 hours at room temperature). Primary antibodies, diluted in blocking solution,

were incubated overnight in a humid chamber at 4ºC. Sections were washed in 0.3% triton in PBS (3x 5 minutes) and secondary antibodies, diluted in blocking solution, were added (1.5 hours at RT). Sections were washed in PBS (5 minutes), Hoechst was added (1 minute), sections were washed again (2x 5 minutes) then Sudan black (0.01% in 70% ethanol) was added for 5 minutes. Sections were washed in 70% ethanol (5 minutes) and PBS (5 minutes). Sections were mounted in Fluoromount.

2.3.4 - Colorimetric IHC on paraffin embedded human tissue

Sections were deparaffinised and antigen retrieval carried out as described above for paraffin embedded rat tissue (2.3.1). Endogenous enzyme activity was blocked with Vector Bloxall (10 minutes) then sections were washed with PBS (5 minutes). Sections were blocked with 2.5% normal horse serum (NHS; from Vector ImmPress kit; 20 minutes) then washed with PBS (5 minutes). The first primary antibody, diluted in antibody diluent (Spring Bioscience) was incubated overnight in a humid chamber at 4ºC. Sections were washed in PBS (5 minutes) and Vector ImmPress secondary was added for 1 hour at RT. Antibodies were visualised with Vector horseradish peroxidase (HRP) NovaRED for 10 minutes before washing in PBS (5 minutes) to stop the reaction. Sections were then blocked with 2.5% NHS (20 minutes) before the second primary antibody, diluted in antibody diluent, was added (overnight in a humid chamber at 4ºC). Sections were washed in PBS (5 minutes) and Vector ImmPress secondary was added for 1 hour at RT. Sections were visualised with Vector alkaline phosphatase (AP) Blue for 30 minutes, before washing in PBS (5 minutes) to stop the reaction. Sections were then rinsed in distilled water before mounting with Fluoromount.

2.3.5 - Fluorescent IHC on ex vivo brain slices

Slices were fixed in 4% PFA for 1 hour before being rinsed in PBS. The outer plastic ring of the cell culture insert was then removed and the slices were further washed in PBS (3x 10 minutes). Slices were incubated with blocking solution (3% HIHS, 2% bovine serum albumin (BSA), 0.5% triton in PBS) for 2 hours at room temperature on

a rocker. Primary antibodies, diluted in blocking solution, were added either overnight at RT on a rocker, or for 2 nights at 4ºC on a rocker (conditioned media experiments only). Slices were washed in blocking solution (10 minutes, then 3x 1 hour) before the secondary antibodies were added overnight at RT on a rocker. Slices were washed with PBS (10 minutes, then 3x 1 hour) then Hoechst was added (1 minute). Slices were rinsed in PBS and mounted with Fluoromount.

2.3.6 - Immunocytochemistry (ICC)

Cells were fixed in 4% PFA (10 minutes) then washed with PBS (3x 5 minutes). Blocking solution (10% HIHS, 0.1% triton in PBS) was added for 1-1.5 hour at RT on a rocker. Cells were then incubated with primary antibodies, diluted in blocking solution, for 1-1.5 hour at RT on a rocker. Cells were washed with PBS (3x 2 minutes) then incubated with secondary antibodies, diluted in blocking solution, for 1 hour at RT on a rocker. Cells were washed with PBS (3x 2 minutes), Hoechst added (1 minute) and washed again with PBS (rinse then 2 minutes) before being mounted with Fluoromount.

2.4 – Analysis of protein levels

2.4.1 - Extraction of protein from tissue

Areas of basal ganglia from fresh, frozen sections of brain tissue, cut using a cryostat onto glass slides, were scraped off with a razor into a solution of 400µl of radioimmunoprecipitation assay (RIPA) buffer with 1% protease inhibitor, aiming for a total of approximately 10mg (10µl by volume size) of tissue. This was homogenised by hand on ice with a plastic pestle before being sonicated (3x 10 seconds sonication followed by 10 seconds on ice). This was spun down in a microfuge (20 minutes at 13,000 RPM at 4ºC) and the supernatant transferred to fresh tubes in 50µl aliquots.

2.4.2 - Extraction of protein from cells

Culture media was removed from wells and approximately 50µl of RIPA buffer with 1% protease inhibitor was added to each well (of a 24 well plate). Cells were scraped with a bent pipette tip and the resultant liquid transferred to a tube. This was spun down in a microfuge (10 minutes at 13,000 RPM at 4^{o}C) and the supernatant collected.

2.4.3 - Quantification of total protein

Protein levels were quantified using a bicinchoninic acid assay (BCA assay), using solutions from a Pierce BCA protein assay kit. BCA working solution was prepared as specified, and 200µl added to each well of a flat bottomed 96-well plate. 10µl of sample was added to each relevant well, and 9 wells were used for a BSA standard curve (2000µg/ml, 1500µg/ml, 1000µg/ml, 750µg/ml, 500µg/ml, 250µg/ml, 125µg/ml, 25µg/ml, and 0µg/ml in RIPA). The plate was incubated at 37^{o}C for 30 minutes and then allowed to cool to RT. The absorbance of each well at 562nm was measured using an Omega Plate Reader. Protein concentration of each sample was then calculated by comparison to the standard curve plotted from the BSA samples.

2.4.4 - Western blotting

Protein lysates were diluted in RIPA and 4x Laemmli buffer (8% sodium dodecyl sulphate (SDS), 40% glycerol, 20% β-mercaptoethanol, 0.4% bromophenol blue, 0.25M Trizma hydrochloride) to a concentration of 5µg of protein in 20µl (20µg of protein in 30µl for ATP11B) in 1x Laemmli buffer. Samples were then boiled at 95^{o}C for 10 minutes and loaded into Pierce ready-cast 4-20% Tris-HEPES gels, in a gel tank filled with HEPES running buffer (Pierce). Samples were run, along with a protein ladder (Bio-Rad) for 1.5 hours at 100 Volts. The gel was then removed and placed into a transfer cassette with a polyvinylidene fluoride (PVDF) membrane (activated in methanol). Gels were transferred in transfer buffer (20mM Trizma base, 150mM glycine, 20% methanol in water) for 2 hours at 400 mAmps. The membrane was removed from the cassette, washed in TBST (tris buffered saline (TBS; 20mM Trizma base, 150mM sodium chloride, 2.7mM potassium chloride in water) + 0.1% tween;

PBST (PBS + 0.05% tween) for ATP11B) and blocked with 4% BSA in TBST (5% milk in PBST for ATP11B) for 1 hour at RT on a rocker. The membrane was then incubated with primary antibodies diluted in block overnight at 4ºC on a rocker. The membrane was washed with TBST (3x 10 minutes; PBST for ATP11B) then incubated with secondary antibodies in block (half as diluted for ATP11B) for 1 hour (2 hours for ATP11B) at RT on a rocker. The membrane was then washed with TBST (PBST for ATP11B) and ECL substrate (femto kit for ATP11B) was put on the membrane for 5 minutes. The excess was dabbed off and the membrane was either exposed to a film which was then developed, or imaged using a LiCor scanner.

2.4.5 - Antibody array

The antibody array was using a kit from Full Moon BioSystems and was carried out according to instructions included with the kit. Briefly, the samples were spun down (18,000g for 15 minutes at 4ºC) and 25µl of the supernatant was incubated with 50µl Labelling Buffer and 3µl Biotin Reagent in N,N-Dimethylformamide (DMF) for 2 hours at RT, vortexing every 10 minutes. The reaction was then stopped with 35µl Stop Reagent, incubated for 30 minutes at RT with regular mixing. During these incubation periods, the antibody array slides were incubated in 30ml Blocking Solution for 30 minutes at RT on an orbital shaker before being rinsed with Milli-Q water (slide was placed in a 50ml tube with 45ml water, shaken for 10 seconds and repeated 10 times). The biotinylated sample was then added to 6ml Coupling Solution, mixed and incubated with an antibody array slide for 2 hours at RT on an orbital shaker. The slide was then washed in Wash Solution (3x 10 minutes at RT on an orbital shaker) and rinsed in Milli-Q water as described above. The slides were then incubated with 30ml streptavidin-800 in Detection Buffer (0.5µg/ml) for 20 minutes at RT on an orbital shaker. The slides were washed with Wash Solution (3x 10 minutes at RT on an orbital shaker) and rinsed in Milli-Q water as described above. The slide was dried by centrifugation (in a 50ml tube at 1300g for 10 minutes) before being scanned and quantified using an Imaris Microarray Slide Scanner, with the help of Dr Bryan Serrels (University of Edinburgh).

2.5 – Molecular biology

2.5.1 - Extraction of deoxyribonucleic acid (DNA)

Tail clips or ear punches from SHRSP and WKY rats were incubated in lysis buffer (1M Trizma hydrochloride), 0.5M EDTA (Sigma-Aldrich), 5M sodium chloride, 10% SDS in water) with 10% proteinase K overnight at 55°C. The samples were then incubated at 95°C for 10 minutes, followed by an incubation at 0ºC for 15 minutes. The samples were centrifuged for 10 minutes and the supernatant collected. This supernatant was diluted 1:10 for polymerase chain reaction (PCR).

2.5.2 - Extraction of ribonucleic acid (RNA)

RNA was extracted from BMECs using the Qiagen RNeasy mini kit and the provided protocol was followed. Briefly, cells were harvested in 200µl lysis buffer (buffer RLT). After adding 1 volume of 70% ethanol, the mixture was centrifuged using a RNeasy spin column. A DNA digestion step was performed to ensure the purity of RNA in the samples. This was followed by 2 washes (buffer RPE). RNA samples were eluted in water and stored at -80°C until synthesis of complement DNA (cDNA) (2.5.3).

2.5.3 - Synthesis of complement DNA (cDNA)

All reagents came as part of SuperScript First-Strand Synthesis System for RT-PCR. 3-8µl of RNA was mixed with 1µl deoxynucleotides (dNTPs) and 1µl hexamer primers (filled up with water to a total volume of 10µl) and incubated for 5 minutes at 65°C. After cooling down for 1 minute on ice, an additional reaction mix was added (2µl RT buffer, 4µl MgCl2, 2µl DTT, 1µl RNase OUT) and incubated for 2 minutes at RT. Then, 1µl Superscript II was added and the samples were incubated for 10 minutes at RT. Subsequently, samples were incubated at 42°C (50 min) and 70°C (15 min). cDNA synthesis was completed by adding 1µl RNAse H and incubating at 37 °C for 20 minutes.

2.5.4 - Polymerase chain reaction (PCR)

PCR was carried out using Promega GoTaq Hot Start Polymerase, which included all the reagents required. To the master mix (10µl 5X PCR buffer, 4µl 25mM MgCl2, 1µl dNTPs, 5µl each of forward and reverse primers (1:10), 0.25µl GoTaq in 22.75µl water per reaction) 2µl of DNA sample was added. After activation of GoTaq polymerase, 30 cycles of amplification were carried out, followed by denaturation by a 2 minute incubation at 94 °C. A touch-down protocol was used for the annealing phase (60-48 °C). For the elongation stage, samples were held at 72 °C for 5 minutes. After the PCR was complete, samples were mixed with dye and visualized on a 1.3% agarose gel to confirm that the reaction worked. PCR products for sequencing were purified using QIAquick PCR purification kit following the provided protocol.

2.5.5 - Sequencing of DNA/complement DNA (cDNA)

Primers were designed, using NCBI primer blast, 300-500 bases either side of the predicted mutation site (primers listed in section 2.11) and the relevant region of (c)DNA was amplified using these primers by PCR. These products were 600-1,000 bases long as any sequencing reads in the first 100 bases or after 800 bases can sometimes be unreliable. These PCR products were sent off, along with forward and reverse primers around the predicted mutation site, to Source Bioscience for sequencing, according to their specifications (16pmol in 5µl of primers per reaction, 50ng in 5µl of each sample per reaction). Sequences were aligned using BioEdit Sequence Alignment Editor (Ibis Biosciences).

2.6 – Other methods

2.6.1 - Assay of nitric oxide synthase (NOS) activity

NOS activity was measured using an assay kit from Merck Millipore which reduced all nitrates in CM to nitrites, and quantified this based on a colour change when Griess reagents were added. The protocol provided with the kit was followed. Briefly: 60µl of each sample and each of a standard curve of nitrate (0µM, 5µM, 10µM, 15µM,

20µM, 25µM) prepared in the presence of unconditioned media were placed in individual wells of a 96-well plate. 10µl of nitrate reductase solution and 10µl of freshly prepared NADPH solution (1mM) was added to each well and incubated for 40 minutes at room temperature. 10µl of cofactors solution and 10µl of LDH solution was added to each well and incubated for 20 minutes at room temperature. Then 50µl each of Griess reagents R1 and R2 were added to each well, and left for 10 minutes at room temperature for the colour to develop. The absorbance at 540nm was then measured using an Omega plate reader. The final nitrate + nitrite concentration was then calculated by comparison to the standard curve.

2.7 – Imaging, analysis and statistics

2.7.1 - Imaging

Fluorescent images were captured using Leica SPE and Leica SP8 confocal microscope systems. Colorimetric images were captured using an AxioScan Slide Scanner.

2.7.2 - Image analysis

With the exception of myelination in slice cultures, all immunostained images were quantified using the FIJI build of ImageJ software (open source). Cells were counted using the Cell Counter plugin, and myelin coverage in tissue was quantified using the pixel count tool. ICC images were blinded before quantification. IHC images were not blinded prior to quantification, however a random selection were quantified again after blinding to confirm the reliability of the quantification. Myelination in slice cultures was quantified with Image Pro Plus (Media Cybernetics) using a macro developed by a previous PhD student in the lab which measures the overlap of myelin and axon staining at each level in a z-stack (Zhang et al., 2011).

2.7.3 - Quantification of western blots

Western blots were analysed using the Western Blot Quantification tool in FIJI, or Image Studio Lite (LI-COR Biosciences), to give the relative intensity of different bands. These were then normalised to the sample loading control.

2.7.4 - Statistics

Graphs were produced and statistics calculated using GraphPad Prism software. All data is presented as mean ± standard error of the mean (SEM), comparing at least three biological repeats each time. Actual numbers of technical and biological repeats are stated in the results sections and in each graphical figure. As all comparisons were between two groups, significance was determined using a Student's t-test. A paired t-test was used for *in vitro* experiments where the same preparation of cells/slices was used for control and experimental conditions, or where control and experimental cells/slices were prepared in parallel, for each biological repeat. An unpaired t-test was used for *in vivo* experiments where control and experimental samples were independent.

2.8 – Materials: human tissue blocks

Human tissue was kindly provided as paraffin embedded blocks by the MRC Sudden Death Brain Bank. All blocks are from the frontal lobes of sudden death patients who died without previously showing signs of SVD. Five blocks were chosen from people who had histopathological signs of SVD upon post-mortem (PM) examination, and five matched controls were chosen from people with no PM signs of SVD. Details are shown in the tables below.

Controls						
Patient Number	**Gender**	**Age**	**Death Certificate**	**PM interval (hours)**	**Block**	**Neuropathology report**
SD015/08	M	53	Suspension by a ligature	42	2I	No significant abnormality.
SD021/08	M	44	Suspension by a ligature	83	2E	No significant abnormality.

SD034/08	M	70	Pulmonary embolism, Deep vein thrombosis, Hypertension, Previous pulmonary embolism	50	2F	No significant abnormality.
SD014/09	M	26	Methadone and diazepam toxicity	44	2F	The white matter appears unremarkable.
SD010/10	M	39	Sudden Adult Death	81	2K	White matter throughout appears unremarkable.

SVD						
Patient Number	**Gender**	**Age**	**Death Certificate**	**PM interval (hours)**	**Block**	**Neuropathology report**
SD019/08	M	58	Myocardial infarction, Small previous infarctions, Coronary arteriosclerosis, General arteriosclerosis, Heart disease	69	2H	Congestion within white matter. Some small vessels with thickened hyalinised walls.
SD020/08	M	51	Ischaemic heart disease, Coronary arteriosclerosis, Heart disease	47	2E	White matter is congested. Some of the smaller vessels have thickened hyalinised walls with surrounding haemosiderin containing macrophages.
SD022/08	F	57	Pulmonary thromboembolism, Heart disease	95	2E	Small vessels with thickened hyalinised walls and surrounding haemosiderin containing macrophages
SD023/08	F	24	Suspension by a ligature	47	2H	Throughout the white matter there are scattered small vessels with thickened hyalinised walls and surrounding haemosiderin containing macrophages. The appearances suggest hyaline arteriosclerosis.
SD031/08	M	55	Acute myocardial ischaemia, Coronary arteriosclerosis, Hypertension, Heart disease	31	2F	Throughout the white matter there are occasional vessels with thickened hyalinised walls.

2.9 – Materials: *in vitro* reagents and plastics

2.9.1 - List of cell culture plastics

Name	Company	Product code
13mm round coverslips	VWR International	631-0149
24-well plates	Costar (Corning)	3524
6-well plates	Costar (Corning)	3516
70µm cell strainer	Fisher Scientific	11597522
Cell culture inserts, 0.4µm	Merck Millipore	PICM0RG50
Dounce tissue grinder	Sigma-Aldrich	P1360 + T0691
Millex 0.22µm syringe filter	Merck Millipore	SLGP033RS
Vented T75 flasks (bEND.3)	Costar (Corning)	430641U
Vented T75 flasks (OPCs)	Falcon (Corning)	353110

2.9.2 - List of cell culture solutions

Name	Company	Product code
22% Bovine serum albumin (chromatographically purified)	First Link UK Ltd.	42-20-850
45% Glucose	Sigma-Aldrich	G8769
Bovine serum albumin (fraction V)	Sigma-Aldrich	A-4919
Chicken serum	Sigma-Aldrich	C5405
Collagen IV	Sigma-Aldrich	C5533
Collagenase/dispase	Roche	10269638001
Dnase I type IV	Sigma-Aldrich	D5025
Dulbecco's modified Eagle medium	Gibco (now Thermo Fisher Scientific)	41966-029
Dulbecco's phosphate buffered saline	Sigma-Aldrich	D8537
Earle's balanced salt solution	Gibco (now Thermo Fisher Scientific)	24010
EDTA	BDH	104245S
Endothelial growth media-2 bullet kit	Lonza	CC-3162
Fetal bovine serum	Gibco (now Thermo Fisher Scientific)	10270106
Fibronectin	Sigma-Aldrich	F1141
Fungizone	Invitrogen (now Thermo Fisher Scientific)	15290-018
Glutamax	Gibco (now Thermo Fisher Scientific)	35050
Hank's balanced salt solution	Life Technologies (now Thermo Fisher Scientific)	14180-046
Heat inactiavted horse serum	Gibco (now Thermo Fisher Scientific)	26050
HEPES	Gibco (now Thermo Fisher Scientific)	15630-049
HSP90α blocking antibody	Enzo Life Sciences	ADI-SPS-771-D
ITS	Sigma-Aldrich	I3146
L-15 medium (Leibovitz)	Sigma-Aldrich	L5520

L-cysteine	Sigma-Aldrich	C7477
Lipofectomine RNAimax	Life Technologies (now Thermo Fisher Scientific)	13778100
L-thyroxine	Sigma-Aldrich	T-1775
Matrigel	Corning	354230
Minimum essential Medium	Gibco (now Thermo Fisher Scientific)	32360
Opti-MEM	Life Technologies (now Thermo Fisher Scientific)	31985062
Papain, suspension	Worthington Biochemical Corporation	LS003127
Penicillin/streptomycin	Gibco (now Thermo Fisher Scientific)	15140
Poly-d-lysine	Sigma-Aldrich	P6407
Progesterone	Sigma-Aldrich	P-8783
Puromycin	Sigma-Aldrich	P8833
Putrescine	Sigma-Aldrich	P-5780
Recombinant HSP90α	Enzo Life Sciences	ADI-SPP-776-D
Tri-iodothyroxine	Sigma-Aldrich	T-6397
Trypsin	Gibco (now Thermo Fisher Scientific)	15090046

2.9.3 - List of siRNAs

Name	**Sequence (sense)**	**Sequence (antisense)**	**Company**	**Catalogue number**
Atp11b siRNA (s94217)	GGGUGAUAUU GUUCGUAUAtt	UAUACGAACA AUAUCACCCac	Ambion (now Thermo Fisher Scientific)	4390771
Non-targeting siRNA	UUACGUCGUC GCGUCGUUAtt	UUACGUCGUC GCGUCGUUAtt	Ambion (now Thermo Fisher Scientific)	4390843

2.10 – Materials: list of antibodies

2.10.1 - Primary antibodies used for IHC and ICC

Name	**Species**	**Dilution**	**Company**	**Catalogue number**	**Notes**
CD34	Goat	1:80	Santa Cruz Biotechnology	sc-7045	
CD68	Rat	1:100	Abcam	ab5344	ICC only
CD68	Mouse	1:100	Dako	M0814	
Cldn5	Rabbit	1:100	Zymed (now Thermo Fisher Scientific)	34-1600	
Cldn5	Rabbit	1:100	Abcam	ab53765	
Fluoroscein	Biotin (Goat)	1:100	Abcam	ab6655	
GFAP	Rabbit	1:500	Dako	Z0334	
Iba1	Rabbit	1:500	Wako Pure Chemical Industries	019-19741	

Ki67	Rabbit	1:200	Abcam	ab9160	ICC only
Ki67	Rabbit	1:200	Abcam	ab16667	ICC only
MBP	Rat	1:300	AbD Serotec (a Bio-Rad company)	MCA409S	
NF	Chicken	1:100	Covance	PCK592-P	
NG2	Mouse	1:200	Merck Millipore (formerly Chemicon)	MAB5384	ICC only
NG2	Rabbit	1:200	Merck Millipore (formerly Chemicon)	AB5320	ICC only
Nogo-A	Mouse	1:100	R&D Systems (a bio-techne brand)	MAB3098	
Olig2	Rabbit	1:100	Merck Millipore (formerly Chemicon)	ab9610	
Olig2	Rabbit	1:100	Atlas Antibodies (now Sigma-Aldrich)	HPA003254	
PCNA	Mouse	1:200	Dako	M0879	
PDGFR-β	Rabbit	1:100	Abcam	ab32570	
PLP	Mouse	1:200	Merck Millipore (formerly Chemicon)	MAB388	
ZO-1	Mouse	1:100	Life Technologies (now Thermo Fisher Scientific)	33-9100	

2.10.2 - Primary antibodies used for western blots

Name	**Species**	**Dilution**	**Company**	**Catalogue number**
ATP11B	Rabbit	1:250	Abcam	ab82640
Cldn5	Rabbit	1:1,000	Zymed (now Thermo Fisher Scientific)	34-1600
eNOS	Rabbit	1:1,000	Abcam	ab5589
GAPDH	Mouse	1:1,000	Merck Millipore	MAB374
Hsp90α	Mouse	1:1,000	Abcam	ab59459

2.10.3 - Secondary antibodies used

Species	**Host**	**Type**	**Dilution**	**Company**	**Catalogue number**
Chicken	Donkey	DyLight 488	1:1,000	Stratech Scientific	703-545-155
Goat	Donkey	Alexa Fluor 555	1:250	Invitrogen (now Thermo Fisher Scientific)	A12432
Goat	Donkey	DyLight 647	1:250	Stratech Scientific	705-605-147
Mouse	Donkey	Alexa Fluor 488	1:1,000	Invitrogen (now Thermo Fisher Scientific)	A21202
Mouse	Donkey	Alexa Fluor 568	1:1,000	Invitrogen (now Thermo Fisher Scientific)	A10037
Mouse	Donkey	Alexa Fluor 647	1:1,000	Invitrogen (now Thermo Fisher Scientific)	A31571
Rabbit	Donkey	Alexa Fluor 488	1:1,000	Invitrogen (now Thermo Fisher Scientific)	A21206

Rabbit	Donkey	Alexa Fluor 568	1:1,000	Invitrogen (now Thermo Fisher Scientific)	A10042
Rabbit	Donkey	Alexa Fluor 647	1:1,000	Invitrogen (now Thermo Fisher Scientific)	A31573
Rat	Donkey	DyLight 549	1:1,000	Stratech Scientific	712-505-153
Rat	Donkey	DyLight 650	1:1,000	Abcam	ab102263
Streptavidin	-	Alexa Fluor 488	1:1,000	Molecular Probes (now Thermo Fisher Scientific)	S32354
Streptavidin	-	IRDye 800CW	1:2,000	Li-Cor Biosciences	925-32230
Goat	Horse	ImmPRESS HRP	-	Vector	MP-7405
Mouse	Horse	ImmPRESS HRP	-	Vector	MP-7402
Mouse	-	ImmPRESS AP	-	Vector	MP-5402
Rabbit	-	ImmPRESS AP	-	Vector	MP-5401
Mouse	Sheep	ECL (HRP-linked)	1:10,000	GE Healthcare	NA934
Rabbit	Donkey	ECL (HRP-linked)	1:10,000	GE Healthcare	NA931

2.11 – Materials: list of primers

Name (gene, direction)	Sequence (5'->3')	Primer length	Product length
Arhgef1 forward	TGTTTACTCACCTTCCGCACC	21	
Arhgef1 reverse	CTTCTGGGTTCTGTTGGGTGG	21	659
Atp11b forward	AAAGGCTACCTACTTGGTTGGG	22	
Atp11b reverse	CAATACTCTCTTCCGCCCACAG	22	659
Col18a1 forward	AATAACGCAGATCCGGTCACTAA	23	
Col18a1 reverse	GTGACGGGAGAAGCTGAGAAC	21	797
Dpp3 forward	GGAGGGTGAAGGAAGGACTGA	21	
Dpp3 reverse	TGTGTGAGATGGTCTTGGGA	20	715
Jak3 forward	GGGAGGCGTGGCAATTAGTAAA	22	
Jak3 reverse	AGAAGAAATGCCTGGAGTCGC	21	626
Ltbp4 forward	AGACCGACCAGAGTTGGACC	20	
Ltbp4 reverse	GAGCGACCAGAGATCCTTGAG	21	614
Atp11b cDNA forward	CCGCAGAAGGAAATGACCCT	20	
Atp11b cDNA reverse	CTCCTGGCAAGCTGTCTCAA	20	916
Col18a1 cDNA forward	CGCTTTGGAGTCAACAGTTCC	21	
Col18a1 cDNA reverse	GCCTTTGGAACCCAGGTCAC	20	699
Jak3 cDNA forward	GGACCAGGGAGAGTTCCTGA	20	
Jak3 cDNA reverse	GTCGGAGAATGTAGGAGCCC	20	728
Ltbp4 cDNA forward	ACAATCTGGGAGTGTGCTGG	20	
Ltbp4 cDNA reverse	GATATGGCCAACCAGTGCCT	20	465

2.12 – Materials: list of kits and other chemicals

Reagent	Company	Product code
10x Phosphate buffered saline	Gibco (now Thermo Fisher Scientific)	70011-036
4-20% Tris-HEPES gels	Thermo Fisher Scientific	25224
Antibody array	Full Moon Biosystems	SET100
Antibody array reagents	Full Moon Biosystems	KAS02
Antibody diluent	Spring Bioscience	ADS-125
Antigen retrieval buffer	Vector	H-3300
BCA protein assay kit	Pierce (now Thermo Fisher Scientific)	23228 + 23224
Bovine serum albumin	Sigma-Aldrich	A7906
Bromophenol blue	Sigma-Aldrich	B8026
Calcium chloride	Sigma-Aldrich	C7902
dNTPs	Promega	U1240
ECL femto kit	Thermo Fisher Scientific	34094
ECL substrate	Thermo Fisher Scientific	80196
EDTA	Sigma-Aldrich	E5134
Ethanol	VWR International	20821.33
Euthatal	Merial	
Fluoromount	Southern Biotech	0100-01
Fluoroscein	Scientific Laboratory Supplies	CHE2032
Glycerol	Sigma-Aldrich	G5516
Glycine	Sigma-Aldrich	G7126
GoTaq Hot Start Polymerase	Promega	M5005
HEPES running buffer	Pierce (now Thermo Fisher Scientific)	10230064
Hoechst	VWR International	BTIU40045
iFX signal enhancer	Molecular Probes (now Thermo Fisher Scientific)	I36933
Kaleidoscope protein ladder	Bio-Rad	1610375
Methanol	Fisher Scientific	M/3900/17
NOS assay kit	Merck Millipore	482702
Optimal cutting temperature compound	CellPath	00.090.112
Paraformaldehyde	Sigma-Aldrich	P6148
Polyvinylidene fluoride membrane	Merck Millipore	IPVH00010
Potassium chloride	Fisher Scientific	P/4280/53
Protease inhibitor	Calbiochem	539134
Proteinase K	Promega	V3021
QIAquick PCR purification kit	Qiagen	28104
Radioimmunoprecipitation assay buffer	Pierce (now Thermo Fisher Scientific)	89900
RNeasy mini kit	Qiagen	74104
SDS	Sigma-Aldrich	5030
Sodium Chloride	Sigma-Aldrich	S7653

Sucrose	Sigma-Aldrich	84100
Sudan black	Sigma-Aldrich	199664
SuperScript First-Strand Synthesis System for RT-PCR	Invitrogen (now Thermo Fisher Scientific)	11904018
Tetramethylrhodamine-dextran	Sigma-Aldrich	42874-aG
Triton x-100	Fisher Scientific	BP151
Trizma base	Sigma-Aldrich	93352
Trizma hydrochloride	Sigma-Aldrich	T5941
Tween	Sigma-Aldrich	P9416
Vector Bloxall	Vector	SP-6000
Vector Blue	Vector	SK-5300
Vector NovaRED	Vector	SK-4800
Xylene	Fisher Scientific	X/0200/17
β-mercaptoethanol	Sigma-Aldrich	M7522

Chapter 3: What are the Early Pathological Changes in Small Vessel Disease: Descriptive Results

3.1 – Introduction

As detailed in Chapter 1, while cerebral small vessel disease (SVD) is becoming better known and more commonly diagnosed, the mechanisms of the disease are not well understood. Part of the problem lies with the fact that the disease is usually only identified in older patients with later stages of the disease, either because they are showing symptoms of the disease or they are undergoing a magnetic resonance imaging (MRI) scan for another reason. In terms of pathology, post-mortem studies to define these factors often use tissue from people who had clear signs of the disease in life, and so by necessity have a later, more developed stage of the disease. However, by looking at the changes which have occurred in patients with the symptomatic disease, researchers will overlook the fact that there are many changes which occur much earlier in the disease course, which can be present without any symptoms (Vermeer et al., 2007).

The first aim of this chapter is therefore to identify the changes which occur in the brain at an early, presymptomatic stage of SVD. This is achieved by studying brain tissue from people who have shown no signs of SVD or hypertension in life, but whose brains were found to have pathological hallmarks of SVD upon post-mortem examination. This tissue is likely to present an earlier, less developed stage of the disease than the tissue from hypertensive patients presenting symptoms of SVD which is more commonly studied. The samples used for this project are from the Edinburgh Sudden Death Brain Bank, part of the MRC Brain Banks (details in chapter 2.8). I am using blocks from subcortical regions of the frontal lobes of five brains of people who showed no symptoms of SVD, however their brains showed pathological signs of SVD upon post-mortem examination. As controls, blocks from five age-matched people with no pathological signs of SVD are used.

Identification of these early pathological changes, however, can only take us so far. While this will allow us to say which changes arise early in the disease course, it will neither give us an idea of which of these occurs first, nor inform us of any changes

which occur in the brain prior to the appearance of classical pathological hallmarks. It is this order of changes which can prove crucial to elucidating the mechanism.

The second aim of this chapter is therefore to understand the order in which these early changes occur. One way to do this would be to study human post-mortem tissue with different severities of classical SVD pathology, defining more severe pathology as being a later stage of the disease. However, the spontaneous nature of SVD means that we cannot currently predict who will go on to develop the disease, or at what rate. Consequently we cannot study changes which occur prior to the development of classic SVD pathology as we cannot know when studying a particular post-mortem specimen whether that particular individual would have gone on to develop SVD.

To overcome this we need an animal model where we know that all individuals in a population will go on to develop SVD at the same rate. With such a model we can study animals at different ages and so discern the order in which early pathological changes are occurring. The model we are using is the Stroke Prone Spontaneously Hypertensive Rat (SHRSP; which for ease I will refer to as Disease Model rat; DM). As described previously (chapter 1.8.3), the SHRSP develops hypertension from six to twelve weeks (Yamori and Horie, 1977), shows classical pathological hallmarks of human SVD from eight weeks and starts suffering strokes from twenty weeks of age (Bailey et al., 2011a; Lin et al., 2001; Yamori et al., 1976). This model appears to be the most relevant model of SVD after extensive systematic review (Bailey et al., 2009, 2011a; Hainsworth and Markus, 2008). As we are interested in the early, presymptomatic changes which are independent of hypertension, we are using animals at three, four and five weeks of age as this is prior to the development of hypertension or classical SVD pathology. As detailed in chapter 1.8.3, few investigations have studied the SHRSPs at this young age, with the only significant finding being a lower total level of claudin-5 in the deep grey and white matter of SHRSP basal ganglia at five weeks of age (Bailey et al., 2011b). As controls, we have Wistar Kyoto rats (WKY; Control), the parent strain of the SHRSP, from a colony maintained in parallel with the SHRSP colony.

The key radiological features of SVD are blood brain barrier (BBB) leakage, white matter hyperintensities (WMH), and enlarged perivascular spaces (PVS) (Wardlaw et

al., 2013a, 2013b). Therefore my initial investigation was to look at molecular correlates of these features and see what changes, if any, I would find. For the BBB, I looked at the different components involved: endothelial cells (ECs), pericytes, astrocytes and tight junction proteins (TJPs) which hold the ECs tightly together (chapter 1.4.2). Specifically, I looked at levels of claudin-5 as this is the tightest TJP and a loss of this protein alone results in severe BBB leakage (Nitta et al., 2003). Enlarged PVS are believed to be caused by a build-up of both fluid and macrophages in the perivascular space between ECs and astrocytes (Doubal et al., 2010). Therefore I studied the number of macrophages and microglia in the brain, which also gives an indication of an inflammatory response. WMH are caused by a loss of white matter, which is composed of myelin producing oligodendrocytes (chapter 1.5). Therefore I looked at myelin levels and the balance between mature, myelinating oligodendrocytes and their precursors, immature oligodendrocyte precursor cells (OPCs). All of these factors were investigated in the first instance by immunohistochemistry on paraffin embedded tissue (see chapter 2.3), which maintains vascular integrity, from the deep white matter around the basal ganglia in the rats and from the frontal lobe in the human cases, as this is where SVD pathology has previously been described both in humans and in this rat model.

3.2 – Results of tissue staining

3.2.1 - BBB tight junctions (TJs)

I found a number of changes in both rat and human diseased tissue compared to control. The first of these to occur in the rat model of the disease was a significant reduction in the number of blood vessels with claudin-5 tight junctions (TJs) compared to age matched controls from three weeks of age (3% ± 0.01% less; mean ± SEM; $p<0.01$, unpaired t-test; n=4; **Figure 3.1 A-F & I, Figure 3.2 A-B**). This is correlated with a similar significant reduction seen in diseased human brains compared to control (6% ± 0.1% less; $p<0.01$, unpaired t-test; n=5; **Figure 3.1 G-I**). Using a western blot, I also showed that there were significantly lower levels of claudin-5 protein in the deep white and grey matter of five week old DM rats (28% ± 3% less; $p<0.05$, unpaired t-

test; n=3; **Figure 3.2 C-D**). This confirms the lower total claudin-5 levels seen at this age in a previous study (Bailey et al., 2011b).

These data show a structural weakness in the BBB in both the DM rat and the diseased human brains. However, this does not demonstrate a functional problem of BBB leakage. This has previously been shown in human disease cases as leakage of gadolinium tracer observed on MRI (**Figure 3.3 C**; Wardlaw et al., 2013b). To investigate this in the rat I perfused a mixture of sodium fluorescein (376 Da), a green fluorescent molecule so small that a slight perturbation in the BBB would allow it to leak out (though this is smaller than the presumed BBB pore size of 800 Da, its charge means that it cannot pass through an intact BBB (Kaya and Ahishali, 2011)), and tetramethylrhodamine-isothiocyanate-dextran (40 kDa), a red fluorescent protein so large that it would remain within the blood vessel, into five week old rats and observed their brains. I found that the small fluorescent molecule leaks out of the BBB and diffuses into the parenchyma in five week old DM rats, whereas it remains entirely within the blood vessel in the control rats (**Figure 3.3 A-B**).

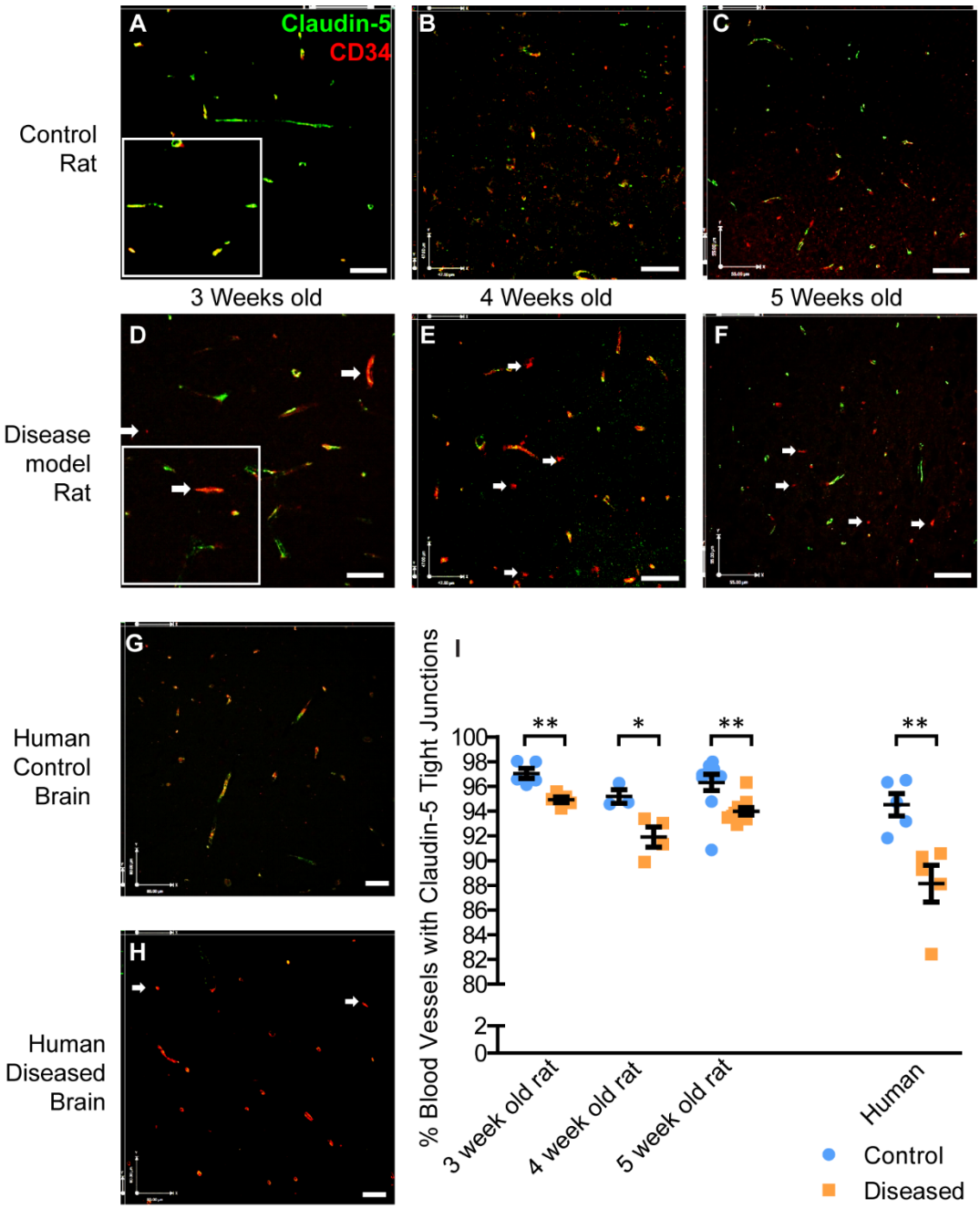


Figure 3.1: Fewer blood vessels with Claudin-5 positive tight junctions from 3 weeks of age in disease model rats and in human brains with SVD. Fluorescent images showing claudin-5 positive tight junctions (TJs; green) on blood vessels (stained with CD34; red) in the deep white matter of brains from control rats (A-C) and disease model rats (D-F) at the ages of 3 weeks (A, D), 4 weeks (B, E) and 5 weeks (C, F), and from control (G) and diseased (H) human brains. White arrows (D-F, H) indicate blood vessels without claudin-5 positive TJs. White boxes (A, D) represent areas which are shown magnified in **Figure 3.2 A-B**. Quantification of the percentage of blood vessels without claudin-5 TJs (I) shows that there are significantly fewer blood vessels with claudin-5 TJs at all ages from 3 weeks in the disease model rats (orange) compared to controls (blue), and in the diseased human brains compared to controls (Mean ± SEM; **: $p<0.01$, *: $p<0.05$, unpaired t-test; 3wk: n=5; 4wk: n=3; 5wk: n=10; human: n=5). Scale bar = 50µm.

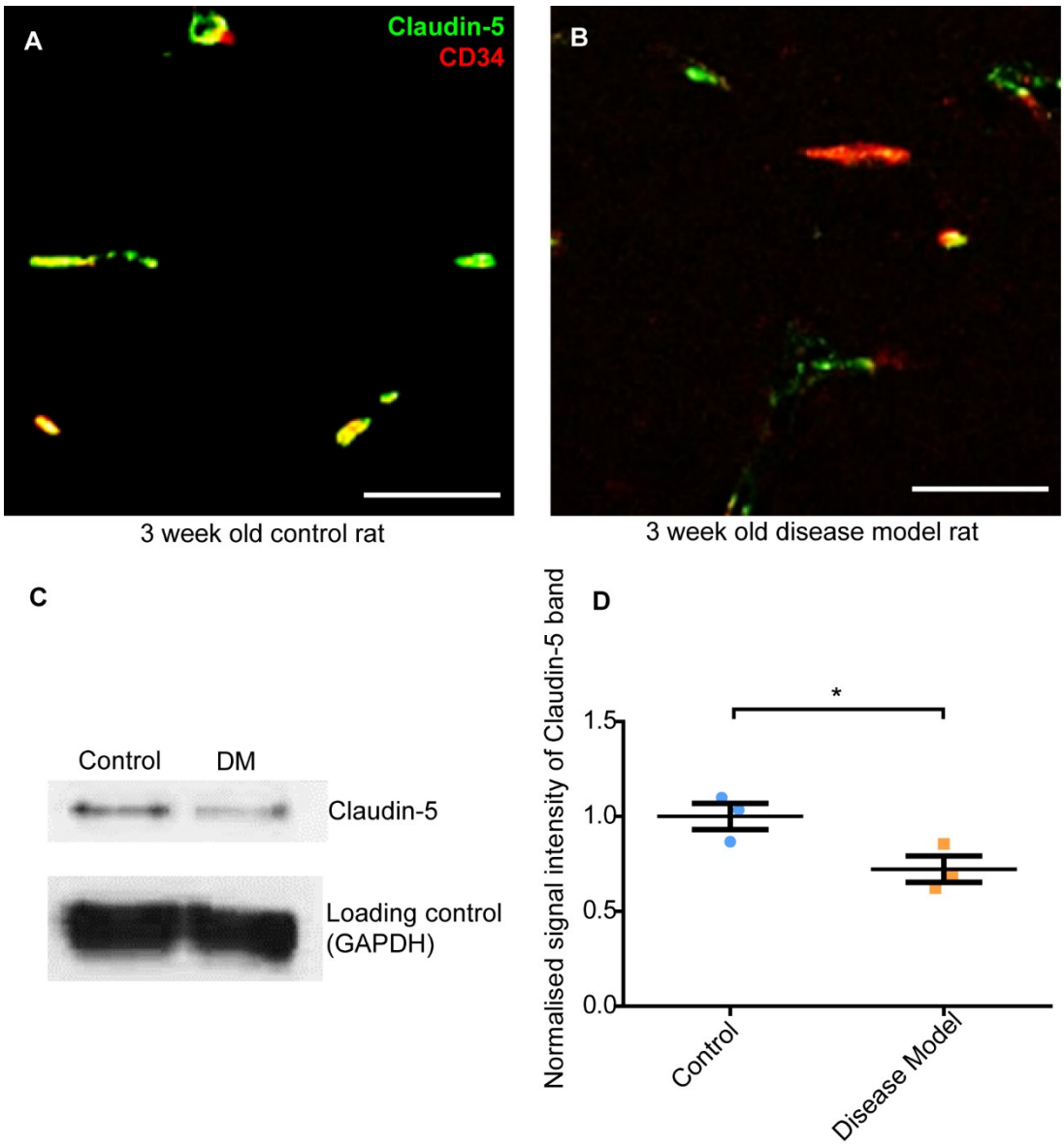


Figure 3.2: Lower levels of claudin-5 protein in the brains of disease model (DM) rats. A-B: fluorescent images showing claudin-5 positive tight junctions (TJs; green) on blood vessels (stained with CD34; red) in the deep white matter of brains from 3 week old control (A) and disease model rats (B). Images are magnified regions of **Figure 3.1 A & D**. C: Western blot showing lower levels of total claudin-5 protein in the brains of 5 week old DM rats compared to controls, indicated by a weaker band in the right hand lane. Also shown is a loading control, demonstrating that the protein gel was loaded evenly. D: Quantification of all western blots to measure total claudin-5 levels. Data are presented as the signal of the claudin-5 band divided by the loading control, normalised to the control levels for that western blot. This shows that there is significantly less claudin-5 in the disease model rats (orange) compared to controls (blue) (Mean ± SEM; *: $p<0.05$, unpaired t-test; n=3). Scale bar = 25µm.

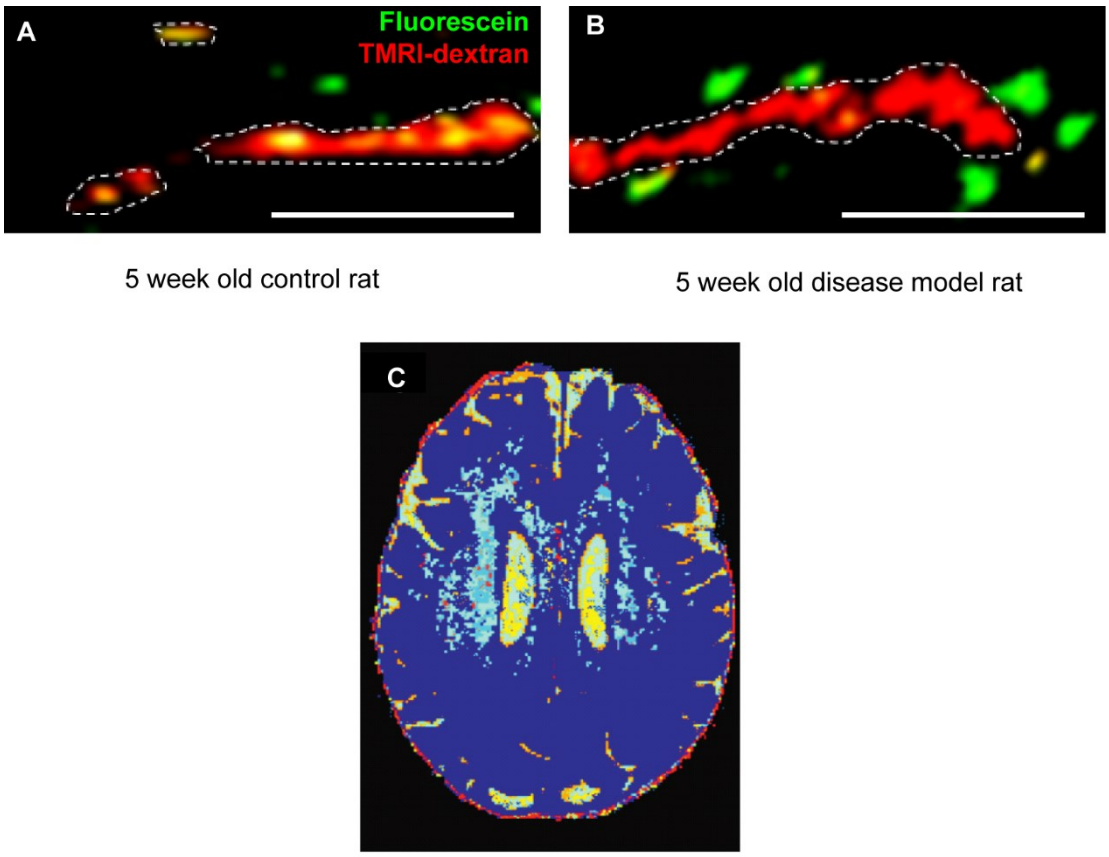


Figure 3.3: Extravasation of tracers shows a functional impairment of the blood brain barrier (BBB). A-B: Fluorescent images showing sodium fluorescein, a small (376 Da) tracer molecule (green), and tetramethylrhodamine-isothiocyanate dextran (TMRI-dextran), a large (40 kDa) tracer molecule (red). Images show blood vessels from five week old control (A) and disease model (B) rat brains fixed immediately after perfusion with a mixture of both tracers. The boundaries of the blood vessels are outlined with dashed white lines. In the control rat both tracers remain within the blood vessel, appearing yellow (A), whereas in the disease model rat the smaller green tracer leaks out through an impaired BBB. The small areas of green in A are background fluorescence. This demonstrates a size-selective loosening of the BBB. C: Colour mapping of cerebrovascular permeability after intravenous administration of a gadolinium tracer in a human with small vessel disease (SVD). Dark blue indicates areas of low vascular permeability, while light blue, yellow and red indicate increasing permeability. The light blue regions show areas where the gadolinium tracer is leaking out of the blood vessels due to an impaired BBB (adapted from Wardlaw et al., 2013b). This indicates a functional impairment of the BBB in humans with SVD. Scale bar = 10μm.

3.2.2 - OPCs

The second change to occur in the DM rat is a significant increase in the number of OPCs compared to controls from four weeks of age. This would normally be quantified using a marker of OPCs, such as platelet derived growth factor receptor alpha (PDGFRα) or neural/glia antigen 2 (NG2) (chapter 1.5.2), however these do not work successfully on paraffin embedded or human tissue. I therefore chose to quantify OPCs using a previously published method, by counting the number of cells which are Olig2 positive (an oligodendroglial lineage marker) but Nogo-A negative (a marker of mature oligodendrocytes; **Figure 1.5**) (Kuhlmann et al., 2007). Using this technique, I found that there was a significant increase in the number of OPCs in DM rats compared to controls from four weeks of age (186% ± 25% more; $p<0.05$, unpaired t-test; n=3; **Figure 3.4 A-F & I**). This change is also seen in the diseased human brains compared to controls (190% ± 20% more; $p<0.01$, unpaired t-test; n=5; **Figure 3.4 G-I**). There are two likely possible explanations for this increase: the OPCs are proliferating more, or there is a block preventing the OPCs from differentiating into mature oligodendrocytes. To study this I looked at levels of OPC proliferation by expression of proliferating cell nuclear antigen (PCNA), which labels cells exclusively during the DNA synthesis phase (s-phase) of the cell cycle. This marker was used as antibodies against it work robustly in paraffin fixed tissue. I found that there were more proliferating OPCs in both the DM rat and diseased human brains compared to controls (Rat: 66% ±5% more, human: 191% ± 46% more; $p<0.05$, unpaired t-test; rat: n=10, human n=5; **Figure 3.5 A-E**). I also found that there were fewer mature oligodendrocytes by counting the number of Nogo-A positive cells (Rat: 7% ± 0.1% less, human: 18% ± 1% less; rat: $p<0.01$, human: $p<0.05$, unpaired t-test; rat: n=3, human: n=5; **Figure 3.4 A-H & Figure 3.5 F**). Together, these data show that there is an early increase in OPC number caused by both proliferation of OPCs and a block in their maturation.

The other aspect of white matter changes is myelin. The optimal method to study the level of myelination would be to immunostain for a marker of axons, such as neurofilament (NF), and a marker of myelin, such as myelin basic protein (MBP), one of the key structural components of compact myelin. From this I would be able to quantify the amount of axonal myelination, rather than simply the amount of myelin

in a given region. Unfortunately, I was not able to find a robust axonal marker for paraffin embedded rat tissue. I therefore chose to stain for MBP alone, and quantify the total levels of MBP. I found that there is significantly less MBP in the DM rats at five weeks, but not at earlier ages (20% ± 0.1% less; $p<0.01$, unpaired t-test; n=4; **Figure 3.6**). The fact that myelin appears normal at earlier ages, but not at five weeks, suggests that the lower levels of myelin are due to myelin degradation, rather than due to abnormal myelin development which would be completed by three weeks of age. The fact that this myelin degradation occurs after the loss of mature oligodendrocytes (at five weeks compared to at four weeks) suggests that it is the loss of oligodendrocytes which causes a loss of myelin, rather than a direct effect on the myelin sheaths.

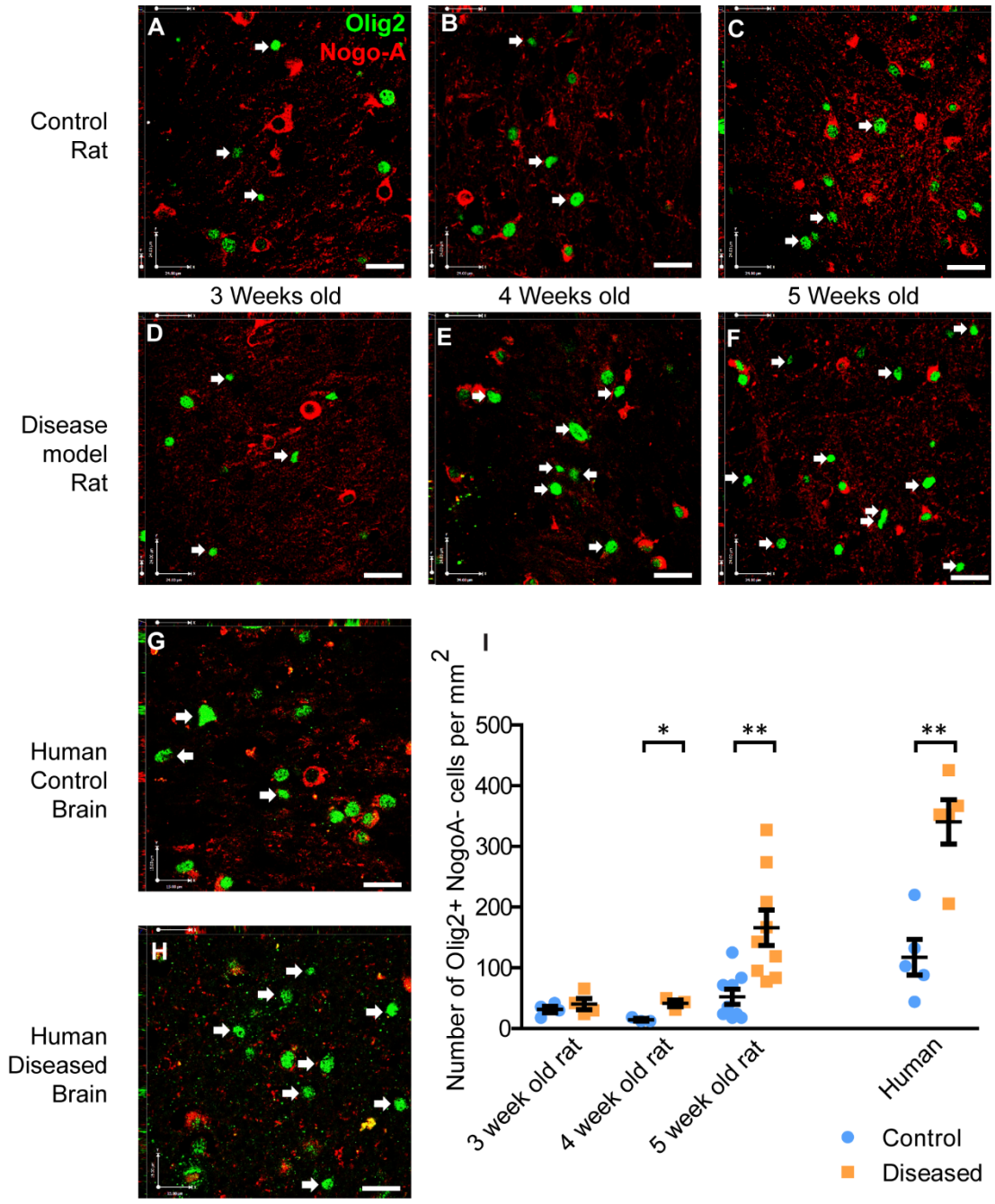


Figure 3.4: More oligodendrocyte precursor cells (OPCs) from 4 weeks of age in disease model rats and in human brains with SVD. Fluorescent images showing Olig2, a nuclear marker of the entire oligodendroglial lineage (green), and Nogo-A, a marker of mature oligodendrocytes (red), in the deep white matter of brains from control rats (A-C) and disease model rats (D-F) at the ages of 3 weeks (A, D), 4 weeks (B, E) and 5 weeks (C, F), and from control (G) and diseased (H) human brains. White arrows indicate OPCs as cells with an Olig2 positive nucleus but no perinuclear Nogo-A. Quantification of the number of OPCs per mm^2 (I) shows that there are significantly more OPCs at all ages from 4 weeks in the disease model rats (orange) compared to controls (blue), and in the diseased human brains compared to controls (Mean ± SEM; **: $p<0.01$, *: $p<0.05$, unpaired t-test; 3wk: n=4; 4wk: n=3; 5wk: n=10; human: n=5). Scale bar = 25µm.

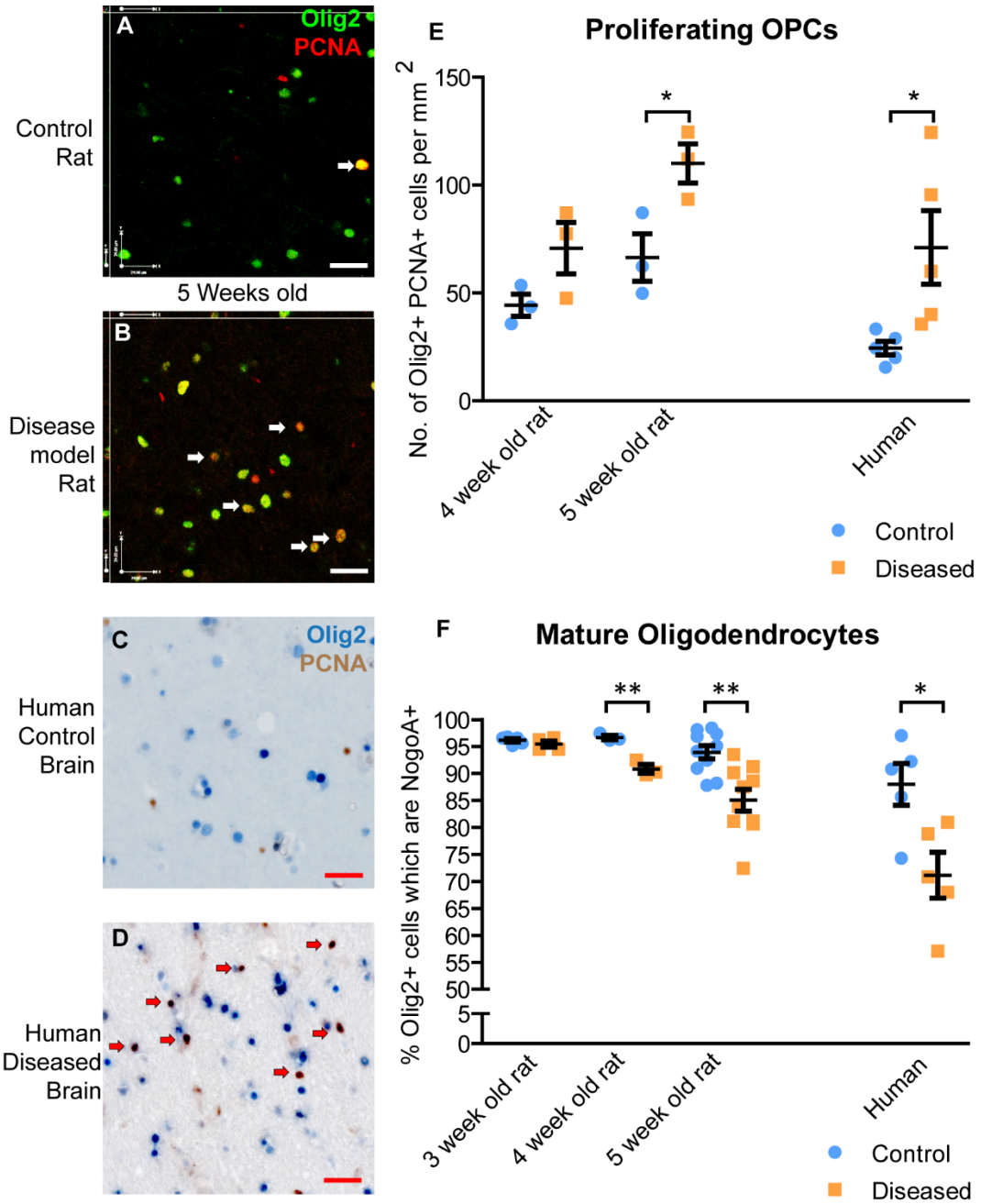


Figure 3.5: Increased number of oligodendrocyte precursor cells (OPCs) due to increased OPC proliferation and fewer mature oligodendrocytes. A-B: Fluorescent images showing Olig2, a nuclear marker of oligodendroglia (green), and proliferating cell nuclear antigen (PCNA), a marker of proliferating nuclei (red), in the deep white matter of brains from 5 week old control rats (A) and disease model rats (B). C-D: Images showing colorimetric staining of Olig2 (blue) and PCNA (brown) in the frontal white matter of control (C) and diseased (D) human brains. Arrows indicate proliferating OPCs as cells expressing both Olig2 and PCNA in their nuclei. E: Quantification of the number of proliferating OPCs per mm^2 shows a trend increase in the number of proliferating OPCs at 4 weeks in the disease model (DM) rats (orange) compared to controls (blue), with a significant increase at 5 weeks in the DM rats and in the diseased human brains (DHBs) compared to controls (Mean ± SEM; *: $p<0.05$, unpaired t-test; rat: n=3; human: n=5). F: Quantification of the percentage of oligodendroglia which are mature oligodendrocytes (cells which are double positive for both Olig2 and Nogo-A in **Figure 3.3 A-H**) shows signifantly fewer mature oligodendrocytes at all ages from 4 weeks in the DM rats and in the DHBs (orange) compared to controls (blue). (Mean ± SEM; **: $p<0.01$, *: $p<0.05$, unpaired t-test; 3wk: n=4; 4wk: n=3; 5wk: n=10; human: n=5). Scale bar = 25µm.

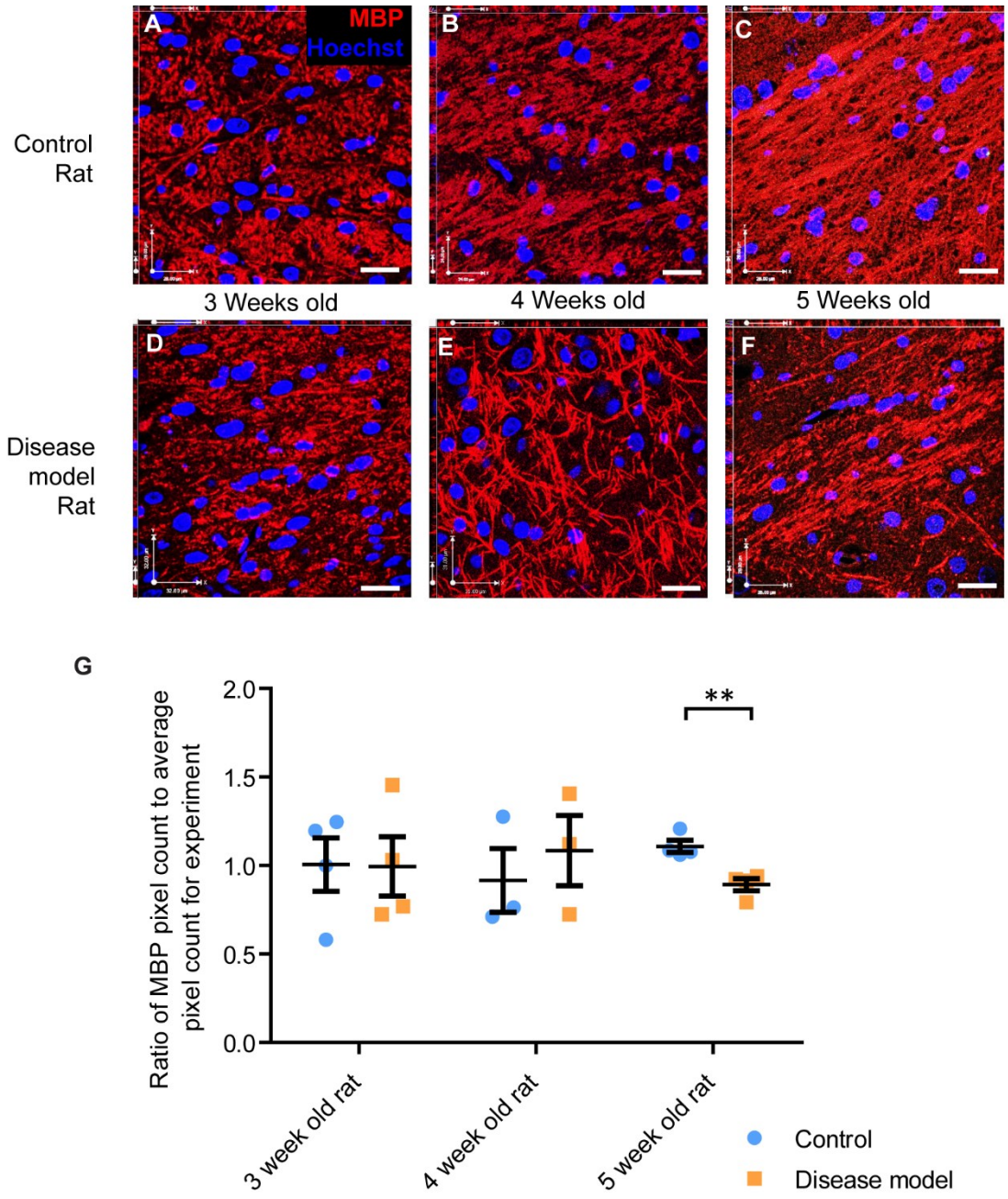


Figure 3.6: More myelin from 5 weeks of age in disease model rats. Fluorescent images showing Myelin Basic Protein (MBP), a component of myelin (red), and Hoechst, a marker of cell nuclei (blue), in the deep white matter of brains from control rats (A-C) and disease model rats (D-F) at the ages of 3 weeks (A, D), 4 weeks (B, E) and 5 weeks (C, F). Quantification of the ratio of MBP pixel count to the average pixel count for the experiment (G) shows that there is significantly less myelin at 5 weeks in the disease model rats (orange) compared to controls (blue) (Mean ± SEM; **: $p<0.01$, unpaired t-test; 3wk: n=4, 4wk: n=3, 5wk: n=4). Scale bar = 25µm.

3.2.3 - Macrophages/microglia

The third change that I observe in the DM rat is a significant increase in the number of microglia and macrophages (counted as the number of cell bodies) compared to controls at the age of five weeks, as measured by the number of ionised calcium binding adapter molecule 1 (Iba1) positive cells (73% ± 7% more; $p<0.001$, unpaired t-test; n=10; **Figure 3.7 A-F & I**). Iba1 was used as it is a robust marker of all macrophages and microglia in rats. However, in human tissue Iba1 can often stain astrocytes as well as macrophages/microglia. I therefore used the marker CD68 in human tissue. While this does not mark exactly the same cells, as it marks activated macrophages/microglia, it still provides a reasonable comparison. There was also an increase in the number of microglia/macrophages as measured by the number of CD68 positive cells in diseased human brains compared to controls (175% ± 32% more; $p<0.05$, unpaired t-test; n=5; **Figure 3.7 G-I**).

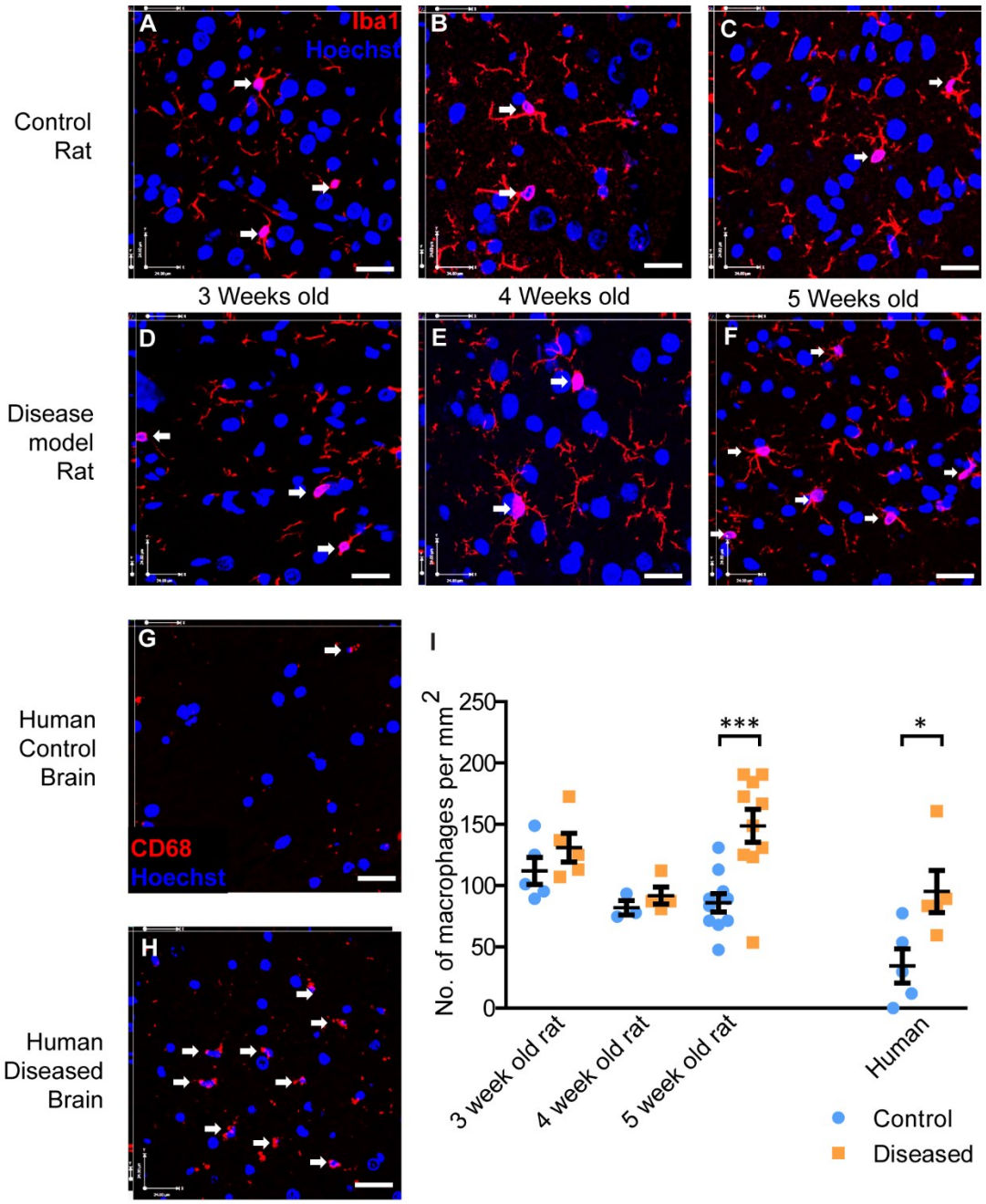


Figure 3.7: More macrophages/microglia at 5 weeks of age in disease model rats and in human brains with SVD. Fluorescent images showing Iba1 (rats) and CD68 (human brains), markers of all macrophages and microglia (red), and Hoechst, a nuclear marker (blue), in the deep white matter of brains from control rats (A-C) and disease model rats (D-F) at the ages of 3 weeks (A, D), 4 weeks (B, E) and 5 weeks (C, F) and from control (G) and diseased (H) human brains. White arrows indicate macrophages/microglia as cells with an Iba1 or CD68 positive cell body (around the nucleus). Quantification of the number of macrophages/microglia per mm^2(I) shows that there are significantly more macrophages/microglia at 5 weeks in the disease model rats (orange) compared to controls (blue), and in the diseased human brains compared to controls (Mean ± SEM; ***: $p<0.001$, *: $p<0.05$, unpaired t-test; 3wk, 4wk: n=4; 5wk: n=10; human: n=5). Scale bar = 25µm.

3.2.4 - Other components of the BBB

There are a number of other features of the BBB which I studied, but which I found to not show any differences between DM rats and controls at any age, or between diseased human brains and controls. As detailed in chapter 1.4.2, one of the other key features of the BBB is the glia limitans, formed by the astrocyte endfeet. I found that there was no difference in total astrocyte density, measured as the pixel count of glial fibrillary acidic protein (GFAP) normalised to the staining intensity for each experiment (**Figure 3.8 A-C**), or the number of blood vessels with astrocyte endfeet, measured using aquaporin 4 (AQP4), a water channel expressed exclusively on astrocyte endfeet (**Figure 3.8 D**). I also described the importance of pericytes in maintaining the BBB phenotype, however I found no difference in the number of blood vessels with pericytes around them (**Figure 3.8 E-F**). These data suggest that the alterations I see in the BBB TJs are induced by changes in the blood or the endothelial cells (ECs), and are not caused due to a loss of astrocyte endfeet or pericytes.

Another feature which might be expected to change with BBB alterations is blood vessel number, however I found no difference in the total number of blood vessels between DM rats/diseased human brains and controls (**Figure 3.1 A-H & Figure 3.8 G**).

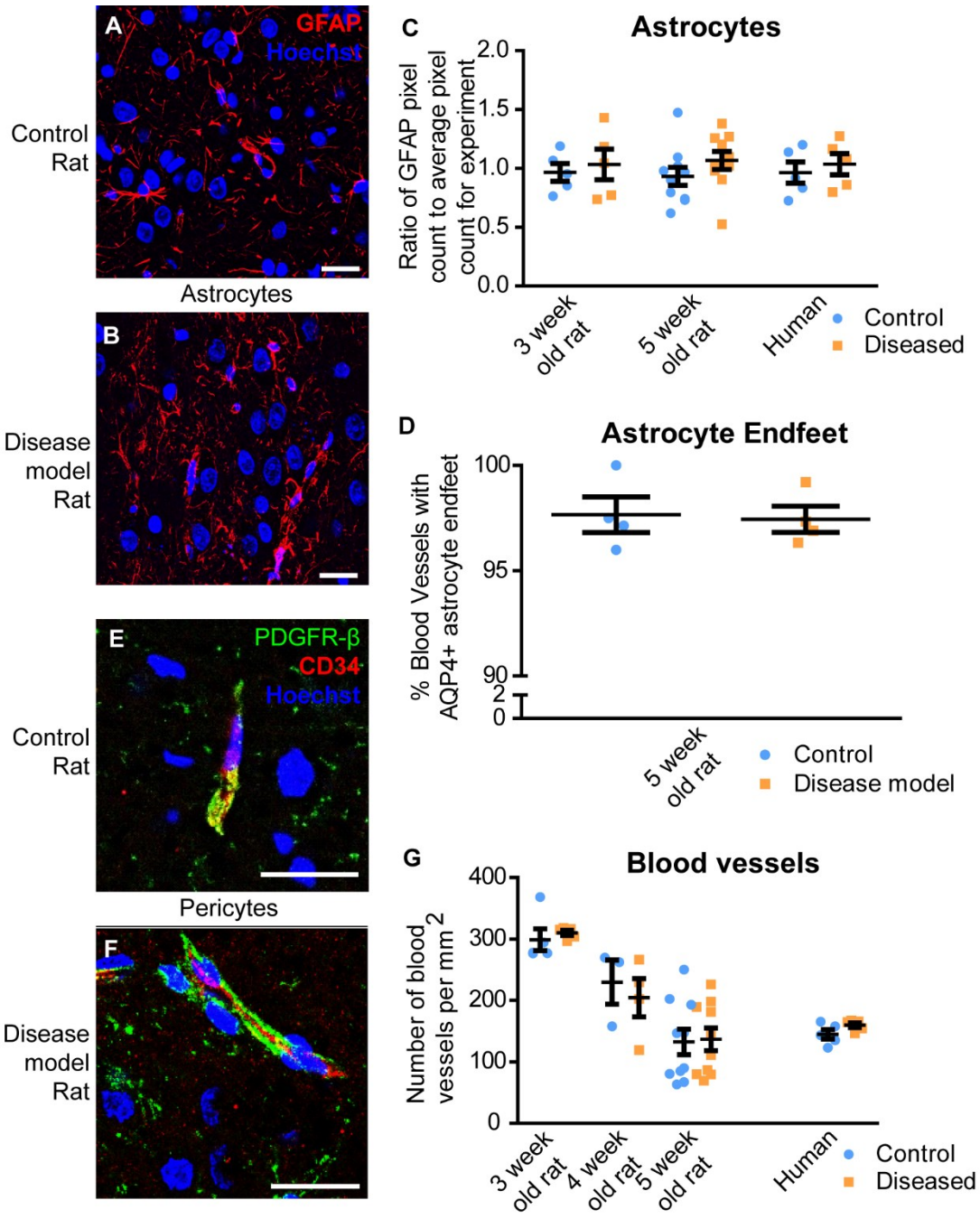


Figure 3.8: No difference in coverage of astrocytes or pericytes, or in blood vessel number. A-B: Fluorescent images showing GFAP, a marker of astrocytes (red), and Hoechst, a nuclear marker (blue), in brains from 4 week old control (A) and disease model (DM) (B) rats. The high density of astrocyte processes makes counting the number of cells unreliable, however, pixel counts of the total amount of GFAP staining, normalised to the average level of staining for each experiment, showed no difference between control and DM rats (C) (Mean ± SEM; 3wk: n=5; 5wk: n=10; human: n=5). D: Quantification of the percentage of blood vessels with aquaporin 4 (AQP4) positive astrocyte endfeet around them shows no difference between DM rats (orange) and controls (blue) (Mean ± SEM; n=4). E-F: Fluorescent images showing PDGFR-β, a marker of pericytes (green), CD34, a marker of endothelial cells (red), and Hoechst, a nuclear marker (blue), in brains from 5 week old control (E) and DM (F) rats. Pericytes can be seen immediately surrounding blood vessel endothelial cells with normal morphology in both control (E) and DM (F) rats. G: Quantification of the number of blood vessels per mm^2 in brains (from images in **Figure 3.1**) shows no difference between DM rats/ diseased human brains (orange) and controls (blue) (Mean ± SEM; 3wk: n=5; 4wk: n=3; 5wk: n=10; human: n=5). Scale bar = 25μm.

3.3 – Discussion I

3.3.1 - BBB changes

The first results that I have shown in this chapter are that from three weeks of age in DM rats, and in human brains with SVD, there is a reduction in the number of blood vessels with claudin-5 TJs, demonstrating a structural loss of BBB integrity (**Figure 3.1**). As I described in the introduction to this chapter, claudin-5 was used as it has been shown that it is the tightest of the TJPs, and that a loss of this TJP alone is sufficient to induce leakage of the BBB (Nitta et al., 2003). While there are other TJPs which compose the BBB (detailed in chapter 1.4.2), studying these would not be as informative. Looking at levels of other TJPs, such as zonula occludens 1 (ZO-1) or occludin, may give us an idea of the extent of the structural damage to the BBB – if the blood vessels in DM rats had lower levels of other TJPs as well as claudin-5, that would suggest that the loss of BBB integrity was more severe. This, however, can be more elegantly demonstrated functionally. As I showed in **Figure 3.3**, the weakening of the BBB in DM rats is size-selective – small molecules (~400 Da) can pass through, but not larger ones (40 kDa). This suggests that the BBB is still partially intact, but it is weaker.

My tracer experiment to investigate the functional impairment of the BBB does have some limitations. I only carried out this experiment on five week old rats, and did not look at younger ages where I also see a structural impairment of the BBB. This was due to technical difficulties – with a smaller animal it is more difficult to ensure that the tracer is not being perfused at such a high pressure that it is simply forced out of the blood vessel. Unfortunately, this means that we cannot tell if the structural impairment of the BBB seen at younger ages also correlates with a functional impairment of the BBB at these ages.

I detailed in chapter 1.8.3 that the only significant change which has previously been shown at a young, prehypertensive age in these DM rats is a decrease in claudin-5 (Bailey et al., 2011b). In this study, the authors looked at rat brains at five, sixteen and twenty-one weeks of age and quantified the total immunoreactivity to claudin-5 by immunohistochemistry, finding reduced levels of claudin-5 at all ages. This essentially measures the total level of protein, and is confirmed by my results showing that total

claudin-5 levels in the basal ganglia of DM rats are lower by western blot (**Figure 3.2 C-D**). This approach is limited, as it does not discern between a generalised, small reduction of claudin-5 levels in all blood vessels, and a large reduction of claudin-5 in some vessels with normal levels in others. My data expands upon this previous study by not only studying the rat at earlier time points, but also demonstrating that the reduction in total claudin-5 is as a result of there being more blood vessels with a complete absence of claudin-5. This resembles other vascular pathologies of SVD, where severe changes are seen in a few blood vessels rather than minor changes in all blood vessels.

3.3.2 - OPC changes

The next results I showed in this chapter were that from four weeks of age in the DM rats there is an increase in the number of OPCs, correlated with an increase in OPC proliferation and a reduction in the number of mature oligodendrocytes (**Figure 3.4-3.5**). I also demonstrated that there are reduced levels of myelin from five weeks of age in the DM rats (**Figure 3.6**). These fit in with the later white matter damage seen in human SVD, both on histopathology (chapter 1.2.1) and radiology (chapter 1.3.3), and suggests that the origins of this damage occur much earlier in the disease course than previously thought. The order of these changes suggests that a loss of mature oligodendrocytes causes the loss of myelin. The proliferation of OPCs may be as a response to this loss of oligodendrocytes, as is seen in other demyelinating diseases (see chapter 1.5.4). In normal circumstances you would expect these extra OPCs to differentiate into mature oligodendrocytes to remyelinate the axons. However, despite this increased number of OPCs, there is still a reduced number of mature oligodendrocytes, suggesting that the OPCs are unable to differentiate normally to remyelinate the axons.

In the rat brain, basal ganglia areas are described as being fully myelinated by the age of three weeks (Downes and Mullins, 2013). Thus, the timing of the myelin changes in the DM rat suggests that there is a loss of myelin by degradation, rather than a developmental problem with myelin formation which would be predicted to be measurable prior to five weeks. As I stated in section 3.2.2 however, my method of

quantifying the total amount of MBP is not the best way to assess this. This method is very sensitive to small technical variations – cutting the tissue block at a slightly different angle or a slightly different location could vastly alter the appearance of myelin density. As stated previously, a better technique would be to stain both myelin and axons, and to quantify the ratio between myelinated axons and unmyelinated axons. This would mitigate any effects of technical variation as in areas of similar myelination an increased amount of myelin would correspond with an increased number of axons. Thus, it could be that myelin differences between DM and control rats appear at earlier ages, which would support the idea that the myelin changes are a defect of myelin formation, but my technique for quantifying myelin is not sensitive enough to pick these up.

To definitively confirm whether myelin is degraded, rather than not developing properly, a loss of myelin could also be quantified by looking for myelin debris. I have tried one antibody apparently specific for myelin debris (Anti-MBP; Merck Millipore; AB5864), but was not able to get it to work on this tissue. There are, however, other antibodies available against myelin debris (e.g. SMI-94; Covance; 836501), and it would be interesting to try these out as well. If DM rats show increased levels of myelin debris at five, or even four, weeks of age, this would further support the theory that the changes I see in OPCs and myelin are indicative of myelin degradation.

3.3.3 - Macrophage/microglia changes

The third set of results I showed demonstrated an increased number of macrophages/microglia in DM rats at five weeks of age, and in diseased human brains. This corresponds with the later increase in macrophages seen on histopathology in human SVD, both in the walls of diseased blood vessels and in lacunar lesions (chapter 1.2.3). These changes could be linked to the OPC changes described above (3.3.2). It has been shown that macrophages/microglia are recruited to areas of demyelination to remove the debris and enable remyelination (see chapter 1.5.4). The macrophages/microglia in the DM rats could be carrying out a similar function. It is also possible that the increased numbers of macrophages/microglia are due to the increased permeability of the BBB – a weaker BBB allows more macrophages from

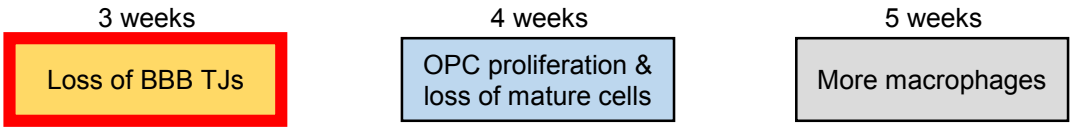
the periphery to enter the brain parenchyma. As the cells recruited to an injury site may be a mixture of both resident microglia and peripheral macrophages, it would be interesting to distinguish these two possibilities. If the increase was due entirely to an increased number of peripheral macrophages, this would suggest that the increase was due to the greater intrusion of these through the damaged BBB. If, however, the increase was caused by both macrophages and microglia, it would suggest that this was caused by increased recruitment and proliferation of these cells. As there is no clear marker to distinguish between macrophages and microglia, this could be achieved by ablating the source of periphery macrophages, the bone marrow, at a young age and repopulating it with fluorescently tagged cells, similarly to a previously published study (Schilling et al., 2003). Thus, any macrophages/microglia seen in the brain with a fluorescent tag would be from the periphery.

As well as an increase in the number of macrophages/microglia, there may also be a change in their activation state. Macrophages/microglia have polarised activated states and can be either pro-inflammatory (sometimes known as M1) or pro-regenerative (sometimes known as M2). The balance between the numbers of such cells in these two states can help explain the pathology – whether the macrophages/microglia are contributing to the damage of the disease, or are helping to repair it. Unfortunately, the antibodies marking these activation states do not work robustly in paraffin embedded tissue, and as yet I have been unable differentiate between these activation states.

3.3.4 - Mechanisms

All of the changes detailed in this chapter were found in both the rat model of the disease and in human brains with an early stage of SVD, though the rat model enabled us to determine the order in which the abnormalities appear. The human data adds weight to the evidence that SHRSP is a valuable model of SVD, and suggests that the changes observed here are not merely artefacts of this specific model.

The data above show that in the rat model of SVD changes occur in the following order:



This order of changes can provide us with clues as to the mechanism of development of SVD. The order of changes, with firstly an early loss of the BBB TJs, suggests that early BBB leakage might be having a causative effect, leading to the other changes. A compromised BBB would allow toxic blood components through into the brain parenchyma. As detailed in chapter 1.4, there are many reasons these are normally kept out of the brain parenchyma, and if allowed in they could do significant damage. These toxic blood components could damage mature oligodendrocytes, leading to the loss of mature oligodendrocytes and myelin described in this chapter. In response to this, we could see an increase in OPC proliferation and macrophage/microglia recruitment, as is seen in other demyelinating diseases (see chapter 1.5.4).

The differences shown here in the DM rat all occurred at ages up to five weeks. This is before the blood pressure (BP) of the DM rat starts rising compared to control rats. This suggests that the changes observed are independent of hypertension and cannot be caused by it as they predate this BP rise, despite many people theorising that hypertension is the primary cause of SVD (chapter 1.7.1). However, early variations in BP between the different rat strains, too small to reliably measure, could still be having an effect. Despite the evidence here, this high blood pressure may still directly cause damage to the brain parenchyma, or indirectly cause damage by damaging the BBB TJs and increasing BBB permeability.

To determine whether either leakage of toxic blood products through a damaged BBB or hypertension are involved in producing this phenotype, I used a model which could completely exclude the effect of BBB leakage and hypertension by removing blood flow completely – the slice culture model.

3.4 – The slice culture model

The slice culture model is well documented as a method of growing sections of brain tissue *in vitro* while maintaining their normal tissue microenvironment (Zhang et al., 2011). It has many advantages over *in vivo* work, allowing multiple sections to be

independently grown from each animal, and far easier manipulation of the tissue. It also has many advantages over *in vitro* single cell cultures as the three dimensional (3D) structure of the brain is maintained with all of the cells present. The extraction of a slice of brain tissue from the animal also includes removing it from any blood flow. This removes any products contained in blood, whose leakage may cause damage, and any blood pressure, which may cause damage by being too high.

Slices were prepared as detailed in chapter 2.2.1. Briefly, 300 micron sections of brain were taken from the basal ganglia region of neonatal (postnatal day 0-2) DM and control rats. These were grown in normal culture conditions for five weeks, the age at which all of the changes described in this chapter are observed *in vivo*, before being fixed and stained (see chapter 2.3.5).

3.5 – Results from slice cultures

In the slice culture model, I looked at all of the features which we see changed in the DM rats – loss of claudin-5, more OPCs, less myelin, more macrophages. In the slices I was unable to immunostain for claudin-5 and blood vessels for technical reasons, however by western blot I found that there was significantly less claudin-5 protein in the slices from DM rats compared to controls (64% ± 7% less; $p<0.05$, paired t-test; n=3 litters; **Figure 3.9**), suggesting that there was still a structural impairment of the BBB. I found that in slices grown from DM rats compared to controls there were significantly more OPCs (102% ± 7% more; $p<0.05$, paired t-test; n=5 litters; **Figure 3.10 A-C**), measured as the number of cells expressing Olig2, but not Nogo-A (3.2.2), mirroring the OPC proliferation seen *in vivo*. Myelin in the slices was quantified as the proportion of axons (marked by NF) which were myelinated (marked with NF and MBP; 3.2.2, 3.3.2), and I found that there was significantly less myelination in slices from DM rats (25% ± 5% less; $p<0.05$, paired t-test; n=4 litters; **Figure 3.10 D-F**), mirroring the loss of myelin and mature oligodendrocytes seen *in vivo*. I also found that there were significantly more microglia in slices from DM rats compared to control (33% ± 3% more; $p< 0.05$, paired t-test; n=5 litters; **Figure 3.11**), as seen *in vivo*.

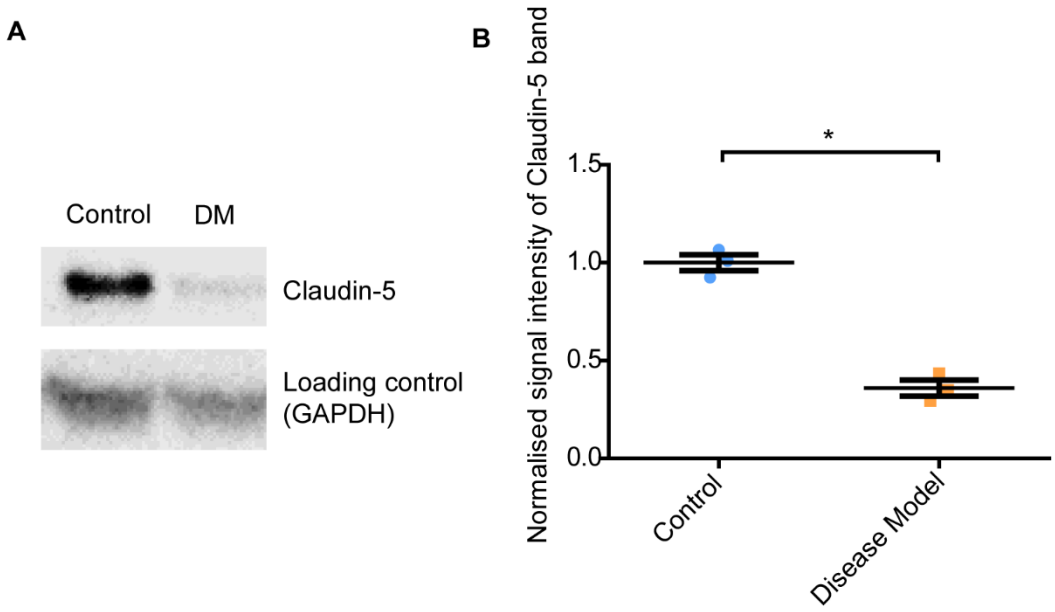


Figure 3.9: Less claudin-5 in brain slices cultured from disease model (DM) rats. A: Western blot showing lower levels of claudin-5 in slices cultured from DM rats for 5 weeks, indicated by a weaker band in the right hand lane. Also shown is a loading control, confirming that the gel was loaded evenly. B: Quantification of the claudin-5 band normalised to the loading control shows that there is significantly less claudin-5 in brain slices grown from DM rat (orange), compared to controls (blue) (Mean ± SEM; *: $p<0.05$, paired t-test; n=3 litters).

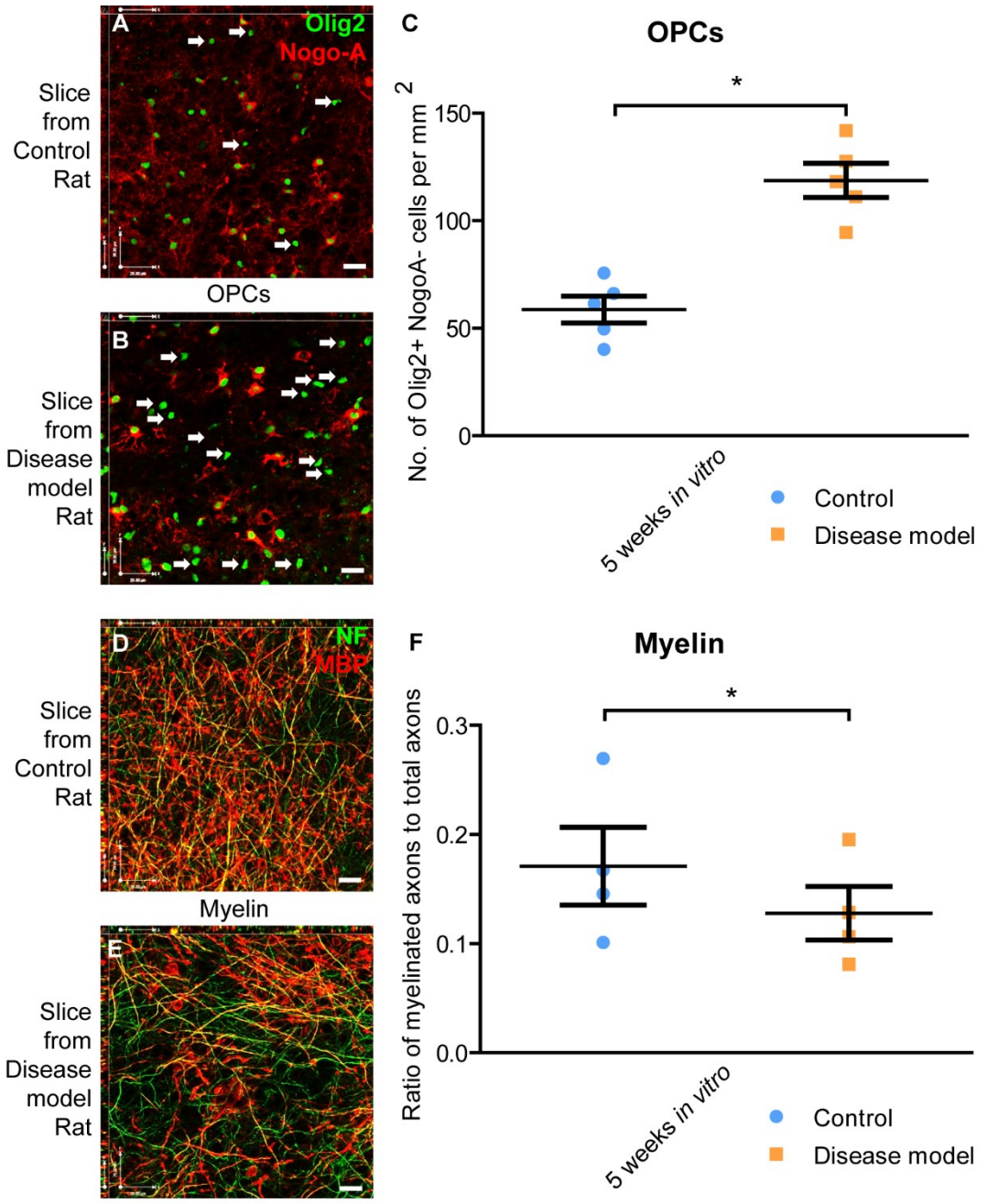


Figure 3.10: More oligodendrocyte precursor cells (OPCs) and less myelin in brain slices cultured from disease model (DM) rats compared to controls. A-B: Fluorescent images showing Olig2, a nuclear marker of the entire oligodendroglial lineage (green), and Nogo-A, a marker of mature oligodendrocytes (red), in brain slices grown in culture for 5 weeks from control (A) and DM (B) rats. White arrows indicate OPCs as cells with an Olig2 positive nucleus but no perinuclear Nogo-A. C: Quantification of the number of OPCs per mm^2 shows that there are significantly more OPCs in slices grown from DM rats (orange) compared to controls (blue) (Mean ± SEM; *: $p<0.05$, paired t-test; n=5 litters). D-E: Fluorescent images showing neurofilament (NF), a marker of axons (green), and myelin basic protein (MBP), a component of myelin (red), in brain slices grown in culture for 5 weeks from control (D) and DM (E) rats. Areas of red and yellow show myelinated axons where NF and MBP overlap, while areas of green show unmyelinated axons with no MBP present. F: Quantification of the ratio of myelinated axons to total axon number shows that there is significantly less myelination in slices grown from DM rats (orange) compared to controls (blue) (Mean ± SEM; *: $p<0.05$, paired t-test; n=4 litters). Scale bar = 25µm.

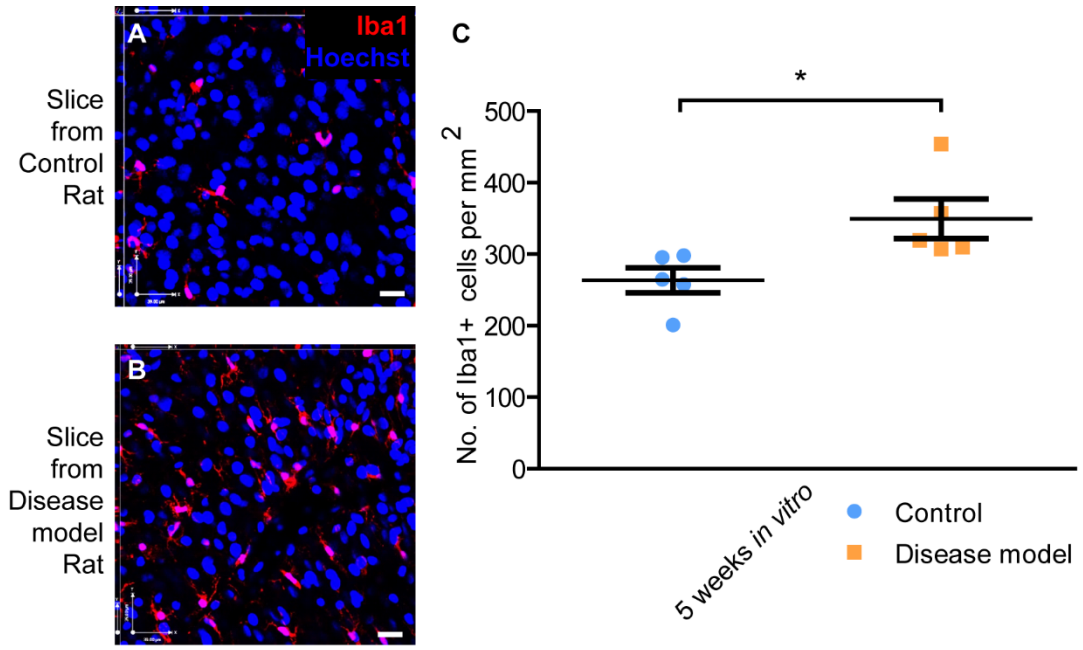


Figure 3.11: More microglia in brain slices cultured from disease model (DM) rats compared to controls. A-B: Fluorescent images showing Iba1, a marker of all macrophages and microglia (red), and Hoechst, a nuclear marker (blue), in brain slices grown in culture for 5 weeks from control (A) and DM (B) rats. Microglia are cells with Iba1 positive cell bodies (around the nucleus). C: Quantification of the number of microglia per mm^2 shows that there are significantly more microglia in slices grown from DM rats (orange) compared to controls (blue) (Mean ± SEM; *: $p<0.05$, paired t-test; n=5 litters). Scale bar = 25µm.

3.6 – Discussion II

The data from the slice culture experiments (chapter 3.5) show that all of the changes observed *in vivo*, also occur in the slice culture model in the absence of blood flow.

These brain slices were taken at postnatal day 0-2, and were grown in culture for five weeks with no blood flow. This means that there was no hypertension during the five weeks that the slices were in culture, and there was unlikely to be any hypertension at the time the slices were extracted from the rat. Despite this, we see all of the same pathological changes in the slices as we do *in vivo* in five week old rats. This means that the pathological changes observed *in vivo* cannot be due to a low level, immeasurable hypertension, as hypertension is not present in this model. The pathological change most likely to be caused by hypertension is the damage of the BBB, as this structure comes into direct contact with the high blood pressure. However, even this change is present in the slice cultures without hypertension.

The lack of blood flow in this model also means that the later pathological changes cannot be caused by BBB leakage. Despite the fact that the earliest change we observe *in vivo* is a structural impairment of the BBB (at three weeks), with BBB leakage demonstrated at a later age (at five weeks), the pathological changes at later time points cannot be caused by toxic blood products leaking into the brain parenchyma, as there is no blood in the slice cultures to leak through a damaged BBB.

The results from the slice culture experiments can also offer some explanations about the increased number of macrophages/microglia observed *in vivo*. In section 3.3.3, I discussed how it was unclear whether this increased number of cells was caused by an increase in the number of peripheral macrophages or resident microglia. In the slice cultures, without blood flow or access to a peripheral source of macrophages, any increase has to come from resident microglia. The fact that we still see this increase in slice cultures suggests that *in vivo*, the increase in macrophages/microglia is at least partly due to an increase in the number of microglia. This supports the theory that the increase is part of a response to damage, rather than due to the increased permeability of the BBB.

These data suggest that rather than SVD being caused by hypertension or leakage through the BBB, a new hypothesis is needed. One theory as to the primary cause of SVD which could explain all the data shown in this chapter is that SVD is caused by an endothelial cell dysfunction, where endothelial cells become more proliferative, necessitating TJ reduction, and produce substances that can detrimentally affect neighbouring cells. This became my new hypothesis, and is explored further in the next chapter.

Chapter 4: What Are the Effects of Endothelial Dysfunction in Small Vessel Disease: *In Vitro* Results

4.1 – Introduction

In the previous chapter, I showed that in a rat model of small vessel disease (SVD) we see an early breakdown of the blood brain barrier (BBB), followed by an increase in oligodendrocyte precursor cell (OPC) proliferation and a block in OPC differentiation, then followed by an increase in the number of macrophages/microglia. Using a slice culture model which excludes blood flow, and hence excludes the leakage of blood products through an impaired BBB, I showed that the subsequent pathological changes are not caused by factors leaking through a damaged BBB and suggested that in fact the root cause of SVD, which could explain all of the features described, could be endothelial cell dysfunction. In the first part of this chapter I will describe what exactly endothelial dysfunction is, and how it has been described in relation to SVD.

4.1.1 - Role of nitric oxide (NO)

At its most basic level, endothelial dysfunction is usually described as a reduced bioavailability of nitric oxide (NO). Under normal conditions, blood vessels will respond to fluctuations in blood pressure or metabolic need by contracting or dilating. This contraction is performed by smooth muscle cells around larger blood vessels, and pericytes around capillaries (see chapter 1.4.2). This response of the smooth muscle cells is mediated by NO produced by endothelial cells (ECs). Increased levels of NO lead to relaxation of the smooth muscle cells and pericytes, and so dilation of the blood vessel, which both reduces local blood pressure and increases the availability of nutrients for the surrounding brain parenchyma. The main source of NO in ECs is the protein endothelial nitric oxide synthase (eNOS; also known as NOS3). The bioavailability of NO is dependent both on its production levels by eNOS, but also on its sequestration by superoxides. In the presence of superoxides, NO is converted to peroxynitrite, which cannot carry out the same functions as NO (reviewed in Beckman and Koppenol, 1996).

4.1.2 - Endothelial nitric oxide synthase (eNOS)

eNOS is one of three nitric oxide synthase (NOS) proteins in the body, the others being neuronal NOS (nNOS) and inducible NOS (iNOS), which all produce NO. While there is also some iNOS expression in ECs, eNOS is the primary producer of NO in ECs. eNOS converts L-arginine to NO and L-citrulline. To carry out this process, eNOS must dimerise and bind a number of cofactors, including flavine adenine dinucleotide (FAD), flavine mononucleotide (FMN) and tetrahydrobiopterin (BH_4) (Huang, 2003). In the absence of sufficient cofactors, eNOS functions as a monomer and converts L-arginine to superoxides, instead of NO (Förstermann and Münzel, 2006; Li and Shah, 2004; Vásquez-Vivar et al., 1998; Yang et al., 2009). These superoxides bind with NO to form peroxynitrites. Thus, when eNOS is active without sufficient cofactors, it in fact functions to reduce NO levels, rather than increasing them.

eNOS is regulated by a number of different factors. It is activated by calcium signalling and phosphorylation, and inhibited by being bound to caveolin-1, the main component of caveolae (Frank et al., 2003; Minshall et al., 2003). The mechanism by which these regulatory factors mediate the response of eNOS to changes in vascular need is unclear. Endothelial dysfunction can be caused by a reduced activation or increased inhibition by these factors, or a reduction in the amount of eNOS (reviewed in Huang, 2003).

4.1.3 - Endothelial dysfunction vs. endothelial activation

The term endothelial dysfunction is sometimes used interchangeably with the term endothelial activation in the literature. Here, I will clarify the distinction between these two terms and explain why this overlap exists. As described in section 4.1.1 above, endothelial dysfunction is defined as a lack of NO bioavailability. Endothelial activation, on the other hand, is defined as an inflammatory state of the endothelium. This state is characterised by the expression of cellular adhesion molecules, such as vascular cellular adhesion molecule 1 (VCAM-1) and intercellular adhesion molecule 1 (ICAM-1), on the surface of ECs (reviewed in Gimbrone et al., 1997). This state is typically induced by pro-inflammatory cytokines, such as tumour necrosis factor alpha

(TNF-α) and interleukin 6 (IL-6), and allows the attachment of circulating leukocytes to the vessel wall, from where they can be easily transported across the endothelial barrier into the parenchyma. Despite these different characterisations, endothelial dysfunction and activation have similar risk factors and similar effects (described in sections 4.1.4 and 4.1.5 respectively), and it has recently been shown that these two states feed into each other (reviewed in Liao, 2013). A reduction in NO in endothelial dysfunction, through a loss of NO's inhibition of nuclear factor kappa-light-chain-enhancer of activated B cells (NF-κB), leads to endothelial activation, and it has been shown that endothelial activation can be reduced by increasing NO levels, using NO donors (De Caterina et al., 1995; Herman and Moncada, 2005). Similarly, the pro-inflammatory cytokines which induce endothelial activation also inhibit expression of eNOS and lead to an increase in superoxides, leading to reduced NO bioavailability and endothelial dysfunction (Gryglewski et al., 1986; Yoshizumi et al., 1993). Thus, though these two states are defined differently, they are closely interlinked, and may in fact be the same thing. Therefore, for the purposes of this thesis, I will exclusively use the term endothelial dysfunction when describing characteristics typically attributed to either endothelial dysfunction or endothelial activation.

4.1.4 - Causes of endothelial dysfunction

There are a number of different risk factors associated with endothelial dysfunction, including hypertension, smoking and diabetes (Johnstone et al., 1993; Ozaki et al., 2010; Panza et al., 1990; Pittilo, 2000). One mechanism by which these may lead to endothelial dysfunction is by increasing superoxide production, leading to a reduced bioavailability of NO (Christ et al., 2002; Dharmashankar and Widlansky, 2010; Heitzer et al., 1996; Hink et al., 2001; Raij et al., 2001). These are explored further in chapter 6.2.1. More generally, as described above, endothelial dysfunction can be caused by anything which reduces the activity or levels of eNOS, such as pro-inflammatory cytokines, or increases the sequestration of NO (reviewed in Huang, 2003).

4.1.5 - Effects of endothelial dysfunction

Endothelial dysfunction can have many varied effects, both on the vasculature and other cells in the body. As described in section 4.1.1 above, the reduced level of NO in endothelial dysfunction leads to vasoconstriction, as NO is required for the contractile smooth muscle cells to relax. NO also inhibits the proliferation of smooth muscle cells, meaning that when NO levels are reduced smooth muscle cells proliferate more, further constricting the vasculature (Mooradian et al., 1995). Another role of NO is to inhibit the adhesion of platelets to the luminal wall of the endothelium (Radomski et al., 1991). Thus, when ECs are dysfunctional, platelets build up more rapidly, and this is believed to be the starting point of atherosclerosis.

Endothelial dysfunction can also lead to the secretion of factors which can have effects on both ECs and other cell types, including vascular endothelial growth factor (VEGF), TNF-α and endothelin 1 (ET-1) (Lip et al., 2000; Pearson, 2000; Rajashekhar et al., 2006). VEGF is a potent proangiogenic factor, and while it has been shown that NO enhances VEGF mediated angiogenesis (Murohara et al., 1998), it has also been shown that endothelial dysfunction leads to increased angiogenesis, suggesting that the increased levels of VEGF still promote angiogenesis in the presence of reduced NO (Patterson and Clauss, 2005; Rajashekhar et al., 2006).

This increased angiogenesis means that ECs are proliferating more, and this may explain the effects of endothelial dysfunction seen in the brain (Dobrogowska et al., 1998). It has been shown that endothelial dysfunction causes leakage of the BBB (Grammas, 2011; Najjar et al., 2013; Staddon and Rubin, 1996; Vandenbroucke et al., 2008). During the process of proliferation, ECs reduce their levels of intercellular junctions, including TJs, to provide room to grow. This leads to leakage of the BBB (Meyer et al., 1991; Zhang et al., 2000). The leakage of the BBB in endothelial dysfunction could also be explained by the pro-inflammatory state induced in ECs. As described in section 4.1.3, dysfunctional ECs express molecules for leukocytes to bind so that they can cross the endothelial barrier transcellularly. It is likely that this also includes a weakening of the barrier to facilitate paracellular leukocyte movement (Fiala et al., 1997).

4.1.6 - Endothelial dysfunction in SVD

There is a wide range of evidence for endothelial dysfunction in SVD, and this will be explored in more detail in chapter 6.2. Briefly, this includes: the overlap of risk factors for SVD and endothelial dysfunction, the presence of markers of endothelial dysfunction, such as ICAM-1, at elevated levels in the blood of SVD patients, and the association of genetic polymorphisms in the gene for eNOS, which cause reduced eNOS activity, with SVD (Elbaz et al., 2000; Hassan et al., 2004a; Poggesi et al., 2015). Despite this, endothelial dysfunction is still rarely thought of as a cause of SVD, compared to risk factors such as hypertension. Endothelial dysfunction is currently believed to contribute to SVD through its mechanisms to initiate atherosclerosis and induce vasoconstriction. This fits in with the assumption, described in Chapter 1, that SVD is caused by vascular occlusion or hypoperfusion. However, as I detailed in chapter 1.2.2, this is unlikely to be the case, as the majority of lacunar lesions have no sign of vascular occlusion (Bailey et al., 2012).

This chapter therefore aims to firstly provide further evidence that endothelial dysfunction is present in humans with SVD, and in the disease model (DM) rat we are using, and then to explore how this can cause the other pathological changes we see in tissue sections from diseased human brains and DM rats.

4.2 – Results: evidence for endothelial dysfunction in SVD and disease model rats

While my results from the previous chapter suggest that we are seeing an early endothelial dysfunction in SVD, I wished to demonstrate this more clearly. I investigated a number of different markers for endothelial dysfunction in both human and rat tissue, and rat cells.

A key sign of endothelial dysfunction is proliferation of ECs (Drab et al., 2001; Rajashekhar et al., 2006). As this was something which can be easily studied in fixed tissue, I was able to look at this in samples of human brains, as well as in the disease model (DM) rats using proliferating cell nuclear antigen (PCNA) which labels cells exclusively during the DNA synthesis phase (s-phase) of the cell cycle. This marker was used as antibodies against it work robustly in paraffin fixed tissue. I found that in

five week old DM rats there were more proliferating ECs than in age matched controls (44% ± 5% more; mean ± SEM; $p<0.05$, unpaired t-test; n=3; **Figure 4.1 A-D, G**), an indication of endothelial dysfunction. I also found that this correlated with an increased number of proliferating ECs in human brains with SVD compared to controls (65% ± 9% more; $p<0.05$, unpaired t-test; n=5; **Figure 4.1 E-G**).

While EC proliferation is associated with endothelial dysfunction, I wanted to look more directly at classical markers for endothelial dysfunction. The most basic marker of endothelial dysfunction is reduced NO production, which can be caused by lower levels or reduced activity of eNOS. While it is difficult to directly measure NO levels in fixed or frozen tissue, as these do not preserve either NO or its metabolites, I was able to study eNOS levels by western blot in control and DM rats. Protein lysates were extracted from basal ganglia regions of the unfixed, frozen brains of five week old rats. Although this is a mixed population of cells, eNOS is exclusively expressed in ECs so other cell types do not affect the results. I found that there is less eNOS in the brains of DM rats compared to controls (33% ± 4% less; $p<0.05$, unpaired t-test; n=3; **Figure 4.2**). Unfortunately I was not able to repeat this western blot using human SVD tissue as we only had access to fixed, paraffin embedded tissue, from which protein extraction for western blot is unreliable.

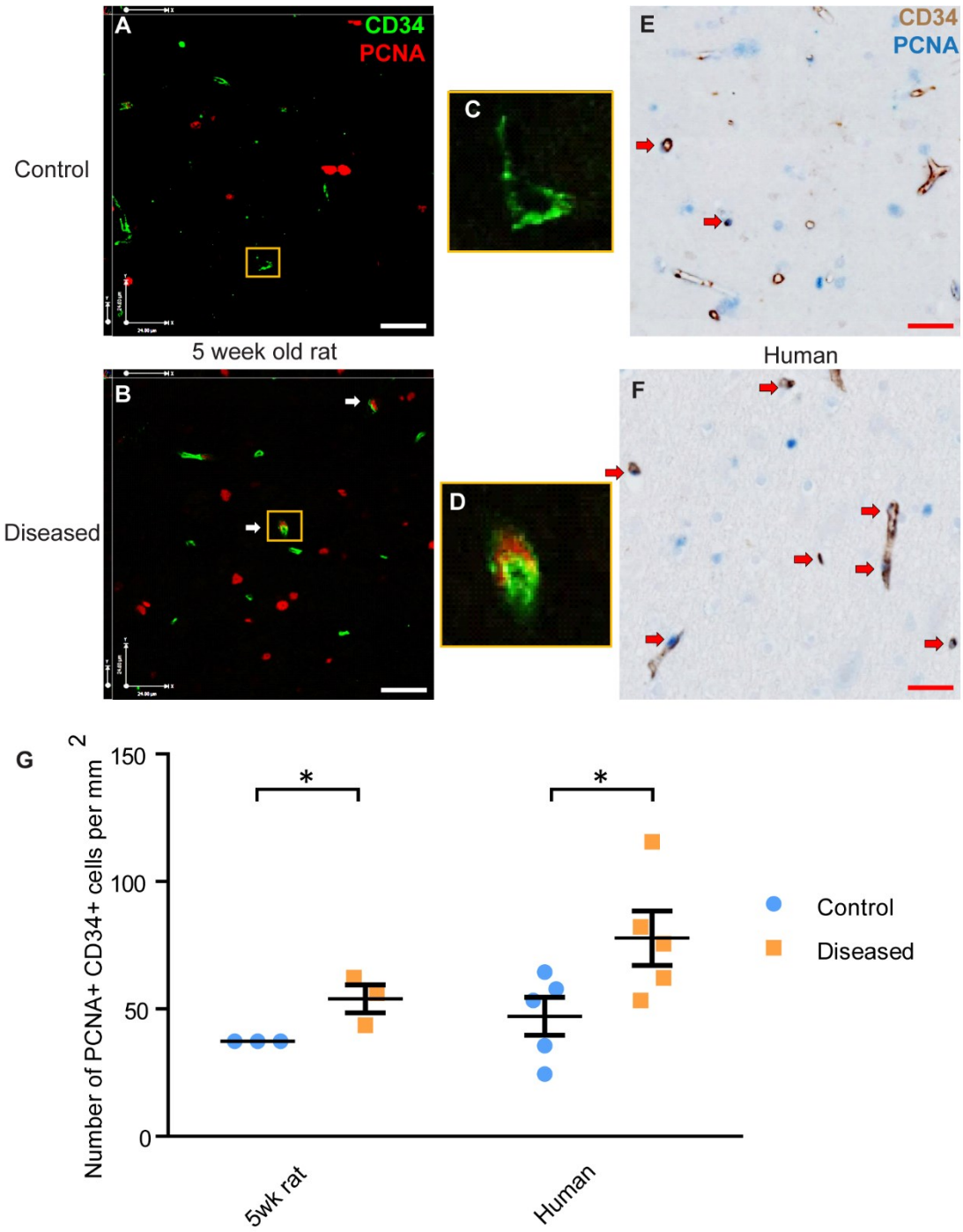


Figure 4.1: More proliferating endothelial cells (ECs) at 5 weeks of age in disease model rats and in human brains with SVD. A-D: Fluorescent images showing CD34, a marker of endothelial cells (green), and proliferating cell nuclear antigen (PCNA), a marker of proliferating cells, in the deep white matter of brains from control rats (A, C) and disease model rats (B, D) at the age of 5 weeks. White arrows indicate proliferating ECs as CD34+ cells with PCNA+ nuclei. C and D show enlargements of the areas within the yellow boxes in A and B respectively to demonstrate more clearly the difference between ECs with and without proliferating nuclei. E-F: Images showing colorimetric staining of CD34 (brown) and PCNA (blue). Red arrows indicate proliferating ECs as CD34+ cells with PCNA+ nuclei. G: Quantification of the number of proliferating ECs per mm^2 shows that there are significantly more proliferating ECs at 5 weeks in the disease model rats (orange) compared to controls (blue), and in the diseased human brains compared to controls (Mean ± SEM; *: $p<0.05$, unpaired t-test; rat n=3; human: n=5). Scale bar = 25µm.

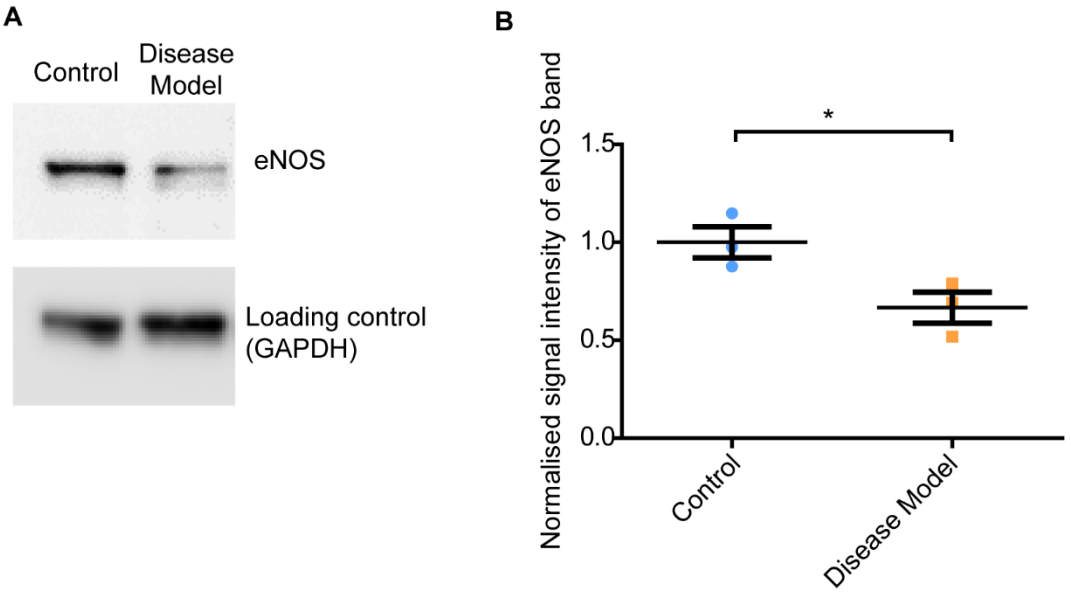


Figure 4.2: Less endothelial nitric oxide synthase (eNOS) in the brains of disease model (DM) rats. A: Western blot showing amounts of eNOS (upper band) and GAPDH as a loading control (lower band) in the brains of control (left column) and DM (right column) rats. The eNOS band is much weaker in the DM rat, while the GAPDH band is similar in both control and DM. B: Quantification of the normalised intensity of the eNOS band compared to its loading control shows lower levels of eNOS in DM (orange) rat brains compared to control (blue) (Mean ± SEM; *: $p<0.05$, unpaired t-test; n=3).

4.3 – Results: effects of endothelial dysfunction in DM rats

The data above demonstrate evidence for endothelial dysfunction in both humans with SVD and in our DM rats. I next asked the question of whether this was inherent to the ECs, rather than being induced by other surrounding cell types, and whether this endothelial dysfunction could be causing all the disease changes we see in tissue sections from diseased human brains and DM rats.

To test if this dysfunction was inherent to ECs, I isolated brain microvascular endothelial cells (BMECs) from DM and control rats and grew them *in vitro* (chapter 2.2.2). The isolation methods and culture conditions meant that the cultures had negligible levels of contaminating cells (less than 1% pericytes or astrocytes) and the cells displayed a typical brain EC phenotype (showing some expression of tight junction proteins, a phenomenon exclusive to ECs extracted from the brain) after a ten day period in culture. To look at endothelial dysfunction in these cultures I studied NO levels in their media by a modified Griess reaction (chapter 2.6.1). This method is based on the fact that in culture any released NO is rapidly oxidised to nitrates and nitrites. The assay I used first reduces any nitrates to nitrites, using nitrate reductase, then causes a colour change based on total nitrite levels, using Griess reagents. I found that BMECs isolated from DM rats produced less NO than those from control rats, indicating an inherent endothelial dysfunction (22% ± 6% less; $p<0.05$, paired t-test; n=3; **Figure 4.3**).

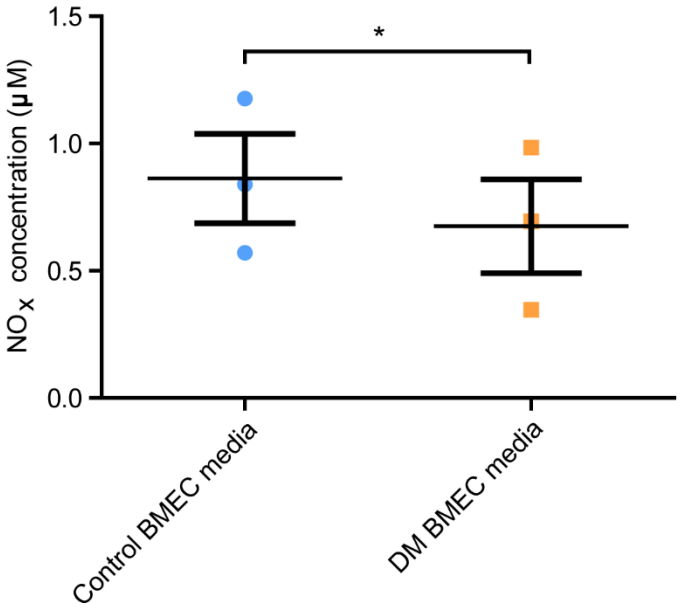


Figure 4.3: Less nitric oxide produced in isolated cultures of brain microvascular endothelial cells (BMECs) from disease model (DM) rats. Quantification of the amount of nitrates and nitrites (NO_x) in the media of isolated BMECs, as a proxy for how much NO the cells are producing, shows lower levels of NO_x, and hence lower levels of NO production, in media from BMECs isolated from DM (orange) rat brains compared to controls (blue) (Mean ± SEM; *: $p<0.05$, paired t-test; n=3 litters).

The isolation of BMECs from DM and control rats allowed me to further study if endothelial dysfunction causes the other changes I see *in vivo*. I was able to look at tight junction proteins (TJPs), the key proteins of the BBB, in BMEC cultures. I found that BMECs isolated from DM rats form less mature tight junctions (TJs) than BMECs from control rats (**Figure 4.4**), as indicated by a reduced localisation of claudin-5, a mature TJP, to the membrane (67% ± 6% less; $p<0.05$, paired t-test; n=3 litters; **Figure 4.4 A-B, D**) despite normal ZO-1, an immature TJP, localisation to the cell membrane (**Figure 4.4 A-C**). TJPs are only functional when localised to the membrane, and while in both control and DM BMECs ZO-1 is localised to the cell membrane in the vast majority of cells, localisation of claudin-5 to the membrane is far less common in DM cultures than control cultures. Claudin-5 is still found around the nucleus in the cytoplasm in both DM and control cultures, suggesting that the protein is still produced to some degree, and demonstrating that the immunocytochemistry is working in the cultures where claudin-5 is absent from cell membranes.

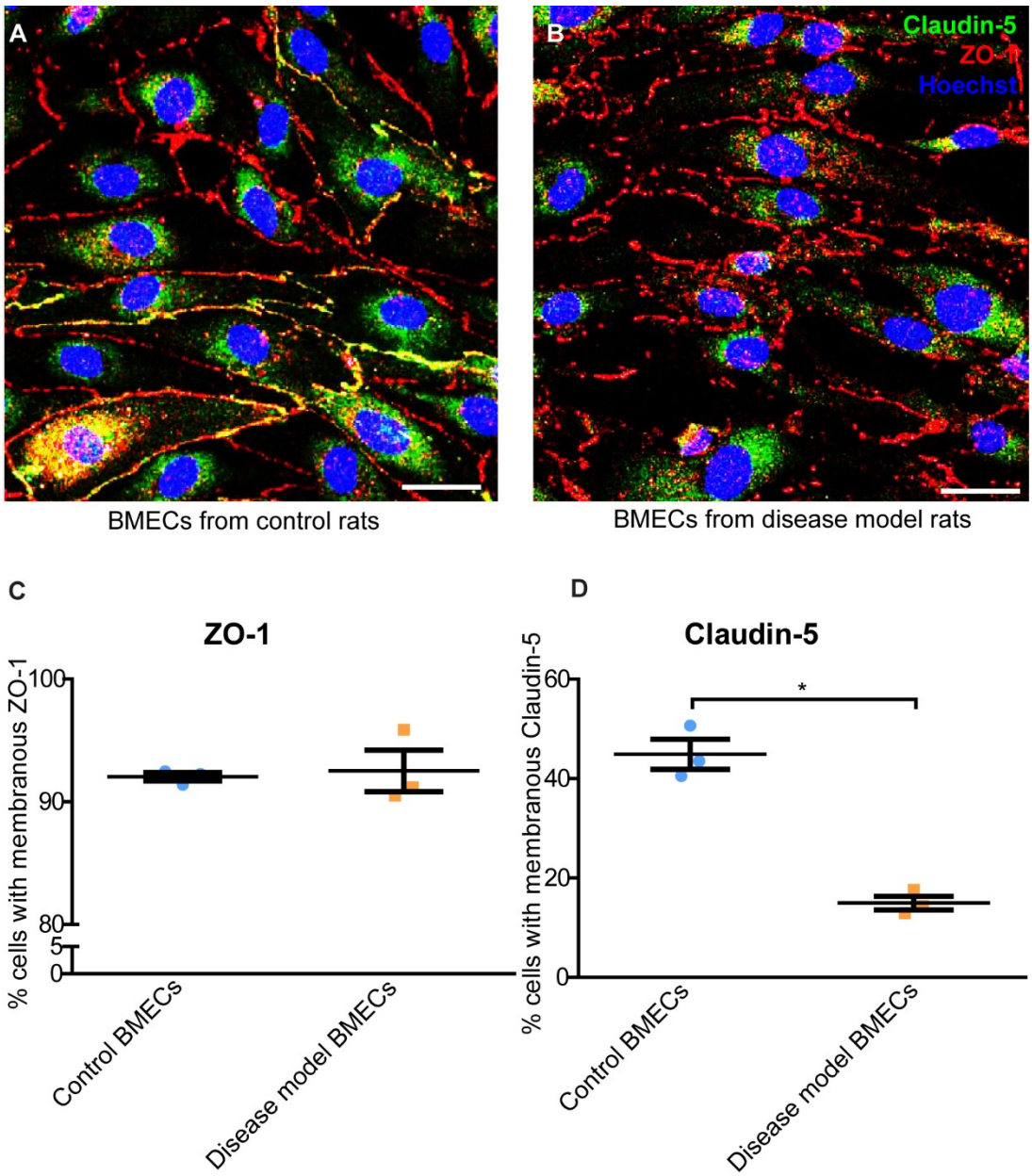


Figure 4.4: Less mature tight junctions (TJs) in brain microvascular endothelial cells (BMECs) isolated from disease model (DM) rats. A-B: Fluorescent images showing claudin-5, a mature TJ protein (green), ZO-1, an immature TJ protein (red), and Hoechst, a nuclear marker (blue), in cultures of BMECs isolated from control (A) and DM (B) rats. TJ proteins are only functional when localised to the cell membrane. While in both control and DM BMECs, ZO-1 (red) is localised to the membrane in the vast majority of cells, localisation of claudin-5 (green) to the membrane (appearing yellow as it colocalises with ZO-1) is far less common in DM cultures than control. C-D: Quantification of the percentage of cells with ZO-1 at the membrane (C) shows no difference between DM BMECs (orange) and control BMECs (blue), however quantification of the percentage of cells with claudin-5 at the membrane (D) shows significantly fewer cells with membranous claudin-5 in DM BMECs compared to controls (Mean ± SEM; *: $p<0.05$, paired t-test; n=3 litters). Scale bar = 25µm.

These data demonstrate that in the DM rats there is an inherent endothelial dysfunction, and this causes the BBB phenotype of reduced mature tight junctions that we see *in vivo*. I next asked whether this could also be causing the other changes we see *in vivo*, notably to OPCs and microglia/macrophages. To study this in the first instance, I took the conditioned media (CM) in which the BMECs were growing and added it to cultures of other cell types. This CM would contain any factors secreted by the BMECs. I chose to investigate secreted factors first as in brain tissue sections OPCs and microglia/macrophages are not always perivascular and do not necessarily have direct cell contact with ECs. Therefore any signal reaching them from ECs would have to be secreted.

When carrying out experiments using CM, care needs to be taken to ensure that any effects observed are not artefacts of the methodology. As cells can behave differently in different types of culture media, CM was produced by growing BMECs in the appropriate media for the target culture, rather than adding BMEC media to other cell types. As even normal ECs will secrete factors which could affect other cell types, CM from control BMECs was used as a control, rather than comparing cells grown in CM from DM BMECs to those grown in unconditioned media. For all CM experiments I have graphically shown the results of cultures grown in unconditioned media for illustrative purposes. In some cases, these show large differences compared to cultures grown in CM. However, monocultures grown *in vitro* are not expected to perfectly model an *in vivo* situation, and cells grown in CM in fact more closely reflect the *in vivo* situation where secreted factors from other cell types will have an effect. Thus, a direct comparison between cells grown in unconditioned media and those grown in CM is not valid. For this reason, I have used a paired t-test to carry out statistical tests in this section, rather than a one-way ANOVA, as there are only two groups between which valid comparisons can be made: control BMEC CM and DM BMEC CM.

I first added CM from DM and control BMECs to cultures of OPCs, isolated from cortices of neonatal (p0-p2) Sprague-Dawley rats by shake off from mixed glial cultures (chapter 2.2.3). OPCs isolated by this method have a purity of at least 90%. When grown in unconditioned media under normal conditions for two days after plating, many of these cells start to differentiate into oligodendrocytes, with some becoming mature enough to express MBP, while many remain as immature OPCs. I

found that in cultures of OPCs grown in CM from DM BMECs there are significantly more cells remaining as NG2 expressing immature OPCS (75% ± 11% more; $p<0.05$, paired t-test; n=3 litters; **Figure 4.5 A-C**), and significantly fewer cells maturing to MBP expressing oligodendrocytes (26% ± 7% less; $p<0.05$, paired t-test; n=3 litters; **Figure 4.5 A-B, D**) compared to those grown in CM from control BMECs after two days *in vitro*. This mirrors the maturation block in oligodendroglial cells we observe in tissue sections from both DM rats and human brains with SVD.

By adding BMEC CM to OPC cultures I also found that OPCs grown in CM from DM BMECs proliferate significantly more than those grown in CM from control BMECs (36% ± 3% more; $p<0.05$, paired t-test; n=3 litters; **Figure 4.6**). Proliferating cells were marked using Ki67, an antigen which is expressed during all active phases of the cell cycle rather than just s-phase, as this antibody was the most robust for immunocytochemistry. This mirrors the OPC proliferation seen in tissue sections from DM rats and human brains with SVD.

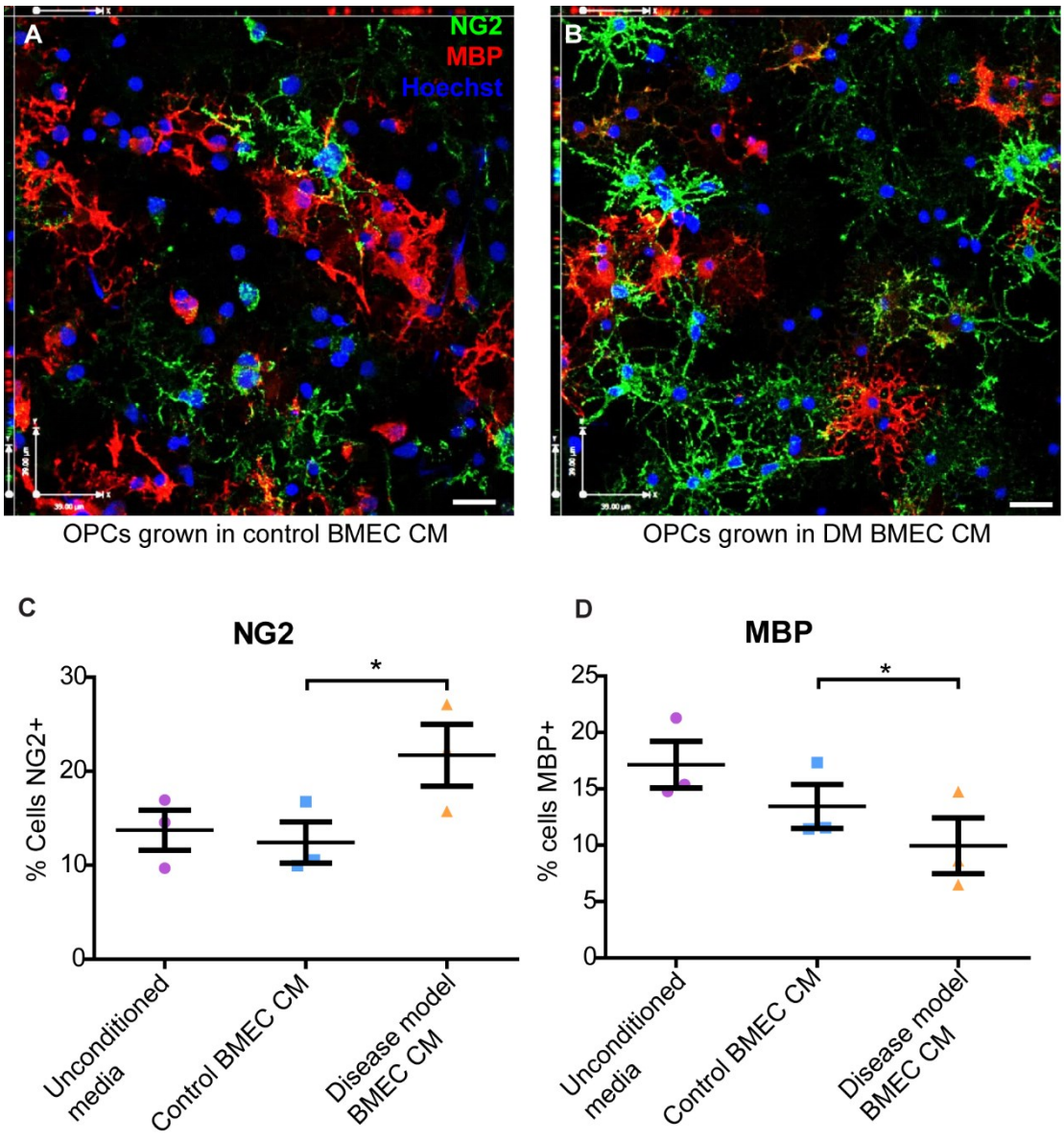


Figure 4.5: Oligodendrocyte precursor cells (OPCs) mature less when grown in conditioned media (CM) from brain microvascular endothelial cells (BMECs) isolated from disease model (DM) rats. A-B: Fluorescent images showing NG2, a marker of immature OPCs (green), MBP, a marker of myelin expressing mature oligodendrocytes (red), and Hoechst, a nuclear marker (blue), in cultures of OPCs grown in control (A) and DM (B) BMEC CM. In the cultures grown in control BMEC CM, there are more mature, MBP expressing cells whereas in the cultures grown in DM BMEC CM there are more immature, NG2 expressing cells. C-D: Quantification of the percentage of NG2+ cells (C) shows more immature OPCs in cultures grown in DM BMEC CM (orange) compared to both control BMEC CM (blue) and unconditioned media (purple), while quantification of the percentage of MBP+ cells (D) shows significantly fewer mature oligodendrocytes in cultures grown in DM BMEC CM compared to control BMEC CM (Mean ± SEM; *: $p<0.05$, paired t-test; n=3 litters). Scale bar = 25µm.

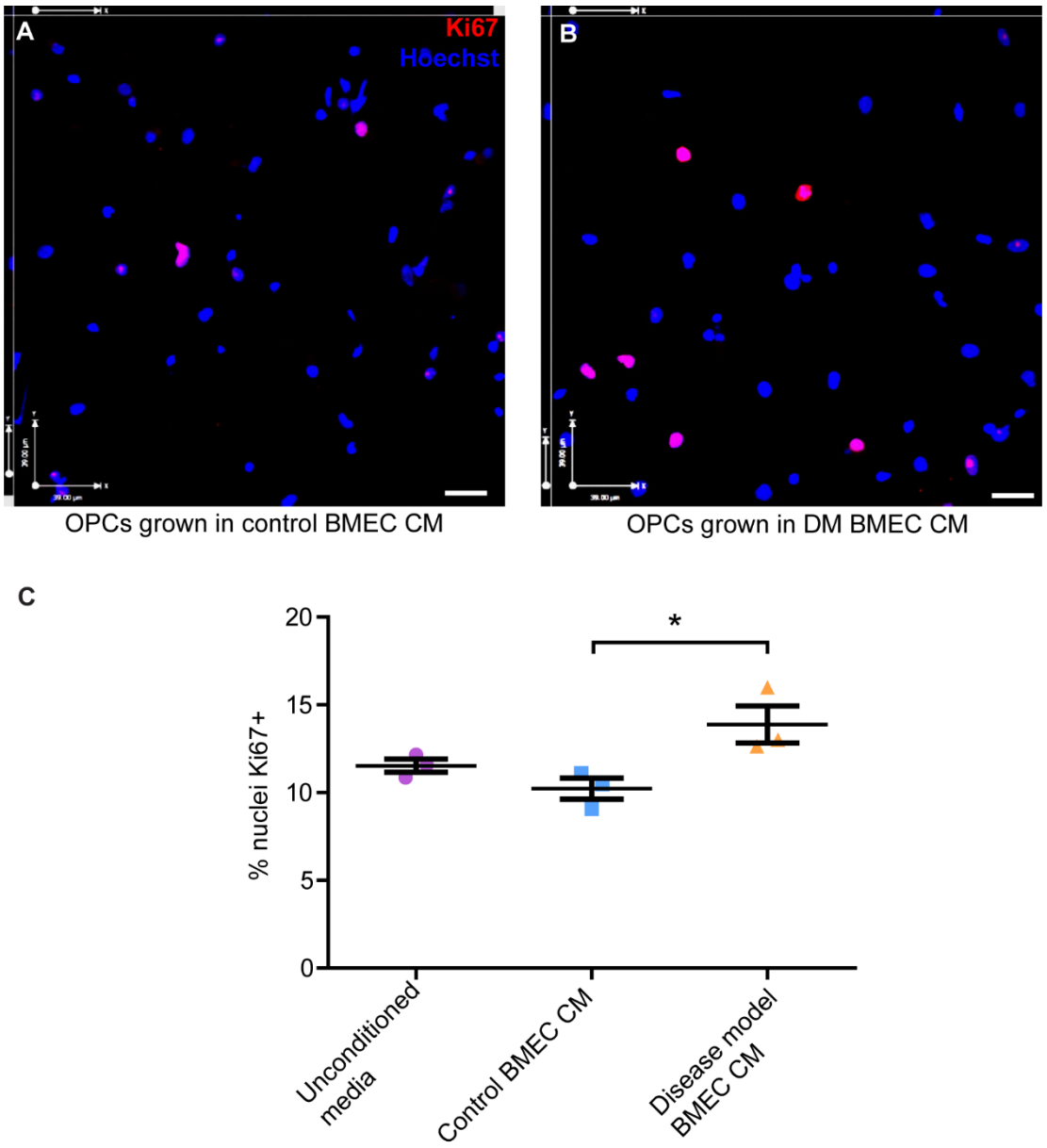


Figure 4.6: Oligodendrocyte precursor cells (OPCs) proliferate more when grown in conditioned media (CM) from brain microvascular endothelial cells (BMECs) isolated from disease model (DM) rats. A-B: Fluorescent images showing Ki67, a marker of proliferating nuclei (red), and Hoechst, a nuclear marker (blue), in cultures of OPCs grown in control (A) and DM (B) BMEC CM. In the cultures grown in DM BMEC CM, there are more proliferating, Ki67 expressing cells compared to cultures grown in control BMEC CM. C: Quantification of the percentage of Ki67+ cells shows more proliferation in cultures grown in DM BMEC CM (orange) compared to both control BMEC CM (blue) and unconditioned media (purple) (Mean ± SEM; *: $p<0.05$, paired t-test; n=3 litters). Scale bar = 25µm.

These data demonstrate that the dysfunctional ECs in DM rats are secreting factors which induce similar changes in OPC cultures to those that we see in OPCs in our DM rats and human brains with SVD. I next wanted to investigate if the pathological changes observed in microglia in tissue sections from DM rats and humans with SVD could be similarly induced by this inherent endothelial dysfunction. To test this I added CM from DM and control BMECs to cultures of microglia, isolated from the same mixed glial cultures as the OPCs, as detailed previously (chapter 2.2.4). I found no difference in microglia number or proliferation between cultures grown in CM from control and DM BMECs (**Figure 4.7**).

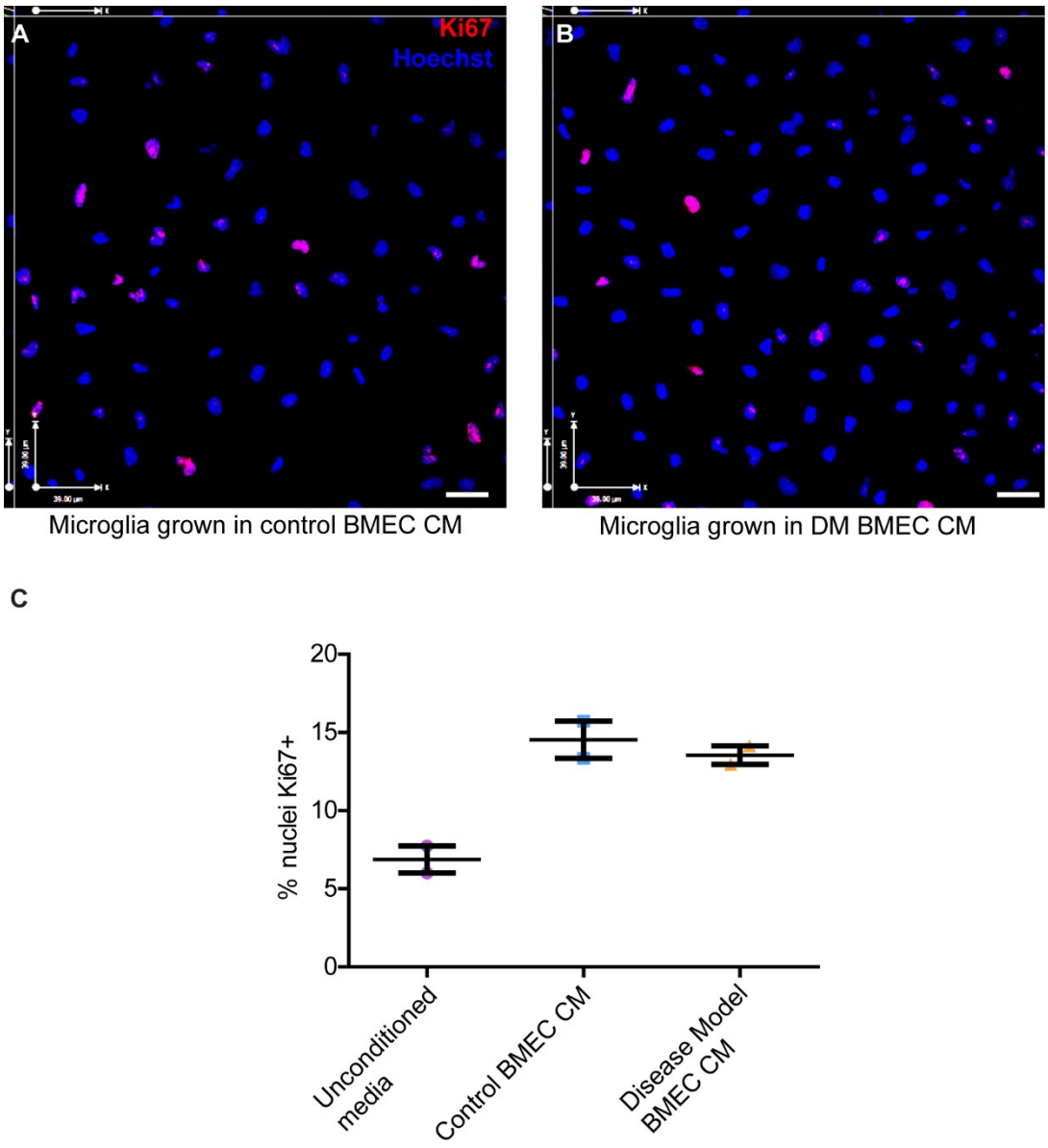


Figure 4.7: No difference in proliferation between microglia grown conditioned media (CM) from brain microvascular endothelial cells (BMECs) isolated from disease model (DM) and control rats. A-B: Fluorescent images showing Ki67, a marker of proliferating nuclei (red), and Hoechst, a nuclear marker (blue), in cultures of microglia grown in control (A) and DM (B) BMEC CM. C: Quantification of the percentage of Ki67+ cells shows no difference in proliferation between cultures grown in DM BMEC CM (orange) and control BMEC CM (blue), though both CM groups show much more proliferation than unconditioned media (purple) (n=2 litters). Scale bar = 25µm.

There are a number of reasons why we may not see similar changes to microglia *in vitro* to what we see in tissue sections from diseased human brains and DM rats. One of these is that the increase in microglia number could be secondary to the changes in OPCs, rather than being directly caused by the dysfunctional ECs. This idea is supported both by the order in which the changes appear in the DM rat *in vivo*, and the range of microglial changes which are known to occur in response to myelin damage in a number of animal models and human diseases (chapter 1.5.4).

One way to test this theory would be to take CM from OPCs which had been grown in CM from DM and control BMECs. This would allow us to see if OPCs, upon being subjected to the changes induced by dysfunctional ECs, secrete factors which affect microglia. However, the interaction between OPCs and microglia might not be mediated by secreted factors, and cell contact may be important. This method also presents a significant technical challenge, as the length of time which the same CM would be used would lead to severe depletion of nutrients in the medium. An alternative is to co-culture OPCs and microglia, and add the BMEC CM to these cells together. This would overcome the issue of nutrient depletion in the medium and would allow cell contact between the OPCs and the microglia. However, this culture would not contain other cell types, such as astrocytes, which may mediate the interaction, and presents technical challenges of its own – namely finding a culture medium in which both OPCs and microglia behave normally.

The optimal method to test this theory is to add CM from DM and control BMECs to wild type slice cultures, detailed in chapter 3.4. These cultures contain all brain cell types in a normal tissue architecture and microenvironment, and so allow normal interactions. These experiments were carried out with the help of a Master's student under my supervision, Silvie Ruigrok. When we grew slice cultures in CM from DM BMECs for five weeks, we found that they show significantly increased OPC numbers, measured as cells expressing Olig2 but not Nogo-A as previously (chapter 3.5), (37% ± 2% more; $p<0.05$, paired t-test; n=3; **Figure 4.8 A-C**), and a significant reduction in myelination, measured as the proportion of axons which are myelinated as previously (chapter 3.5), (19% ± 2% less; $p<0.05$, paired t-test; n=3; **Figure 4.8 D-F**) compared to slices grown in CM from control BMECs. Again, this mirrors what we see in tissue sections from diseased human brains and DM rats, further demonstrating that factors

secreted from isolated ECs are alone sufficient to recapitulate the pathological changes in OPCs.

However, when we looked at microglia numbers in slices grown in CM from DM BMECs, measured as the percentage of Iba1 expressing cells as previously (chapter 3.5), we found no difference compared to those grown in CM from control BMECS (**Figure 4.9**).

These data suggest a number of alternative possibilities. It may be that the OPC changes induced in the slices by DM BMEC CM are not large enough or present for long enough to induce changes in microglia numbers, or that the microglia require direct cell contact with dysfunctional ECs to undergo changes, and secreted factors alone are not enough to mediate this. These possibilities are explored further in the discussion below (section 4.5.1).

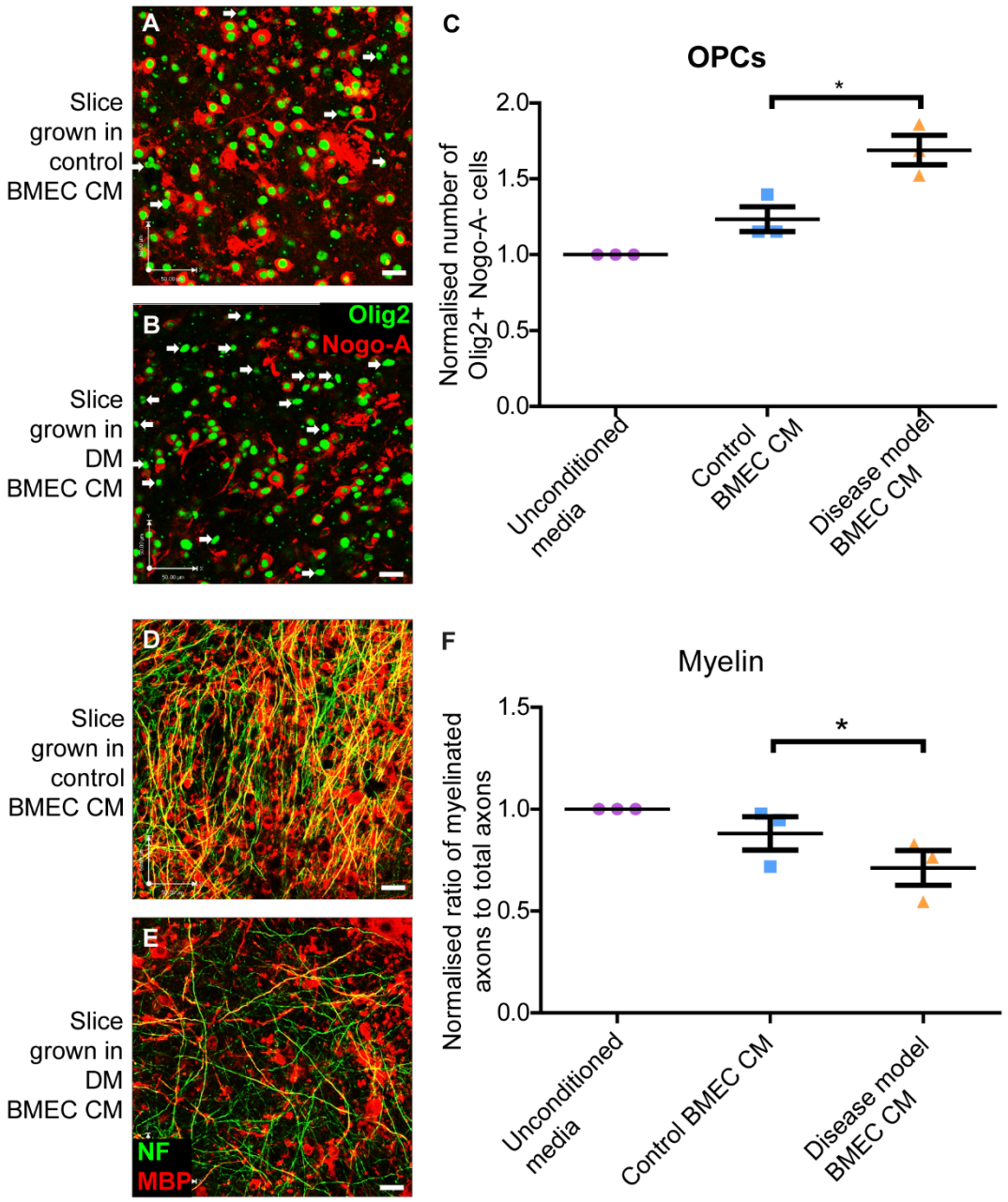


Figure 4.8: More oligodendrocyte precursor cells (OPCs) and less myelin in slice cultures grown in conditioned media (CM) of brain microvascular endothelial cells (BMECs) from disease model (DM) rats. A-B: Fluorescent images showing Olig2, a nuclear marker of the entire oligodendroglial lineage (green), and Nogo-A, a marker of mature oligodendrocytes (red), in wild type brain slices grown in culture for 5 weeks in CM from control (A) and DM (B) BMECs. Arrows indicate OPCs as cells with an Olig2 positive nucleus but no perinuclear Nogo-A. C: Quantification of the number of Olig2+ Nogo-A- cells normalised to slices grown in unconditioned media (purple) shows significantly more OPCs in slices grown in BMEC CM from DM rats (orange) compared to controls (blue) (Mean ± SEM; *: $p<0.05$, paired t-test; n=3). D-E: Fluorescent images showing neurofilament (NF), a marker of axons (green), and myelin basic protein (MBP), a component of myelin (red), in slices grown in culture for 5 weeks in CM from control (D) and DM (E) BMECs. Areas of red and yellow show myelinated axons where NF and MBP overlap, while areas of green show unmyelinated axons with no MBP present. F: Quantification of the ratio of myelinated axons to total axon number normalised to unconditioned media (purple) shows that there is significantly less myelination in slices grown in BMEC CM from DM rats (orange) compared to controls (blue) (Mean ± SEM; *: $p<0.05$, paired t-test; n=3). Scale bar = 25µm.

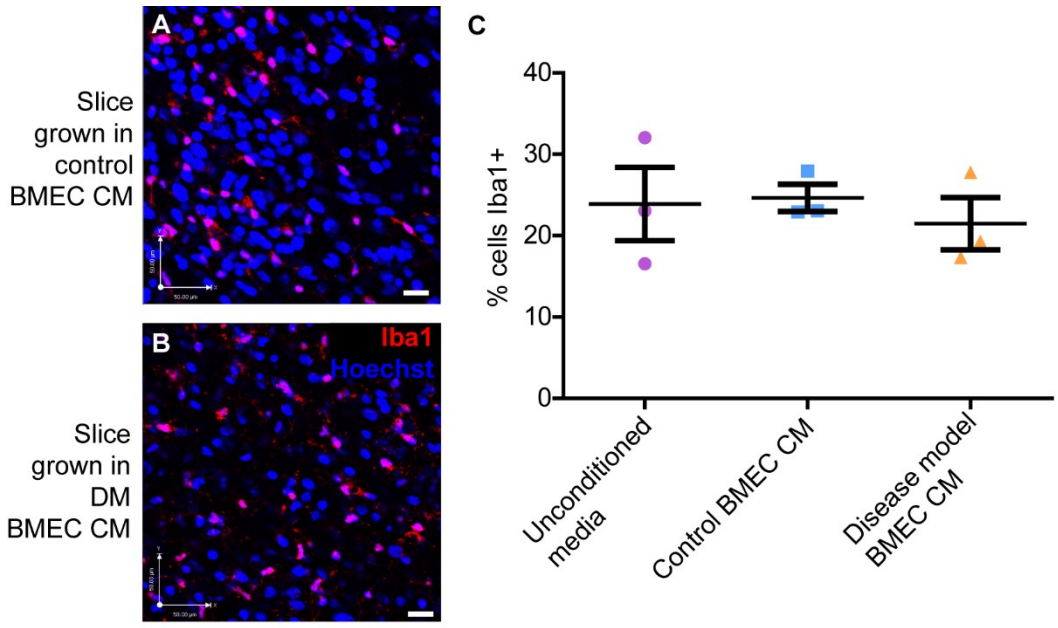


Figure 4.9: No difference in numbers of microglia between slice cultures grown in conditioned media (CM) of brain microvascular endothelial cells (BMECs) from disease model (DM) and control rats. A-B: Fluorescent images showing Iba1, a marker of all microglia (red), and Hoechst, a marker of cell nuclei (blue), in wild type brain slices grown in culture for 5 weeks in CM from control (A) and DM (B) BMECs. C: Quantification of the percentage of cells which are Iba1+ shows no difference between slices grown in BMEC CM from DM rats (orange) and controls (blue) (Mean ± SEM; n=3). Scale bar = 25μm.

4.4 – Results: what mediates the effects of endothelial dysfunction in the DM rat

The data so far in this chapter demonstrate that at least part of the later phenotype of SVD, the changes in OPCs, is mediated by factors secreted by dysfunctional ECs. This begs the question: what are these secreted factors?

There are a number of ways we could study this. The most technologically reliable way would be to study messenger ribonucleic acid (mRNA) levels in DM and control BMECs using a microarray or RNA-seq, and enrich the results for secreted factors. However, mRNA levels do not always directly correspond to protein levels as some mRNA is degraded before it can be translated, and we would be left uncertain as to whether the mRNA differences we were measuring were actually reflected in altered levels of secreted protein.

To study protein levels directly instead of mRNA, the optimal, unbiased approach would be to carry out a proteomics screen on the CM from DM and control BMECs. This would pick up every protein secreted into the medium without us having to choose a specific candidate list. However, current proteomics technology is limited in its sensitivity, and may not pick up proteins which are at a low level, even though these may be important. Proteomics is also limited in how well it works with CM containing serum, and so serum-free culture conditions for the BMECs would need to be devised, which may affect their phenotype.

Therefore we initially chose to investigate the factors secreted into CM by DM BMECs using a commercial antibody array in the first instance. We used the Signalling Explorer array from Full Moon Bioscience, which contains antibodies against 1358 different proteins, and compared CM from control BMECs to CM from DM BMECs. While a number of the antibodies gave off very low levels of fluorescence, as the array was optimised for human not rat samples, we discovered a number of hits where the fluorescence of the spot on the array was high, the log fold change was high, and the quality of the spot on the array was high (**Figure 4.10 A**). In the first instance, we were looking for factors which were at higher levels in CM from DM BMECs than control as the OPCs grown in control BMEC CM are no different to those grown in unconditioned media (**Figure 4.5 C-D, Figure 4.6 C**), so we know that the differences are due to additional factors in DM BMEC CM, rather than factors from control BMEC

CM being absent in DM BMEC CM. I initially found three factors of interest: Actin-alpha 1, heat shock protein 90 alpha (HSP90α) and matrix metalloprotease 2 (MMP-2). However, after further quality control steps (accounting for the consistency of fluorescence across an individual antibody spot and the variation between repeats) this was narrowed down to one robust change: heat shock protein 90 alpha (HSP90α). This increased level of HSP90α secreted by BMECs from DM rats compared to BMECs from control rats was confirmed by western blot of the CM using an antibody specific for HSP90α (24% ± 0.5% higher; $p<0.05$, paired t-test; n=3; **Figure 4.10 B-C**). The bands were smaller (~75 kDa) than the expected size of HSP90α (~86 kDa), however the antibody was validated by running recombinant HSP90α on the western blot, which was the expected size (data not shown). This suggests that the secreted HSP90α is cleaved (see section 4.5.3). As this western blot is carried out on CM, rather than cell or tissue lysates, there was no housekeeping protein I could use as a loading control. I instead stained the membranes with Ponceau S, which stains all proteins red. Where there is an abundant protein this appears as a distinct band. In this case, bovine serum albumin (BSA; the major component of fetal bovine serum (FBS)) is highly abundant in the CM, and I was able to normalise to this, visualised on Ponceau staining.

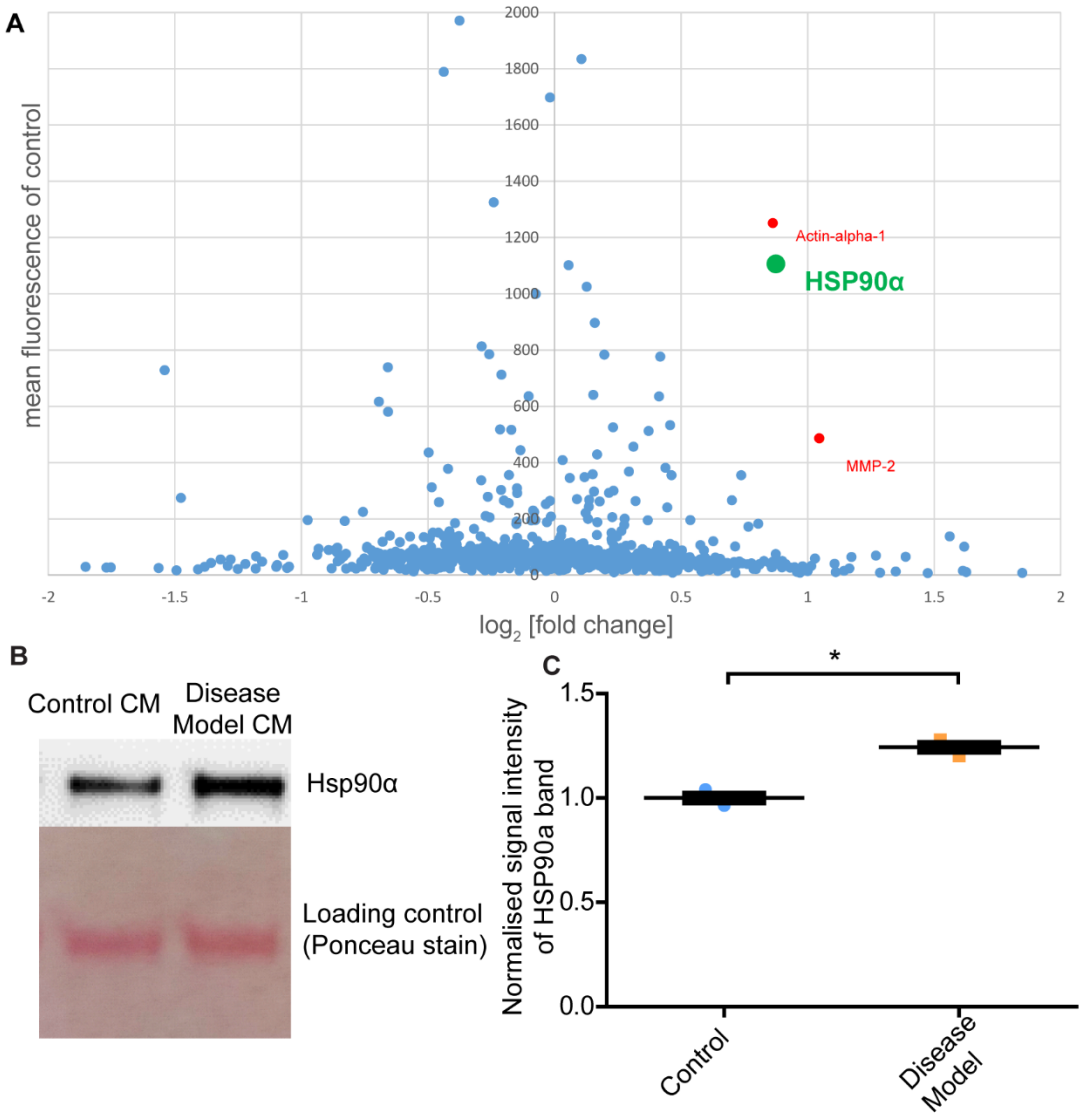


Figure 4.10: Hsp90α is secreted by brain microvascular endothelial cells (BMECs) isolated from disease model (DM) rats. A: Graph showing the results from the Full Moon Signalling Explorer antibody array. Each point represents a different protein detected by the array. The y-axis shows the mean fluorescence of the spots for that protein on the array of the control conditioned media (CM). The x-axis shows the $\log_2$ of the fold change between the DM CM and control CM (i.e. brightness of spot in DM CM divided by brightness of spot in control CM). Points further to the right represent proteins which are at higher levels in DM CM, while those on the left represent proteins which are at lower levels in DM CM compared to controls. Spots with a mean fluorescence below 400 are unreliable (as this is too close to the negative control) and those with $\log_2$ [fold change] less than 0.5 don't show a very different level between DM and control CM. This leaves three candidate proteins, indicated in red and green. Using other quality control methods (consistency of fluorescence across the spot, variation between repeats) HSP90α, indicated in green, was chosen as the first candidate to investigate. B: Western blot showing HSP90α levels in CM from control (left) and DM (right) BMECs. The darker band in DM CM demonstrates that there is more HSP90α in DM BMEC CM, confirming the findings from the antibody array. These bands were smaller (~75kDa) than the expected size of HSP90α (~86kDa), suggesting that the protein has been cleaved. Also shown is a ponceau stain of the membrane, which stains total protein on the gel and shows a band for bovine serum albumin (BSA) which is present in the culture media, as a loading control, demonstrating that the protein gel was loaded evenly. B: Quantification of western blots, showing the signal of the HSP90α band normalised to the loading control of that lane, across different samples shows that the increase in HSP90α secretion is significant (Mean ± SEM; *: $p<0.05$, paired t-test; n=3).

To see if HSP90α is the secreted factor responsible for the changes in OPCs, I first added recombinant HSP90α (rHSP90α) to cultures of OPCs. I initially added this at a range of doses at which the recombinant protein had previously been shown to have an effect in a wound healing assay (Li et al., 2007) and found the optimal dose to be 1μg/ml. I added the recombinant protein when the cells were plated, and cultured the cells for the same amount of time as the CM experiments, two days. I found that the addition of rHSP90α alone was enough to mimic the blocked maturation phenotype of OPCs which I see with DM BMEC CM, causing increased numbers of immature OPCs (49% ± 17% more; $p<0.05$, paired t-test; n=4; **Figure 4.11 A-C**) and reduced numbers of mature oligodendrocytes (13% ± 5% less; $p<0.05$, paired t-test; n=4; **Figure 4.11 A-B, D**) compared to controls without rHSP90α added. However, the addition of rHSP90α was not able to recapitulate the proliferation phenotype of OPCs which I see with DM BMEC CM, causing no change in the number of proliferating cells (**Figure 4.12**). This suggests that the addition of HSP90α is sufficient to cause the blocked maturation of OPCs I see in human brains with SVD and DM rats, but not the increased proliferation of OPCs.

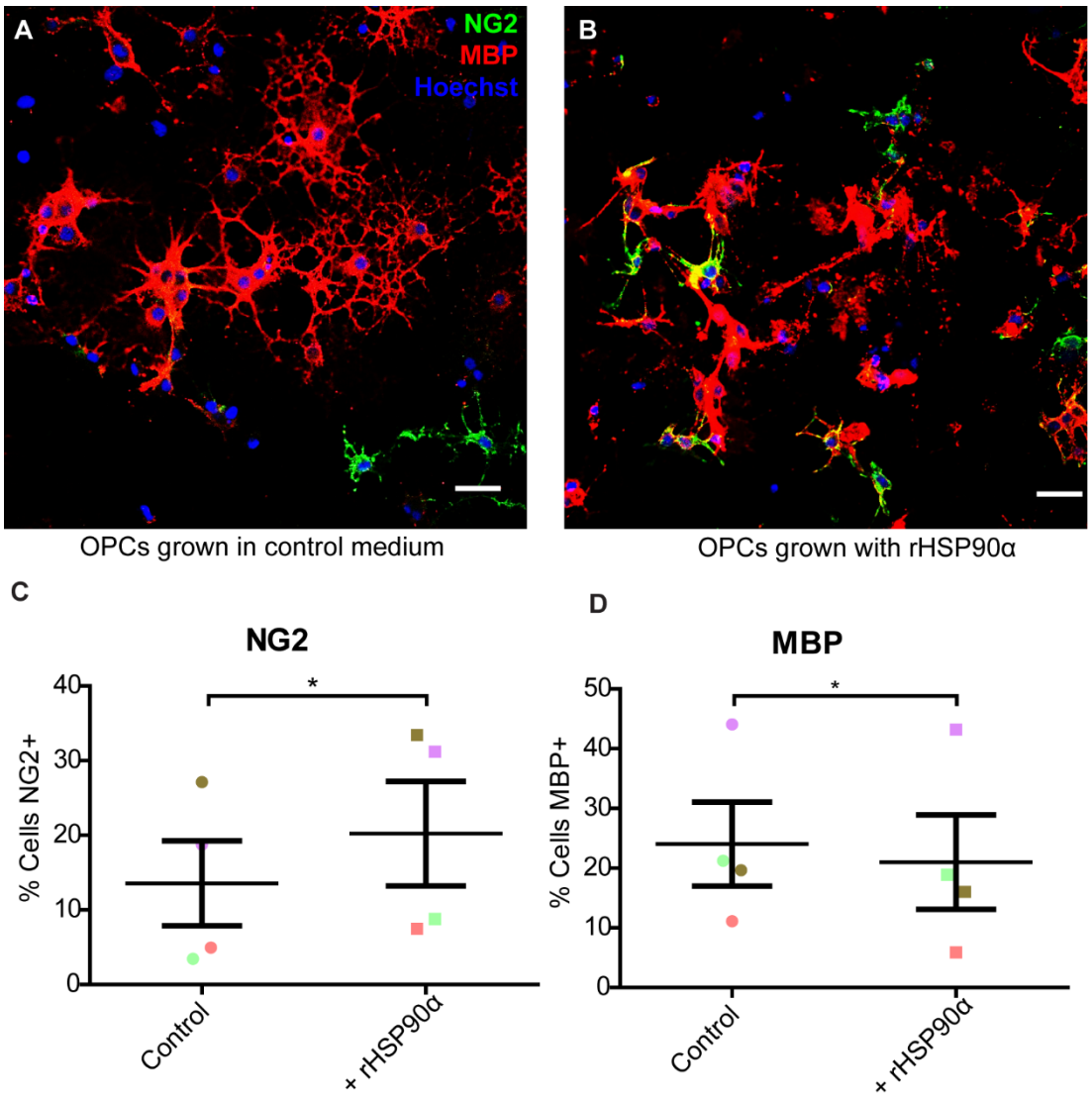


Figure 4.11: Oligodendrocyte precursor cells (OPCs) mature less when grown with recombinant heat shock protein 90 alpa (rHSP90α). A-B: Fluorescent images showing NG2, a marker of immature OPCs (green), MBP, a marker of myelin expressing mature oligodendrocytes (red), and Hoechst, a nuclear marker (blue), in cultures of OPCs grown in control conditions (A) and with rHSP90α added (B). In the cultures grown in control conditions, there are more mature, MBP expressing cells whereas in the cultures grown with HSP90α there are more immature, NG2 expressing cells. C-D: Quantification of the percentage of NG2+ cells (C) shows more immature OPCs in cultures grown with rHSP90α (squares) compared to those grown without (circles), while quantification of the percentage of MBP+ cells (D) shows significantly fewer mature oligodendrocytes in cultures grown with rHSP90α compared to control. Each colour represents a different paired repeat (Mean ± SEM; *: $p<0.05$, paired t-test; n=4). Scale bar = 25µm.

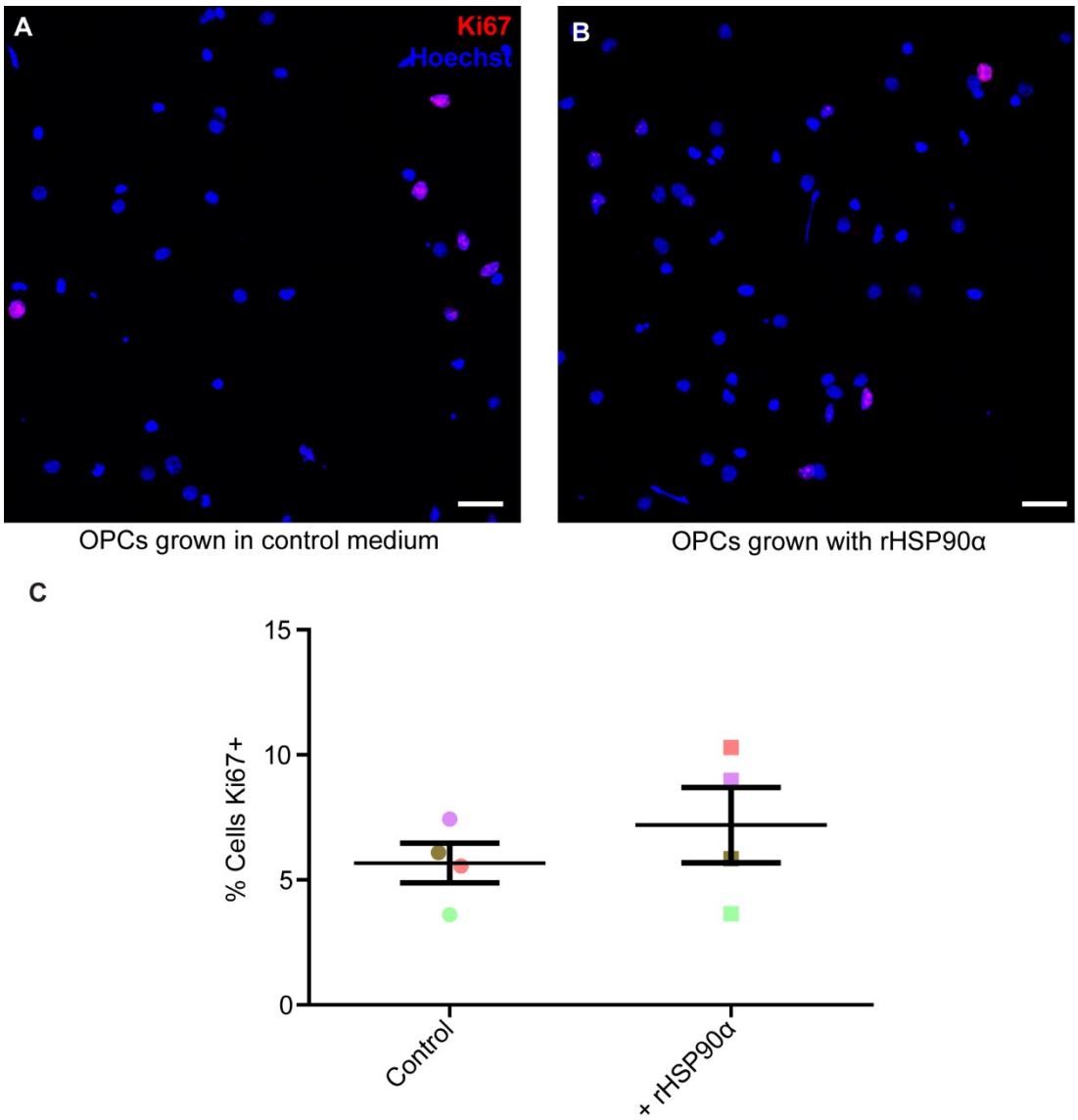


Figure 4.12: Oligodendrocyte precursor cells (OPCs) do not proliferate more with recombinant heat shock protein 90 alpha (rHSP90α). A-B: Fluorescent images showing Ki67, a marker of proliferating nuclei (red), and Hoechst, a nuclear marker (blue), in cultures of OPCs grown in control conditions (A) and with rHSP90α (B). C: Quantification of the percentage of Ki67+ cells shows no difference in proliferation between cultures grown with rHSP90α (squares) and those without (circles). Each colour represents a different paired repeat (Mean ± SEM; n=4). Scale bar = 25μm.

I next added a blocking antibody to HSP90α with CM from control and DM BMECs to see if this would block the effects which DM BMEC CM has on OPCs. Though inhibitors exist for HSP90, these are not specific to the alpha form of the protein. As with the recombinant protein, I initially added this blocking antibody at a range of concentrations shown to be effective in a wound healing assay (Li et al., 2007), and found the optimum dose to be 1.7μg/ml. I found that adding the blocking antibody to HSP90α with DM CM blocks the maturation phenotype, stopping the increased number of immature OPCs (**Figure 4.13 A-D**) and reduced number of mature oligodendrocytes (**Figure 4.13 A-C, E**) normally seen with DM CM (**Figure 4.5**). However, blocking HSP90α does not alter the effect of DM BMEC CM on the proliferation of OPCs (**Figure 4.14**).

These data demonstrate that HSP90α is both necessary and sufficient to induce the maturation block of OPCs observed in SVD, but not the increased proliferation of OPCs.

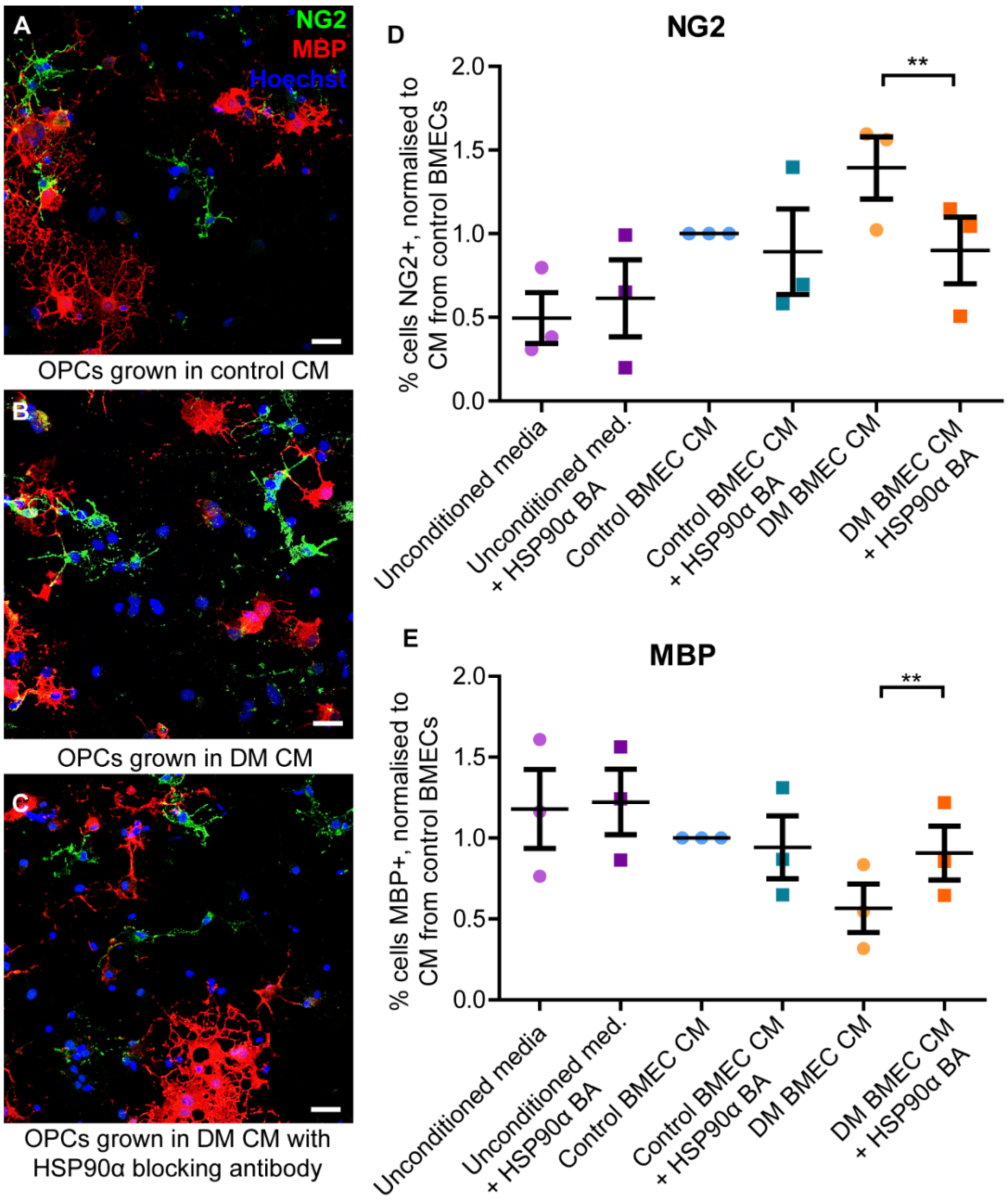


Figure 4.13: Blocking antibody (BA) against heat shock protein 90 alpha (HSP90α) blocks the reduced maturation of oligodendrocyte precursor cells (OPCs) caused by conditioned media (CM) from brain microvascular endothelial cells (BMECs) isolated from disease model (DM) rats. A-C: Fluorescent images showing NG2, a marker of immature OPCs (green), MBP, a marker of myelin expressing mature oligodendrocytes (red), and Hoechst, a nuclear marker (blue), in cultures of OPCs grown in control BMEC CM (A), DM BMEC CM (B), and DM BMEC CM with HSP90α BA added (C). In the cultures grown in control CM, there are more mature, MBP expressing cells whereas in the cultures grown in DM CM there are more immature, NG2 expressing cells. However, with HSP90α BA added to DM CM we see a return to more mature, MBP expressing cells. D-E: Quantification of the percentage of NG2+ cells normalised to control CM (D) shows more immature OPCs in cultures grown in DM CM (orange) compared to both those grown in control CM (blue) and those in unconditioned media, while quantification of the percentage of MBP+ cells normalised to control CM (E) shows significantly fewer mature oligodendrocytes in cultures grown in DM CM compared to control CM. In both of these graphs the addition of HSP90α BA (squares) returns cell numbers with DM CM to that of control CM. (Mean ± SEM; **: $p<0.01$, paired t-test; n=3). Scale bar = 25μm.

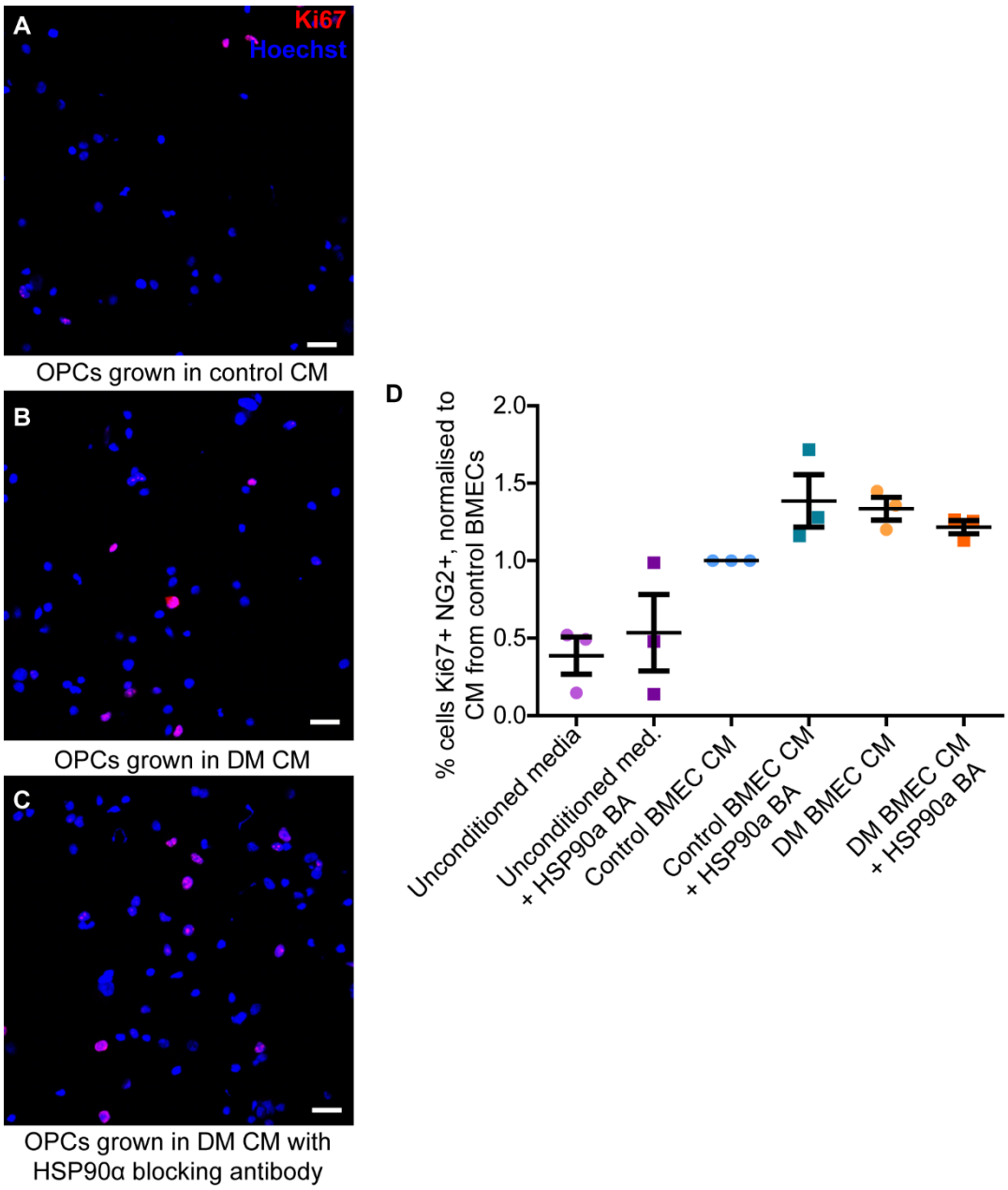


Figure 4.14: Blocking antibody (BA) against heat shock protein 90 alpha (HSP90α) has no effect on the proliferation of oligodendrocyte precursor cells (OPCs) caused by conditioned media (CM) from brain microvascular endothelial cells (BMECs) isolated from disease model (DM) rats. A-C: Fluorescent images showing Ki67, a marker of proliferating nuclei (red), and Hoechst, a nuclear marker (blue), in cultures of OPCs grown in control BMEC CM (A), DM BMEC CM (B), and DM BMEC CM with HSP90α BA added (C). In the cultures grown in DM CM there are more proliferating cells than in those grown in control CM. The addition of HSP90α BA to DM CM has no effect on this. D: Quantification of the percentage of Ki67+ cells shows more proliferating cells in cultures grown in DM CM (orange) compared to both those grown in control CM (blue) and those in unconditioned media. The addition of HSP90α BA (squares) has no consistent effect on this. (Mean ± SEM; n=3). Scale bar = 25μm.

4.5 – Discussion

4.5.1 - The effects of endothelial dysfunction on microglia

The early results in this chapter demonstrate that in both human brains with SVD and in our rat model of the disease there are dysfunctional ECs, and in the DM rat these alone are sufficient to cause the weakened BBB, OPC proliferation and OPC maturation block which I observe *in vivo*. However, I was not able to recapitulate the increase in microglia using CM, either in isolated cultures or in *ex vivo* slice cultures. This rules out the idea that the microglia changes are caused either directly by secreted factors from dysfunctional ECs, or by the OPC changes induced by dysfunctional ECs. There are a number of possible explanations for this.

One explanation is that the increase in microglia is a response to the increase in OPCs or the loss of myelin, but these changes are not marked enough in the slices grown in DM CM to cause this. While the number of OPCs in slices grown in DM CM is 37% ± 2% higher than in slices grown in control DM, we see a 102% ± 7% increase in the number of OPCs slices isolated from DM rats compared to controls (**Figure 3.10**). Similarly while the amount of myelination in slices grown in DM CM is 19% ± 2% lower than slices grown in control CM, the amount of myelination in slices isolated from DM rats is 25% ± 5% lower than slices from controls (**Figure 3.10**). This theory could be tested by growing slices in DM CM for a longer period of time to establish if this causes a more severe OPC and myelin phenotype, and hence induce a microglia phenotype.

An alternative explanation for the lack of microglial increase in CM experiments is that microglia require direct cell contact with dysfunctional ECs. While ECs are present in slice cultures, we have no evidence that CM from DM BMECs can induce endothelial dysfunction in wild-type endothelial cells. I initially attempted to test this theory by adding CM from DM BMECs to cultured ECs from an EC cell line, as these represent a wild type brain endothelial cell which grows more consistently than primary cells. However, these cells did not grow well in CM from primary BMECs.

The final possibility is that microglia from DM rats have an innate sensitivity to either factors secreted from dysfunctional ECs, or myelin damage. This theory seems less

likely, as it would suggest that humans with SVD, who also show increased numbers of microglia/macrophages (**Figure 3.7**), also have microglia which are more susceptible to damage. This idea could be tested by isolating microglia from DM rat brains, and growing them in CM from control and DM BMECs or adding them to wild-type slice cultures grown in CM from control and DM BMECs.

4.5.2 – Recombinant protein and blocking antibody experiments

The later results in this chapter demonstrate that HSP90α is both sufficient and necessary to cause the reduced maturation of OPCs, using rHSP90α and HSP90α BA. However, there are confounding factors which could be affecting these results.

The recombinant protein used in these experiments was produced in *E. coli*. Though it is a purified human protein, there is the possibility that it also contains fragments of other bacterial proteins, and these may be contributing to the effects observed. This could be controlled by adding a non-reactive recombinant protein produced by a similar method to cultures grown in parallel. However, this approach also poses problems with selection of a non-reactive protein, as it is difficult to predict what effect a given protein will have on OPC cultures.

The use of a polyclonal blocking antibody raised in rabbit raises many similar issues – it is unclear if the effects we are seeing are due to a blocking of HSP90α in the CM, a non-specific blocking of another protein, or a direct effect of the antibody on the cells. To test if the antibody is behaving in a non-specific manner, I could add other monoclonal antibodies against HSP90α. As there is less chance of all of the antibodies producing the same non-specific effect, the reproduction of these results by this method would confirm that the effect is specific. To test if the antibody itself is having an effect on the cells, a control culture could be set up where rabbit IgG fragments are added. These would mimic the effect of the blocking antibody on the cells without specifically depleting HSP90α. However, the possibility of a direct effect of the antibody on the cells could be more elegantly ruled out by depleting the CM of HSP90α without adding antibody to the media. One method to do this is to pass the CM through a column which has HSP90α BA bound to it.

4.5.3 - Heat shock protein 90 alpha (HSP90α)

The later results in this chapter show that the reduced maturation of OPCs induced by dysfunctional ECs is mediated, at least in part, by HSP90α, but this is not involved in the increased proliferation of OPCs. The HSP90 family consists of three members in rodents: HSP90α, HSP90β, and glucose-regulated protein 94 (GRP-94; also known as endoplasmin). HSP90α and HSP90β both have a similar function in overlapping locations, the cytosol or plasma membrane, and their protein sequences are 85% identical (Langer and Fasold, 2001). The differences appear to be in their activity – both are constitutively active, but only HSP90α increases in response to stress (Taherian et al., 2008) – and their capacity to function extracellularly – only HSP90α has been shown to be secreted from cells and have effects on other cells extracellularly (Eustace et al., 2004; Liao et al., 2000). GRP-94 only shows a 47% sequence similarity and is localised to the endoplasmic reticulum (Koch et al., 1986).

Together, the HSP90 proteins comprise 1% of all cytosolic proteins in the body in unstressed conditions (Lai et al., 1984). All three variants of the protein are highly expressed in all the major cell types in the brain, including ECs. The name HSP90 derives from the fact that expression of the proteins greatly increases when cells are subjected to heat shock, and all the members are approximately 90kDa. However, despite the name, HSP90 has far more functions than simply responding to stressful conditions. HSP90's best defined function is as a chaperone protein, involved in assisting protein folding, by preventing the aggregation of unfolded proteins, and stabilising folded proteins (reviewed in Picard, 2002). Though HSP90 proteins contain an adenosine triphosphate (ATP) binding site, these functions are not always ATP-dependent. A large portion of studies into the function and structure of HSP90 come from the cancer field, as HSP90 has a known anti-apoptotic effect and inhibition of HSP90 appears to be a promising target for anti-cancer therapies (Jhaveri et al., 2012). However, HSP90 is important beyond the field of cancer.

HSP90 has many well-documented interactions with eNOS, a key regulator of endothelial function. These will be explored further in chapter 6.1.2. In this section, I will focus on the role of HSP90α as a secreted molecule. HSP90α has been shown to be secreted from many cell types, including vascular smooth muscle cells and

endothelial cells (Liao et al., 2000; Song et al., 2010). The mechanism by which HSP90α is secreted has not been well characterised, but some evidence suggests that it is translocated to the surface membrane, mediated by protein kinase A (PKA) dependent phosphorylation, where it is cleaved off (Wang et al., 2009). This idea that HSP90α secretion involves cleavage of the protein is supported by the fact that I found secreted HSP90α to be smaller than normal by western blot (**Figure 4.10 B**). The impetus for a cell to secrete HSP90α is again unclear, but many studies suggest that HSP90α is secreted by cells undergoing hypoxia or oxidative stress (Liao et al., 2000; Wang et al., 2009). In ECs, HSP90α secretion is increased when the cells are proliferating (Song et al., 2010).

Secreted HSP90α can have many effects. As mentioned above, one of the main areas of focus in relation to the HSP90 proteins is cancer, and from these studies it has been shown that extracellular HSP90α can increase angiogenesis (Song et al., 2010). This effect is mediated by stabilising MMP-2, in an ATP-independent manner (Eustace et al., 2004; Song et al., 2010). The fact that this process does not involve ATP means that many HSP90 inhibitors, which target the ATP binding site of HSP90 proteins, do not stop it. This is another reason why, in my experiments investigating the necessity of HSP90α in mediating EC effects on OPCs, I used a blocking antibody which would block all the functions of HSP90α, not an inhibitor which would only block the ATP-dependent functions. This increase in angiogenesis caused by secreted HSP90α could explain why it is secreted by cells which are hypoxic or in oxidative stress – to draw more blood, and hence more oxygen, to the cells.

HSP90 also plays a role in cell migration. Extracellular HSP90α has been shown to increase skin cell migration in wound healing (Li et al., 2007). This again demonstrates a role of extracellular HSP90α in repairing a hypoxic insult, suggesting that HSP90α is secreted by hypoxic cells. HSP90 on the cell surface has also been shown to be involved in neuronal and glial migration during development (Sidera et al., 2004).

For the purposes of this thesis, we are interested in what effects extracellular HSP90α has on OPCs. Specifically, we are interested in how HSP90α secreted from dysfunctional ECs can prevent OPC maturation

4.5.4 - HSP90 and OPCs

A few studies have looked at HSP90 in OPCs in response to the finding that antibodies against HSP90β are often found circulating in the blood of patients with a demyelinating disease, multiple sclerosis (MS) (Cid et al., 2004). It has been shown that HSP90β is highly expressed on the surface of OPCs, and that the addition of anti-HSP90β antibodies isolated from MS patients is toxic to OPCs in culture (Cid et al., 2004). It has also been shown that inhibitors of HSP90 kill OPCs *in vitro*, though in very low doses HSP90 inhibitors can protect OPCs from the toxic effects of anti-HSP90β antibodies isolated from MS patients (Alcazar and Cid, 2009; Cid and Alcazar, 2010). Together, these data suggest that unimpeded expression of HSP90β on the cell surface plays a role in OPC survival, as any interference with these surface proteins causes the death of OPCs.

In section 4.5.3, I described how HSP90α and HSP90β are functionally very similar, and differ largely in their normal localisation. It therefore follows that if increased expression of HSP90β at the cell surface increases OPC survival, then increased levels of HSP90α would do the same if localised similarly. Thus, if there is a mechanism by which extracellular HSP90α is localised to the cell surface of OPCs, this could explain the results shown in this chapter. HSP90α secreted by dysfunctional ECs could cause a reduction in OPC maturation by increasing the survival of OPCs, at the expense of mature oligodendrocytes.

One such mechanism by which this could happen is by the binding of HSP90α to the receptor low density lipoprotein receptor-related protein 1 (LRP1; also known as CD91). LRP1 is expressed at the plasma membrane and is involved in receptor mediated endocytosis. It has been shown that extracellular HSP90 binds to LRP1, is endocytosed and then expressed on the cell surface (Basu et al., 2001). Though this has not been shown specifically in OPCs, LRP1 is highly expressed in OPCs, with the expression level decreasing as OPCs mature, to the point where the expression level is over 50 times lower in mature myelinating oligodendrocytes (Barres Brain RNA-Seq Database, described in chapter 5.2 (Zhang et al., 2014)). Thus, exogenous HSP90α could preferentially enter OPCs over mature oligodendrocytes, increasing OPC survival at the expense of mature oligodendrocytes. This theory could be tested by

quantifying cell survival in cultures of OPCs, both with and without rHSP90α and DM BMEC CM, using a terminal deoxynucleotidyl transferase dUTP nick end labelling (TUNEL) assay for apoptosis. If OPCs grown in DM BMEC CM or with rHSP90α show less cell death than those grown in control media, with no reduction in cell death in mature oligodendrocytes, this would support the theory detailed above.

Though a mechanism linking HSP90 expression to OPC survival has not been shown, this could be mediated by the Akt pathway. The Akt pathway is an intracellular cell signalling pathway, and HSP90α plays a crucial role in the pathway by both stabilising and activating Akt (Basso et al., 2002; Sato et al., 2000). A number of studies have shown that activation of the Akt pathway plays an important role in OPC survival, including one looking at the effects of ECs on OPC survival (Arai and Lo, 2009; Flores et al., 2000). HSP90α stabilisation and activation of Akt could also be affecting OPC maturation more directly, as Akt activation has been shown to be involved in suppressing OPC maturation (Sussman, 2005). The theory that the effects of HSP90α on OPCs are mediated by the Akt pathway could be tested by first measuring levels of Akt and activated Akt in OPCs after the addition of rHSP90α. If that suggests that the Akt pathway is activated in OPCs in the presence of extracellular HSP90α, inhibitors and activators of the Akt pathway could be added along with rHSP90α to see if they modulate its effects.

4.5.5 - Other secreted factors

While these data show that HSP90α secreted by DM BMECs is responsible for the block in OPC maturation, it does not seem to have an effect on the proliferation of OPCs, suggesting another mechanism, and another secreted factor, is involved. In the first instance we could try and identify this by reanalysing the data from the antibody array, to see if there are any other hits. The next most reliable hit was matrix metalloprotease 2 (MMP-2), a protein involved in the breakdown of extracellular matrix. This has been linked previously to hypoxic myelin breakdown, whereby an inhibitor of MMP-2 prevents myelin breakdown, but not oligodendrocyte loss, in a mouse model of hypoxic hypoperfusion (Walker and Rosenberg, 2010). MMPs have also been linked to genetic forms of SVD, with a genetic polymorphism in MMP-2

associated with SVD (Zhang et al., 2015) and the implication of MMP involvement in inherited forms of SVD (reviewed in Joutel et al., 2015). The fact that HSP90α is known to work synergistically with MMP-2 extracellularly (section 4.5.3) also makes this a promising target. However, this and the other potential hits from the array were excluded initially due to the low confidence in the fluorescent spots on the array, and we may not be able to confirm these by western blot. Therefore we could search for further hits by extracting RNA from control and DM BMECs and carrying out RNA-Seq. This would not only allow us to identify other factors which may be secreted by DM BMECs, but would also allow us to compare the expression profiles between the two cell types, providing further evidence that DM BMECs are dysfunctional, and what this dysfunctional signature consists of.

The data in this chapter demonstrate that many of the changes we see in SVD are downstream of a primary endothelial dysfunction. However, this does not explain what is causing the endothelial dysfunction in the first place. While in humans there are a myriad of environmental factors (e.g. hypertension, smoking, diabetes) or genetic polymorphisms (e.g. in the gene for eNOS) which could cause this, the origin of this in our DM rats is less clear. In the next chapter, I will explore the genetic background of these rats to try and pinpoint the upstream cause of the endothelial dysfunction.

Chapter 5: What Are the Causes of Endothelial Dysfunction in the Disease Model Rat: Genetics Results

5.1 – Introduction

In the previous chapters, I have demonstrated that in a rat model of small vessel disease (SVD) we see a range of changes early on, before classical pathology. These start with an early loss of blood brain barrier (BBB) integrity, followed by a differentiation block and proliferation of oligodendrocyte precursor cells (OPCs), followed by an increase in the number of macrophages/microglia. I also demonstrated that all of these changes occur in an early stage of the human disease.

I then went on to demonstrate that rather than the later changes being caused by leakage of blood products through an impaired BBB, all of these changes are in fact caused by a primary endothelial cell (EC) dysfunction, inherent to the ECs. I showed that these dysfunctional ECs cause the changes in OPCs through secreted factors, and that one of the secreted factors responsible for the block in OPC maturation is HSP90α.

These data show the downstream effects of endothelial dysfunction, but it is also interesting to consider what is upstream and causing the endothelial dysfunction in the first place.

In humans there are a range of possibilities, and the lack of clear understanding of what can cause SVD makes it hard to pinpoint definitively what could be causing endothelial dysfunction. One possibility is that it may be caused by environmental factors. Hypertension, smoking and diabetes mellitus have all been previously associated with SVD, though none have shown a strong correlation (see chapter 1.7). These environmental factors are also all known causes of endothelial dysfunction (Johnstone et al., 1993; Ozaki et al., 2010; Panza et al., 1990; Pittilo, 2000). This is explored further in chapter 6.2.1. The weak correlation of these risk factors individually with SVD could be due to the fact that these work together or in concert with other elements to lead to endothelial dysfunction severe enough to cause SVD.

These other elements could be genetic. Aside from the monogenic inherited forms of SVD (see chapter 1.6) it has also been shown that certain genetic polymorphisms can increase susceptibility to or protect against SVD, discussed in chapter 6.2.4. Amongst

these are a number of studies which have shown that certain polymorphisms in endothelial nitric oxide synthase (eNOS), a key protein for normal endothelial function, can protect against small vessel disease (Elbaz et al., 2000; Hassan et al., 2004a; Poggesi et al., 2015).

To elucidate these polymorphisms further, larger genome wide association studies (GWAS) would need to be carried out on sufferers of SVD, to try and pinpoint what genetic polymorphisms may pose risk factors. Some GWAS have already been carried out on SVD patients, showing some interesting gene variants which may be related to endothelial dysfunction (reviewed in Haffner et al., 2015). These will be explored in chapter 6.2.5. However, developing this further in humans is beyond the scope of this project.

Instead, I was interested in discovering what genetic factors might play a role in causing endothelial dysfunction in the disease model (DM) rat. The aim of this chapter is to explore this further.

The DM rat I am using is the stroke prone spontaneously hypertensive rat (SHRSP), an inbred substrain of the spontaneously hypertensive rat (SHR) which is in turn an inbred strain derived from the Wistar Kyoto rat (WKY) (Okamoto, 1974). The SHR was initially bred for its hypertensive phenotype, but shows no signs of strokes or SVD. The SHRSP however, shows classic pathological signs of SVD from 8 weeks of age, and starts to suffer strokes from 20 weeks of age (Bailey et al., 2011a; Lin et al., 2001; Yamori et al., 1976). The inbred nature of these rats means that it is not clear what genetic factors may be causing the changes we see, including endothelial dysfunction. We can, however, exploit a study published in 2013 which sequenced 27 different rat strains, including all of the strains above (Atanur et al., 2013). In this study, the authors analysed a number of different hypertensive rat strains to search for common genes or pathways involved in hypertension. By reanalysing this data, I was instead able to search for genes which may be involved in causing the SVD-like changes we see in our DM rat.

5.2 – Reanalysis of genetic data

The Atanur et al. (2013) study was led by a group based at Imperial College, London and involved sequencing 25 new rat strains and analysing them together with two rat strains which they had previously sequenced. These strains included 11 widely used models of hypertension, diabetes and insulin resistance, along with the relevant control strains. Though the colonies of these different strains are kept at different locations around the world and deoxyribonucleic acid (DNA) samples were gathered at these locations, all the sequencing was carried out in the same location to reduce variability. The sequencing was carried out using a next generation Illumina high throughput system with at least 20x coverage for all strains. Segments of the sequence of one of the strains (LE/Stm) were compared with a publicly available sequence of the same strain carried out by Sanger sequencing, and from this the authors were able to calculate a false positive rate for variant calls in this study of 0.38% for single nucleotide variants (SNVs) and 3.75% for indels (insertion/deletion mutations), and a false negative rate of 8.1% for SNVs and 10.98% for indels. Genomic variants were detected using the Genome Analysis Toolkit (GATK). These genomic variants were then analysed across all strains to discover co-evolved clusters of genes which may contribute to the hypertensive phenotype of these different rat strains. Alongside their published analysis of genes underlying hypertension, the authors also provided lists of: clusters of SNVs, frameshift mutations (insertion or deletion of a number of bases indivisible by three, which will cause changes in multiple codons) in coding regions and SNVs predicted to lead to the gain of a STOP codon (stop-gain).

For my initial analysis, I chose to look for mutations which were the most likely to lead to non-functioning proteins. Though coding and non-coding SNVs have been documented to have deleterious effects in many diseases, these effects are more difficult to predict. I therefore analysed the lists of coding frameshift mutations and stop-gain mutations in the first instance, and found 78 such mutations in SHRSP compared to WKY control. As an initial method of filtering, to focus on the most likely candidates, I decided to exploit the fact that the SHRSP and SHR are genetically very similar, but the SHR shows no signs of SVD. I therefore looked for genes which were homozygous mutated (as a phenotype consistent across all individuals and stable across generations must be caused by a homozygous mutation) in SHRSP, but normal

in SHR. This excludes any mutations present in both SHR and SHRSP, which likely contribute to hypertension and are unlikely to be important for SVD as SHR does not show signs of SVD. From a candidate list of 78 mutations, this reduced the list to 32 mutations which were only present in SHRSP, but not SHR (**Figure 5.1 A**).

I then used the Variant Effect Predictor (VeP) tool from ENSEMBL (Cunningham et al., 2015; Release 66) to determine which of the frameshift mutations was expected to lead to a truncated protein, as this is more likely to predictably cause a severe phenotype. This narrowed down the list to 30 mutations.

The next stage of filtering was to determine where the genes are expressed. As the disease is neurological, I focussed on genes which are expressed in the brain, determined using the Allen Brain Atlas (Lein et al., 2007) (Website: © 2015 Allen Institute for Brain Science. Allen Mouse Brain Atlas [Internet]. Available from: http://mouse.brain-map.org) (**Figure 5.1 C**). This tool shows data from in situ hybridisations (ISH) which have been carried out to measure messenger ribonucleic acid (mRNA) levels throughout the mouse brain, displayed in a format which allows easy visualisation of the whole brain in a three dimensional format. Unfortunately a similar tool is not available for mRNA expression in the rat brain, however I compared the results from this tool with a similar tool for the human brain and worked under the assumption that a gene which is expressed in both mouse and human brains is likely to also be expressed in rat brains.

The fact that I have shown that the initial cause of the disease phenotype is an endothelial dysfunction which is cell autonomous means that I initially only looked for mutations in genes which are expressed in endothelial cells, determined using the Barres Brain RNA-Seq Database (Zhang et al., 2014) (**Figure 5.1 D**). This tool displays relative expression levels of genes in different brain cell types (astrocytes, neurons, OPCs, newly formed oligodendrocytes, myelinating oligodendrocytes, microglia and endothelial cells), using RNA sequencing data generated from sorted cells from normal adult mouse brain. As a similar tool does not exist using cells from rat brain, I worked under the assumption that a given gene would have a similar cellular expression pattern in both rat and mouse. This led to a list of 6 candidate genes which appeared mutated in SHRSP and may cause its pathology. I am aware that these genes

have been chosen using various assumptions, but I believe that this is a reasonable first pass analysis.

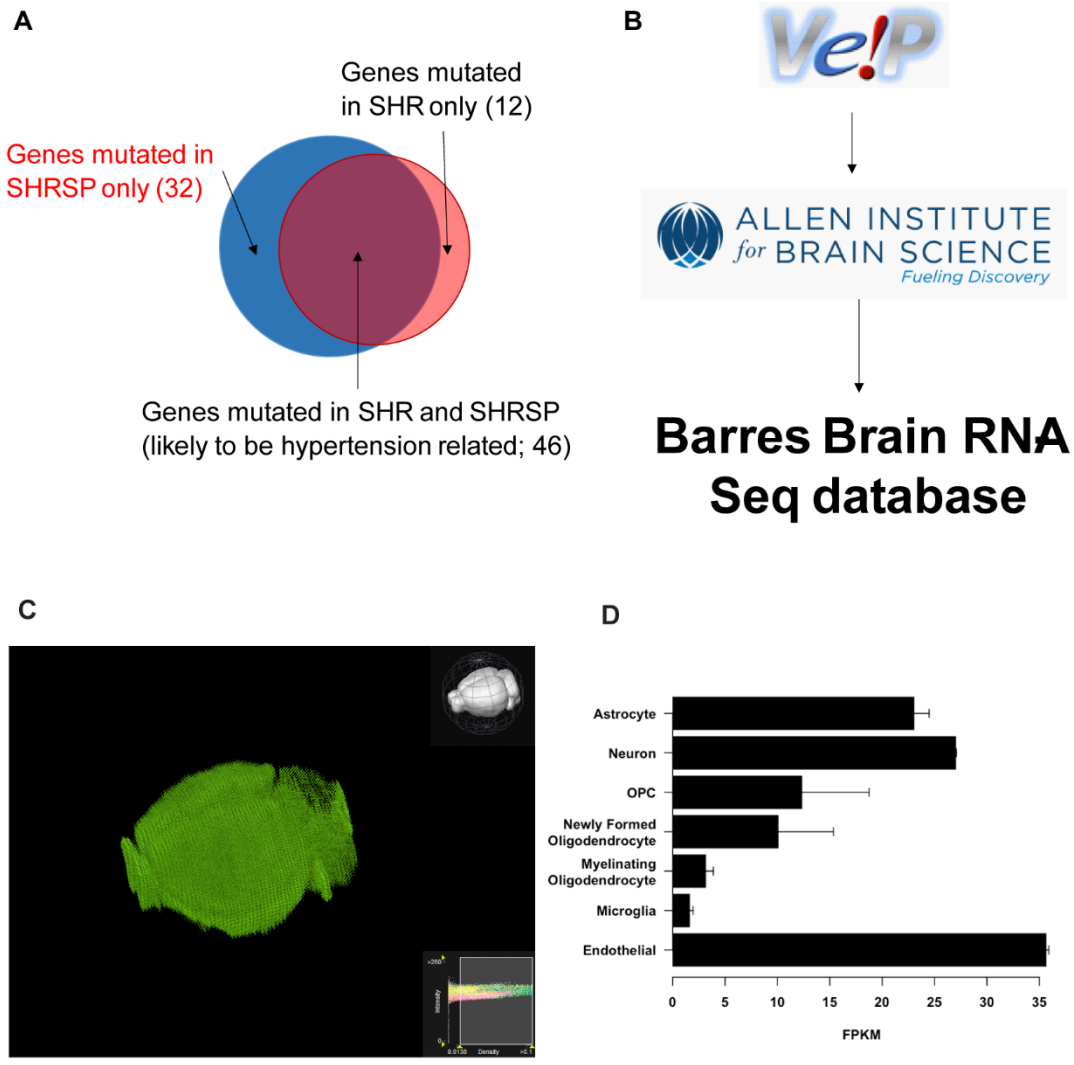


Figure 5.1: Methods for reanalysing and filtering genome sequencing data from Atanur et al., 2013. A: Venn diagram illustrating the overlap between genes mutated in our disease model rat, the stroke prone spontaneously hypertensive rat (SHRSP), and its nearest relative which develops hypertension but no small vessel disease (SVD) like pathology, the spontaneously hypertensive rat (SHR). Of the 78 genes predicted to have frameshift or stop-gain mutations in SHRSP, 46 are also predicted to be mutated in SHR and are likely to contribute to the hypertensive phenotype of both rat strains, rather than the SVD phenotype unique to SHRSP. B: Diagram illustrating the filtering steps undertaken. The mutations were first run through the Variant Effect Predictor (VeP) tool from ENSEMBL (Cunningham et al., 2015; Release 66) to assess which frameshift mutations were predicted to lead to truncated proteins. The list of genes was then run through the Allen Mouse Brain Atlas (Lein et al., 2007; Website: © 2015 Allen Institute for Brain Science. Allen Mouse Brain Atlas [Internet]. Available from: http://mouse.brain-map.org) to determine which were expressed in the brain. This list was finally run through the Barres Brain RNA-Seq database (Zhang et al., 2014) to determine which genes were expressed in brain endothelial cells. C-D: Example data using the gene *Atp11b* from the Allen Brain Atlas (C) and the Barres Brain RNA-Seq database (D). These data show that the gene *Atp11b* is expressed throughout the brain (green dots present throughout in C) and is highly expressed in brain endothelial cells (Lower bar showing a high FPKM (Fragments Per Kilobase of transcript per Million mapped reads; measure of relative expresssion level) in D).

5.3 – Results: validation of genetic mutations

The reanalysis of a published dataset described above led me to a list of 6 genetic mutations which could be responsible for the changes I see in the DM rats: in the genes rho guanine nucleotide exchange factor 1 (*Arhgef1*), dipeptidyl peptidase 3 (*Dpp3*), collagen XVIII alpha 1 (*Col18a1*), latent transforming growth factor beta binding protein 4 (*Ltbp4*), janus kinase 3 (*Jak3*), and ATPase, Class VI, 11B (*Atp11b*). However, before any further work could be done on these genes, the mutations first needed to be validated. This validation was carried out by a Master's student under my supervision, Silvie Ruigrok.

There are two main reasons why the mutations may not be present in the DM rat as predicted from my analysis. The first is the reliability of high throughput sequencing. In traditional Sanger sequencing (also known as chain-terminator sequencing), the sequence of a length of DNA is determined sequentially, with a polymerisation reaction starting at the beginning of the sequence and prematurely stopped at each individual base. However, the lengths of sequences involved when sequencing a whole genome make this unfeasible, both technologically, as the DNA polymerase will fall off after a certain length, and practically, as this process is relatively slow. Therefore for high throughput sequencing, the length of DNA is randomly split into many small fragments, each of which is individually sequenced and then aligned to a reference genome. To increase reliability, each region of the genome is covered by at least 20 individual fragments, and the random splitting of the DNA into fragments means that there are overlaps between fragments. For SNVs, this method is very reliable, with the false discovery rate (FDR; the chance of a base being classed as mutated when it is not) in the data we are using being 0.38% (Atanur et al., 2013). However, because this method relies on aligning each fragment of DNA sequence to a reference sequence it has an increased chance of failure when there is a deletion or insertion of DNA, as this reduces the similarity between a DNA fragment and the reference sequence. Therefore for frameshift mutations the FDR is much higher, calculated at 3.75% for our data (Atanur et al., 2013). To confirm whether the mutations are real, or are simply an artefact of the sequence alignment, we need to Sanger sequence the DNA around the site where the mutation is expected to be, for a more reliable readout of the actual sequence of bases. To do this we extracted DNA from tail clips or ear punches of DM

and control rats (chapter 2.5.1), designed primers 300-500 base pairs either side of the predicted mutation site (chapter 2.11) and amplified this region using polymerase chain reaction (PCR) to give us a product 600-1,000 base pairs in length (chapter 2.5.4). This length was chosen as the first 50-100 reads of a sequencing reaction can be unreliable, as are any reads after 800-1,000. We then sent off the amplified products to be sequenced by Source BioScience (chapter 2.5.5). As well as sequencing samples from multiple animals to give us biological repeats, we also sequenced each PCR product from both the forward and reverse primers as a technical repeat.

The other form of validation required is to confirm that the mutations are actually in coding regions. While intronic mutations have been well documented to cause severe effects and are implicated in a number of diseases (Tazi et al., 2009), these are difficult to predict, and often do not even affect the gene in which the intron is located. I therefore wanted to confirm that the mutation was in an exon, and would cause a truncated protein as expected, as this is more likely to cause a predictable and testable effect. The reason that the mutations may not be exonic, despite being predicted to be so, is that the study in which the sequencing was carried out used RGSC3.4, the latest version of the rat genome reference sequence at the time, for sequence alignment and determining the boundaries between exons and introns. The current version of the rat genome reference sequence is Rnor_6.0, in which a number of gene sequences, and many predicted exon locations have changed. As any mutation within a coding region of the gene will be transcribed into mRNA, we determined whether or not the mutations are in coding regions of the gene by extracting mRNA from brain microvascular endothelial cells (BMECs) isolated from control and DM rats (as the high expression of the target genes in brain endothelial cells means that the mRNA would be enriched in these cells compared to tissue) (chapter 2.5.2), reverse transcribing it into complement DNA (cDNA) (chapter 2.5.3) and Sanger sequencing the product as described for DNA above.

From my filtered list of six candidate genes we found that two did not in fact have the genomic mutation they were predicted to have: *Arhgef1* and *Dpp3*. Of the remaining four, only one gene had the mutation in a coding region: ATPase, Class VI, type 11B (*Atp11b*) which contains a 28 base deletion (**Figure 5.2 A-C**).

ATP11B is a P4-ATPase, part of a family of phospholipid flippases which are involved in moving phospholipid molecules from the outer leaflet (extracellular or intra-vesicular) to the inner leaflet (cytoplasmic) of the membrane (reviewed in Palmgren and Nissen, 2011). While the majority of the literature on P4-ATPases does not look specifically at ATP11B, the few studies investigating it have shown that it plays an important role in vesicular transport (Moreno-Smith et al., 2013).

These data demonstrate that *Atp11b* is mutated as predicted in a coding region of DNA. To demonstrate that this causes an effect in the actual protein produced I carried out a western blot on brain tissue lysates from control and DM rats. I found that rather than leading to a truncated protein, as predicted, the mutation in fact leads to a total loss of protein (**Figure 5.2 D**). This could be because the extent of the protein truncation is so severe – a loss of one third of the amino acids – that the incomplete protein is targeted for degradation (Heck et al., 2010).

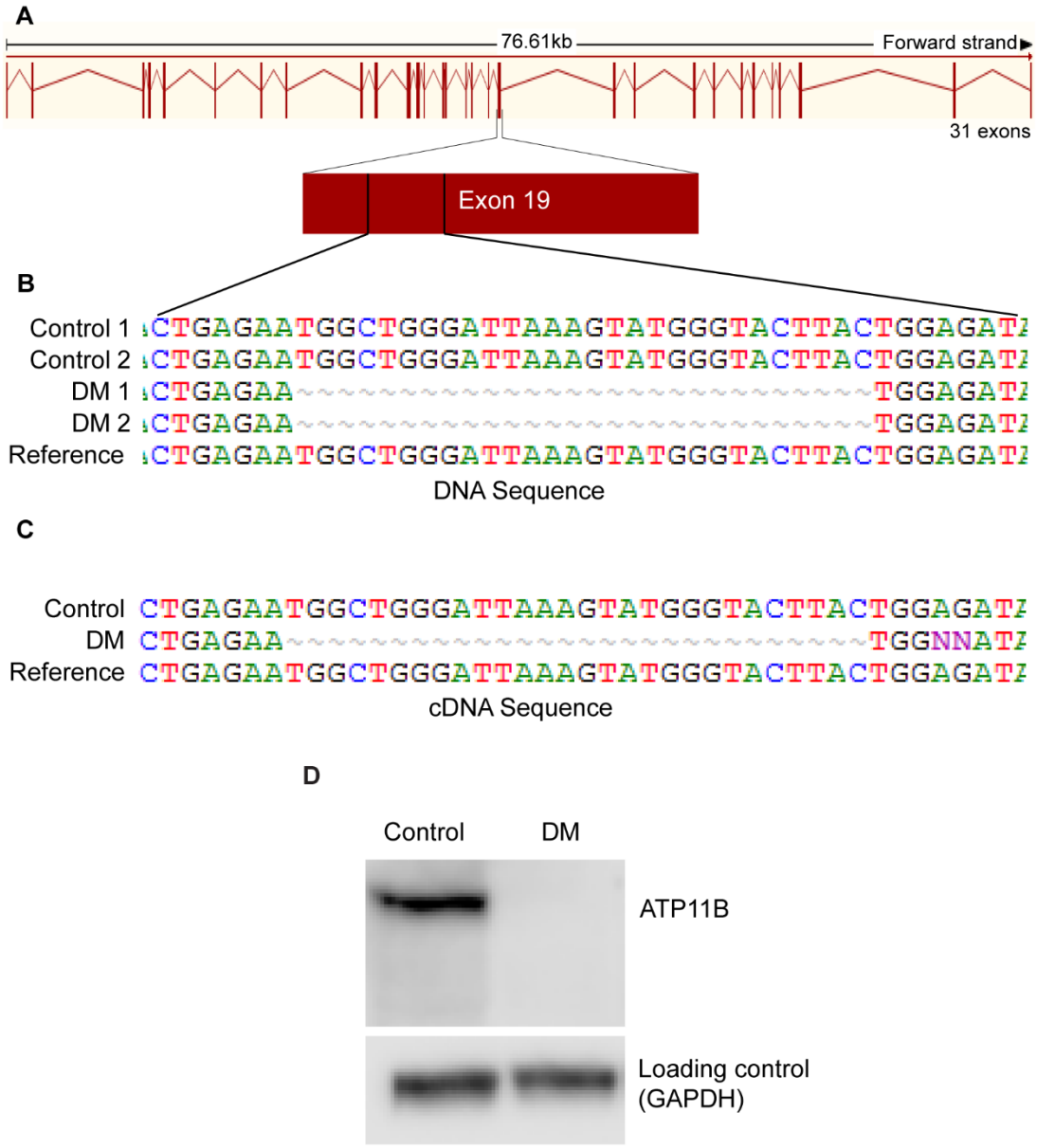


Figure 5.2: *Atp11b* is mutated in disease model (DM) rats, leading to a loss of the protein ATP11B. A: Diagram illustrating the genomic organisation of the *Atp11b* gene and where the mutation is located (adapted from ENSEMBL; Cunningham et al., 2015). B: Sequencing data showing the results of sequencing a region of deoxyribonucleic acid (DNA) amplified by polymerase chain reaction (PCR) around the predicted mutation site of *Atp11b*. The top two rows show data from control rats, the next two rows show data from DM rats, and the bottom row shows the reference sequence for comparison. A indicates an adenine base, T indicates a thymine base, C indicates a cytosine base and G indicates a guanine base. The ~ symbol indicates where there is a gap and the sequence has been adjusted in this visualisation to be aligned, thus the sequence goes from the base preceding the first ~ immediately to the base following the final ~. This data shows that in the DM samples there is a 28 base pair deletion in the *Atp11b* gene, indicated by the 28 ~ in the middle, not present in the controls. C: Sequencing data showing the results of sequencing a region of complement DNA (cDNA) reverse transcribed from messenger ribonucleic acid (mRNA) and amplified by PCR around the predicted mutation site of *Atp11b*. This demonstrates that the 28 base deletion present in the DNA sequence of DM rats is also present in mRNA, and hence is in a coding region of the gene. D: Western blot showing levels of ATP11B in the brains of control (left column) and DM (right column) rats. The absence of a band in the DM rat indicates that the mutation in *Atp11b* leads to a complete loss of the ATP11B protein.

5.4 – Results: effects of knocking down *Atp11b* in ECs

5.4.1 - Knocking down Atp11b

So far in this chapter, I have demonstrated that in the DM rats there is a frameshift mutation in the *Atp11b* gene which causes a loss of the ATP11B protein. To see if this mutation could be the cause of endothelial dysfunction, and ultimately the SVD-like changes, in the DM rats I wanted to see what the effect would be of knocking down the gene in wild-type endothelial cells. To do this I used small interfering RNA (siRNA). siRNAs are small strands of RNA whose sequence complements a section of the mRNA of the target gene. By binding to the mRNA of the target gene they target the mRNA for degradation and so stop it being translated to form the protein (reviewed in Carthew and Sontheimer, 2009). Despite their small size, the high negative charge of siRNAs prevents their normal uptake into a cell. The most common and simplest method to overcome this is to package the siRNA into liposomes which can then bind with the lipid bilayer of the cell surface membrane, a process known as transfection. While this is possible in primary cells, transfection efficiency is much higher in cell lines (Gresch and Altrogge, 2012; Ovcharenko et al., 2005), leading to a more consistent phenotype across the culture. Therefore I initially used an immortalised mouse brain endothelial cell line, known as bEND.3, for these experiments. While the use of this cell line poses disadvantages, as it is a mouse line and may have abnormal characteristics, achieving a similar transfection efficiency in primary BMECs, which could be done using short hairpin RNA (shRNA) transfected in a viral vector, is far more time-consuming and expensive. I therefore used lipofectamine based transfection into a cell line for my initial experiments.

I optimised my transfection protocol by trying different timelines for transfection, different plating densities of the bEND.3 cells, and different siRNAs targeted against different regions of the *Atp11b* gene as well as different siRNAs in combination. As bEND.3 cells reach maturity (defined by showing mature tight junctions) 4-7 days after becoming confluent (Koto et al., 2007), and the mutation in DM rats is present throughout development I grew the cells for 7 days in vitro (DIV) and transfected them early. As the effects of the siRNA wear off as the siRNA degrades I also tried transfecting the cells multiple times. The process of transfecting a population of cells

can also have effects on its own, so as a control I also transfected cells with a siRNA which was not targeted to any gene. I found optimal transfection with one of the siRNAs targeted against *Atp11b* when the cells were plated at a 50% confluent density and transfected twice, once one day after plating and once four days after plating (chapter 2.2.8). With this method I was able to knock down *Atp11b* and get lower levels of protein compared to bEND.3 cells transfected with a non-targeting siRNA (61% ± 20% less; $p<0.05$, paired t-test; n=3; **Figure 5.3**).

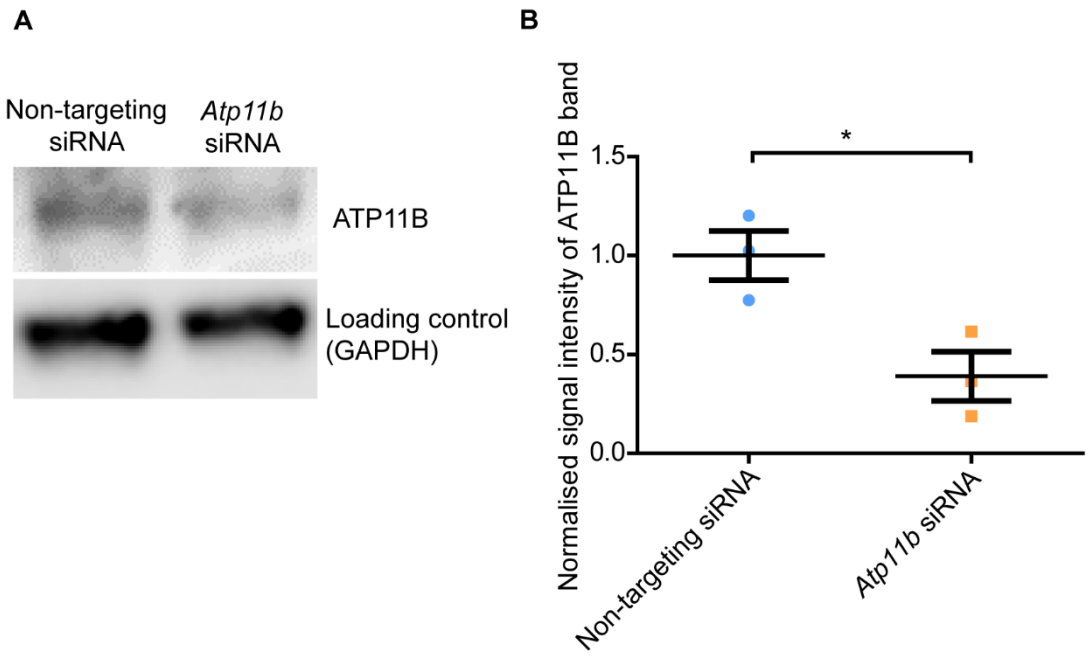


Figure 5.3: siRNA against *Atp11b* successfully knocks down levels of ATP11B protein in bEND.3 cells. A: Western blot showing levels of ATP11B protein in bEND.3 cells treated with non-targeting siRNA (left) and cells treated with siRNA against *Atp11b* (right), demonstrating a reduced level of ATP11B protein when siRNA against *Atp11b* is added. Also shown is a loading control, demonstrating that the protein gel was loaded evenly. B: Quantification of western blots, showing the signal of the ATP11B band normalised to the loading control of that lane, across different samples shows that the reduction in ATP11B levels is significant (Mean ± SEM; *: $p<0.05$, paired t-test; n=3).

5.4.2 - Effects of knocking down Atp11b on ECs

To see if knocking down *Atp11b* was causing these ECs to become dysfunctional, I looked at the proliferation of siRNA treated cells, using an antibody against Ki67 which marks cells at all active stages of the cell cycle, and found that cells transfected with *Atp11b* siRNA proliferated more than those transfected with non-targeting siRNA (57% ± 5% higher; $p<0.05$, paired t-test; n=3; **Figure 5.4**), indicating that they are dysfunctional.

I then wanted to see if this endothelial dysfunction was causing the same changes as I see in primary BMECs isolated from DM rats. To do this, I initially looked at tight junctions (TJs), and found that cells transfected with siRNA against *Atp11b* have less mature TJs compared to those transfected with non-targeting siRNA, as indicated by fewer cells having membranous claudin-5 (29% ± 4% less; $p<0.05$, paired t-test; n=3; **Figure 5.5 A-B, D**), despite normal localisation of ZO-1 to the membrane (**Figure 5.5 A-C**). As detailed previously (chapter 4.3), TJ proteins are only functional when localised to the cell surface membrane, and while normal localisation of ZO-1 is seen in the vast majority of cells, there is less localisation of claudin-5 to the membrane in bEND.3 cells transfected with siRNA against *Atp11b* compared to those transfected with non-targeting siRNA.

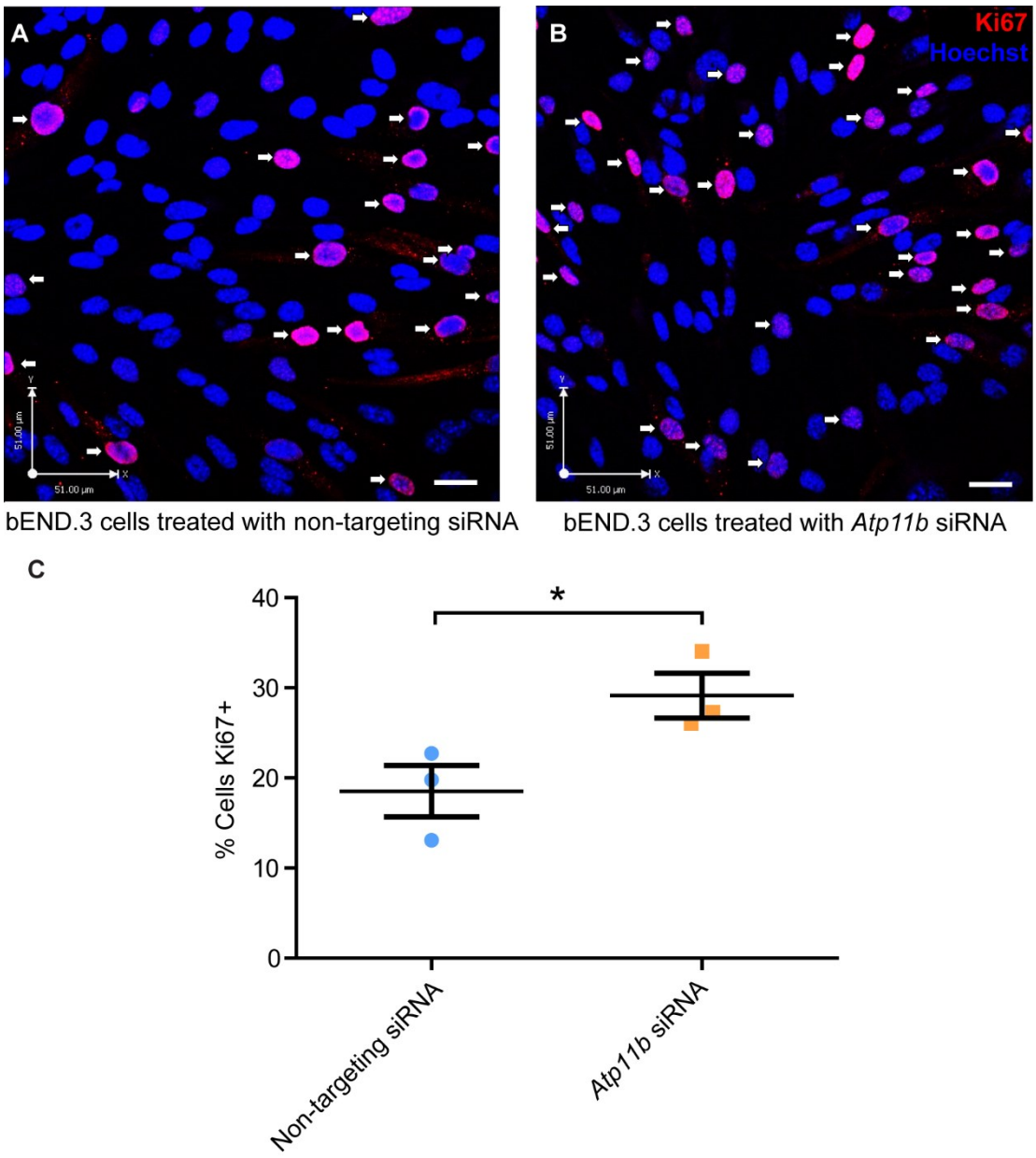


Figure 5.4: More proliferating cells in a mouse brain endothelial cell line (bEND.3 cells) treated with siRNA against *Atp11b*. A-B: Fluorescent images showing Ki67, a marker of proliferating nuclei (red), and Hoechst, a nuclear marker (blue), in cultures of bEND.3 cells treated with non-targeting siRNA (A) and siRNA against *Atp11b* (B). There are more Ki67 positive nuclei (appearing magenta, indicated by white arrows) indicating proliferating cells in cultures treated with siRNA against *Atp11b* than in those treated with non-targeting siRNA. C: Quantification of the percentage of cells which are Ki67+ shows that there are significantly more proliferating cells in cultures treated with siRNA against *Atp11b* (orange), than those treated with non-targeting siRNA (blue) (Mean ± SEM; *: $p<0.05$, paired t-test; n=3). Scale bar = 25µm.

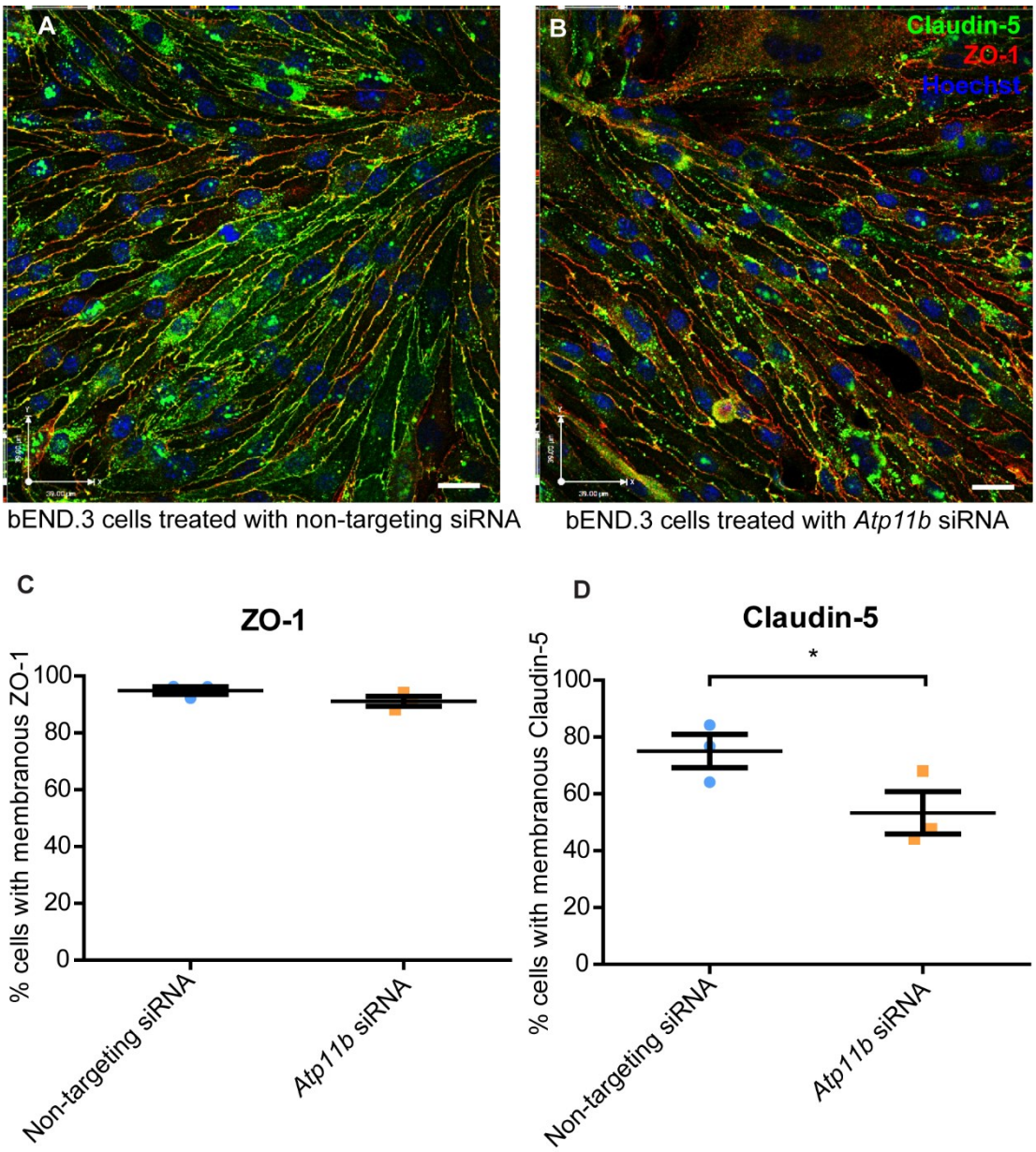


Figure 5.5: Less mature tight junctions (TJs) in a mouse brain endothelial cell line (bEND.3 cells) treated with siRNA against *Atp11b*. A-B: Fluorescent images showing claudin-5, a mature TJ protein (green), ZO-1, an immature TJ protein (red), and Hoechst, a nuclear marker (blue), in cultures of bEND.3 cells treated with non-targeting siRNA (A) and siRNA against *Atp11b* (B). TJ proteins are only functional when localised to the cell membrane. While in cultures treated with both non-targeting and *Atp11b* siRNA ZO-1 (red) is localised to the membrane in the vast majority of cells, localisation of claudin-5 (green) to the membrane (appearing yellow as it colocalises with ZO-1) is far less common in cultures treated with siRNA against *Atp11b*. C-D: Quantification of the percentage of cells with ZO-1 at the membrane (C) shows no difference between cells treated with non-targeting siRNA (blue) and siRNA against *Atp11b* (orange), however quantification of the percentage of cells with claudin-5 at the membrane (D) shows significantly fewer cells with membranous claudin-5 in cultures treated with siRNA against *Atp11b* (Mean ± SEM; *: $p<0.05$, paired t-test; n=3). Scale bar = 25µm.

5.4.3 - Effects on OPCs

To further investigate whether the knockdown of *Atp11b* is sufficient to recapitulate the phenotype I see in DM rats, and in BMECs isolated from DM rats, I took the conditioned media (CM) from siRNA treated bEND.3 cells and added it to cultures of OPCs. This allows us to see whether the knockdown of *Atp11b* causes all the aspects of endothelial dysfunction we see in primary BMECs, including secretion of the same factors inducing the same changes in OPC maturation and proliferation. As the levels of OPC maturation and proliferation vary both between preparations of OPCs and between CM from different passages of bEND.3 cells, these data are presented normalised to levels for OPCs with CM from untreated bEND.3 cells added for each experiment.

I found that adding CM from bEND.3 cells with *Atp11b* knocked down to OPC cultures increased the number of immature OPCs, expressing NG2 (16% ± 1% more; $p<0.05$, paired t-test; n=4; **Figure 5.6 A-C**), and reduced the number of mature oligodendrocytes, expressing myelin basic protein (MBP) (22% ± 3% less; $p<0.05$, paired t-test; n=4; **Figure 5.6 A-B, C**), compared to CM from bEND.3 cells treated with non-targeting siRNA. This mirrors the maturation block in OPC cultures observed when CM from DM BMECs is added, and the maturation block of OPCs seen in tissue sections from DM rats and human brains with SVD.

I also found that adding CM from bEND.3 cells with *Atp11b* knocked down increased the proliferation of OPCs in culture, measured as the percentage of cells expressing Ki67 (15% ± 1% more; $p<0.05$, paired t-test; n=3; **Figure 5.7**). This mirrors the increased OPC proliferation seen when CM from DM BMECs is added, and the increase in OPC proliferation seen in tissue sections from DM rats and human brains with SVD.

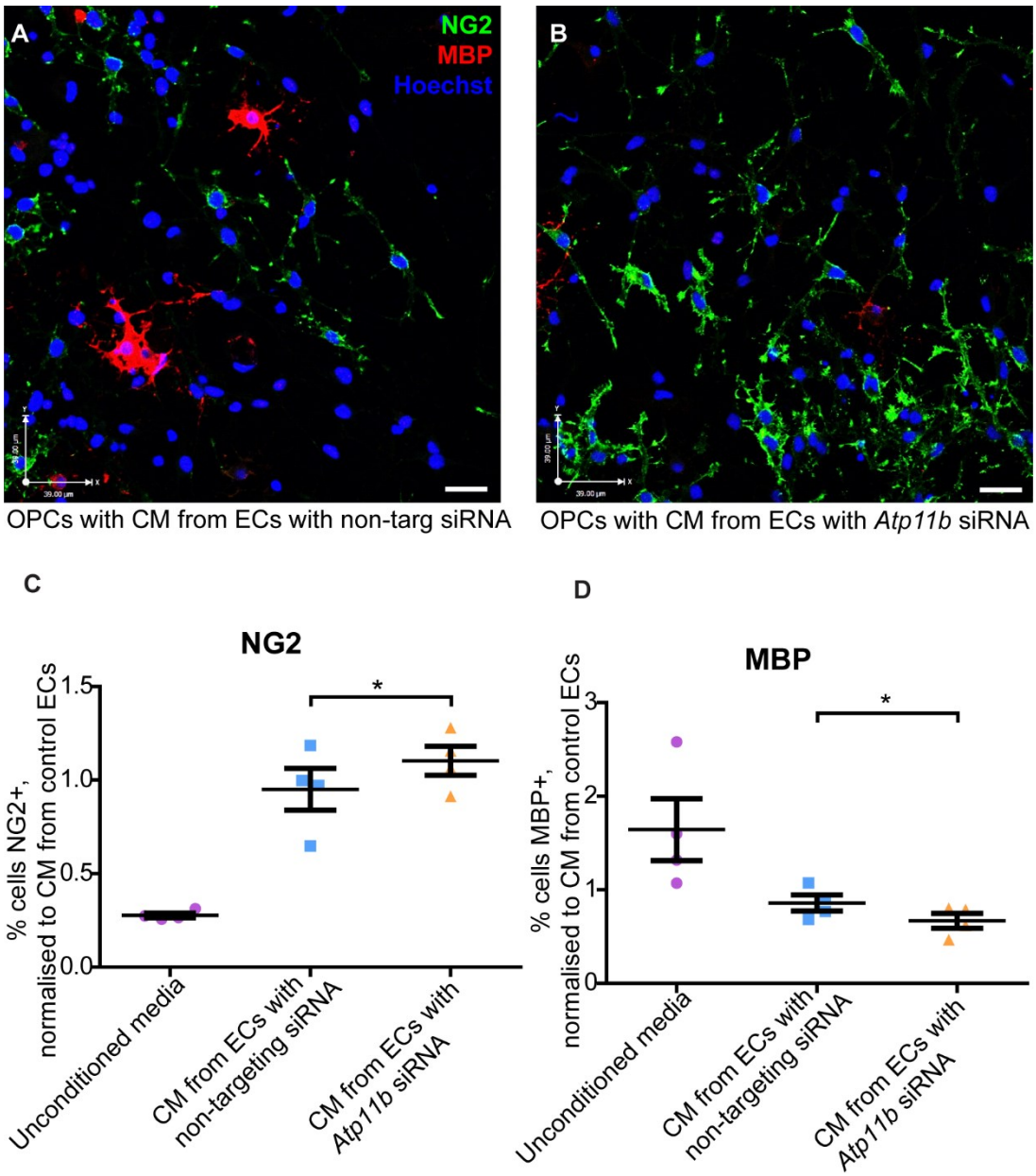


Figure 5.6: Oligodendrocyte precursor cells (OPCs) mature less when grown in conditioned media (CM) from bEND.3 cells treated with *Atp11b* siRNA. A-B: Fluorescent images showing NG2, a marker of immature OPCs (green), MBP, a marker of myelin expressing mature oligodendrocytes (red), and Hoechst, a nuclear marker (blue), in cultures of OPCs grown in CM from bEND.3 cells treated with non-targeting (A) and *Atp11b* (B) siRNA. In the cultures grown in CM from non-targeting siRNA treated bEND.3 cells, there are more mature, MBP expressing cells whereas in the cultures grown in CM from *Atp11b* siRNA treated bEND.3 cells there are more immature, NG2 expressing cells. C-D: Quantification of the percentage of NG2+ cells normalised to levels in cultures grown in CM from untreated bEND.3 cells (such that 1 = an average of 47% NG2+) (C) shows more immature OPCs in cultures grown in CM from *Atp11b* siRNA treated bEND.3 cells (orange) compared to control CM from non-targeting siRNA treated bEND.3 cells (blue) and unconditioned media (purple), while quantification of the percentage of MBP+ cells similarly normalised (such that 1 = an average of 15% MBP+) (D) shows significantly fewer mature oligodendrocytes in cultures grown in CM from *Atp11b* siRNA treated bEND.3 cells compared to non-targeting siRNA treated bEND.3 cells (Mean ± SEM; *: $p<0.05$, paired t-test; n=4). Scale bar = 25µm.

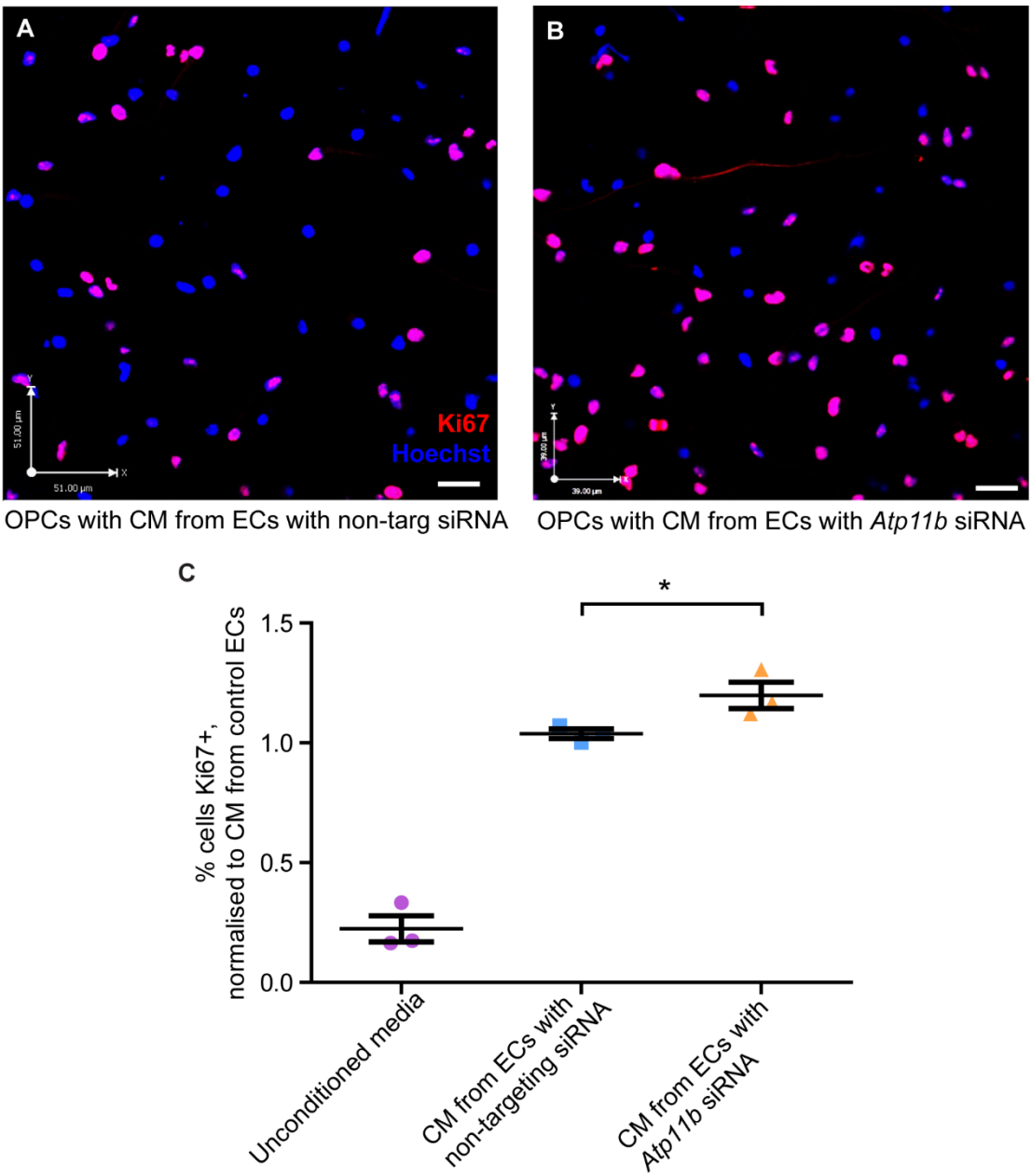


Figure 5.7: Oligodendrocyte precursor cells (OPCs) proliferate more when grown in conditioned media (CM) from bEND.3 cells treated with *Atp11b* siRNA. A-B: Fluorescent images showing Ki67, a marker of proliferating nuclei (red), and Hoechst, a nuclear marker (blue), in cultures of OPCs grown in CM from bEND.3 cells treated with non-targeting (A) and *Atp11b* (B) siRNA. In the cultures grown in CM from non-targeting siRNA treated bEND.3 cells, there are more proliferating OPCs, expressing Ki67 (appearing magenta). C: Quantification of the percentage of Ki67+ cells normalised to levels in cultures grown in CM from untreated bEND.3 cells (such that 1 = an average of 44% Ki67+ cells) shows more proliferating OPCs in cultures grown in CM from *Atp11b* siRNA treated bEND.3 cells (orange) compared to control CM from non-targeting siRNA treated bEND.3 cells (blue) and unconditioned media (purple) (Mean ± SEM; *: $p<0.05$, paired t-test; n=3). Scale bar = 25µm.

To determine whether these downstream effects of endothelial dysfunction in bEND.3 cells treated with *Atp11b* siRNA may be happening by a similar mechanism to the downstream effects of endothelial dysfunction in DM BMECs, I quantified the amount of HSP90α secreted into the media by bEND.3 cells treated with *Atp11b* siRNA. I found that CM from bEND.3 cells with *Atp11b* knocked down contained more HSP90α than CM from cells treated with non-targeting siRNA (30% ± 0.6% more; $p<0.05$, paired t-test; n=3; **Figure 5.8**). This suggests that cells with *Atp11b* knocked down may be causing their downstream effects on OPCs through a similar mechanism to DM BMECs.

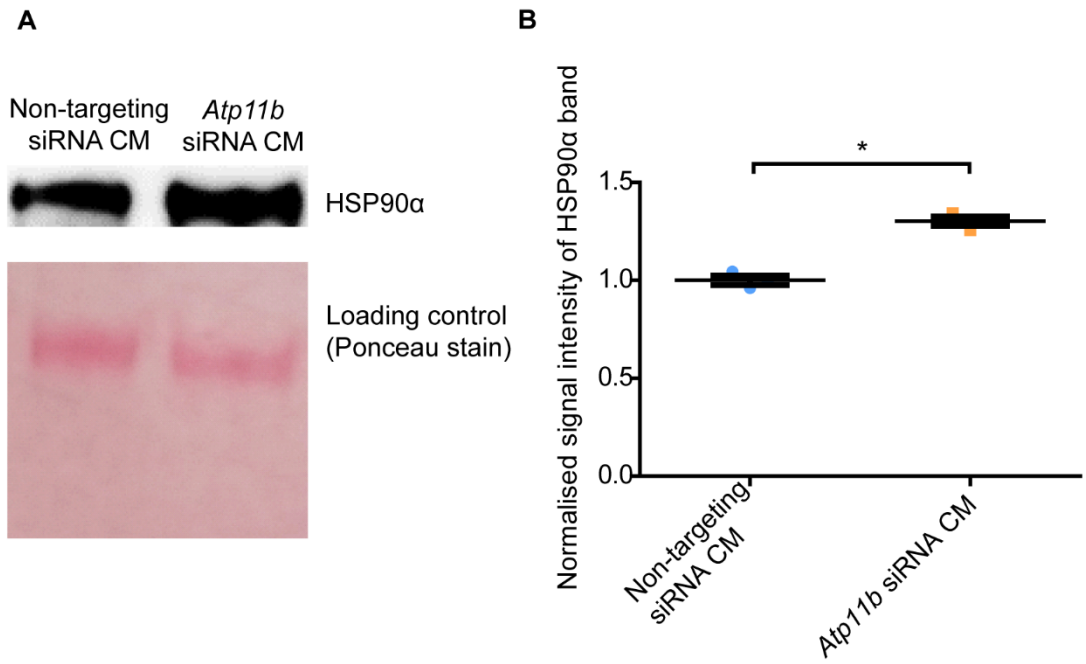


Figure 5.8: bEND.3 cells treated with siRNA against *Atp11b* secrete more HSP90α. A: Western blot showing levels of HSP90α protein in conditioned media (CM) collected from bEND.3 cells treated with non-targeting siRNA (left) and cells treated with siRNA against *Atp11b* (right), demonstrating an increased level of HSP90α secretion when siRNA against *Atp11b* is added. Also shown is a ponceau stain of the membrane, which stains total protein on the gel and shows a band for bovine serum albumin (BSA) which is present in the culture media, as a loading control, demonstrating that the protein gel was loaded evenly. B: Quantification of western blots, showing the signal of the HSP90α band normalised to the loading control of that lane, across different samples shows that the increase in HSP90α secretion is significant (Mean ± SEM; *: $p<0.05$, paired t-test; n=3).

5.5 – Discussion

5.5.1 - Analysis of genome sequence of DM rat

In this chapter, I firstly showed that the gene *Atp11b* is mutated in the DM rats which we are using to model SVD, causing a loss of the ATP11B protein. While I went on to show how this mutation can contribute to the pathological changes we see in the DM rats, there may be other mutated genes which contribute to this pathology which did not appear in my reanalysis of the genome sequence data from Atanur et al., 2013.

There are two main reasons why other mutations may have been missed. Firstly, the filtering process I used for discovering mutations was very stringent. I did not explore genes with SNV mutations, which are liable to having equally or more severe effects than mutations leading to truncated proteins as a change in a single amino acid can cause a large conformational change in the protein, leading to a non-functioning or dominant negative protein. These were initially excluded as the effects of this type of mutation are more difficult to predict. However, a list of non-synonymous coding SNVs in SHRSPs was kindly provided by the lead author of the sequencing study, Santosh Atanur, and reanalysis of this data shows seven SNVs which are unique to SHRSPs and are in genes which are expressed in brain endothelial cells, and these will be worth validating and exploring further. These genes are: afadin (*Mllt4*), heat shock protein 90 beta (*Hsp90ab1*), mitochondrial ribosomal protein L14 (*Mrpl14*), pikachurin (*Egflam*), proteinase-activated receptor 1 (*F2r*), NF-κB inhibitor beta (*Nfkbib*), and succinate dehydrogenase assembly factor 1 (*Sdhaf1*). I also excluded genes which were not expressed in brain endothelial cells. While the data in this thesis suggest that SVD originates in brain ECs, the later changes may be reliant on mutated genes expressed in other cell types, such as OPCs or microglia. The initial stage of my filtering process also excluded any mutations related to hypertension, by excluding mutations which were also present in the SHR. However, there is the possibility that these mutations may contribute to SVD as well as hypertension, especially as hypertension can contribute to endothelial dysfunction (Dharmashankar and Widlansky, 2010). While validating and testing all of these other mutations may yield interesting results, this will be a very lengthy process, and the filters in this study were

chosen to give the greatest chance of discovering a mutation contributing to the SVD-like pathology observed in DM rats in a first study.

The second reason I may have missed important genes is due to the fact that the original analysis of the sequence of the DM rats was carried out using an older version of the rat genome reference sequence, RGSC3.4. As I demonstrated, this led to many false hits due to imperfect definitions of intron/exon boundaries. Rather than the expected FDR of 3.75% for the presence of an insertion/deletion mutation (Atanur et al., 2013), I in fact had a FDR of 33% for the presence of a mutation, and an effective FDR of 83% for the presence of a coding mutation. This higher than expected level of false positives also means that there are likely to have been more false negatives (mutations which are in coding regions but were predicted to be intronic, and so were not flagged up in my analysis) than the expected 10.98%. A comparison of the genes I tested to the most up to date rat genome reference sequence (Rnor_6) shows that many of the false positives would no longer be considered positives if compared to the latest reference sequence, suggesting that many predicted intron/exon boundaries have changed in the reference sequence. To study this, we would need to reanalyse the data from the original study using the latest rat genome reference sequence. This would hopefully give us more targets to explore.

5.5.2 - Knockdown of Atp11b

I next knocked down *Atp11b* in endothelial cells *in vitro* by transfecting siRNA targeted against *Atp11b* into an immortalised mouse brain endothelial cell line, bEND.3. This cell line was originally immortalised by transformation of a middle T antigen (Montesano et al., 1990; Sikorski et al., 1993; Williams et al., 1988). I used this cell line as they have been shown previously to be very receptive to transfection with siRNA (Koto et al., 2007; Zhang et al., 2006). However, while these cells display typical brain endothelial cell characteristics, such as formation of mature TJs, they do not always behave in exactly the same way as primary cells in culture. They are also mouse cells, rather than rat cells, and so may behave differently. It would therefore be ideal to confirm the results shown in this chapter using primary BMECs isolated from rats. However, transfection of primary cells with siRNA by chemical means is far less

efficient (Gresch and Altrogge, 2012; Ovcharenko et al., 2005) and so may lead to inconsistency both within and between cultures, and a smaller effect. Though higher transfection rates can be achieved in primary cells by viral transfection of shRNA constructs or electroporation, these techniques have their own problems, including lower rates of cell survival. The optimal way to test this would therefore be to generate a rat line with *Atp11b* knocked out and isolate BMECs from these rats. These BMECs would be directly comparable with BMECs isolated from DM rats and would not require transfection with siRNA. Alternatively, embryonic stem (ES) cells could be generated with *Atp11b* knocked out and differentiated to BMECs *in vitro*, which could provide more cells more easily, but these cells would not be directly comparable to primary BMECs.

Generating a transgenic rat with *Atp11b* knocked out would also allow us to answer a number of other questions raised by the results in this chapter. While these data demonstrate that knocking down *Atp11b* is sufficient to produce many of the effects we see with DM BMECs *in vitro*, they do not prove that the *Atp11b* mutation is the sole factor causing the SVD-like pathology in our DM rats. The *in vitro* assays used in this chapter do not demonstrate if the loss of ATP11B is sufficient to cause the increase in microglia we see in tissue sections from DM rats or the later increase in strokes observed *in vivo*. To demonstrate this we would need to either completely knock out the gene, or introduce the same frameshift mutation as in DM rats, in wild type rats and study them throughout development to see if they develop the same pathological changes as DM rats in the same order.

This could be done using CRISPR-Cas9 technology. CRISPRs (clustered regularly interspaced short palindromic repeat) allow targeting of a nuclease (Cas9) to a very specific point in the genome (Cong et al., 2013; Garneau et al., 2010; Horvath and Barrangou, 2010). This causes a double strand break (DSB) in the genome, which can lead to two types of repair. In the absence of a template, the two cut ends of DNA will be joined together by non-homologous end joining (NHEJ) which can cause random insertions or deletions of bases (Sander and Joung, 2014). This can lead to a prematurely terminated or non-functional protein. If, however, donor template DNA is introduced concurrently with the DSB, the DNA will undergo homology directed repair (HDR) and copy in the bases from the donor template (Sander and Joung, 2014).

This allows a very specific modification to be introduced into the DNA. CRISPR-Cas9 is especially good for this purpose as it is relatively cheap and easy to design a CRISPR to target a specific point in your gene, and it has a high transfection efficiency (Wang et al., 2013). For the purposes of this study, CRISPR-Cas9 technology would easily allow us to either knock out the *Atp11b* gene, or introduce the specific mutation of the gene found in DM rats, in a rat embryo and then implant this embryo into a mother to give rise to a rat with *Atp11b* knocked out. We could then study these knockout rats to discover similarities to DM rats.

This very specific genome editing which CRISPR-Cas9 technology facilitates means that we can also use this technology to repair the mutation in *Atp11b* in DM rats. While the data in this chapter demonstrate that knocking down *Atp11b* is sufficient to cause many of the changes seen in BMECs from DM rats, they do not demonstrate that this is the only mutation having this effect. By repairing the mutation in *Atp11b* using CRISPR-Cas9 technology we could see if this stops the development of pathological changes seen in tissue sections and the effects of endothelial dysfunction seen in BMECs isolated from DM rats.

5.5.3 - Function of ATP11B

I have shown in this chapter that knocking down *Atp11b* in endothelial cells *in vitro* is sufficient to induce all of the effects of endothelial dysfunction I see in primary BMECs isolated from DM rats, including formation of less mature TJs and secreting factors which cause a differentiation block in OPCs and OPC proliferation. In this section I will discuss how knocking down *Atp11b* might be having these effects.

ATP11B is a P4-type ATPase, a family of proteins thought to have 14 members in mammals whose best characterised function is as a phospholipid flippase (van der Mark et al., 2013; Tang et al., 1996). Cell membranes, including those of the cell surface (plasma membrane), organelles and vesicles, are composed of a phospholipid bilayer. This consists of two layers of phospholipids, consisting of a hydrophilic phosphate ‘head’, which faces out of the membrane, and a hydrophobic lipid ‘tail’, facing the lipid tail of the other half of the membrane (Branton, 1969). Also present

within cell membranes are sphingolipids (SL) such as sphingomyelin (SM). There are four main phospholipids in cellular membranes, which vary in their lipid 'tail' component: phosphatidylcholine (PC), phosphatidylserine (PS), phosphatidylethanolamine (PE) and phosphatidylinositol (PI). At the plasma membrane, and in some organelles such as the Golgi, these different lipids have an asymmetrical distribution: PS, PE and PI are enriched in the cytosolic leaflet while SL and PC are enriched in the luminal (organelle) or extracellular (plasma membrane) leaflet (reviewed in Daleke, 2003; Op den Kamp, 1979; van der Velden et al., 2010). Maintenance of this membrane asymmetry is crucial for many cell functions. Flippases, such as ATP11B, as well as floppases and scramblases carry out the maintenance of this membrane asymmetry (reviewed in Daleke, 2003). Flippases transport lipids from the outer/luminal leaflet to inner/cytosolic leaflet of the membrane, predominantly PS and PE (van der Velden et al., 2010). Floppases transport lipids from the inner/cytosolic leaflet to the outer/luminal surface of the membrane, predominantly PC and SL (Bitbol and Devaux, 1988). Scramblases transport lipids in both directions in a non-specific, ATP-independent manner (Bassé et al., 1996; Comfurius et al., 1996).

Maintenance of membrane asymmetry is thought to be important for many cell functions. One of these is cell signalling, as PI and PS both play important roles in many cell signalling pathways (Leonard and Hurley, 2011; Leventis and Grinstein, 2010). Membrane asymmetry is also important for cell polarity and rigidity, as PI and PS are more negatively charged than PC or SL (reviewed in Paulusma and Oude Elferink, 2010). Another key role of membrane asymmetry is facilitating vesicle budding, as an increase in the number of phospholipids in the cytosolic leaflet is important to cause the initial curve in the membrane (Graham, 2004; Muthusamy et al., 2009).

Loss of P4-type ATPases, and loss of membrane asymmetry, have been shown to cause severe phenotypes in both animal models and in humans (van der Mark et al., 2013). The best studied of these in humans are mutations causing a loss of ATP8B1. A lack of ATP8B1 causes poor fat absorption in the liver, impaired bile flow and ultimately liver failure (Bull et al., 1998). This is thought to be due to an excess of PS in the outer leaflet of epithelial cell membranes in the bile canaliculi (where bile is drained). This

excess of PS, caused by a lack of ATP8B1 activity transporting PS to the inner leaflet of the membrane, reduces the relative levels of SM and cholesterol in the outer leaflet which provide the membrane with rigidity and resistance to breakdown by bile salts (Paulusma and Oude Elferink, 2010). Other less thoroughly studied effects of a loss of P4-type ATPases in humans include mental retardation, insulin resistance and colorectal tumour metastasis (van der Mark et al., 2013).

As mentioned above, There are few studies which have thoroughly studied the function of ATP11B itself. However, one study has looked in detail at its function in a very specific context from which we can learn a lot about what other roles it might play: platinum resistance in ovarian cancer (Moreno-Smith et al., 2013). In this study, the authors showed that human ovarian tumours which were resistant to cisplatin, a platinum based cytotoxic treatment, had higher levels of *ATP11B*, and that silencing this gene in human cancer cell lines *in vitro* increased their sensitivity to cisplatin. They then studied the mechanism of this in more detail in mouse cells *in vitro* and found that ATP11B is involved in the efflux of cisplatin from the cell. They showed that ATP11B is usually localised to the trans-Golgi network (TGN) and was found to colocalise with syntaxin 6 (STX6) and vesicular associated membrane protein 4 (VAMP4) (Moreno-Smith et al., 2013). The results of this study correlate with the idea that membrane asymmetry and P4-type ATPases are important for vesicular transport. The colocalisation of ATP11B with STX6 and VAMP4, proteins which are both known to be important in vesicular transport particularly from the TGN (Steegmaier et al., 1999), and the localisation of ATP11B at the TGN suggest that ATP11B plays a role in vesicular transport from the Golgi to the plasma membrane or secreted endosomes.

5.5.4 - Atp11b and endothelial dysfunction

These details about the function of P4-type ATPases, and in particular ATP11B, allows us to form some theories as to how the *Atp11b* mutation in DM rats may be causing endothelial dysfunction and SVD-like pathology. As the only study looking at ATP11B specifically suggests a role in vesicular transport from the TGN, I will first explore how this may cause the changes we see. This could be due to a change in the

subcellular localisation of eNOS, a protein whose activity is crucial for endothelial function. It has been shown that eNOS is commonly localised to either the Golgi or the plasma membrane, but is more active, and more responsive to external cues, when localised to the plasma membrane (Jin, 2006). It is unclear why this is, however it could be due to increased binding of inhibitors, such as caveolin-1, when eNOS is localised to the Golgi. If ATP11B is important in transporting eNOS from the Golgi to the plasma membrane, then a loss of ATP11B in DM rats would lead to less eNOS at the plasma membrane, leading to lower eNOS activity and endothelial dysfunction. This could be tested by studying the subcellular localisation of both ATP11B and eNOS by immunocytochemistry in both bEND.3 cells and in BMECs isolated from control and DM rats. This would allow us to study the normal localisation of ATP11B and eNOS, and see if in BMECs from DM rats or bEND.3 cells treated with siRNA against *Atp11b* eNOS is preferentially localised to the Golgi rather than the plasma membrane compared to controls. I have attempted this, but have as yet been unable to get antibodies against either ATP11B or eNOS to reliably work for immunocytochemistry.

Though ATP11B has been shown to play a role in vesicular transport in ovarian cancer cells, it may well exert its phospholipid flippase effects in other ways in different cell types. Another way in which a loss of ATP11B could lead to endothelial dysfunction is by causing a relatively increased amount of cholesterol in the inner leaflet of the plasma membrane. In the same way as a loss of ATP8B1 is described above as leading to relatively lower levels of cholesterol in the outer leaflet of the plasma membrane by not transporting other lipids away, a loss of ATP11B could lead to relatively higher levels of cholesterol in the inner leaflet of the plasma membrane by not transporting in other lipids to dilute it. Higher levels of cholesterol can inhibit eNOS activity (Feron et al., 1999) and so lead to endothelial dysfunction. This could be tested by blocking the production of cholesterol using a drug, such as simvastatin which has previously been shown to be functionally active in BMECs (Jiang et al., 2012). If the effects of endothelial dysfunction in DM BMECs and bEND.3 cells treated with siRNA against *Atp11b* are still found in the presence of simvastatin, then this would suggest that a loss of ATP11B was not exerting its effect by altering relative cholesterol concentrations.

Finally a loss of ATP11B may lead to endothelial dysfunction by disrupting tight junctions (TJs). Throughout this thesis I have been working under the assumption that endothelial dysfunction leads to a loss of TJs, as it has been well documented both *in vivo* and *in vitro* that endothelial dysfunction leads to impairment of the BBB (Grammas, 2011; Lum and Roebuck, 2001; Mazzon et al., 2002; Staddon and Rubin, 1996; Vandenbroucke et al., 2008). However, some studies have suggested that disrupting TJs can cause endothelial dysfunction, though they are mechanistically unclear as to how this might occur (Lopez-Ramirez et al., 2012). A loss of ATP11B, by affecting membrane asymmetry, could alter the polarity of the plasma membrane and so disrupt the anchoring of TJ proteins. This may in turn lead to endothelial dysfunction. This could be tested by treating cells with *Atp11b* knocked down with a compound which increases endothelial function, such as acetylcholine or bradykinin. These substances activate eNOS and so increase NO production and reduce endothelial dysfunction. If ATP11B is weakening TJs independently of endothelial dysfunction, then the activation of eNOS should not have an effect on the loss of TJs observed in bEND.3 cells treated with siRNA against *Atp11b*.

Chapter 6: General Discussion

6.1 – Mechanism of development of small vessel disease (SVD)

6.1.1 - Summary of results

In this thesis I first showed that in a rat model of small vessel disease (SVD), the Stroke Prone Spontaneously Hypertensive Rat (SHRSP; disease model; DM), a number of pathological changes occur from a young age before the DM rat begins to develop classical SVD-like pathology or symptoms, and even before the DM rat begins to develop hypertension. These begin with a weakening of the blood brain barrier (BBB) at three weeks of age, demonstrated by a decrease in the number of blood vessels with claudin-5 positive tight junctions (TJs; **Figure 3.1**). This is followed by an increase in the number of oligodendrocyte precursor cells (OPCs) at four weeks of age (**Figure 3.4**), caused by an increase in OPC proliferation and a block in OPC maturation (**Figure 3.5**). This is then followed by an increase in the number of macrophages/microglia at five weeks of age (**Figure 3.7**). I also showed that all of these changes occur in brains from humans who had died of unrelated causes but had an early stage of SVD, defined as having no symptoms of SVD but having SVD pathology upon post-mortem examination.

While this order of changes in the DM rat suggested an early involvement of BBB breakdown in the pathology of SVD, I went on to show that the later changes are not reliant on blood products leaking out of a damaged BBB using an *ex vivo* slice culture model. In this model there is no blood flow, so nothing to leak out of a damaged BBB, yet after five weeks *in vitro* the same changes were still present, demonstrating that these changes are independent of blood leakage (**Figures 3.9-3.11**). The lack of blood flow in this system also excludes hypertension, further confirming that these changes are not caused by a low level hypertension.

This led me to hypothesise that the initial cause of SVD may in fact be endothelial dysfunction, which is characterised by reduced nitric oxide (NO) production and increased endothelial cell (EC) proliferation, and is known to cause BBB damage and cause ECs to secrete a variety of different factors. I then went on to show that both the human brains with SVD and the DM rat brains had dysfunctional ECs, demonstrated

by an increased proliferation of ECs (**Figure 4.1**). In the DM rat brains I further confirmed this by showing that there were lower levels of endothelial nitric oxide synthase (eNOS; **Figure 4.2**), the protein responsible for the majority of NO production in ECs and a key regulator of endothelial function. To show that this endothelial dysfunction was inherent to ECs, and not induced by another cell type, I extracted brain microvascular endothelial cells (BMECs) from control and DM rats and found that BMECs from DM rats produced less NO (**Figure 4.3**). I also showed that BMECs isolated from DM rats form less mature TJs, having fewer cells with membranous claudin-5, than BMECs from control rats (**Figure 4.4**), demonstrating that this inherent endothelial dysfunction is responsible for the BBB phenotype I see in tissue sections from DM rats and human SVD brains. To see if this endothelial dysfunction was causing the other changes I see in tissue sections from DM rats and human brains with SVD, I took conditioned media (CM) from these BMECs and added it to cultures of OPCs and microglia, and slice cultures. I showed that CM from BMECs isolated from DM rats was able to cause the increased OPC proliferation and OPC differentiation block I see in tissue sections from DM rats and human brains with SVD (**Figures 4.5 & 4.6**), but not the increased number of microglia (**Figure 4.7**), even when CM was added to slice cultures where microglia could respond to changes in OPCs (**Figure 4.9**).

Using an antibody array, I showed that one of the factors secreted by DM BMECs into CM is HSP90α (**Figure 4.10**), and by adding recombinant HSP90α to OPC cultures, or a blocking antibody against HSP90α with DM BMEC CM to OPC cultures, I demonstrated that HSP90α is both sufficient and necessary to induce the differentiation block of OPCs, but not the increased proliferation (**Figures 4.11-4.14**).

To determine what is causing the endothelial dysfunction in the DM rats I reanalysed gene sequencing data from a previous study (Atanur et al., 2013) and showed that a mutation in the *Atp11b* gene causes an absence of the ATP11B protein in DM rats (**Figure 5.2**). By adding siRNA against *Atp11b* to an endothelial cell line I showed that a loss of this protein alone is able to make these ECs dysfunctional (**Figure 5.4**) leading to TJ problems in these ECs (**Figure 5.5**) and causing them to secrete factors which block OPC differentiation and increase OPC proliferation (**Figures 5.6 & 5.7**). Furthermore, I showed that ECs treated with siRNA against *Atp11b* secrete increased

levels of HSP90α (**Figure 5.8**), suggesting that they exert their effects on OPCs through a similar mechanism to DM BMECs.

These data lead me to a mechanism of SVD whereby the primary cause is an endothelial dysfunction, caused by environmental and genetic factors (a mutation in *Atp11b* in the DM rats), which causes a breakdown in the BBB and causes ECs to secrete factors, including HSP90α, which cause OPCs to proliferate more and have a blocked maturation. Ultimately, these changes will lead to a neuronal vulnerability and neuronal loss, causing the motor and cognitive defects which are symptomatic of SVD.

6.1.2 - Possible mechanisms of action

In the preceding chapters, I have explored separately how HSP90α might cause a differentiation block in OPCs (chapter 4.5.4), and how a loss of ATP11B may cause endothelial dysfunction (chapter 5.5.4). Here I will explore some possible mechanisms which link these proteins.

The role of HSP90α in endothelial function has been well characterised (Averna et al., 2008; García-Cardeña et al., 1998; Lei et al., 2007; Takahashi and Mendelsohn, 2003). HSP90α binds to eNOS, a key regulator of endothelial function, both activating eNOS and protecting eNOS from breakdown by activated calpain (Averna et al., 2008). A reduction in intracellular HSP90α activity, either using a blocking antibody against HSP90α or a HSP90 inhibitor, geldanomycin, can lead to lower levels of eNOS activity and lower levels of total eNOS (Averna et al., 2008). This reduction in total eNOS levels is similar to what we see in brains from our DM rats (**Figure 4.2**).

While a definitive mechanism by which HSP90 is secreted has not yet been shown (reveiwed in Li et al., 2013), many mechanisms have been demonstrated which cause HSP90 to become localised to the plasma membrane (Lei et al., 2007; Wang et al., 2009), and it has been theorised that from the plasma membrane HSP90 can be shed in exosomes or cleaved off, causing a large part of the protein to be secreted (Clayton et al., 2005; Wang et al., 2009). In this project I found that secreted HSP90α appears smaller than normal by western blot (**Figure 4.10**), supporting the cleavage hypothesis. One mechanism by which HSP90 moves to the plasma membrane involves the

activation of calpain by high glucose levels which goes on to activate protein kinase A (PKA). PKA then phosphorylates HSP90 at a specific site (Threonine 89) which targets the protein for translocation to the plasma membrane (Lei et al., 2007). This mechanism links a known risk factor for SVD (high glucose caused by diabetes) to a displacement of HSP90 which uncouples HSP90 and eNOS allowing eNOS to be broken down by activated calpain. Lower levels of eNOS means that less NO is being produced, making ECs dysfunctional.

It is expected that this process would occur with natural fluctuations in glucose levels, and that without persistently high glucose levels HSP90 would normally return to the cytoplasm from the plasma membrane, and so would shuttle back and forth from the cytoplasm to the plasma membrane with fluctuating intracellular glucose levels. There are, however, different ways in which a loss of the ATP11B protein could disrupt this process. As described in chapter 5.5.3, ATP11B is a P4-type ATPase involved in flipping phospholipids from the outer leaflet to the inner leaflet of the membrane. Through this, it plays an important role in both cell polarity and vesicle budding. By disrupting cell polarity, a loss of ATP11B could disrupt the normal localisation of GLUT-1 glucose transporters, and so lead to a persistently high intracellular glucose level leading to a permanent activation of the mechanism described above targeting HSP90 to the plasma membrane. Alternatively, by disrupting vesicle budding a loss of ATP11B could disrupt the normal trafficking of HSP90 back into the cell from the plasma membrane after a return of glucose concentrations to normal levels.

The mechanisms suggested above could be tested in the first instance by looking at the levels of HSP90α in control and DM endothelial cells. If HSP90α secretion is happening as part of a process which reduces the levels of HSP90α inside the cell which can bind to eNOS, as opposed to the cell increasing HSP90α production causing some to be secreted, we would expect to see lower levels of HSP90α inside DM BMECs. The idea that the loss of ATP11B is causing endothelial dysfunction through HSP90α, rather than ATP11B causing endothelial dysfunction through another mechanism, which then leads to HSP90α secretion, could be further tested by inducing endothelial dysfunction in ECs by another method. If a direct disruption of eNOS and NO production leads to EC secretion of HSP90α, then that would suggest that endothelial dysfunction leads to HSP90α secretion, rather than HSP90α secretion

being involved in causing endothelial dysfunction in our DM rats. One method to do this would be to treat cells with nitro-L-arginine methyl ester hydrochloride (L-NAME). This is an analogue of L-arginine which eNOS will process in preference to L-arginine, but which cannot be converted into NO. Therefore the addition of L-NAME to ECs will cause a lower production of NO, and so endothelial dysfunction. As a control, other ECs would be treated with nitro-D-arginine methyl ester hydrochloride (D-NAME), the inactive chiral form. The outputs of this experiment would be to see if the treatment increased EC proliferation and reduced the formation of mature TJs, measuring the amount of HSP90α secreted by western blot, and adding CM from treated cells to OPCs as a bioassay to see if this CM causes OPCs to proliferate more or have blocked differentiation. If the CM from ECs treated with L-NAME contains increased levels of HSP90α and has effects on OPCs, then this would suggest that endothelial dysfunction causes HSP90α to be secreted, even in the absence of any changes to ATP11B. If, however, adding L-NAME causes endothelial dysfunction, as measured by increased EC proliferation and a reduction in mature TJ formation, but the CM from L-NAME treated cells has no increased HSP90α and no effect on OPCs, this would suggest that a loss of ATP11B directly increases HSP90α secretion, through a mechanism described above, which in turn increases endothelial dysfunction. However, while the effects of L-NAME in reducing NO production are well characterised in short term studies (<6 hours), few studies have administered L-NAME over longer timescales (>24 hours) and it has even been shown that long-term administration of L-NAME can actually cause an increase in the production of NO (Rivas-Cabanero et al., 1996). As we would want to grow ECs in the presence of L-NAME over longer timescales to mirror our previous experiments, this would require optimisation of the L-NAME treatment protocol and verification that treatment with L-NAME is actually causing endothelial dysfunction, by studying endothelial proliferation and formation of mature TJs.

6.2 – Relevance of rat model findings to human disease

The mechanisms described above, and the majority of the results in this thesis, pertain to our rat model of SVD, and this naturally begs the question of how much relevance

this bears to human disease: Do my findings that endothelial dysfunction is the primary cause of SVD-like pathology in DM rats mean that endothelial dysfunction is also the cause of SVD in humans? The following section will address this question.

In the introduction to this thesis, I discussed the necessity of using an animal model to better understand the development of SVD, and explored the range of animal models available (chapter 1.8). I concluded that the SHRSP, our DM rat, was one of the best models of sporadic SVD due to the wide range of pathologies and symptoms it displays (Bailey et al., 2009, 2011a; Hainsworth and Markus, 2008). These similarities between the DM rat and SVD in humans were given further traction in the third chapter of this thesis where I showed that all the changes which we see early on in the development of disease in the DM rats, upon which the later work in this thesis is based, are also present in human brains with early stage SVD. These overlapping pathologies, both early on and late in disease development, between the DM rat and human SVD, suggest that there are also overlapping mechanisms. The idea that this disease mechanism may be rooted in endothelial dysfunction is supported by the data in this thesis demonstrating that in human brains with an early stage of SVD there are more proliferating ECs, a key marker of endothelial dysfunction (**Figure 4.1**). While this study is among the first to demonstrate that endothelial dysfunction plays a causative role in the non-vascular changes associated with SVD, there is also further evidence of endothelial dysfunction playing an important role in SVD beyond the data in this thesis, from a number of different aspects of SVD which have been studied.

6.2.1 - SVD risk factors associated with endothelial dysfunction

In chapter 1.7 I described the wide array of different risk factors which have been associated with SVD, and discussed the strength of these associations. Of these risk factors, those with the most consistent associations with human SVD are hypertension, smoking and diabetes (van Dijk et al., 2004; Jackson et al., 2010; Vermeer et al., 2007; Wardlaw et al., 2014). These risk factors are also associated with endothelial dysfunction, as defined by reduced NO production and vascular reactivity, independently of their association with SVD (Johnstone et al., 1993; Ozaki et al., 2010; Panza et al., 1990; Pittilo, 2000). Hypertension is thought to both play a causal role in

endothelial dysfunction, by increasing production of reactive oxygen species (Dharmashankar and Widlansky, 2010), and be caused as an output of endothelial dysfunction, due to decreased vascular reactivity (Huang et al., 1995; Sander et al., 1999). Smoking has been shown to impair endothelial function by increasing vascular production of superoxides, which reduce the bioavailability of NO (Heitzer et al., 1996; Raij et al., 2001). A number of different mechanisms have been proposed for the effects of diabetes on endothelial function. As described previously in this chapter (section 6.1.2), high glucose can activate calpain which ultimately leads to translocation of HSP90α to the cell surface and a reduction in eNOS activity (Lei et al., 2007). It has also been shown that high glucose can lead to an increased expression of eNOS, without an associated increase in cofactors, and increased levels of NAD(P)H, causing increased production of superoxides (Christ et al., 2002; Hink et al., 2001), reducing the bioavailability of NO. The fact that all of these SVD risk factors are independently associated with endothelial dysfunction, and have been shown to cause endothelial dysfunction, provides further evidence that this plays an important role in SVD in humans.

6.2.2 - Markers of endothelial dysfunction in humans with SVD

Further evidence for the presence of endothelial dysfunction in humans with SVD comes from studies looking at circulating biomarkers (reviewed in Poggesi et al., 2015). These are proteins which have been detected in the blood or cerebrospinal fluid (CSF) of SVD patients at higher levels than in controls. Many of these circulating biomarkers are proteins associated with endothelial dysfunction, including factors thought to contribute to endothelial dysfunction and factors expressed as a result of endothelial dysfunction.

An example of a factor thought to cause endothelial dysfunction is homocysteine, a homologue of the amino acid cysteine. Higher levels of homocysteine in the blood have been shown to be associated with SVD in a number of studies (Hassan et al., 2004b; Jeon et al., 2014). Increased levels of homocysteine have also been shown to contribute to endothelial dysfunction, as defined by reduced vascular reactivity (McDowell and Lang, 2000). The mechanisms by which homocysteine contributes to

endothelial dysfunction are unknown, though there is evidence that it has this effect by increasing levels of asymmetric dimethylarginine (ADMA), a competitive inhibitor of eNOS which supplants L-arginine (Stühlinger et al., 2001).

An example of a factor expressed as a result of endothelial dysfunction is intercellular adhesion molecule 1 (ICAM-1). ICAM-1 is usually found at low concentrations on the cell surface of ECs and leukocytes. In certain pathological conditions, including endothelial dysfunction (usually described as endothelial activation, however, as described in chapter 4.1.3, these two terms overlap), the levels of ICAM-1 on the EC surface are increased, allowing leukocytes to bind to ECs to facilitate their transcellular migration and move from the blood into the brain parenchyma (Smith et al., 1988). Studies have not only shown that higher levels of ICAM-1 circulating in the blood are associated with SVD (Hassan et al., 2003; Wiseman et al., 2014), but they have also shown that the higher the level of ICAM-1 in the blood, the faster the rate of progression of SVD (Markus et al., 2005). These data suggest that higher levels of endothelial dysfunction are associated with disease progression.

Investigating the levels of circulating biomarkers does have some limitations. Chief amongst these is the fact that a study of circulating biomarkers does not differentiate between a systemic endothelial dysfunction (present in all ECs in the body), a peripheral endothelial dysfunction (all non-cerebral ECs), and a cerebral endothelial dysfunction, as these circulating biomarkers could be coming from anywhere in the body. One study which has attempted to address this by looking for some of these markers in tissue sections of human brains with SVD in fact found no link between ICAM-1 expression and SVD (Giwa et al., 2012), though the low levels of ICAM-1 detectable in all tissue sections made any differences hard to discern in that study. Overall, while the data from studies of circulating biomarkers have limitations, and do not demonstrate that endothelial dysfunction plays a causal role in later stages of SVD in humans, they, along with studies showing reduced vascular reactivity in SVD patients (Stevenson et al., 2010), provide further evidence that endothelial dysfunction is an important, common feature of SVD.

6.2.3 - Endothelial dysfunction in Mendelian forms of SVD

In chapter 1.6 I described the different variants of SVD which are inheritable. As well as providing support that sporadic SVD is an actual disease, rather than an aspect of normal ageing, these forms of SVD also allow us to more easily understand the disease process, due to their more consistent and predictable disease development. We can therefore investigate what is known about the mechanisms of Mendelian forms of SVD and see if endothelial dysfunction is implicated in any of them. I will focus on the three best characterised forms of Mendelian SVD: cerebral autosomal dominant arteriopathy with subcortical infarcts and leukoencephalopathy (CADASIL), cerebral autosomal recessive arteriopathy with subcortical infarcts and leukoencephalopathy (CARASIL), and *COL4A1/A2*-related angiopathies.

CADASIL is caused by a mutation in the *NOTCH3* gene (Joutel et al., 1996) which leads to an increase in accumulation of the NOTCH3 extracellular domain ($NOTCH3^{ECD}$) in small vessels. This accumulated $NOTCH3^{ECD}$ then sequesters other extracellular matrix proteins, such as vitronectin (VTN) and tissue inhibitor of metalloprotease 3 (TIMP3) (Monet-Leprêtre et al., 2013). Cerebrovascular dysfunction has already been well-characterised in a mouse model of CADASIL (Joutel et al., 2010) and the sequestration of proteins by accumulated $NOTCH3^{ECD}$ provides a number of possible mechanisms by which this may occur. One such mechanism is based around the accumulation of TIMP3. TIMP3 inhibits TNFα-converting-enzyme (TACE; also known as ADAM17) (Amour et al., 1998) which is involved in the shedding of heparin binding epidermal growth factor (HB-EGF) (Lee et al., 2003). HB-EGF in turn increases eNOS expression and activates eNOS by phosphorylation (Mehta et al., 2008). Thus, accumulation of TIMP3, through inhibition of ADAM17-mediated shedding of HB-EGF, reduces the amount and activation of eNOS, leading to endothelial dysfunction. Another mechanism by which $NOTCH3^{ECD}$ accumulation can lead to endothelial dysfunction lies with another protein which is sequestered by accumulated $NOTCH3^{ECD}$, latent transforming growth factor beta binding protein 1 (LTBP1) (Kast et al., 2014). As the name suggests, LTBP1 binds transforming growth factor beta (TGF-β), which has been shown to reduce NOS activity in vascular smooth muscle (Schini et al., 1992), though no studies have yet looked at the effects of TGF-β on eNOS specifically.

Reduced NOS activity by elevated TGF-β levels can also provide a mechanism for reduced endothelial function in CARASIL. CARASIL is caused by a loss of function mutation in the gene HtrA Serine Peptidase 1 (*HTRA1*) (Hara et al., 2009), whose derived protein is involved in cleaving pro-TGF-β to modulate and lower TGF-β levels (Beaufort et al., 2014; Shiga et al., 2011). Thus a loss of HTRA1 would lead to elevated levels of TGF-β, which can inhibit NOS activity as described above.

The involvement of TGF-β in *COL4A1/A2*-related angiopathies is unknown. These forms of SVD are characterised by mutations in either collagen type IV alpha-1 chain (*COL4A1*) or collagen type IV alpha-2 chain (*COL4A2*) (Gould et al., 2006). COL4A1 and COL4A2 together form the heterotrimer collagen IV, a major component of the basement membrane around blood vessels. These mutations can cause both an altered interaction with other ECM proteins outside the cell, and an accumulation of mutated heterotrimer inside the cell (Kuo et al., 2012). Though the downstream pathological mechanisms of these mutated proteins are yet to be elucidated, it has been shown that mice with *Col4a1* mutations have reduced NOS activity and reduced vascular function (Van Agtmael et al., 2010).

The fact that three of the most common forms of Mendelian SVD all display endothelial dysfunction further supports the data in this thesis demonstrating a key role for endothelial dysfunction in driving the pathology of SVD.

6.2.4 - Genetic polymorphisms linked to SVD and endothelial dysfunction

As well as Mendelian forms of SVD, whereby inheritance of a specific genetic mutation directly causes SVD in either a dominant or recessive fashion, there are also genetic polymorphisms, natural variations in the sequence of a gene, which have been shown to be associated with an increased risk of SVD. Many of these are in genes associated with endothelial dysfunction. Most notable amongst these are a number of studies which have shown that polymorphisms in the gene coding for eNOS, the key regulator of endothelial function, are associated with SVD (Elbaz et al., 2000; Hassan et al., 2004a). These include a polymorphism in a coding region (G294T (base G replaced with base T at position 294), causing amino acid change Glu298Asp)

whereby the G variant is more commonly found in patients with SVD than controls (Elbaz et al., 2000). The T variant is associated with enhanced vascular responsiveness (Philip et al., 1999) suggesting that there is reduced endothelial function in people with the G variant. Other eNOS polymorphisms linked to SVD are in a promoter region (T-786C) and an intron (intron4ab; a repeated region of 27 base pairs where a = deletion of a repeat and b = insertion of an extra repeat), whereby the T and a variants respectively have been shown to have a protective effect against SVD (Hassan et al., 2004a). These protective polymorphisms are thought to increase the expression level of eNOS, and have also been shown to be associated with increased levels of nitrates and nitrites (NO_x levels), the metabolites of NO and indicative of endothelial function, in the blood (Hassan et al., 2004a).

There are also polymorphisms associated with SVD in genes other than eNOS, which may lead to endothelial dysfunction. One of these is found in the gene methylenetetrahydrofolate reductase (*MTHFR*). The T variant of the C677T polymorphism in this gene leads to increased levels of homocysteine and is associated with SVD (Hassan et al., 2004b; Jeon et al., 2014). In section 6.2.2, I described how increased levels of homocysteine can lead to endothelial dysfunction. Another SVD-associated polymorphism is in the gene coding for angiotensin converting enzyme (ACE) at a deletion/insertion site. The deletion allele is associated with both increased levels of ACE in the blood and SVD (Markus et al., 1995). ACE has previously been shown to inhibit eNOS, and so cause endothelial dysfunction (Lüscher, 2000). The association of many genetic polymorphisms which cause endothelial dysfunction with SVD supports the hypothesis that endothelial dysfunction plays an important part in the development of SVD.

6.2.5 - Genome wide association studies (GWAS) and endothelial dysfunction

As mentioned in chapter 5.1, a key source of information as to what might be causing endothelial dysfunction in humans with sporadic SVD is data from genome wide association studies (GWAS) to determine what gene variants are more commonly associated with SVD. While some GWAS which include SVD patients have either not subdivided their results by stroke subtype or not had enough SVD patients to provide

significant results, many of them have still found interesting results (reviewed in Haffner et al., 2015). Some of these results come from meta-analyses, which are studies which gather and reanalyse the data from many GWAS, so increasing the number of SVD patients studied and the power of the results. Many of the gene variants which have been discovered in these studies have been in the same genes which cause Mendelian forms of SVD, such as mutations in *COL4A1* or *COL4A2* (Rannikmäe et al., 2015). It is thought that these variants would cause mechanistically similar, though less severe, changes to their relevant Mendelian forms.

There are also a number of other genes which have come out of these studies as having variants associated with aspects of SVD. One of these is the gene *PRKCH* (Kubo et al., 2007; Li et al., 2012; Serizawa et al., 2008; Wu et al., 2009) which codes for the protein protein kinase C, eta (PKC-η). This protein is a member of the PKC family which is highly expressed in brain endothelial cells, as well as having some expression in microglia (Barres brain RNA-Seq database (Zhang et al., 2014)). While the function of PKC-η has not been well characterised in endothelial cells, we can learn what its effects might be by looking at studies of other members of the PKC family. Both PKC-α and PKC-ε have been studied in endothelial cells and have been shown to have significant effects on endothelial function (Rask-Madsen and King, 2008). Knockdown of PKC-α by siRNA was shown to increase vascular endothelial growth factor (VEGF) dependent phosphorylation (and activation) of eNOS, while PKC-ε knockdown leads to reduced VEGF dependent phosphorylation of eNOS and endothelial dysfunction (Rask-Madsen and King, 2008). Of these two mechanisms, PKC-η is more likely to behave in a similar fashion to PKC-ε, as it is in the same class of PKC proteins – novel PKCs, which are activated independently of calcium. This suggests that a mutation in *PRKCH* leading to a less active PKC-η may cause endothelial dysfunction.

The contribution of PKC family proteins to endothelial dysfunction also provides us with another possible mechanism as to how the *Atp11b* mutation in our DM rats could be inducing endothelial dysfunction. PKC activation is dependent on the presence of a phospholipid, usually phosphatidylserine (Newton, 1995). As detailed in chapter 5.5, a loss of ATP11B, a phospholipid flippase, would likely lead to a reduction in the

relative levels of PS in the inner leaflet of the plasma membrane. This in turn may lead to reduced activation of PKC, and hence endothelial dysfunction.

Another gene variant of interest shown to be associated with SVD is in the gene *FOXC1* (French et al., 2014). FOXC1 is a transcription factor which is highly expressed in brain endothelial cells, as well as having some expression in OPCs (Barres brain RNA-Seq database (Zhang et al., 2014)). Mutations in the *FOXC1* gene leading to both increased and reduced levels of protein are shown to cause SVD pathology and symptoms in both human patients and animal models, including developmentally in patients as young as one year old (French et al., 2014). This dual effect at both increased and reduced levels can be explained by the dual role FOXC1 plays in endothelial function. Deletion of *FOXC1* in endothelial cells leads to increased levels of matrix metalloprotease 3 (MMP-3), MMP-9 and MMP-19, which exert proangiogenic effects by increasing the bioavailability of VEGF-A (Koo and Kume, 2013). Deletion of *FOXC1* also leads to increased levels of soluble VEGF receptor 1 (sVEGFR-1) which exerts an anti-angiogenic effect (Koo and Kume, 2013). Ultimately the balance of these changes leads to increased angiogenesis, and so reduced endothelial function when *FOXC1* is lost. When *FOXC1* is expressed at higher than normal levels, it is possible that the balance of these two functions will change, so similarly leading to increased angiogenesis and endothelial dysfunction.

Thus, the results of GWAS also show that gene variants likely to lead to endothelial dysfunction are associated with SVD.

6.3 – Clinical relevance of findings

The data in this thesis demonstrate that endothelial dysfunction plays a key early role in causing the later pathological changes associated with SVD. The preceding section provides evidence that far from being an artefact of the animal model we have used, this endothelial dysfunction has been well documented as being associated with SVD, and in some cases is even implicated as a cause. Given that trials of treatments for SVD largely have mixed results, in this section I will explore how the data from this

thesis can be used to inform future clinical trials, and potentially lead to improved therapies.

6.3.1 - Treatments tested to help SVD

There are many treatments that have been tried in SVD targeting a wide range of different pathways (reviewed in Bath and Wardlaw, 2015; Mok and Kim, 2015). The efficacy of these treatments has largely been assessed by either monitoring the progression of certain radiological features of SVD (such as white matter hyperintensities (WMH) or lacunar infarcts) over time or the number of incidences of strokes. In some cases, radiological signs of SVD have even been shown to be reversible (Wardlaw et al., 2015). Many of the treatments tested for SVD are those which are normally used for treating large vessel strokes, such as thrombolytic or antiplatelet therapies. Other trials involve targeting known SVD risk factors, such as the use of B vitamins to treat high levels of homocysteine, or statins to lower cholesterol levels. I described in section 6.2.2 how high levels of homocysteine can cause endothelial dysfunction by increasing levels of ADMA, an inhibitor of eNOS, in ECs (Stühlinger et al., 2001). Lowering homocysteine levels with B vitamins has been shown to slow the progression of severe SVD (Cavalieri et al., 2012). In chapter 5.5.3 I described how increased cholesterol levels can cause endothelial dysfunction by inhibiting eNOS. Lowering cholesterol levels with statin treatment has been shown to reduce progression of SVD in some trials (Amarenco et al., 2009; Fu et al., 2010). The results from these trials suggest that by lowering the levels of substances known to cause endothelial dysfunction, it is possible to improve outcomes in patients with SVD. However, trials of B vitamins or statins to treat SVD tend to be limited to those patients with elevated levels of homocysteine or cholesterol respectively. By far the most common form of treatment tried with patients with SVD is antihypertensive therapy.

6.3.2 - Clinical trials involving antihypertensive therapy

As detailed in chapter 1.7.1, hypertension has long been considered the primary risk factor for SVD, partly due to the fact that 70% of patients with SVD are also hypertensive (Lammie et al., 1997; Thrift et al., 1998). This means that a standard treatment that many SVD patients are taking is antihypertensive therapy, and a number of trials have been carried out to assess the efficacy of this treatment for SVD as well as hypertension. While the majority of these trials show some benefit of antihypertensive therapy in reducing the progression of SVD, in many cases this benefit is not significant (SPS3 Group, 2013). For the purposes of this thesis however, we are less interested in the overall efficacy of antihypertensive treatment, and more interested in if there is any difference in the effectiveness of different antihypertensive drugs, which may have different actions on endothelial dysfunction. As detailed in section 6.2.1, hypertension can be both a cause of endothelial dysfunction and a symptom of endothelial dysfunction. It is therefore unclear, according to my model of endothelial dysfunction as the driver of SVD, whether simply lowering blood pressure would have an effect on SVD, as this may simply treat one of the symptoms of the underlying endothelial dysfunction, rather than the root cause. However, these possibilities can be differentiated by comparing the many different classes of antihypertensive drugs which are used, which work using different mechanisms. These include diuretics, which work by reducing the salt and water content of the blood, beta blockers, which reduce heart rate and cause vasodilation, angiotensin converting enzyme (ACE) inhibitors, which prevent production of angiotensin II (a potent vasoconstrictor), and angiotensin II receptor blockers (ARBs). While all of these classes of drugs lower blood pressure, only some of them have direct effects on endothelial function. Diuretics have not been shown to have any effect on endothelial function. Some beta-blockers have been shown to increase eNOS activity and NO production, but this does not occur with some of the most commonly used beta-blockers such as atenolol (Funovic et al., 2008). ACE inhibitors protect against endothelial dysfunction by multiple mechanisms. One of these is the prevention of angiotensin II production, as angiotensin II inhibits eNOS itself, while also leading to the production of endothelin 1 (ET-1) which also inhibits eNOS (Lüscher, 2000). ACE inhibitors also prevent the breakdown of bradykinin, a potent activator of eNOS, by

ACE (Lüscher, 2000). ARBs reduce endothelial dysfunction by preventing the inhibitive functions of angiotensin II. Thus, of the four classes of antihypertensives listed here, ACE inhibitors have the greatest potential effect on improving endothelial function, while ARBs are a close second.

When trying to determine whether the effectiveness of antihypertensive therapies in reducing the progression of SVD is based upon the effects of these drugs on endothelial function, we are faced with some problems. One of these is that in many trials these drugs are tested in mixed groups of stroke patients, including patients with large vessel stroke as well as those with SVD. Their results are often not considered separately, as there are too few patients within each group from which to calculate meaningful statistics (HSCS Group, 1974). The other is that many trials used a variety of different classes of antihypertensive therapies within the same trial, aiming only for reduced blood pressure rather than targeting a particular molecular mechanism (SPS3 Group, 2013). From the studies which do make these distinctions, we can see that those using ACE inhibitors tend to show a better outcome for SVD (Chapman et al., 2004; Dufouil et al., 2005) than those using beta blockers (Eriksson et al., 1995) or ARBs (Weber et al., 2012; Yusuf et al., 2008). This suggests that the improved patient outcome seen with antihypertensive therapy may be due to direct improvements in endothelial function, rather than a reduction in blood pressure. While more work obviously needs to be done in this area to compare different classes of antihypertensive therapy in SVD patient outcome, the results of these trials, together with the data in this thesis, clearly suggest that treatment with ACE inhibitors would be better for SVD patients than other antihypertensive therapies. This would involve only a minor alteration to the treatment regimens currently used for hypertension in SVD patients, but could make a large difference to disease outcome.

6.3.3 - Other therapies to improve endothelial function

The role of endothelial function in producing SVD pathology suggests that therapies which are specifically targeted at improving endothelial function could have a beneficial impact on patients with SVD. The most common treatments of this type are a class of therapies known as NO donors, which chemically increase the levels of NO

in the blood. These therapies are commonly used to treat angina, and some trials have been carried out to look at their effect on strokes, but like many of the antihypertensive trials described above these studies did not differentiate between the effects on large vessel and small vessel stroke (Bath et al., 2001; Rashid et al., 2003). There are, however, a number of ongoing clinical trials which make this distinction and are investigating the effects of NO donors on patients with SVD, including treatment with glyceryl trinitrate (http://www.controlled-trials.com/ISRCTN99414122), and cilostazol and isosorbide mononitrate (http://www.controlled-trials.com/ISRCTN12580546). If positive, these trials could provide further evidence of the involvement of endothelial dysfunction in SVD.

6.4 – Future directions

At the end of the preceding results chapters, I described experiments which would help to answer questions raised by the results of those chapters. In this section I will briefly revisit those ideas, and expand upon them further.

6.4.1 - Effects of secreted factors downstream of endothelial dysfunction

In Chapter 4, I showed that HSP90α secreted by BMECs isolated from DM rats was both necessary and sufficient to cause a differentiation block in OPCs, similar to that which I see in tissue sections from DM rats and human brains with SVD. I described future experiments which would allow us to elucidate how secreted HSP90α from DM BMECs causes this phenotype in OPCs. As CM from DM BMECs also causes OPCs to proliferate more, I described methods by which we could discover other factors secreted by DM BMECs into conditioned media. One of these methods was to sequence the mRNA in DM and control BMECs and look for genes coding for secreted factors which are more highly expressed in DM BMECs.

Sequencing RNA from DM BMECs would also allow us to do far more than just identify other factors secreted by DM BMECS. It would also provide us with a full profile of gene expression, which could give us further details about the mechanisms of endothelial dysfunction, and allow us to compare the expression pattern of these

cells to known expression patterns of endothelial dysfunction, further reinforcing our evidence that these ECs are dysfunctional. Using BMECs isolated from DM rats for this purpose, rather than extracting ECs from tissue using techniques such as laser capture microdissection, would allow us to obtain RNA of a high enough quality more easily, and to be certain that there are not any contaminating cells.

6.4.2 - Upstream causes of endothelial dysfunction

In Chapter 5, I demonstrated that a 28 base pair deletion in the *Atp11b* gene leads to a loss of the ATP11B protein in DM rats, and that knocking down this gene in a wild-type endothelial cell line is sufficient to cause endothelial dysfunction and an impairment of mature TJ formation, as well as causing secretion of molecules into CM which have the same effect on OPC maturation and proliferation as CM from DM BMECs. Based on the function of ATP11B as a phospholipid flippase, I proposed a number of possible mechanisms as to how this mutation could cause endothelial dysfunction, both in chapter 5.5.3 and earlier in this chapter, and described experiments which could be carried out to test these hypotheses.

Some of these proposed mechanisms were based around the effects that a loss of ATP11B may have on membrane polarity. However, the role of ATP11B in membrane polarity could be better studied if a three dimensional (3D) culture system for ECs was developed. In the culture systems used in this thesis, both for primary BMECs and the bEND.3 cell line, cells are grown in a two dimensional (2D) monolayer, with one surface attached to the cell culture plate. This serves as an imperfect model for ECs *in vivo* for a number of reasons. Key amongst this is the lack of a different milieu on either side of the EC – *in vivo* the apical and basal surfaces are exposed to very different environments: the blood on one side and cell contact with astrocytes, pericytes and microglia on the other (reveiwed in Abbott et al., 2006). Also absent from a 2D culture is any aspect of blood flow. The shear stress which blood flow places on ECs is thought to play a crucial role in the development of TJs *in vivo*, and the lack of this could explain the relatively low rate of mature TJ formation in my primary BMEC cultures (Cucullo et al., 2011; Ye et al., 2014). All of these factors affect cell polarity. While the polarity between the inner and outer leaflets of the plasma membrane would be

maintained in a 2D culture, the apical-basal polarity between different cell surfaces may not be. This affects localisation of key receptors which could be crucial in endothelial cell function, such as GLUT-1, a glucose transporter (Simpson, 2001). A number of different 3D models for EC growth have been developed. One involves growing ECs on a permeable membrane, and then once attached turning the membrane upside down and growing other brain cells such as astrocytes on the other side (Sansing et al., 2012). While this allows for different environments on either side of the EC, and direct contact with other cell types, it does not fully recapitulate the 3D environment, and would not allow substances to be perfused through tubes of ECs. Another model involves seeding ECs in spinning microfluidic channels (Bischel et al., 2013). As these channels are spinning, the ECs would be spread evenly along the surface. Once the ECs grow to confluence, they would form vessel-like structures through which a blood substitute could be flowed. Other cell types, such as astrocytes or OPCs, could also be seeded along the outside. Growing BMECs from DM rats, or ECs with *Atp11b* knocked down, in these models could give us a better idea about the role of cell polarity in both endothelial dysfunction and the development of SVD.

While these studies of the function of ATP11B in ECs will help to elucidate the mechanism of endothelial dysfunction in the DM rat, there are other factors to consider upstream of endothelial dysfunction which could help us discover what causes endothelial dysfunction in humans with SVD.

One aspect of SVD in humans which could be important in causing endothelial dysfunction is genetic factors, both mutations in Mendelian forms of SVD and polymorphisms in sporadic SVD. A simple way to test the effects of Mendelian mutations on endothelial dysfunction would be to extract BMECs from existing mouse lines which have these mutations and recapitulate the disease *in vivo* (Gould et al., 2006; Joutel et al., 2010). By culturing BMECs extracted from these mice, we can utilise the techniques used in this thesis to test for endothelial dysfunction – western blot for eNOS, measuring NO_x levels in the media, and immunostaining for proliferation and assessment of TJ maturity. We could also take CM from these BMECs and add it to OPCs as a bioassay of dysfunctional ECs, to assess the effect of the CM on OPC proliferation and maturation. These experiments would allow us to

see if genetic mutations which cause SVD in humans and in mice *in vivo* also cause endothelial dysfunction *in vitro*, and what the mechanisms might be behind this.

We could further study the role of genetics in causing endothelial dysfunction in human SVD by creating induced pluripotent stem cells (iPSCs) from human patient skin samples, differentiating these into ECs and studying these *in vitro*. iPSCs are pluripotent stem cells generated by reprogramming differentiated adult cells using a set of defined factors (Takahashi and Yamanaka, 2006). These cells are genetically identical to the person from whom the adult cells were taken, including the presence of any genetic mutations or polymorphisms. These iPSCs can then be differentiated to form mature brain ECs (Lippmann et al., 2012), grown in culture and assessed for endothelial dysfunction using the techniques described in the preceding paragraph. Using this method we could study the genetic contributions to endothelial dysfunction in humans with Mendelian SVD, and humans with sporadic SVD with and without known genetic polymorphisms, independently of any environmental factors which may contribute to any dysfunctional phenotype measured directly in the patients. Though the use of iPSCs can sometimes pose problems with variability, both between different lines and between different passages of the same line, using this technique would be more feasible than extracting cells from human post-mortem brains, both technically – the long, and variable, post-mortem interval between death and tissue extraction would preclude the extraction of viable cells – and practically – iPSCs allow us to grow cells from multiple patients simultaneously and conveniently, rather than waiting for a post-mortem sample to become available.

As well as genetic mutations and polymorphisms, there are also environmental factors associated with SVD which may contribute to endothelial dysfunction. Notable amongst these are hypertension, smoking and diabetes (described in chapter 1.7 and section 6.2.1). While these factors are all associated with SVD, there is little evidence as to whether they cause or modulate the disease phenotype. If, however, we could demonstrate that they cause or exacerbate endothelial dysfunction then, together with the data in this thesis, we could derive a mechanism by which these factors cause SVD. These factors could all be tested *in vitro* by growing wild-type BMECs, exposing them to these different environmental factors and assaying the BMECs for endothelial dysfunction as described above. The effects of diabetes on cells in the body is mediated

by exposure to elevated levels of glucose in the blood. Therefore we could model the effects of diabetes by growing BMECs in media with elevated glucose levels. To model the effects of smoking, a commonly used technique is the addition of cigarette smoke extract (CSE), made by bubbling cigarette smoke through phosphate buffered saline (PBS), to the culture (Prasad et al., 2015). Adding CSE to BMECs would allow us to see the effects of all the chemicals in cigarettes, rather than just nicotine, on endothelial dysfunction. Using these techniques to model the effects of smoking and diabetes on brain endothelial cells has already been shown to be effective, in a study which demonstrated that these two factors, both separately and together, cause weakening of TJs and reduced integrity of the BBB, suggesting that they indeed induced endothelial dysfunction (Prasad et al., 2015). However, it would be interesting to study this in more detail looking at claudin-5, a key TJ protein, direct markers of endothelial dysfunction, and downstream effects of endothelial dysfunction on other brain cell types.

Modelling hypertension in the 2D BMEC cultures used in this thesis would not be possible, as there is no way to flow a liquid across the endothelial cells at different pressures. However, by using a 3D culture technique for ECs, described above, we would be able to form tubes of ECs through which liquid could be perfused. By perfusing liquid at different pressures we could model hypertension and assay for endothelial dysfunction using the techniques described above. A 3D model would also allow us to better model diabetes and smoking, as in the body ECs will be maximally exposed to these environmental factors on the luminal surface.

It would also be interesting to see the effects of these environmental factors on cells which are not wild-type. It is likely that in many cases SVD is caused by a combination of genetic susceptibility and exposure to environmental factors. Thus, it would be interesting to test all of these environmental variables *in vitro* on both well-defined diseased cells – such as those from our DM rats, mouse models of Mendelian SVD or ECs derived from iPSCs from patients with Mendelian SVD – to see if these environmental factors exacerbate the disease changes, and also on cells with less well-defined SVD – such as ECs derived from iPSCs from patients with sporadic SVD, with and without known genetic polymorphisms – to see if these cells are more susceptible to environmental factors than control cells.

6.4.3 - In vivo experiments

In chapter 5.5.2, I described how the key way to demonstrate beyond any doubt that the *Atp11b* mutation in DM rats is responsible for endothelial dysfunction and downstream SVD-like pathology and symptoms is to generate a rat which has only the *Atp11b* gene mutated. This could be done using CRISPR-Cas9 technology to introduce a precise mutation into a specific point in the genome.

Confirming the effect of the *Atp11b* mutation is not the only experiment we could do using this gene editing technology. We could test more generally whether or not endothelial dysfunction causes SVD by introducing mutations into, for example, the gene for eNOS or one of the co-enzymes it requires to function. This could, however, simply lead to a non-viable embryo as a total loss of eNOS with no NO production throughout development could be lethal. This could be avoided by being more targeted to simply reduce the function of eNOS rather than eliminating it. For example, the eNOS polymorphisms in humans, described above as increasing the risk of SVD, could be inserted. A similar study to this has recently been carried out whereby a mouse with a partial deficiency of eNOS was generated by knocking out one copy of the *eNOS* gene (Tan et al., 2015). The cognitive functions and brains of these mice were studied at a range of ages, and these mice were shown to have hypoperfusion, BBB leakage, microbleeds, microinfarctions, cerebral amyloid angiopathy, an increase in the number of macrophages/microglia and cognitive decline (Tan et al., 2015) – findings all of which occur in SVD. The data from this study strongly support the conclusions of this thesis – that the later stages of SVD are caused by an early endothelial dysfunction. This study does, however, have some limitations. The authors did not look for any signs of changes in myelin or oligodendrocytes, despite the fact that white matter changes in the form of WMH are amongst the most common radiological signs of SVD. Similarly, an interesting expansion to this study would be to look at the brains of these mice by MRI, to see if they exhibit similar radiological features to human SVD. The key limitation of this study is that the partial deficiency of eNOS was constitutively present, and so the mice would have had dysfunctional ECs throughout development. While this may recapitulate the situation of humans with Mendelian

forms of SVD, or genetic polymorphisms causing endothelial dysfunction, the late onset of sporadic SVD suggests that many patients only start to experience endothelial dysfunction later in life, possibly as a result of environmental factors. One way to model this genetically would be to design the partial knockout of eNOS to be a time conditional knockout. This could be achieved by placing lox-P sites either side of a portion of the eNOS gene and inserting an ER-Cre (which is only active when tamoxifen is administered) elsewhere in the genome. As eNOS is only expressed in ECs, ER-Cre expression could be driven by a constitutively active promoter region, such as in the *Rosa26* locus. This ER-Cre could be activated at a later stage of the mouse's life by administering tamoxifen, at which point the ER-Cre would excise the section of the eNOS gene between the lox-P sites, inactivating the gene, and so only induce the endothelial dysfunction at that stage.

Another way to test if late onset endothelial dysfunction leads to SVD-like pathology *in vivo* would be to chemically block endothelial function in the brains of adult rats. A recently published study tried something similar to this, by injecting ET-1 and L-NAME into the internal capsule of the brains of adult mice (Uchida et al., 2015). The authors used these molecules due to their known vasoconstrictive effects, however these vasoconstrictive effects arise from endothelial dysfunction leading to less vasodilating NO being produced. ET-1 both inhibits eNOS activity by upregulating caveolin-1 and increases NO degradation via oxygen radicals (Iglarz and Clozel, 2007). L-NAME inhibits eNOS activity by mimicking arginine, as detailed in section 6.1.2. The authors showed that injection of these two molecules into the internal capsule leads to a loss of myelin and an increase in microglia/macrophages (Uchida et al., 2015), similar to what we saw in our DM rats. They also showed a loss of axons and behavioural defects (Uchida et al., 2015). Their data provide further evidence that endothelial dysfunction is the cause of SVD. However, their study does not look in detail at oligodendrocytes, OPCs or TJs, and also has the limitation that it was performed in mice, not rats, where the smaller size of the brain makes comparison with human SVD pathology more difficult. This study would be worth repeating, but using different inhibitors of endothelial dysfunction separately to rule out any effects caused by combinations of molecules.

6.5 – Concluding remarks

In this thesis I have demonstrated that endothelial dysfunction is amongst the earliest features of SVD, and this endothelial dysfunction drives the development of much of the later pathology. While there is much work to be done to strengthen the assertion that endothelial dysfunction is the root cause of SVD, this idea provides us with new avenues to explore for treatment options for a disease which to date has few therapies available.

List of abbreviations

2D	Two dimensional
3D	Three dimensional
ACE	Angiotensin converting enzyme
AD	Alzheimer's disease
ADMA	Asymmetric dimethylarginine
AP	Alkaline phosphatase
AQP4	Aquaporin 4
ARB	Angiotensin II receptor blocker
Arhgef	Rho guanine nucleotide exchange factor 1
Atp11b	ATPase, Class VI, 11B (gene)
ATP11B	ATPase, Class VI, 11B (protein)
ATP8B1	ATPase, Class I, Type 8B, Member 1
BA	Blocking antibody
BBB	Blood brain barrier
BCA	Bicinchoninic acid
BDNF	Brain derived neurotrophic factor
BH_4	Tetrahydrobiopterin
BMEC	Brain microvascular endothelial cell
BP	Blood pressure
BSA	Bovine serum albumin
BSA (cp)	Bovine serum albumin (chromatographically purified)
CADASIL	Cerebral autosomal dominant arteriopathy with subcortical infarcts and leukoencephalopathy
CARASIL	Cerebral autosomal recessive arteriopathy with subcortical infarcts and leukoencephalopathy
cDNA	Complement deoxyribonucleic acid
CM	Conditioned media
CNS	Central nervous system
CO_2	Carbon dioxide
Col18a1	Collagen XVIII alpha 1

COL4	Collagen IV
COL4A1	Collagen type IV alpha-1 chain
COL4A2	Collagen type IV alpha-2 chain
CRISPR	Clustered regularly interspaced short palindromic repeat
CSE	Cigarette smoke extract
Da	Daltons
DHB	Diseased human brain
DIV	Days in vitro
DM	Disease model
DMEM	Dulbecco's modified Eagle medium
DMF	N,N-dimethylformamide
DNA	Deoxyribonucleic acid
D-NAME	Nitro-D-arginine methyl ester hydrochloride
dNTP	Deoxynucleotide
DPBS	Dulbecco's phosphate buffered saline
Dpp3	Dipeptidyl peptidase 3
DSB	Double strand break
DWI	Diffusion weighted imaging
EBSS	Earle's balanced salt solution
EC	Endothelial cell
EDTA	Ethylenediaminetetraacetic acid
Egflam	Pikachurin
EGM-2	Endothelial growth media 2 bullet kit
eNOS	Endothelial nitric oxide synthase
ET-1	Endothelin 1
F2r	Proteinase-activated receptor 1
FAD	Flavine adenine dinucleotide
FBS	Fetal Bovine Serum
FDR	False discovery rate
FLAIR	Fluid-attenuated inversion recovery
FMN	Flavine mononucleotide
FPKM	Fragments per kilobase of transcript per million mapped reads

GATK	Genome analysis toolkit
GFAP	Glial fibrillary acidic protein
GLUT-1	Glucose transporter 1
GRP-94	Glucose regulated protein 94
GWAS	Genome wide association studies
HB-EGF	Heparin binding epidermal growth factor
HBSS	Hank's balanced salt solution
HDR	Homology directed repair
hEGF	Human epidermal growth factor
hFGF-beta	Human fibroblast growth factor beta
HIHS	Heat inactivated horse serum
HRP	Horseradish peroxidase
HSP90	Heat shock protein 90
Hsp90ab1	Heat shock protein 90 beta (gene)
HSP90α	Heat shock protein 90 alpha
HSP90β	Heat shock protein 90 beta (protein)
HTRA1	HtrA serine peptidase 1
Iba1	Ionised calcium binding adapter molecule 1
ICAM-1	Intercellular adhesion molecule 1
ICC	Immunocytochemistry
IGF-1	Insulin-like growth factor 1
IHC	Immunohistochemistry
IHR	Inducible hypertensive rat
IL-6	Interleukin 6
indel	Insertion/deletion mutation
iNOS	Inducible nitric oxide synthase
iPSC	Induced pluripotent stem cell
ISH	In situ hybridisation
Jak3	Janus kinase 3
JAM	Junctional adhesion molecule
kDa	KiloDaltons
kg	Kilogram(s)

L-NAME	Nitro-L-arginine methyl ester hydrochloride
LRP1	Lipoprotein receptor-related protein 1
LSR	Lipolysis-stimulated lipoprotein receptor
LTBP1	Latent transforming growth factor beta binding protein 1
Ltbp4	Latent transforming growth factor beta binding protein 4
M	Molar
MAG	Myelin associated glycoprotein
mAmps	MilliAmps
MBP	Myelin basic protein
MCAO	Middle cerebral artery occlusion
MCT1	Monocarboxylate transporter 1
MEM	Minimum essential medium
mg	Milligram(s)
ml	Milliitre(s)
Mllt4	Afadin
mM	Millimolar
MMP	Matrix metalloprotease
MMP-19	Matrix metalloprotease 19
MMP-2	Matrix metalloprotease 2
MMP-3	Matrix metalloprotease 3
MMP-9	Matrix metalloprotease 9
MOG	Myelin/oligodendrocyte glycoprotein
MRI	Magnetic resonance imaging
mRNA	messenger ribonucleic acid
Mrpl14	Mitochondiral ribosomal protein L14
MS	Multiple Sclerosis
MTHFR	Methylenetetrahydrfolate reductase
NAD(P)H	Nicotinamide adenine dinucleotide (phosphate) oxidase
NF	Neurofilament
Nfkbib	Nuclear factor kappa-light-chain-enhancer of activated B cells inhibitor beta
NF-κB	Nuclear factor kappa-light-chain-enhancer of activated B cells

ng	Nanogram(s)
NG2	Neural/glial antigen 2
NHEJ	Non-homologous end joining
NHS	Normal horse serum
nm	Nanometre(s)
nNOS	Neuronal nitric oxide synthase
NO	Nitric oxide
NOS	Nitric oxide synthase
$NOTCH3^{ECD}$	NOTCH3 extracellular domain
NO_x	Nitrates and nitrites
OCT	Optimal cutting temperature compond
OPC	Oligodendrocyte precursor cell
PBS	Phosphate buffered saline
PC	Phosphatidylcholine
PCNA	Proliferating cell nuclear antigen
PCR	Polymerase chain reaction
PDGFRα	Platelet derived frowth factor receptor alpha
PDL	Poly-D-lysine
PE	Phosphatidylethanolamine
pen/strep	Penicillin/streptomycin
PFA	Paraformaldehyde
PI	Phosphatidylinositol
PKA	Protein kinase A
PKC	Protein kinase C
PKC-α	Protein kinase C alpha
PKC-ε	Protein kinase C epsilon
PKC-η	Protein kinase C eta (protein)
PLP	Proteolipid protein
PM	Post-mortem
pmol	Picomole(s)
PNS	Peripheral nervous system
PRKCH	Protein kinase C eta (gene)

PS	Phosphatidylserine
PVDF	Polyvinylidene fluoride
PVS	Perivascular space(s)
R3-IGF-1	Recombinant insulin-like growth factor 1
rHSP90α	Recombinant heat shock protein 90 alpha
RIPA	Radioimmunoprecipitation assay
RNA	Ribonucleic acid
RPM	Revolutions per minute
RT	Room temperature
RVCL	Retinal vasculopathy with cerebral leukodystrophy
Sdhaf1	Succinate dehydrogenase assembly factor 1
SDS	Sodium dodecyl sulphate
SEM	Standard error of the mean
SHR	Spontaneously hypertensive rat
shRNA	Short hairpin ribonucleic acid
SHRSP	Stroke prone spontaneously hypertensive rat
siRNA	Small interferfering ribonucleic acid
SL	Sphingolipids
SM	Sphingomyelin
SNV	Single nucleotide variant
STX6	Syntaxin 6
SVD	Small vessel disease
sVEGFR-1	Soluble vascular endothelial growth factor receptor 1
TACE	Tumour necrosis factor alpha converting enzyme
TBS	Tris buffered saline
TGF-β	Transforming growth factor beta
TGN	Trans-Golgi network
TIMP3	Tissue inhibitor of metalloprotease 3
TJ	Tight junction
TJP	Tight junction protein
TMRI-dextran	Tetramethylrhodamine-isothicyanate dextran
TNF-α	Tumour necrosis factor alpha

TUNEL	Terminal deoxynucleotidyl transferase dUTP nick end labelling
VAMP4	Vesicular associated membrane protein 4
VCAM-1	Vascular cellular adhesion molecule 1
VEGF	Vascular endothelial growth factor
VeP	Varant effect predictor
VTN	Vitronectin
WKY	Wistar Kyoto rat
WMH	White matter hyperintensity(ies)
WML	White matter lesion
ZO-1	Zonula occludens 1
ZO-2	Zonula occludens 2
ZO-3	Zonula occludens 3
µg	Microgram(s)
µl	Microlitre(s)
µm	Micrometre(s)
µM	Micromolar

References

Abbott, N.J., Hughes, C.C., Revest, P. a, and Greenwood, J. (1992). Development and characterisation of a rat brain capillary endothelial culture: towards an in vitro blood-brain barrier. J. Cell Sci. *103 (Pt 1*, 23–37.

Abbott, N.J., Rönnbäck, L., and Hansson, E. (2006). Astrocyte-endothelial interactions at the blood-brain barrier. Nat. Rev. Neurosci. *7*, 41–53.

Acharya, N.K., Goldwaser, E.L., Forsberg, M.M., Godsey, G. a., Johnson, C. a., Sarkar, A., DeMarshall, C., Kosciuk, M.C., Dash, J.M., Hale, C.P., et al. (2015). Sevoflurane and Isoflurane induce structural changes in brain vascular endothelial cells and increase blood−brain barrier permeability: Possible link to postoperative delirium and cognitive decline. Brain Res. *1620*, 29–41.

Van Agtmael, T., Bailey, M. a, Schlötzer-Schrehardt, U., Craigie, E., Jackson, I.J., Brownstein, D.G., Megson, I.L., and Mullins, J.J. (2010). Col4a1 mutation in mice causes defects in vascular function and low blood pressure associated with reduced red blood cell volume. Hum. Mol. Genet. *19*, 1119–1128.

Alcazar, A., and Cid, C. (2009). High cytotoxic sensitivity of the oligodendrocyte precursor cells to HSP90 inhibitors in cell cultures. Exp. Neurol. *216*, 511–514.

Alzheimer's Society, U.K. (2012). Demography. Web: http://www.alzheimers.org.uk/site/scripts/documents_info.php?documentID=412 [Accesed: 01/06/2013]

Amarenco, P., Benavente, O., Goldstein, L.B., Callahan, A., Sillesen, H., Hennerici, M.G., Gilbert, S., Rudolph, A.E., Simunovic, L., Zivin, J.A., et al. (2009). Results of the Stroke Prevention by Aggressive Reduction in Cholesterol Levels (SPARCL) trial by stroke subtypes. Stroke. *40*, 1405–1409.

Amour, A., Slocombe, P.M., Webster, A., Butler, M., Knight, C.G., Smith, B.J., Stephens, P.E., Shelley, C., Hutton, M., Knäuper, V., et al. (1998). TNF-α converting enzyme (TACE) is inhibited by TIMP-3. FEBS Lett. *435*, 39–44.

Arai, K., and Lo, E.H. (2009). An oligovascular niche: cerebral endothelial cells promote the survival and proliferation of oligodendrocyte precursor cells. J. Neurosci. *29*, 4351–4355.

Atanur, S.S., Diaz, A.G., Maratou, K., Sarkis, A., Rotival, M., Game, L., Tschannen, M.R., Kaisaki, P.J., Otto, G.W., John Ma, M.C., et al. (2013). Genome Sequencing Reveals Loci under Artificial Selection that Underlie Disease Phenotypes in the Laboratory Rat. Cell *154*, 691–703.

Averna, M., Stifanese, R., De Tullio, R., Passalacqua, M., Salamino, F., Pontremoli, S., and Melloni, E. (2008). Functional role of HSP90 complexes with endothelial

nitric-oxide synthase (eNOS) and calpain on nitric oxide generation in endothelial cells. J. Biol. Chem. *283*, 29069–29076.

Baezner, H., Blahak, C., Poggesi, A., Pantoni, L., Inzitari, D., Chabriat, H., Erkinjuntti, T., Fazekas, F., Ferro, J.M., Langhorne, P., et al. (2008). Association of gait and balance disorders with age-related white matter changes: The LADIS Study. Neurology *70*, 935–942.

Bailey, E.L., McCulloch, J., Sudlow, C., and Wardlaw, J.M. (2009). Potential animal models of lacunar stroke: a systematic review. Stroke. *40*, e451–e458.

Bailey, E.L., Smith, C., Sudlow, C.L.M., and Wardlaw, J.M. (2011a). Is the spontaneously hypertensive stroke prone rat a pertinent model of sub cortical ischemic stroke? A systematic review. Int. J. Stroke *6*, 434–444.

Bailey, E.L., Wardlaw, J.M., Graham, D., Dominiczak, a F., Sudlow, C.L.M., and Smith, C. (2011b). Cerebral small vessel endothelial structural changes predate hypertension in stroke-prone spontaneously hypertensive rats: a blinded, controlled immunohistochemical study of 5- to 21-week-old rats. Neuropathol. Appl. Neurobiol. *37*, 711–726.

Bailey, E.L., Smith, C., Sudlow, C.L.M., and Wardlaw, J.M. (2012). Pathology of lacunar ischemic stroke in humans--a systematic review. Brain Pathol. *22*, 583–591.

Bamford, J., Sandercock, P., Jones, L., and Warlow, C. (1987). The natural history of lacunar infarction: the Oxfordshire Community Stroke Project. Stroke. *18*, 545–551.

Bamford, J., Sandercock, P., Dennis, M., Burn, J., and Warlow, C. (1991). Classification and natural history of clinically identifiable subtypes of cerebral infarction. Ann. Intern. Med. *115*, 89.

Bassé, F., Stout, J.G., Sims, P.J., and Wiedmer, T. (1996). Isolation of an erythrocyte membrane protein that mediates Ca2+-dependent transbilayer movement of phospholipid. J. Biol. Chem. *271*, 17205–17210.

Basso, A.D., Solit, D.B., Chiosis, G., Giri, B., Tsichlis, P., and Rosen, N. (2002). Akt forms an intracellular complex with heat shock protein 90 (Hsp90) and Cdc37 and is destabilized by inhibitors of Hsp90 function. J. Biol. Chem. *277*, 39858–39866.

Basu, S., Binder, R.J., Ramalingam, T., and Srivastava, P.K. (2001). CD91 is a common receptor for heat shock proteins gp96, hsp90, hsp70, and calreticulin. Immunity *14*, 303–313.

Batchelor, P.E., Liberatore, G.T., Wong, J.Y., Porritt, M.J., Frerichs, F., Donnan, G. a, and Howells, D.W. (1999). Activated macrophages and microglia induce dopaminergic sprouting in the injured striatum and express brain-derived neurotrophic factor and glial cell line-derived neurotrophic factor. J. Neurosci. *19*,

1708–1716.

Bath, P.M., and Wardlaw, J.M. (2015). Pharmacological treatment and prevention of cerebral small vessel disease: a review of potential interventions. Int. J. Stroke *10*, 469–478.

Bath, P.M., Pathansali, R., Iddenden, R., and Bath, F.J. (2001). The effect of transdermal glyceryl trinitrate, a nitric oxide donor, on blood pressure and platelet function in acute stroke. Cerebrovasc. Dis. *11*, 265–272.

Baumann, N., and Pham-Dinh, D. (2001). Biology of oligodendrocyte and myelin in the mammalian central nervous system. Physiol. Rev. *81*, 871–927.

Beaufort, N., Scharrer, E., Kremmer, E., Lux, V., Ehrmann, M., Huber, R., Houlden, H., Werring, D., Haffner, C., and Dichgans, M. (2014). Cerebral small vessel disease-related protease HtrA1 processes latent TGF-β binding protein 1 and facilitates TGF-β signaling. Proc. Natl. Acad. Sci. *111*, 16496–16501.

Bechmann, I., Galea, I., and Perry, V.H. (2007). What is the blood-brain barrier (not)? Trends Immunol. *28*, 5–11.

Beckman, J.S., and Koppenol, W.H. (1996). Nitric oxide, superoxide, and peroxynitrite: the good, the bad, and ugly. Am. J. Physiol. *271*, C1424–C1437.

Bianchi, S., Zicari, E., Carluccio, A., Di Donato, I., Pescini, F., Nannucci, S., Valenti, R., Ragno, M., Inzitari, D., Pantoni, L., et al. (2014). CADASIL in central Italy: a retrospective clinical and genetic study in 229 patients. J. Neurol. *262*, 134–141.

Bischel, L.L., Young, E.W.K., Mader, B.R., and Beebe, D.J. (2013). Tubeless microfluidic angiogenesis assay with three-dimensional endothelial-lined microvessels. Biomaterials *34*, 1471–1477.

Bitbol, M., and Devaux, P.F. (1988). Measurement of outward translocation of phospholipids across human erythrocyte membrane. Proc. Natl. Acad. Sci. U. S. A. *85*, 6783–6787.

Boggs, J.M. (2006). Myelin basic protein: a multifunctional protein. Cell. Mol. Life Sci. *63*, 1945–1961.

Branton, D. (1969). Membrane Structure. Annu. Rev. Plant Physiol. *20*, 209–238.

Bridges, L.R., Andoh, J., Lawrence, A.J., Khoong, C.H.L., Poon, W.W., Esiri, M.M., Markus, H.S., and Hainsworth, A.H. (2014). Blood-Brain Barrier Dysfunction and Cerebral Small Vessel Disease (Arteriolosclerosis) in Brains of Older People. J. Neuropathol. Exp. Neurol. *73*, 1026–1033.

Bull, L.N., van Eijk, M.J., Pawlikowska, L., DeYoung, J. a, Juijn, J. a, Liao, M.,

Klomp, L.W., Lomri, N., Berger, R., Scharschmidt, B.F., et al. (1998). A gene encoding a P-type ATPase mutated in two forms of hereditary cholestasis. Nat. Genet. *18*, 219–224.

Carmichael, O. (2010). Longitudinal Changes in White Matter Disease and Cognition in the First Year of the Alzheimer Disease Neuroimaging Initiative. Arch. Neurol. *67*, 1370.

Carré, J.-L., Goetz, B.D., O'Connor, L.T., Bremer, Q., and Duncan, I.D. (2002). Mutations in the rat myelin basic protein gene are associated with specific alterations in other myelin gene expression. Neurosci. Lett. *330*, 17–20.

Carthew, R.W., and Sontheimer, E.J. (2009). Origins and Mechanisms of miRNAs and siRNAs. Cell *136*, 642–655.

De Caterina, R., Libby, P., Peng, H.B., Thannickal, V.J., Rajavachisth, T.B., Gimbrone Jr., M. a, Shin, W.S., and Laio, J.K. (1995). Nitric oxide decreases cykotine-induced endothelial activation. Nitric oxide selectively redeuced endothelial expression of adhesion molecules and pro inflamatory cytokines. J Clin Invest *96*, 60–68.

Catterall, W.A. (2012). Voltage-gated sodium channels at 60: structure, function and pathophysiology. J. Physiol. *590*, 2577–2589.

Cavalieri, M., Schmidt, R., Chen, C., Mok, V., de Freitas, G.R., Song, S., Yi, Q., Ropele, S., Grazer, A., Homayoon, N., et al. (2012). B Vitamins and Magnetic Resonance Imaging-Detected Ischemic Brain Lesions in Patients With Recent Transient Ischemic Attack or Stroke: The VITAmins TO Prevent Stroke (VITATOPS) MRI-Substudy. Stroke *43*, 3266–3270.

Chabriat, H., Vahedi, K., Bousser, M.., Iba-Zizen, M.., Joutel, A., Nibbio, A., Nagy, T.., Tournier Lasserve, E., Krebs, M.., Julien, J., et al. (1995). Clinical spectrum of CADASIL: a study of 7 families. Lancet *346*, 934–939.

Chabriat, H., Joutel, A., Dichgans, M., Tournier-Lasserve, E., and Bousser, M.-G. (2009). Cadasil. Lancet Neurol. *8*, 643–653.

Chapman, N., Huxley, R., Anderson, C., Bousser, M.G., Chalmers, J., Colman, S., Davis, S., Donnan, G., MacMahon, S., Neal, B., et al. (2004). Effects of a Perindopril-Based Blood Pressure-Lowering Regimen on the Risk of Recurrent Stroke According to Stroke Subtype and Medical History: The PROGRESS Trial. Stroke *35*, 116–121.

Chastain, E.M.L., and Miller, S.D. (2012). Molecular mimicry as an inducing trigger for CNS autoimmune demyelinating disease. Immunol. Rev. *245*, 227–238.

Christ, M., Bauersachs, J., Liebetrau, C., Heck, M., and Gu, A. (2002). Glucose

Increases Endothelial-Dependent Superoxide Formation in Coronary Arteries by NAD(P)H Oxidase. Diabetes *51*, 2648–2652.

Cid, C., and Alcazar, A. (2010). Protection of oligodendrocyte precursor cells by low doses of HSP90 inhibitors in cell culture. Exp. Neurol. *225*, 29–33.

Cid, C., Alvarez-Cermeño, J.C., Camafeita, E., Salinas, M., and Alcázar, A. (2004). Antibodies reactive to heat shock protein 90 induce oligodendrocyte precursor cell death in culture. Implications for demyelination in multiple sclerosis. FASEB J. *18*, 409–411.

Clayton, A., Turkes, A., Navabi, H., Mason, M.D., and Tabi, Z. (2005). Induction of heat shock proteins in B-cell exosomes. J. Cell Sci. *118*, 3631–3638.

Comfurius, P., Williamson, P., Smeets, E.F., Schlegel, R. a., Bevers, E.M., and Zwaal, R.F. a (1996). Reconstitution of phospholipid scramblase activity from human blood platelets. Biochemistry *35*, 7631–7634.

Cong, L., Ran, F.A., Cox, D., Lin, S., Barretto, R., Habib, N., Hsu, P.D., Wu, X., Jiang, W., Marraffini, L.A., et al. (2013). Multiplex genome engineering using CRISPR/Cas systems. Science *339*, 819–823.

Cooper, M.E., Bonnet, F., Oldfield, M., and Jandeleit-Dahm, K. (2001). Mechanisms of Diabetic Vasculopathy : An Overview. Am. J. Hypertens. *7061*, 475–486.

Cordonnier, C., Al-Shahi Salman, R., and Wardlaw, J. (2007). Spontaneous brain microbleeds: systematic review, subgroup analyses and standards for study design and reporting. Brain *130*, 1988–2003.

Cserr, H.F., and Bundgaard, M. (1984). Blood-brain interfaces in vertebrates: a comparative approach. Am. J. Physiol. *246*, R277–R288.

Cucullo, L., Hossain, M., Puvenna, V., Marchi, N., and Janigro, D. (2011). The role of shear stress in Blood-Brain Barrier endothelial physiology. BMC Neurosci. *12*, 40.

Cunningham, F., Amode, M.R., Barrell, D., Beal, K., Billis, K., Brent, S., Carvalho-Silva, D., Clapham, P., Coates, G., Fitzgerald, S., et al. (2015). Ensembl 2015. Nucleic Acids Res. *43*, D662–D669.

Daleke, D.L. (2003). Regulation of transbilayer plasma membrane phospholipid asymmetry. J. Lipid Res. *44*, 233–242.

Daneman, R., Zhou, L., Kebede, A. a, and Barres, B. a (2010). Pericytes are required for blood-brain barrier integrity during embryogenesis. Nature *468*, 562–566.

Dawson, M.R.L., Polito, A., Levine, J.M., and Reynolds, R. (2003). NG2-expressing glial progenitor cells: an abundant and widespread population of cycling cells in the adult rat CNS. Mol. Cell. Neurosci. *24*, 476–488.

Debette, S., and Markus, H.S. (2010). The clinical importance of white matter hyperintensities on brain magnetic resonance imaging: systematic review and meta-analysis. BMJ *341*, c3666.

Dermietzel, R., Spray, D.C., and Needergard, M. (2006). Blood-Brain Barriers (Weinheim, Germany: Wiley-VCH Verlag GmbH & Co. KGaA).

Dharmashankar, K., and Widlansky, M.E. (2010). Vascular endothelial function and hypertension: insights and directions. Curr. Hypertens. Rep. *12*, 448–455.

van Dijk, E.J., Breteler, M.M.B.B., Schmidt, R., Berger, K., Nilsson, L.-G.L.-G., Oudkerk, M., Pajak, A., Sans, S., de Ridder, M., Dufouil, C., et al. (2004). The association between blood pressure, hypertension, and cerebral white matter lesions: cardiovascular determinants of dementia study. Hypertension *44*, 625–630.

Van Dijk, E.J., Prins, N.D., Vrooman, H. a., Hofman, A., Koudstaal, P.J., and Breteler, M.M.B. (2008). Progression of cerebral small vessel disease in relation to risk factors and cognitive consequences: Rotterdam scan study. Stroke *39*, 2712–2719.

Dobrogowska, D.H., Lossinsky, a S., Tarnawski, M., and Vorbrodt, a W. (1998). Increased blood-brain barrier permeability and endothelial abnormalities induced by vascular endothelial growth factor. J. Neurocytol. *27*, 163–173.

Doubal, F.N., MacLullich, A.M.J., Ferguson, K.J., Dennis, M.S., and Wardlaw, J.M. (2010). Enlarged perivascular spaces on MRI are a feature of cerebral small vessel disease. Stroke. *41*, 450–454.

Downes, N., and Mullins, P. (2013). The Development of Myelin in the Brain of the Juvenile Rat. Toxicol. Pathol.

Dozono, K., Ishii, N., Nishihara, Y., and Horie, a (1991). An autopsy study of the incidence of lacunes in relation to age, hypertension, and arteriosclerosis. Stroke. *22*, 993–996.

Drab, M., Verkade, P., Elger, M., Kasper, M., Lohn, M., Lauterbach, B., Menne, J., Lindschau, C., Mende, F., Luft, F.C., et al. (2001). Loss of caveolae, vascular dysfunction, and pulmonary defects in caveolin-1 gene-disrupted mice. Science *293*, 2449–2452.

Dufouil, C., Chalmers, J., Coskun, O., Besançon, V., Bousser, M.G., Guillon, P., MacMahon, S., Mazoyer, B., Neal, B., Woodward, M., et al. (2005). Effects of blood pressure lowering on cerebral white matter hyperintensities in patients with stroke: The PROGRESS (Perindopril Protection Against Recurrent Stroke Study) Magnetic Resonance Imaging Substudy. Circulation *112*, 1644–1650.

Ehrlich, P. (1885). Das Sauerstoff-Bedürfniss des Organismus, eine

farbenanalytische Studie von Professor Dr P. Ehrlich,... (A. Hirschwald).

Elbaz, A., Poirier, O., Moulin, T., Chédru, F., Cambien, F., and Amarenco, P. (2000). Association between the Glu298Asp polymorphism in the endothelial constitutive nitric oxide synthase gene and brain infarction. The GENIC Investigators. Stroke. *31*, 1634–1639.

Engel, O., Kolodziej, S., Dirnagl, U., and Prinz, V. (2011). Modeling Stroke in Mice - Middle Cerebral Artery Occlusion with the Filament Model. J. Vis. Exp. e2423.

Eriksson, S., Olofsson, B., and Wester, P. (1995). Atenolol in Secondary Prevention after Stroke. Cerebrovasc. Dis. *5*, 21–25.

Esiri, M.M., Wilcock, G.K., and Morris, J.H. (1997). Neuropathological assessment of the lesions of significance in vascular dementia. J. Neurol. Neurosurg. Psychiatry *63*, 749–753.

Eustace, B.K., Sakurai, T., Stewart, J.K., Yimlamai, D., Unger, C., Zehetmeier, C., Lain, B., Torella, C., Henning, S.W., Beste, G., et al. (2004). Functional proteomic screens reveal an essential extracellular role for hsp90 alpha in cancer cell invasiveness. Nat. Cell Biol. *6*, 507–514.

Farrall, A.J., and Wardlaw, J.M. (2009). Blood-brain barrier: ageing and microvascular disease--systematic review and meta-analysis. Neurobiol. Aging *30*, 337–352.

Feng, D., Nagy, J.A., Pyne, K., Dvorak, H.F., and Dvorak, A.M. (1998). Neutrophils emigrate from venules by a transendothelial cell pathway in response to FMLP. J. Exp. Med. *187*, 903–915.

Feron, O., Dessy, C., Moniotte, S., Desager, J.P., and Balligand, J.L. (1999). Hypercholesterolemia decreases nitric oxide production by promoting the interaction of caveolin and endothelial nitric oxide synthase. J. Clin. Invest. *103*, 897–905.

Fiala, M., Looney, D.J., Stins, M., Way, D.D., Zhang, L., Gan, X., Chiappelli, F., Schweitzer, E.S., Shapshak, P., Weinand, M., et al. (1997). TNF-alpha opens a paracellular route for HIV-1 invasion across the blood-brain barrier. Mol. Med. *3*, 553–564.

Fisher, C.M. (1969). The arterial lesions underlying lacunes. Acta Neuropathol. *12*, 1–15.

Flores, A.I., Mallon, B.S., Matsui, T., Ogawa, W., Rosenzweig, A., Okamoto, T., and Macklin, W.B. (2000). Akt-mediated survival of oligodendrocytes induced by neuregulins. J. Neurosci. *20*, 7622–7630.

Förstermann, U., and Münzel, T. (2006). Endothelial nitric oxide synthase in vascular disease: From marvel to menace. Circulation *113*, 1708–1714.

Frank, P.G., Woodman, S.E., Park, D.S., and Lisanti, M.P. (2003). Caveolin, caveolae, and endothelial cell function. Arterioscler. Thromb. Vasc. Biol. *23*, 1161–1168.

Franklin, R.J.M., and ffrench-Constant, C. (2008). Remyelination in the CNS: from biology to therapy. Nat. Rev. Neurosci. *9*, 839–855.

Fredriksson, K., Nordborg, C., Kalimo, H., Olsson, Y., and Johansson, B.B. (1988). Cerebral microangiopathy in stroke-prone spontaneously hypertensive rats. Acta Neuropathol. *75*, 241–252.

French, C.R., Seshadri, S., Destefano, A.L., Fornage, M., Arnold, C.R., Gage, P.J., Skarie, J.M., Dobyns, W.B., Millen, K.J., Liu, T., et al. (2014). Mutation of FOXC1 and PITX2 induces cerebral small-vessel disease. J. Clin. Invest. *124*, 4877–4881.

Fu, J.H., Mok, V., Lam, W., Wong, A., Chu, W., Xiong, Y., Ng, P.W., Tsoi, T.H., Yeung, V., and Wong, K.S. (2010). Effects of statins on progression of subclinical brain infarct. Cerebrovasc. Dis. *30*, 51–56.

Fukutake, T. (2011). Cerebral autosomal recessive arteriopathy with subcortical infarcts and leukoencephalopathy (CARASIL): from discovery to gene identification. J. Stroke Cerebrovasc. Dis. *20*, 85–93.

Funovic, P., Korda, M., Kubant, R., Barlag, R.E., Jacob, R.F., Mason, R.P., and Malinski, T. (2008). Effect of beta-blockers on endothelial function during biological aging: a nanotechnological approach. J. Cardiovasc. Pharmacol. *51*, 208–215.

Furuse, M., Hirase, T., Itoh, M., Nagafuchi, a., Yonemura, S., Tsukita, S., and Tsukita, S. (1993). Occludin: A novel integral membrane protein localizing at tight junctions. J. Cell Biol. *123*, 1777–1788.

Furuse, M., Fujita, K., Hiiragi, T., Fujimoto, K., and Tsukita, S. (1998). Claudin-1 and -2: novel integral membrane proteins localizing at tight junctions with no sequence similarity to occludin. J. Cell Biol. *141*, 1539–1550.

García-Cardeña, G., Fan, R., Shah, V., Sorrentino, R., Cirino, G., Papapetropoulos, a, and Sessa, W.C. (1998). Dynamic activation of endothelial nitric oxide synthase by Hsp90. Nature *392*, 821–824.

Garneau, J.E., Dupuis, M.-È., Villion, M., Romero, D. a, Barrangou, R., Boyaval, P., Fremaux, C., Horvath, P., Magadán, A.H., and Moineau, S. (2010). The CRISPR/Cas bacterial immune system cleaves bacteriophage and plasmid DNA. Nature *468*, 67–71.

Geren, B. Ben, and Schmitt, F.O. (1954). The Structure of the Schwann Cell and its Relation to the Axon in Certain Invertebrate Nerve Fibers. Proc. Natl. Acad. Sci. *40*, 863–870.

Gimbrone, M.A., Nagel, T., and Topper, J.N. (1997). Biomechanical Activation: an Emerging Paradigm in Endothelial Adhesion Biology. J. Clin. Invest. *99*, 1809–1813.

Giwa, M.O., Williams, J., Elderfield, K., Jiwa, N.S., Bridges, L.R., Kalaria, R.N., Markus, H.S., Esiri, M.M., and Hainsworth, a H. (2012). Neuropathologic evidence of endothelial changes in cerebral small vessel disease. Neurology *78*, 167–174.

Go, A.S., Mozaffarian, D., Roger, V.L., Benjamin, E.J., Berry, J.D., Borden, W.B., Bravata, D.M., Dai, S., Ford, E.S., Fox, C.S., et al. (2013). Heart disease and stroke statistics--2013 update: a report from the American Heart Association. Circulation *127*, e6–e245.

Gorelick, P.B., Scuteri, A., Black, S.E., Decarli, C., Greenberg, S.M., Iadecola, C., Launer, L.J., Laurent, S., Lopez, O.L., Nyenhuis, D., et al. (2011). Vascular contributions to cognitive impairment and dementia: A statement for healthcare professionals from the American Heart Association/American Stroke Association. Stroke *42*, 2672–2713.

Gould, D.B., Phalan, F.C., van Mil, S.E., Sundberg, J.P., Vahedi, K., Massin, P., Bousser, M.G., Heutink, P., Miner, J.H., Tournier-lasserve, E., et al. (2006). Role of COL4A1 in Small-Vessel Disease and Hemorrhagic Stroke. N. Engl. J. Med. *354*, 1489–1496.

Gouw, A.A., Seewann, A., van der Flier, W.M., Barkhof, F., Rozemuller, A.M., Scheltens, P., and Geurts, J.J.G. (2011). Heterogeneity of small vessel disease: a systematic review of MRI and histopathology correlations. J. Neurol. Neurosurg. Psychiatry *82*, 126–135.

Graham, T.R. (2004). Flippases and vesicle-mediated protein transport. Trends Cell Biol. *14*, 670–677.

Grammas, P. (2011). Neurovascular dysfunction, inflammation and endothelial activation: implications for the pathogenesis of Alzheimer's disease. J. Neuroinflammation *8*, 26.

Gresch, O., and Altrogge, L. (2012). Protein Expression in Mammalian Cells (Totowa, NJ: Humana Press).

Griffiths, I. (1998). Axonal Swellings and Degeneration in Mice Lacking the Major Proteolipid of Myelin. Science *280*, 1610–1613.

Groeschel, S., Chong, W.K., Surtees, R., and Hanefeld, F. (2006). Virchow-Robin spaces on magnetic resonance images: Normative data, their dilatation, and a review of the literature. Neuroradiology *48*, 745–754.

Gryglewski, R.J., Palmer, R.M.J., and Moncada, S. (1986). Superoxide anion is

involved in the breakdown of endothelium-derived vascular relaxing factor. Nature *320*, 264–265.

Haffner, C., Malik, R., and Dichgans, M. (2015). Genetic factors in cerebral small vessel disease and their impact on stroke and dementia. J. Cereb. Blood Flow Metab. 1–10.

Hainsworth, A.H., and Markus, H.S. (2008). Do in vivo experimental models reflect human cerebral small vessel disease? A systematic review. J. Cereb. Blood Flow Metab. *28*, 1877–1891.

Hallbergson, A.F., Gnatenco, C., and Peterson, D. a. (2003). Neurogenesis and brain injury: Managing a renewable resource for repair. J. Clin. Invest. *112*, 1128–1133.

Hara, K., Shiga, A., Fukutake, T., Nozaki, H., Miyashita, A., Yokoseki, A., Kawata, H., Koyama, A., Arima, K., Takahashi, T., et al. (2009). Association of HTRA1 mutations and familial ischemic cerebral small-vessel disease. N. Engl. J. Med. *360*, 1729–1739.

Hassan, a., Gormley, K., O'Sullivan, M., Knight, J., Sham, P., Vallance, P., Bamford, J., and Markus, H. (2004a). Endothelial Nitric Oxide Gene Haplotypes and Risk of Cerebral Small-Vessel Disease. Stroke *35*, 654–659.

Hassan, A., Hunt, B.J., O'Sullivan, M., Parmar, K., Bamford, J.M., Briley, D., Brown, M.M., Thomas, D.J., and Markus, H.S. (2003). Markers of endothelial dysfunction in lacunar infarction and ischaemic leukoaraiosis. Brain *126*, 424–432.

Hassan, A., Hunt, B.J., O'Sullivan, M., Bell, R., D'Souza, R., Jeffery, S., Bamford, J.M., and Markus, H.S. (2004b). Homocysteine is a risk factor for cerebral small vessel disease, acting via endothelial dysfunction. Brain *127*, 212–219.

Hawkins, B., and Davis, T. (2005). The blood-brain barrier/neurovascular unit in health and disease. Pharmacol. Rev. *57*, 173–185.

Heck, J.W., Cheung, S.K., and Hampton, R.Y. (2010). Cytoplasmic protein quality control degradation mediated by parallel actions of the E3 ubiquitin ligases Ubr1 and San1. Proc. Natl. Acad. Sci. U. S. A. *107*, 1106–1111.

Heitzer, T., Just, H., and Mu¨nzel, T. (1996). Antioxidant Vitamin C Improves Endothelial Dysfunction in Chronic Smokers. Circulation *94*, 6–9.

Herman, A.G., and Moncada, S. (2005). Therapeutic potential of nitric oxide donors in the prevention and treatment of atherosclerosis. Eur. Heart J. *26*, 1945–1955.

Herrmann, L.L., Le Masurier, M., and Ebmeier, K.P. (2007). White matter hyperintensities in late life depression: a systematic review. J. Neurol. Neurosurg. Psychiatry *79*, 619–624.

Hink, U., Li, H., Mollnau, H., Oelze, M., Matheis, E., Hartmann, M., Skatchkov, M., Thaiss, F., Stahl, R.A., Warnholtz, A., et al. (2001). Mechanisms underlying endothelial dysfunction in diabetes mellitus. Circ Res *88*, E14–E22.

Holland, P.R., Searcy, J.L., Salvadores, N., Scullion, G., Chen, G., Lawson, G., Scott, F., Bastin, M.E., Ihara, M., Kalaria, R., et al. (2015). Gliovascular disruption and cognitive deficits in a mouse model with features of small vessel disease. J. Cereb. Blood Flow Metab. 1–10.

Horvath, P., and Barrangou, R. (2010). CRISPR/Cas, the immune system of bacteria and archaea. Science *327*, 167–170.

HSCS Group (1974). Effect of Antihypertensive Treatment on Stroke Recurrence. JAMA *229*, 409.

Huang, P.L. (2003). Endothelial nitric oxide synthase and endothelial dysfunction. Curr. Hypertens Rep *5*, 473–480.

Huang, P.L., Huang, Z., Mashimo, H., Bloch, K.D., Moskowitz, M. a, Bevan, J. a, and Fishman, M.C. (1995). Hypertension in mice lacking the gene for endothelial nitric oxide synthase. Nature *377*, 239–242.

Huxley, A.F., and Stampfli, R. (1949). Saltatory transmission of the nervous impulse. Arch. Sci. Physiol. (Paris). *3*, 435–448.

Iglarz, M., and Clozel, M. (2007). Mechanisms of ET-1-induced Endothelial Dysfunction. J. Cardiovasc. Pharmacol. *50*, 621–628.

Iida, S., Baumbach, G.L., Lavoie, J.L., Faraci, F.M., Sigmund, C.D., and Heistad, D.D. (2005). Spontaneous stroke in a genetic model of hypertension in mice. Stroke *36*, 1253–1258.

Jackson, C. a., Hutchison, A., Dennis, M.S., Wardlaw, J.M., Lindgren, A., Norrving, B., Anderson, C.S., Hankey, G.J., Jamrozik, K., Appelros, P., et al. (2010). Differing risk factor profiles of ischemic stroke subtypes: Evidence for a distinct lacunar arteriopathy? Stroke *41*, 624–629.

Jeon, S.-B., Kang, D.-W., Kim, J.S., and Kwon, S.U. (2014). Homocysteine, small-vessel disease, and atherosclerosis: An MRI study of 825 stroke patients. Neurology *83*, 695–701.

Jhaveri, K., Taldone, T., Modi, S., and Chiosis, G. (2012). Advances in the clinical development of heat shock protein 90 (Hsp90) inhibitors in cancers. Biochim. Biophys. Acta *1823*, 742–755.

Jiang, X., Guo, M., Su, J., Lu, B., Ma, D., Zhang, R., Yang, L., Wang, Q., Ma, Y., and Fan, Y. (2012). Simvastatin blocks blood-brain barrier disruptions induced by elevated cholesterol both in vivo and in vitro. Int. J. Alzheimers. Dis. *2012*, 109324.

Jin, Z.-G. (2006). Where is endothelial nitric oxide synthase more critical: plasma membrane or Golgi? Arterioscler. Thromb. Vasc. Biol. *26*, 959–961.

Johns, T.G., and Bernard, C.C. a (1999). The structure and function of myelin oligodendrocyte glycoprotein. J. Neurochem. *72*, 1–9.

Johnstone, M.T., Creager, S.J., Scales, K.M., Cusco, J.A., Lee, B.K., and Creager, M.A. (1993). Impaired endothelium-dependent vasodilation in patients with insulin-dependent diabetes mellitus. Circulation *88*, 2510–2516.

Joutel, A., and Faraci, F.M. (2014). Cerebral Small Vessel Disease: Insights and Opportunities From Mouse Models of Collagen IV-Related Small Vessel Disease and Cerebral Autosomal Dominant Arteriopathy With Subcortical Infarcts and Leukoencephalopathy. Stroke *45*, 1215–1221.

Joutel, A., Corpechot, C., Ducros, A., Vahedi, K., Chabriat, H., Mouton, P., Alamowitch, S., Domenga, V., Cécillion, M., Marechal, E., et al. (1996). Notch3 mutations in CADASIL, a hereditary adult-onset condition causing stroke and dementia. Nature *383*, 707–710.

Joutel, A., Monet-Leprêtre, M., Gosele, C., Baron-Menguy, C., Hammes, A., Schmidt, S., Lemaire-Carrette, B., Domenga, V., Schedl, A., Lacombe, P., et al. (2010). Cerebrovascular dysfunction and microcirculation rarefaction precede white matter lesions in a mouse genetic model of cerebral ischemic small vessel disease. J. Clin. Invest. *120*, 433–445.

Joutel, A., Haddad, I., Ratelade, J., and Nelson, M.T. (2015). Perturbations of the cerebrovascular matrisome: a convergent mechanism in small vessel disease of the brain? J. Cereb. Blood Flow Metab. 1–10.

Kalaria, R.N., and Erkinjuntti, T. (2006). Small vessel disease and subcortical vascular dementia. J Clin Neurol *2*, 1–11.

Kast, J., Hanecker, P., Beaufort, N., Giese, A., Joutel, A., Dichgans, M., Opherk, C., and Haffner, C. (2014). Sequestration of latent TGF-β binding protein 1 into CADASIL-related Notch3-ECD deposits. Acta Neuropathol. Commun. *2*, 96.

Kaya, M., and Ahishali, B. (2011). Assessment of Permeability in Barrier Type of Endothelium in Brain Using Tracers: Evans Blue, Sodium Fluorescein, and Horseradish Peroxidase. In Permeability Barrier SE - 25, K. Turksen, ed. (Humana Press), pp. 369–382.

Khan, U., Porteous, L., Hassan, A., and Markus, H.S. (2006). Risk factor profile of cerebral small vessel disease and its subtypes. J. Neurol. Neurosurg. Psychiatry *78*, 702–706.

Klein, L.W. (1984). Cigarette smoking, atherosclerosis and the coronary

hemodynamic response: A unifying hypothesis. J. Am. Coll. Cardiol. *4*, 972–974.

Kloppenborg, R.P., Nederkoorn, P.J., Grool, A.M., Vincken, K.L., Mali, W.P.T.M., Vermeulen, M., Van Der Graaf, Y., and Geerlings, M.I. (2012). Cerebral small-vessel disease and progression of brain atrophy : The SMART-MR study. Neurology *79*, 2029–2036.

Koch, G., Smith, M., Macer, D., Webster, P., and Mortara, R. (1986). Endoplasmic reticulum contains a common, abundant calcium-binding glycoprotein, endoplasmin. J. Cell Sci. *86*, 217–232.

Koo, H.-Y., and Kume, T. (2013). FoxC1-dependent regulation of vascular endothelial growth factor signaling in corneal avascularity. Trends Cardiovasc. Med. *23*, 1–4.

Korn, J., Christ, B., and Kurz, H. (2002). Neuroectodermal origin of brain pericytes and vascular smooth muscle cells. J. Comp. Neurol. *442*, 78–88.

Koto, T., Takubo, K., Ishida, S., Shinoda, H., Inoue, M., Tsubota, K., Okada, Y., and Ikeda, E. (2007). Hypoxia disrupts the barrier function of neural blood vessels through changes in the expression of claudin-5 in endothelial cells. Am. J. Pathol. *170*, 1389–1397.

Kotter, M.R., Zhao, C., van Rooijen, N., and Franklin, R.J.M. (2005). Macrophage-depletion induced impairment of experimental CNS remyelination is associated with a reduced oligodendrocyte progenitor cell response and altered growth factor expression. Neurobiol. Dis. *18*, 166–175.

Kotter, M.R., Li, W.-W., Zhao, C., and Franklin, R.J.M. (2006). Myelin impairs CNS remyelination by inhibiting oligodendrocyte precursor cell differentiation. J. Neurosci. *26*, 328–332.

Kubo, M., Hata, J., Ninomiya, T., Matsuda, K., Yonemoto, K., Nakano, T., Matsushita, T., Yamazaki, K., Ohnishi, Y., Saito, S., et al. (2007). A nonsynonymous SNP in PRKCH (protein kinase C eta) increases the risk of cerebral infarction. Nat Genet *39*, 212–217.

Kuhlmann, T., Remington, L., Maruschak, B., Owens, T., and Brück, W. (2007). Nogo-A is a reliable oligodendroglial marker in adult human and mouse CNS and in demyelinated lesions. J. Neuropathol. Exp. Neurol. *66*, 238–246.

Kuo, D.S., Labelle-Dumais, C., and Gould, D.B. (2012). COL4A1 and COL4A2 mutations and disease: insights into pathogenic mechanisms and potential therapeutic targets. Hum. Mol. Genet. *21*, R97–R110.

de Laat, K.F., Tuladhar, A.M., van Norden, A.G.W., Norris, D.G., Zwiers, M.P., and de Leeuw, F.-E. (2011). Loss of white matter integrity is associated with gait

disorders in cerebral small vessel disease. Brain *134*, 73–83.

Lai, B.T., Chin, N.W., Stanek, a E., Keh, W., and Lanks, K.W. (1984). Quantitation and intracellular localization of the 85K heat shock protein by using monoclonal and polyclonal antibodies. Mol. Cell. Biol. *4*, 2802–2810.

Lammie, G.A. (2000). Pathology of small vessel stroke. Br. Med. Bull. *56*, 296–306.

Lammie, G.A. (2002). Hypertensive cerebral small vessel disease and stroke. Brain Pathol. *12*, 358–370.

Lammie, G.A., Brannan, F., Slattery, J., and Warlow, C. (1997). Nonhypertensive cerebral small-vessel disease an autopsy study. Stroke *28*, 2222–2229.

Langer, T., and Fasold, H. (2001). Isolation and quantification of the heat shock protein 90 alpha and beta isoforms from rat liver. Protoplasma *218*, 54–56.

Lee, D.C., Sunnarborg, S.W., Hinkle, C.L., Myers, T.J., Stevenson, M.Y., Russell, W.E., Castner, B.J., Gerhart, M.J., Paxton, R.J., Black, R. a, et al. (2003). TACE/ADAM17 processing of EGFR ligands indicates a role as a physiological convertase. Ann. N. Y. Acad. Sci. *995*, 22–38.

Lee, Y., Morrison, B.M., Li, Y., Lengacher, S., Farah, M.H., Hoffman, P.N., Liu, Y., Tsingalia, A., Jin, L., Zhang, P., et al. (2012). Oligodendroglia metabolically support axons and contribute to neurodegeneration. Nature *487*, 443–448.

Lei, H., Venkatakrishnan, A., Yu, S., and Kazlauskas, A. (2007). Protein kinase A-dependent translocation of Hsp90?? impairs endothelial nitric-oxide synthase activity in high glucose and diabetes. J. Biol. Chem. *282*, 9364–9371.

Lein, E.S., Hawrylycz, M.J., Ao, N., Ayres, M., Bensinger, A., Bernard, A., Boe, A.F., Boguski, M.S., Brockway, K.S., Byrnes, E.J., et al. (2007). Genome-wide atlas of gene expression in the adult mouse brain. Nature *445*, 168–176.

Leonard, T. a, and Hurley, J.H. (2011). Regulation of protein kinases by lipids. Curr. Opin. Struct. Biol. *21*, 785–791.

Leventis, P.A., and Grinstein, S. (2010). The Distribution and Function of Phosphatidylserine in Cellular Membranes. Annu. Rev. Biophys. *39*, 407–427.

Levi, G., and Meyer, H. (1941). Nouvelles recherches sur le tissu nerveux cultivé in vitro: Morphologie, croissance et relations réciproques des neurones (Vaillant-Carmanne).

Lewandowski, M. (1900). Zur Lehre von der Cerebrospinalflüssigkeit. Z. Klein Forsch. *40*, 480–494.

Li, J.-M., and Shah, A.M. (2004). Endothelial cell superoxide generation: regulation and relevance for cardiovascular pathophysiology. Am. J. Physiol. Regul. Integr.

Comp. Physiol. *287*, R1014–R1030.

Li, C., Trapp, B., Ludwin, S., Peterson, a, and Roder, J. (1998). Myelin associated glycoprotein modulates glia-axon contact in vivo. J. Neurosci. Res. *51*, 210–217.

Li, J., Luo, M., Xu, X., and Sheng, W. (2012). Association between 1425G/A SNP in PRKCH and ischemic stroke among Chinese and Japanese populations: a meta-analysis including 3686 cases and 4589 controls. Neurosci. Lett. *506*, 55–58.

Li, W., Li, Y., Guan, S., Fan, J., Cheng, C.-F., Bright, A.M., Chinn, C., Chen, M., and Woodley, D.T. (2007). Extracellular heat shock protein-90alpha: linking hypoxia to skin cell motility and wound healing. EMBO J. *26*, 1221–1233.

Li, W., Tsen, F., Sahu, D., Bhatia, A., Chen, M., Multhoff, G., and Woodley, D.T. (2013). Extracellular Hsp90 (eHsp90) as the Actual Target in Clinical Trials: Intentionally or Unintentionally. Int. Rev. Cell Mol. Biol. *303*, 203–235.

Liao, J.K. (2013). Linking endothelial dysfunction with endothelial cell activation. J. Clin. Invest. *123*, 540–541.

Liao, D.F., Jin, Z.G., Baas, a S., Daum, G., Gygi, S.P., Aebersold, R., and Berk, B.C. (2000). Purification and identification of secreted oxidative stress-induced factors from vascular smooth muscle cells. J. Biol. Chem. *275*, 189–196.

Lin, J.-X., Tomimoto, H., Akiguchi, I., Wakita, H., Shibasaki, H., and Horie, R. (2001). White matter lesions and alteration of vascular cell composition in the brain of spontaneously hypertensive rats. Neuroreport *12*, 1835–1839.

Linker, R.A., Lee, D.-H., Demir, S., Wiese, S., Kruse, N., Siglienti, I., Gerhardt, E., Neumann, H., Sendtner, M., Lühder, F., et al. (2010). Functional role of brain-derived neurotrophic factor in neuroprotective autoimmunity: therapeutic implications in a model of multiple sclerosis. Brain *133*, 2248–2263.

Lip, P.L., Belgore, F., Blann, A.D., Hope-Ross, M.W., Gibson, J.M., and Lip, G.Y.H. (2000). Plasma VEGF and soluble VEGF receptor FLT-1 in proliferative retinopathy: Relationship to endothelial dysfunction and laser treatment. Investig. Ophthalmol. Vis. Sci. *41*, 2115–2119.

Lippmann, E.S., Azarin, S.M., Kay, J.E., Nessler, R.A., Wilson, H.K., Al-Ahmad, A., Palecek, S.P., and Shusta, E. V (2012). Derivation of blood-brain barrier endothelial cells from human pluripotent stem cells. Nat. Biotechnol. *30*, 783–791.

Lopez-Ramirez, M.A., Fischer, R., Torres-Badillo, C.C., Davies, H.A., Logan, K., Pfizenmaier, K., Male, D.K., Sharrack, B., and Romero, I.A. (2012). Role of Caspases in Cytokine-Induced Barrier Breakdown in Human Brain Endothelial Cells. J. Immunol. *189*, 3130–3139.

Lum, H., and Roebuck, K. a (2001). Oxidant stress and endothelial cell dysfunction.

Am. J. Physiol. Cell Physiol. *280*, C719–C741.

Lüscher, T.F. (2000). Endothelial dysfunction: the role and impact of the renin-angiotensin system. Heart *84*, 20i – 22.

Macdonald, R.L., Kowalczuk, A., and Johns, L. (1995). Emboli Enter Penetrating Arteries of Monkey Brain in Relation to Their Size. Stroke *26*, 1247–1251.

MacLullich, A.M.J. (2004). Enlarged perivascular spaces are associated with cognitive function in healthy elderly men. J. Neurol. Neurosurg. Psychiatry *75*, 1519–1523.

Maeda, S., Nakayama, H., Isaka, K., Aihara, Y., and Nemoto, S. (1976). Familial Unusual Encephalopathy of Binswanger's Type without Hypertension. Psychiatry Clin. Neurosci. *30*, 165–177.

van der Mark, V.A., Oude Elferink, R.P.J., and Paulusma, C.C. (2013). P4 ATPases: flippases in health and disease. Int. J. Mol. Sci. *14*, 7897–7922.

Markus, H.S., Barley, J., Lunt, R., Bland, J.M., Jeffery, S., Carter, N.D., and Brown, M.M. (1995). Angiotensin-Converting Enzyme Gene Deletion Polymorphism: A New Risk Factor for Lacunar Stroke but not Carotid Atheroma. Stroke *26*, 1329–1333.

Markus, H.S., Hunt, B., Palmer, K., Enzinger, C., Schmidt, H., and Schmidt, R. (2005). Markers of endothelial and hemostatic activation and progression of cerebral white matter hyperintensities: Longitudinal results of the Austrian Stroke Prevention Study. Stroke *36*, 1410–1414.

Martìn-Padura, I., Lostaglio, S., Schneemann, M., Williams, L., Romano, M., Fruscella, P., Panzeri, C., Stoppacciaro, A., Ruco, L., Villa, A., et al. (1998). Junctional Adhesion Molecule, a Novel Member of the Immunoglobulin Superfamily That Distributes at Intercellular Junctions and Modulates Monocyte Transmigration. J. Cell Biol. *142*, 117–127.

Mazzon, E., De Sarro, A., Caputi, A.P., and Cuzzocrea, S. (2002). Role of tight junction derangement in the endothelial dysfunction elicited by exogenous and endogenous peroxynitrite and poly(ADP-ribose) synthetase. Shock *18*, 434–439.

McAllister, M.S., Krizanac-Bengez, L., Macchia, F., Naftalin, R.J., Pedley, K.C., Mayberg, M.R., Marroni, M., Leaman, S., Stanness, K.A., and Janigro, D. (2001). Mechanisms of glucose transport at the blood-brain barrier: An in vitro study. Brain Res. *904*, 20–30.

McCarthy, K.D., and de Vellis, J. (1980). Preparation of separate astroglial and oligodendroglial cell cultures from rat cerebral tissue. J. Cell Biol. *85*, 890–902.

McDowell, I.F., and Lang, D. (2000). Homocysteine and endothelial dysfunction: a

link with cardiovascular disease. J. Nutr. *130*, 369S – 372S.

Mehta, V.B., Zhou, Y., Radulescu, A., and Besner, G.E. (2008). HB-EGF stimulates eNOS expression and nitric oxide production and promotes eNOS dependent angiogenesis. Growth Factors *26*, 301–315.

Meyer, J., Rauh, J., and Galla, H.J. (1991). The susceptibility of cerebral endothelial cells to astroglial induction of blood-brain barrier enzymes depends on their proliferative state. J. Neurochem. *57*, 1971–1977.

Minshall, R.D., Sessa, W.C., Stan, R. V, Anderson, R.G.W., and Malik, A.B. (2003). Caveolin regulation of endothelial function. Am. J. Physiol. Lung Cell. Mol. Physiol. *285*, L1179–L1183.

Mok, V., and Kim, J.S. (2015). Prevention and Management of Cerebral Small Vessel Disease. J. Stroke *17*, 111–122.

Monet-Leprêtre, M., Haddad, I., Baron-Menguy, C., Fouillot-Panchal, M., Riani, M., Domenga-Denier, V., Dussaule, C., Cognat, E., Vinh, J., and Joutel, A. (2013). Abnormal recruitment of extracellular matrix proteins by excess Notch3 ECD: A new pathomechanism in CADASIL. Brain *136*, 1830–1845.

Montesano, R., Pepper, M.S., Möhle-Steinlein, U., Risau, W., Wagner, E.F., and Orci, L. (1990). Increased proteolytic activity is responsible for the aberrant morphogenetic behavior of endothelial cells expressing the middle T oncogene. Cell *62*, 435–445.

Mooradian, D.L., Hutsell, T.C., and Keefer, L.K. (1995). Nitric oxide (NO) donor molecules: effect of NO release rate on vascular smooth muscle cell proliferation in vitro. J Cardiovasc Pharmacol *25*, 674–678.

Moreau, F., Patel, S., Lauzon, M.L., McCreary, C.R., Goyal, M., Frayne, R., Demchuk, A.M., Coutts, S.B., and Smith, E.E. (2012). Cavitation After Acute Symptomatic Lacunar Stroke Depends on Time, Location, and MRI Sequence. Stroke *43*, 1837–1842.

Moreno-Smith, M., Halder, J., Meltzer, P.S., Gonda, T.A., Mangala, L.S., Rupaimoole, R., Lu, C., Nagaraja, A.S., Gharpure, K.M., Kang, Y., et al. (2013). ATP11B mediates platinum resistance in ovarian cancer. J. Clin. Invest. *123*, 2119–2130.

Morita, K., Sasaki, H., Furuse, M., and Tsukita, S. (1999). Endothelial claudin: claudin-5/TMVCF constitutes tight junction strands in endothelial cells. J. Cell Biol. *147*, 185–194.

Morris, Z., Whiteley, W.N., Longstreth, W.T., Weber, F., Lee, Y., Tsushima, Y., Alphs, H., Ladd, S.C., Warlow, C., Wardlaw, J.M., et al. (2009). Incidental findings

on brain magnetic resonance imaging: systematic review and meta-analysis. BMJ *339*, b3016.

Muldoon, L.L., Alvarez, J.I., Begley, D.J., Boado, R.J., del Zoppo, G.J., Doolittle, N.D., Engelhardt, B., Hallenbeck, J.M., Lonser, R.R., Ohlfest, J.R., et al. (2013). Immunologic privilege in the central nervous system and the blood–brain barrier. J. Cereb. Blood Flow Metab. *33*, 13–21.

Muller, W. a (2011). Mechanisms of leukocyte transendothelial migration. Annu. Rev. Pathol. *6*, 323–344.

Mungas, D., Jagust, W.J., Reed, B.R., Kramer, J.H., Weiner, M.W., Schuff, N., Norman, D., Mack, W.J., Willis, L., and Chui, H.C. (2001). MRI predictors of cognition in subcortical ischemic vascular disease and Alzheimer's disease. Neurology *57*, 2229–2235.

Murohara, T., Asahara, T., Silver, M., Bauters, C., Masuda, H., Kalka, C., Kearney, M., Chen, D., Symes, J.F., Fishman, M.C., et al. (1998). Nitric oxide synthase modulates angiogenesis in response to tissue ischemia. J. Clin. Invest. *101*, 2567–2578.

Muthusamy, B.P., Natarajan, P., Zhou, X., and Graham, T.R. (2009). Linking phospholipid flippases to vesicle-mediated protein transport. Biochim. Biophys. Acta - Mol. Cell Biol. Lipids *1791*, 612–619.

Najjar, S., Pearlman, D.M., Devinsky, O., Najjar, A., and Zagzag, D. (2013). Neurovascular unit dysfunction with blood-brain barrier hyperpermeability contributes to major depressive disorder: a review of clinical and experimental evidence . J. Neuroinflammation *10*, 142.

Narayan, S.K., Gorman, G., Kalaria, R.N., Ford, G.A., and Chinnery, P.F. (2012). The minimum prevalence of CADASIL in northeast England. Neurology *78*, 1025–1027.

Nedergaard, M., Ransom, B., and Goldman, S. a. (2003). New roles for astrocytes: Redefining the functional architecture of the brain. Trends Neurosci. *26*, 523–530.

Newton, A.C. (1995). Protein Kinase C : Structure , Function , and Regulation. J. Biol. Chem. *270*, 28495–28498.

Nitta, T., Hata, M., Gotoh, S., Seo, Y., Sasaki, H., Hashimoto, N., Furuse, M., and Tsukita, S. (2003). Size-selective loosening of the blood-brain barrier in claudin-5-deficient mice. J. Cell Biol. *161*, 653–660.

Noseworthy, J.H., Lucchinetti, C., Rodriguez, M., and Weinshenker, B.G. (2000). MS - Clinical course and diagnosis. N. Engl. J. Med. *343*, 938–952.

Nozaki, H., Nishizawa, M., and Onodera, O. (2014). Features of cerebral autosomal

recessive arteriopathy with subcortical infarcts and leukoencephalopathy. Stroke. *45*, 3447–3453.

Oide, T., Nakayama, H., Yanagawa, S., Ito, N., Ikeda, S.I., and Arima, K. (2008). Extensive loss of arterial medial smooth muscle cells and mural extracellular matrix in cerebral autosomal recessive arteriopathy with subcortical infarcts and leukoencephalopathy (CARASIL). Neuropathology *28*, 132–142.

Okamoto, K. (1974). Establishment of the stroke-prone spontaneously hypertensive rat (SHR). Cir. Res. *34*, 143–153.

Op den Kamp, J.A.F. (1979). Lipid Asymmetry in Membranes. Annu. Rev. Biochem. *48*, 47–71.

Ovcharenko, D., Jarvis, R., Hunicke-Smith, S., Kelnar, K., and Brown, D. (2005). High-throughput RNAi screening in vitro: from cell lines to primary cells. RNA *11*, 985–993.

Ozaki, K., Hori, T., Ishibashi, T., Nishio, M., and Aizawa, Y. (2010). Effects of chronic cigarette smoking on endothelial function in young men. J. Cardiol. *56*, 307–313.

Palmgren, M.G., and Nissen, P. (2011). P-type ATPases. Annu. Rev. Biophys. *40*, 243–266.

Panza, J.A., Quyyumi, A.A., Brush, J.E., and Epstein, S.E. (1990). Abnormal Endothelium-Dependent Vascular Relaxation in Patients with Essential Hypertension. N. Engl. J. Med. *323*, 22–27.

Patel, B., Lawrence, A.J., Chung, A.W., Rich, P., Mackinnon, A.D., Morris, R.G., Barrick, T.R., and Markus, H.S. (2013). Cerebral Microbleeds and Cognition in Patients With Symptomatic Small Vessel Disease. Stroke. 356–361.

Patterson, C.E., and Clauss, M. (2005). Perspectives on Lung Endothelial Barrier Function (Elsevier).

Paulusma, C.C., and Oude Elferink, R.P.J. (2010). P4 ATPases - The physiological relevance of lipid flipping transporters. FEBS Lett. *584*, 2708–2716.

Pearson, J.D. (2000). Normal endothelial cell function. Lupus *9*, 183–188.

Pevsner, P.H., Eichenbaum, J.W., Miller, D.C., Pivawer, G., Eichenbaum, K.D., Stern, A., Zakian, K.L., and Koutcher, J. a. (2001). A photothrombotic model of small early ischemic infarcts in the rat brain with histologic and MRI correlation. J. Pharmacol. Toxicol. Methods *45*, 227–233.

Philip, I., Plantefeve, G., Vuillaumier-Barrot, S., Vicaut, E., LeMarie, C., Henrion, D., Poirier, O., Levy, B.I., Desmonts, J.M., Durand, G., et al. (1999). G894T

polymorphism in the endothelial nitric oxide synthase gene is associated with an enhanced vascular responsiveness to phenylephrine. Circulation *99*, 3096–3098.

Picard, D. (2002). Heat-shock protein 90, a chaperone for folding and regulation. Cell. Mol. Life Sci. *59*, 1640–1648.

Pittilo, R.M. (2000). Cigarette smoking, endothelial injury and cardiovascular disease. Int. J. Exp. Pathol. *81*, 219–230.

Poggesi, A., Pasi, M., Pescini, F., Pantoni, L., and Inzitari, D. (2015). Circulating biologic markers of endothelial dysfunction in cerebral small vessel disease: a review. J. Cereb. Blood Flow Metab. 1–15.

Pöschl, E., Schlötzer-Schrehardt, U., Brachvogel, B., Saito, K., Ninomiya, Y., and Mayer, U. (2004). Collagen IV is essential for basement membrane stability but dispensable for initiation of its assembly during early development. Development *131*, 1619–1628.

Potter, G.M., Doubal, F.N., Jackson, C.A., Chappell, F.M., Sudlow, C.L., Dennis, M.S., and Wardlaw, J.M. (2010). Counting Cavitating Lacunes Underestimates the Burden of Lacunar Infarction. Stroke *41*, 267–272.

Potter, G.M., Marlborough, F.J., and Wardlaw, J.M. (2011). Wide Variation in Definition, Detection, and Description of Lacunar Lesions on Imaging. Stroke *42*, 359–366.

Prasad, S., Sajja, R.K., Park, J.H., Naik, P., Kaisar, M.A., and Cucullo, L. (2015). Impact of cigarette smoke extract and hyperglycemic conditions on blood–brain barrier endothelial cells. Fluids Barriers CNS *12*, 18.

Prins, N.D., van Dijk, E.J., den Heijer, T., Vermeer, S.E., Jolles, J., Koudstaal, P.J., Hofman, A., and Breteler, M.M.B. (2005). Cerebral small-vessel disease and decline in information processing speed, executive function and memory. Brain *128*, 2034–2041.

Radomski, M.W., Palmer, R.M.J., and Moncada, S. (1991). Modulation of platelet aggregation by an l-arginine-nitric oxide pathway. Trends Pharmacol. Sci. *12*, 87–88.

Raij, L., DeMaster, E.G., and Jaimes, E. a (2001). Cigarette smoke-induced endothelium dysfunction: role of superoxide anion. J. Hypertens. *19*, 891–897.

Rajashekhar, G., Willuweit, A., Patterson, C.E., Sun, P., Hilbig, A., Breier, G., Helisch, A., and Clauss, M. (2006). Continuous endothelial cell activation increases angiogenesis: Evidence for the direct role of endothelium linking angiogenesis and inflammation. J. Vasc. Res. *43*, 193–204.

Ramsauer, M., Krause, D., and Dermietzel, R. (2002). Angiogenesis of the blood-brain barrier in vitro and the function of cerebral pericytes. FASEB J. *16*, 1274–

1276.

Rannikmäe, K., Davies, G., Thomson, P.A., Bevan, S., Devan, W.J., Falcone, G.J., Traylor, M., Anderson, C.D., Battey, T.W.K., Radmanesh, F., et al. (2015). Common variation in COL4A1/COL4A2 is associated with sporadic cerebral small vessel disease. Neurology *84*, 918–926.

Rashid, P., Weaver, C., Leonardi-Bee, J., Bath, F., Fletcher, S., and Bath, P. (2003). The effects of transdermal glyceryl trinitrate, a nitric oxide donor, on blood pressure, cerebral and cardiac hemodynamics, and plasma nitric oxide levels in acute stroke. J. Stroke Cerebrovasc. Dis. *12*, 143–151.

Rask-Madsen, C., and King, G.L. (2008). Differential regulation of VEGF signaling by PKC-alpha and PKC-epsilon in endothelial cells. Arterioscler. Thromb. Vasc. Biol. *28*, 919–924.

Readhead, C., Takasashi, N., Shine, H.D., Saavedra, R., Sidman, R., and Hood, L. (1990). Role of Myelin Basic Protein in the Formation of Central Nervous System Myelin. Ann. N. Y. Acad. Sci. *605*, 280–285.

Rehman, H.U. (2000). Primary Angiitis of the Central Nervous System. In Journal of the Royal Society of Medicine, (Elsevier), pp. 586–588.

Reimer, M.M., McQueen, J., Searcy, L., Scullion, G., Zonta, B., Desmazieres, A., Holland, P.R., Smith, J., Gliddon, C., Wood, E.R., et al. (2011). Rapid disruption of axon-glial integrity in response to mild cerebral hypoperfusion. J. Neurosci. *31*, 18185–18194.

Richardson, W.D., Young, K.M., Tripathi, R.B., and McKenzie, I. (2011). NG2-glia as Multipotent Neural Stem Cells: Fact or Fantasy? Neuron *70*, 661–673.

Ritchie, J.M., and Rogart, R.B. (1977). Density of sodium channels in mammalian myelinated nerve fibers and nature of the axonal membrane under the myelin sheath. Proc. Natl. Acad. Sci. *74*, 211–215.

Rivas-Cabanero, L., Valedivielso, J.M., and Lopez-Novoa, J.M. (1996). NG-Nitro-L-Arginine Methyl Ester Causes Glomeruloar Nitrite Production in Long-Term Incubations. Nephron *73*, 97–98.

Ruckh, J.M., Zhao, J.-W., Shadrach, J.L., Wijngaarden, P. Van, Nageswara, T., van Wijngaarden, P., Rao, T.N., Wagers, A.J., and Franklin, R.J.M. (2012). Rejuvenation of regeneration in the aging central nervous system. Cell Stem Cell *10*, 96–103.

Ryu, W.-S., Woo, S.-H., Schellingerhout, D., Chung, M.K., Kim, C.K., Jang, M.U., Park, K.-J., Hong, K.-S., Jeong, S.-W., Na, J.-Y., et al. (2014). Grading and interpretation of white matter hyperintensities using statistical maps. Stroke. *45*, 3567–3575.

Saher, G., Brügger, B., Lappe-Siefke, C., Möbius, W., Tozawa, R., Wehr, M.C., Wieland, F., Ishibashi, S., and Nave, K.-A. (2005). High cholesterol level is essential for myelin membrane growth. Nat. Neurosci. *8*, 468–475.

Sander, J.D., and Joung, J.K. (2014). CRISPR-Cas systems for editing, regulating and targeting genomes. Nat. Biotechnol. *32*, 347–355.

Sander, M., Chavoshan, B., and Victor, R.G. (1999). A Large Blood Pressure Raising Effect of Nitric Oxide Synthase Inhibition in Humans. Hypertension *33*, 937–942.

Sandoval, K.E., and Witt, K.A. (2008). Blood-brain barrier tight junction permeability and ischemic stroke. Neurobiol. Dis. *32*, 200–219.

Sansing, H. a, Renner, N. a, and MacLean, A.G. (2012). An inverted blood-brain barrier model that permits interactions between glia and inflammatory stimuli. J. Neurosci. Methods *207*, 91–96.

Sato, S., Fujita, N., and Tsuruo, T. (2000). Modulation of Akt kinase activity by binding to Hsp90. Proc. Natl. Acad. Sci. *97*, 10832–10837.

Schilling, M., Besselmann, M., Leonhard, C., Mueller, M., Ringelstein, E.B., and Kiefer, R. (2003). Microglial activation precedes and predominates over macrophage infiltration in transient focal cerebral ischemia: a study in green fluorescent protein transgenic bone marrow chimeric mice. Exp. Neurol. *183*, 25–33.

Schini, V.B., Durante, W., Elizondo, E., Scott-Burden, T., Junquero, D.C., Schafer, A.I., and Vanhoutte, P.M. (1992). The induction of nitric oxide synthase activity is inhibited by TGF-β1, PDGFAB and PDGFBB in vascular smooth muscle cells. Eur. J. Pharmacol. *216*, 379–383.

Schmidt, R., Schmidt, H., Haybaeck, J., Loitfelder, M., Weis, S., Cavalieri, M., Seiler, S., Enzinger, C., Ropele, S., Erkinjuntti, T., et al. (2011). Heterogeneity in age-related white matter changes. Acta Neuropathol. *122*, 171–185.

Schreiber, S., Bueche, C.Z., Garz, C., Kropf, S., Angenstein, F., Goldschmidt, J., Neumann, J., Heinze, H.-J., Goertler, M., Reymann, K.G., et al. (2012). The pathologic cascade of cerebrovascular lesions in SHRSP: is erythrocyte accumulation an early phase? J. Cereb. Blood Flow Metab. *32*, 278–290.

Serizawa, M., Nabika, T., Ochiai, Y., Takahashi, K., Yamaguchi, S., Makaya, M., Kobayashi, S., and Kato, N. (2008). Association between PRKCH gene polymorphisms and subcortical silent brain infarction. Atherosclerosis *199*, 340–345.

Shiga, A., Nozaki, H., Yokoseki, A., Nihonmatsu, M., Kawata, H., Kato, T., Koyama, A., Arima, K., Ikeda, M., Katada, S., et al. (2011). Cerebral small-vessel disease protein HTRA1 controls the amount of TGF-β1 via cleavage of proTGF-β1.

Hum. Mol. Genet. *20*, 1800–1810.

Shimizu, F., Sano, Y., Tominaga, O., Maeda, T., Abe, M.-A., and Kanda, T. (2013). Advanced glycation end-products disrupt the blood–brain barrier by stimulating the release of transforming growth factor–β by pericytes and vascular endothelial growth factor and matrix metalloproteinase–2 by endothelial cells in vitro. Neurobiol. Aging *34*, 1902–1912.

Sidera, K., Samiotaki, M., Yfanti, E., Panayotou, G., and Patsavoudi, E. (2004). Involvement of cell surface HSP90 in cell migration reveals a novel role in the developing nervous system. J. Biol. Chem. *279*, 45379–45388.

Sikorski, E.E., Hallmann, R., Berg, E.L., and Butcher, E.C. (1993). The Peyer's patch high endothelial receptor for lymphocytes, the mucosal vascular addressin, is induced on a murine endothelial cell line by tumor necrosis factor-alpha and IL-1. J. Immunol. *151*, 5239–5250.

Simpson, I.A. (2001). Glucose Transporter Asymmetries in the Bovine Blood-Brain Barrier. J. Biol. Chem. *276*, 12725–12729.

Smallwood, A., Oulhaj, A., Joachim, C., Christie, S., Sloan, C., Smith, a D., and Esiri, M. (2012). Cerebral subcortical small vessel disease and its relation to cognition in elderly subjects: a pathological study in the Oxford Project to Investigate Memory and Ageing (OPTIMA) cohort. Neuropathol. Appl. Neurobiol. *38*, 337–343.

Smith, C.W., Rothlein, R., Hughes, B.J., Mariscalco, M.M., Rudloff, H.E., Schmalstieg, F.C., and Anderson, D.C. (1988). Recognition of an endothelial determinant for CD 18-dependent human neutrophil adherence and transendothelial migration. J. Clin. Invest. *82*, 1746–1756.

Sohet, F., Lin, C., Munji, R.N., Lee, S.Y., Ruderisch, N., Soung, a., Arnold, T.D., Derugin, N., Vexler, Z.S., Yen, F.T., et al. (2015). LSR/angulin-1 is a tricellular tight junction protein involved in blood-brain barrier formation. J. Cell Biol. *208*, 703–711.

Sommer, I., and Schachner, M. (1981). Monoclonal antibodies (O1 to O4) to oligodendrocyte cell surfaces: An immunocytological study in the central nervous system. Dev. Biol. *83*, 311–327.

Song, X., Wang, X., Zhuo, W., Shi, H., Feng, D., Sun, Y., Liang, Y., Fu, Y., Zhou, D., and Luo, Y. (2010). The regulatory mechanism of extracellular Hsp90α on matrix metalloproteinase-2 processing and tumor angiogenesis. J. Biol. Chem. *285*, 40039–40049.

Sourander, P., and Walinder, J. (1977). Hereditary multi-infarct dementia. Acta Neuropathol. *39*, 247–254.

SPS3 Group, T. (2013). Blood-pressure targets in patients with recent lacunar stroke: the SPS3 randomised trial. Lancet *382*, 507–515.

Sriram, S. (2011). Role of glial cells in innate immunity and their role in CNS demyelination. J. Neuroimmunol. *239*, 13–20.

Staddon, J.M., and Rubin, L.L. (1996). Cell adhesion, cell junctions and the blood-brain barrier. Curr. Opin. Neurobiol. *6*, 622–627.

Steegmaier, M., Klumperman, J., Foletti, D.L., Yoo, J.S., and Scheller, R.H. (1999). Vesicle-associated membrane protein 4 is implicated in trans-Golgi network vesicle trafficking. Mol. Biol. Cell *10*, 1957–1972.

Stevenson, S.F., Doubal, F.N., Shuler, K., and Wardlaw, J.M. (2010). A systematic review of dynamic cerebral and peripheral endothelial function in lacunar stroke versus controls. Stroke *41*, 434–443.

Stühlinger, M.C., Tsao, P.S., Her, J.H., Kimoto, M., Balint, R.F., and Cooke, J.P. (2001). Homocysteine impairs the nitric oxide synthase pathway: role of asymmetric dimethylarginine. Circulation *104*, 2569–2575.

Sussman, C.R. (2005). The ErbB4 Neuregulin Receptor Mediates Suppression of Oligodendrocyte Maturation. J. Neurosci. *25*, 5757–5762.

Swieten, J.C. Van, Hout, J.H.W. Van Den, Ketel, B. a. Van, Hijdra, a., Wokke, J.H.J., and Gijn, J. Van (1991). Periventricular Lesions in the White Matter on Magnetic Resonance Imaging in the Elderly. Brain *114*, 761–774.

Tagami, M., Nara, Y., Kubota, A., Sunaga, T., Maezawa, H., Fujino, H., and Yamori, Y. (1987). Ultrastructural characteristics of occluded perforating arteries in stroke-prone spontaneously hypertensive rats. Stroke *18*, 733–740.

Taherian, A., Krone, P.H., and Ovsenek, N. (2008). A comparison of Hsp90alpha and Hsp90beta interactions with cochaperones and substrates. Biochem. Cell Biol. *86*, 37–45.

Takahashi, K., and Yamanaka, S. (2006). Induction of Pluripotent Stem Cells from Mouse Embryonic and Adult Fibroblast Cultures by Defined Factors. Cell *126*, 663–676.

Takahashi, S., and Mendelsohn, M.E. (2003). Synergistic Activation of Endothelial Nitric-oxide Synthase (eNOS) by HSP90 and Akt. J. Biol. Chem. *278*, 30821–30827.

Tan, X.-L., Xue, Y.-Q., Ma, T., Wang, X., Li, J.J., Lan, L., Malik, K.U., McDonald, M.P., Dopico, A.M., and Liao, F.-F. (2015). Partial eNOS deficiency causes spontaneous thrombotic cerebral infarction, amyloid angiopathy and cognitive impairment. Mol. Neurodegener. *10*, 24.

Tang, X., Halleck, M.S., Schlegel, R. a, and Williamson, P. (1996). A subfamily of P-type ATPases with aminophospholipid transporting activity. Science *272*, 1495–1497.

Tasaki, I. (1939). The electro-saltatory transmission of the nerve impulse and the effect of narcosis upon the nerve fiber. J. Physiol. *127*, 211–227.

Tazi, J., Bakkour, N., and Stamm, S. (2009). Alternative splicing and disease. Biochim. Biophys. Acta - Mol. Basis Dis. *1792*, 14–26.

Thrift, A.G., McNeil, J.J., Forbes, A., and Donnan, G.A. (1998). Three Important Subgroups of Hypertensive Persons at Greater Risk of Intracerebral Hemorrhage. Hypertension *31*, 1223–1229.

Tournier-Lasserve, E., Iba-Zizen, M.T., Romero, N., and Bousser, M.G. (1991). Autosomal dominant syndrome with strokelike episodes and leukoencephalopathy. Stroke *22*, 1297–1302.

Tsukita, S., Katsuno, T., Yamazaki, Y., Umeda, K., Tamura, A., and Tsukita, S. (2009). Roles of ZO-1 and ZO-2 in establishment of the belt-like adherens and tight junctions with paracellular permselective barrier function. Ann. N. Y. Acad. Sci. *1165*, 44–52.

Uchida, H., Sakata, H., Fujimura, M., Niizuma, K., Kushida, Y., Dezawa, M., and Tominaga, T. (2015). Experimental model of small subcortical infarcts in mice with long-lasting functional disabilities. Brain Res. *1629*, 318–328.

Valdés Hernández, M.D.C., Maconick, L.C., Muñoz Maniega, S., Wang, X., Wiseman, S., Armitage, P. a., Doubal, F.N., Makin, S., Sudlow, C.L.M., Dennis, M.S., et al. (2015). A comparison of location of acute symptomatic vs. “silent” small vessel lesions. Int. J. Stroke *10*, 1044–1050.

Vandenberg, J.I., and Waxman, S.G. (2012). Hodgkin and Huxley and the basis for electrical signalling: a remarkable legacy still going strong. J. Physiol. *590*, 2569–2570.

Vandenbroucke, E., Mehta, D., Minshall, R., and Malik, A.B. (2008). Regulation of Endothelial Junctional Permeability. Ann. N. Y. Acad. Sci. *1123*, 134–145.

Vásquez-Vivar, J., Kalyanaraman, B., Martásek, P., Hogg, N., Masters, B.S., Karoui, H., Tordo, P., and Pritchard, K. a (1998). Superoxide generation by endothelial nitric oxide synthase: the influence of cofactors. Proc. Natl. Acad. Sci. *95*, 9220–9225.

van der Velden, L.M., van de Graaf, S.F.J., and Klomp, L.W.J. (2010). Biochemical and cellular functions of P4 ATPases. Biochem. J. *431*, 1–11.

Verbeek, E., Meuwissen, M.E., Verheijen, F.W., Govaert, P.P., Licht, D.J., Kuo, D.S., Poulton, C.J., Schot, R., Lequin, M.H., Dudink, J., et al. (2012). COL4A2

mutation associated with familial porencephaly and small-vessel disease. Eur. J. Hum. Genet. *20*, 844–851.

Verdelho, a., Madureira, S., Moleiro, C., Ferro, J.M., Santos, C.O., Erkinjuntti, T., Pantoni, L., Fazekas, F., Visser, M., Waldemar, G., et al. (2010). White matter changes and diabetes predict cognitive decline in the elderly: The LADIS Study. Neurology *75*, 160–167.

Vermeer, S.E., Longstreth, W.T., and Koudstaal, P.J. (2007). Silent brain infarcts: a systematic review. Lancet Neurol. *6*, 611–619.

Vernooij, M.W., van der Lugt, A., Ikram, M.A., Wielopolski, P.A., Niessen, W.J., Hofman, A., Krestin, G.P., and Breteler, M.M.B. (2008). Prevalence and risk factors of cerebral microbleeds: The Rotterdam Scan Study. Neurology *70*, 1208–1214.

Walker, E.J., and Rosenberg, G. a. (2010). Divergent role for MMP-2 in myelin breakdown and oligodendrocyte death following transient global ischemia. J. Neurosci. Res. *88*, 764–773.

Wang, K., and Walz, W. (2003). Unusual topographical pattern of proximal astrogliosis around a cortical devascularizing lesion. J. Neurosci. Res. *73*, 497–506.

Wang, H., Yang, H., Shivalila, C.S., Dawlaty, M.M., Cheng, A.W., Zhang, F., and Jaenisch, R. (2013). One-step generation of mice carrying mutations in multiple genes by CRISPR/cas-mediated genome engineering. Cell *153*, 910–918.

Wang, X., Song, X., Zhuo, W., Fu, Y., Shi, H., Liang, Y., Tong, M., Chang, G., and Luo, Y. (2009). The regulatory mechanism of Hsp90 secretion and its function in tumor malignancy. Proc. Natl. Acad. Sci. *106*, 21288–21293.

Wardlaw, J.M. (2008). What is a lacune? Stroke. *39*, 2921–2922.

Wardlaw, J.M., Sandercock, P. a G., Dennis, M.S., and Starr, J. (2003). Is breakdown of the blood-brain barrier responsible for lacunar stroke, leukoaraiosis, and dementia? Stroke. *34*, 806–812.

Wardlaw, J.M., Smith, E.E., Biessels, G.J., Cordonnier, C., Fazekas, F., Frayne, R., Lindley, R.I., O'Brien, J.T., Barkhof, F., Benavente, O.R., et al. (2013a). Neuroimaging standards for research into small vessel disease and its contribution to ageing and neurodegeneration. Lancet Neurol. *12*, 822–838.

Wardlaw, J.M., Smith, C., and Dichgans, M. (2013b). Mechanisms of sporadic cerebral small vessel disease: insights from neuroimaging. Lancet Neurol. *12*, 483–497.

Wardlaw, J.M., Allerhand, M., Doubal, F.N., Valdes Hernandez, M., Morris, Z., Gow, A.J., Bastin, M., Starr, J.M., Dennis, M.S., and Deary, I.J. (2014). Vascular risk factors, large-artery atheroma, and brain white matter hyperintensities.

Neurology *82*, 1331–1338.

Wardlaw, J.M., Valdés Hernández, M.C., and Muñoz-Maniega, S. (2015). What are White Matter Hyperintensities Made of? Relevance to Vascular Cognitive Impairment. J. Am. Heart Assoc. *4*, 001140.

Waxman, S.G., and Ritchie, J.M. (1985). Organization of ion channels in the myelinated nerve fiber. Science *228*, 1502–1507.

Weber, R., Weimar, C., Blatchford, J., Hermansson, K., Wanke, I., Möller-Hartmann, C., Gizewski, E.R., Forsting, M., Demchuk, A.M., Sacco, R.L., et al. (2012). Telmisartan on top of antihypertensive treatment does not prevent progression of cerebral white matter lesions in the prevention regimen for effectively avoiding second strokes (PRoFESS) MRI substudy. Stroke *43*, 2336–2342.

Wilkins, A., Chandran, S., and Compston, A. (2001). A role for oligodendrocyte-derived IGF-1 in trophic support of cortical neurons. Glia *36*, 48–57.

Williams, R.L., Courtneidge, S.A., and Wagner, E.F. (1988). Embryonic lethalities and endothelial tumors in chimeric mice expressing polyoma virus middle T oncogene. Cell *52*, 121–131.

Wiseman, S., Marlborough, F., Doubal, F., Webb, D.J., and Wardlaw, J. (2014). Blood markers of coagulation, fibrinolysis, endothelial dysfunction and inflammation in lacunar stroke versus non-lacunar stroke and non-stroke: Systematic review and meta-analysis. Cerebrovasc. Dis. *37*, 64–75.

Wolburg, H., and Lippoldt, A. (2002). Tight junctions of the blood-brain barrier: development, composition and regulation. Vascul. Pharmacol. *38*, 323–337.

Wu, G.F., and Alvarez, E. (2011). The immunopathophysiology of multiple sclerosis. Neurol. Clin. *29*, 257–278.

Wu, L., Shen, Y., Liu, X., Ma, X., Xi, B., Mi, J., Lindpaintner, K., Tan, X., and Wang, X. (2009). The 1425G/A SNP in PRKCH is associated with ischemic stroke and cerebral hemorrhage in a Chinese population. Stroke. *40*, 2973–2976.

y Cajal, S.R. (1928). Degeneration & regeneration of the nervous system (Oxford University Press, Humphrey Milford).

Yamori, Y., and Horie, R. (1977). Developmental course of hypertension and regional cerebral blood flow in stroke-prone spontaneously hypertensive rats. Stroke *8*, 456–461.

Yamori, Y., Horie, R., Handa, H., Sato, M., and Fukase, M. (1976). Pathogenetic Similarity of Strokes in Stroke-Prone Spontaneously Hypertensive Rats and Humans. Stroke *7*, 46–53.

Yang, Y.-M., Huang, A., Kaley, G., and Sun, D. (2009). eNOS uncoupling and endothelial dysfunction in aged vessels. Am. J. Physiol. Heart Circ. Physiol. *297*, H1829–H1836.

Ye, M., Sanchez, H.M., Hultz, M., Yang, Z., Bogorad, M., Wong, A.D., and Searson, P.C. (2014). Brain microvascular endothelial cells resist elongation due to curvature and shear stress. Sci. Rep. *4*, 4681.

Yoon, S.S.S., Ostchega, Y., and Louis, T. (2010). Recent trends in the prevalence of high blood pressure and its treatment and control, 1999-2008. NCHS Data Brief 1–8.

Yoshizumi, M., Perrella, M.A., Burnett, J.C., and Lee, M.-E. (1993). Tumor necrosis factor downregulates an endothelial nitric oxide synthase mRNA by shortening its half- life. Circ. Res. *73*, 205–209.

Yusuf, S., Diener, H.-C., Sacco, R.L., Cotton, D., Ounpuu, S., Lawton, W. a, Palesch, Y., Martin, R.H., Albers, G.W., Bath, P., et al. (2008). Telmisartan to prevent recurrent stroke and cardiovascular events. N. Engl. J. Med. *359*, 1225–1237.

Zhang, G., Fahmy, R.G., DiGirolamo, N., and Khachigian, L.M. (2006). JUN siRNA regulates matrix metalloproteinase-2 expression, microvascular endothelial growth and retinal neovascularisation. J. Cell Sci. *119*, 3219–3226.

Zhang, H., Jarjour, A. a, Boyd, A., and Williams, A. (2011). Central nervous system remyelination in culture--a tool for multiple sclerosis research. Exp. Neurol. *230*, 138–148.

Zhang, M., Zhu, W., Yun, W., Wang, Q., Cheng, M., Zhang, Z., Liu, X., Zhou, X., and Xu, G. (2015). Correlation of matrix metalloproteinase-2 single nucleotide polymorphisms with the risk of small vessel disease (SVD). J. Neurol. Sci. *356*, 61–64.

Zhang, Y., Chen, K., Sloan, S.A., Bennett, M.L., Scholze, A.R., O'Keeffe, S., Phatnani, H.P., Guarnieri, P., Caneda, C., Ruderisch, N., et al. (2014). An RNA-Sequencing Transcriptome and Splicing Database of Glia, Neurons, and Vascular Cells of the Cerebral Cortex. J. Neurosci. *34*, 11929–11947.

Zhang, Z.G., Zhang, L., Jiang, Q., Zhang, R., Davies, K., Powers, C., Van Bruggen, N., and Chopp, M. (2000). VEGF enhances angiogenesis and promotes blood-brain barrier leakage in the ischemic brain. J. Clin. Invest. *106*, 829–838.